SELF-COMPACTING
HIGH AND ULTRA HIGH PERFORMANCE
CONCRETES

Akbar Ghanbari

Ph.D.   2011

SELF-COMPACTING
HIGH AND ULTRA HIGH PERFORMANCE
CONCRETES

Akbar Ghanbari

B.Sc., M.Sc.

Submitted for the degree of

Doctor of Philosophy

CARDIFF
UNIVERSITY

PRIFYSGOL
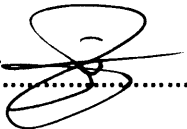CAERDYⱰ

Department of Civil Engineering

Cardiff University, UK

April 2011

In the Name of God
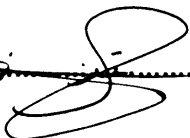
the Most Compassionate and the Most Merciful

DECLARATION

This work has not previously been accepted in substance for any degree and is not concurrently submitted in candidature for any degree.

Signed...A.- Ghanbari...............(candidate)   Date 5./.7./.201 1
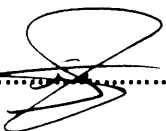
STATEMENT 1

This thesis is being submitted in partial fulfilment of the requirements for the degree of Doctor of Philosophy.

Signed...A.- Ghanba.ri...............(candidate)   Date 5./.7./.2011
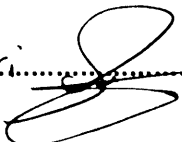
STATEMENT 2

This thesis is the result of my own independent work/investigations, except where otherwise stated. Other sources are acknowledged by explicit references.

Signed...A.- Ghanbari...............(candidate)   Date 5./.7./.2011

STATEMENT 3

I hereby give consent for my thesis, if accepted, to be made available for photocopying and for inter-library loan, and for the title and summary to be made available to outside organisations.

Signed...A.- Ghanbari...............(candidate)   Date 5./.7./.2011

To Forouzan and Parinaz

ACKNOWLEDGEMENT

My deepest gratitude is to my supervisor, Professor B.L. Karihaloo. It has been an honour to be his Ph.D. student. He has been always ready to listen and give advice. I am grateful to him for sharing his valuable time and knowledge. He offered me so much advice, patiently supervising me, and always guiding me in the right direction. I have learned a lot from him, without his help I could not have finished my dissertation successfully. I am also thankful to him for encouraging the use of correct grammar and consistent notation in my writings and for carefully reading and commenting on revisions of this dissertation.

My co-supervisor, Dr S. Kulasegaram has been always helpful. I am deeply grateful to him for valuable discussions we had during my research project.

Sincere thanks are conveyed to Faculty of Civil Engineering at Cardiff University and my friends.

I am also grateful to my parents who helped me stay sane through these years. Their support and care helped me to overcome setbacks and stay focused on my graduate study.

Last but not least, I am greatly indebted to my devoted wife Forouzan and my daughter Parinaz. They form the backbone and origin of my happiness. Their love and support without any complaint or regret has enabled me to complete this Ph.D. project. Being both a mother and father while I was away was not an easy thing for my wife. She took every responsibility and suffered all the bitterness to take care of my daughter and my family. I owe my every achievement to both of them.

SYNOPSIS

This thesis describes the steps taken to develop self-compacting high and ultra high-performance concretes with (SCHPFRC/SCUHPFRC) and without steel fibres (SCHPC/SCUHPC). For the self-compacting concrete mixes without steel fibres the fulfilment of the flow and cohesiveness criteria are found to be sufficient for the mix design. However, for the design of self-compacting concrete mixes with steel fibres it is found that they must additionally meet the passing ability criterion.

Micromechanical constitutive models are used to predict the plastic viscosity of SCHPFRC/SCUHPFRC from the measured plastic viscosity of the paste. The concrete is regarded as a two-phase suspension in which the solid phase is suspended in a viscous liquid phase. The liquid matrix phase consists of cement, water and any viscosity modifying agent (VMA) to which the solids (fine and coarse aggregates and fibres) are added in succession. The predictions are shown to correlate very well with available experimental data.

A Lagrangian particle based method, the smooth particle hydrodynamics (SPH), is used to model the flow of SCHPC/SCUHPC with or without short steel fibres. An incompressible SPH method is employed to simulate the flow of such non-Newtonian fluids whose behaviour is described by a Bingham-type model, in which the kink in the shear stress versus shear strain rate diagram is first appropriately smoothed out. The basic equations solved in the SPH are the incompressible mass conservation and Navier-Stokes equations. The solution procedure uses prediction-correction fractional steps with the temporal velocity field integrated forward in time without enforcing incompressibility in the prediction step. The resulting temporal velocity field is used in the mass conservation equation to satisfy incompressibility through a pressure Poisson equation derived from an approximate pressure equation. The results of the numerical simulation are benchmarked against actual slump tests carried out in the laboratory. The numerical results are in excellent agreement with test results, thus demonstrating the capability of SPH and a proper rheological model to predict self-compacting concrete flow behaviour.

The simulations of SCC mixes are also used as an aid at the mix design stage of such concretes. Self-compacting high and ultra-high performance concrete (SCHPC/SCUHPC) mixes with and without steel fibres (SCHPFRC/SCUHPFRC) are proportioned to cover a wide range of plastic viscosity. All these mixes meet the flow and passing ability criteria, thus ensuring that they will flow properly into the moulds.

TABLE OF CONTENTS

Chapter 3: An Introduction to the Rheology of Self-Compacting Concrete and Methods of Simulating its Flow   43

X

Chapter 4: Development of Self-Compacting High and Ultra High Performance Concretes with and without Steel Fibres 83

Chapter 5: Prediction of the Plastic Viscosity of Self-Compacting High and Ultra High Performance Concretes With and Without Steel Fibres 109

Chapter 6: Modelling the Flow of Self-Compacting High and Ultra High Performance Concretes With and Without Steel Fibres   141

Chapter 7: Guidelines for Mix Proportioning of Self-Compacting High and Ultra High Performance Concretes With and Without Steel Fibres   168

Chapter 8: Conclusions and Recommendations for Future Research   186

List of Figures

XVIII

XIX

List of Tables

Chapter 1

Introduction

1.1 Research background

Reinforced concrete is one of the most versatile and widely used construction materials on the planet. With new structural demands due to more and more ambitious design, the reinforcement in concrete structures is becoming extremely dense and clustered. With such dense rebar arrangements, it is becoming increasingly harder to pour and fully compact the concrete into the formwork. As a result of the poor placement, compaction and homogeneity of concrete, the mechanical characteristics and the visual appearance of reinforced concrete structures are affected. The aforementioned difficulties resulting from the passing and flowing restrictions introduced by high percentage of reinforcement are overcome by the use of self-compacting concrete (SCC).

The self-compacting concrete is a comparatively new type of concrete that differs from the conventional vibrated concrete in that it contains a superplasticiser and a stabiliser, which contribute significantly to increasing the ease and rate of its flow. A self-compacting concrete can fill any part of formwork only under its own weight, without the need for compaction or external vibration. It was first developed in Japan in 1988 and spread to Europe through Holland and Sweden in the 1990s. It is a good alternative to conventional concretes in structural elements of complex and difficult shapes, e.g. very thin or curved members, in which the conventional concrete maybe difficult to compact, especially in the presence of congested reinforcement. Moreover, SCC offers many health and safety benefits. The elimination of vibratory compaction on site means that the workers are no longer exposed to vibration and its related illnesses, e.g. white finger syndrome, besides providing a quieter working environment.

Despite its many advantages, such as good filling ability, passing ability and segregation resistance, normal SCCs are still prone to low durability and low tensile capacity in a similar manner to conventional vibrated concrete.

Over the past few decades many researchers have explored ways of overcoming the drawbacks of conventional vibrated concretes. The majority of work done in this field is related to changing the constituents of the vibrated concrete to improve the interfacial bond between the mortar matrix and aggregates. The concretes so produced are the so-called high performance concretes (HPC). In order to produce a HPC some modifications need to be made to both the mixing and curing processes. The benefits of using HPCs are compaction

without segregation, higher tensile capacity, toughness, early age strength, high compressive strength (from 40 MPa for normal concretes to about 80 MPa for HPCs), etc.

An alternative in the advancement of concrete technology is to combine the important characteristics of the conventional vibrated HPC and the SCC to produce self-compacting high performance concretes (SCHPC). The major disadvantage of a HPC, namely its low flow-ability and filling ability, is overcome by using a viscosity modifying admixture (VMA) or superplasticiser, while cement replacement materials (CRM) e.g. ground granulated blast furnace slag, fly ash and/or silica fume are used to overcome the drawbacks of the SCC, i.e. its low strength and durability. Even the SCHPC has low tensile strength and low strain capacity. To overcome this, short steel fibres can be added to SCHPC to increase its ductility and energy absorption capacity, thereby improving its durability.

Self-compacting high performance fibre reinforced concretes (SCHPFRC) exhibit a significant strain-hardening response that leads to an improvement in their tensile strength and toughness in comparison with normal SCHPCs.

To improve the performance further self-compacting ultra-high performance fibre reinforced concretes (SCUHPFRC) can be produced through the use of only fine quartz sands as aggregates, a high content of cement and silica fume (or CRMs), a high dosage of an effective superplasticiser (preferably based on poly-carboxylic ethers) and short steel fibres.

An example of the ultra-high performance fibre reinforced concrete (UHPFRC) is CARDIFRC. CARDIFRC is characterised by high compressive strength (in excess of 200 MPa), high splitting/flexural strength (up to 30 MPa) and high energy absorption capacity (in excess of 17,000 J/m^2). The matrix contains only very fine graded quartz sand and about 6% of short steel fibres of two lengths (6 and 13 mm long, 0.16 mm diameter). The mix without the fibres is very dense, viscous and flowable, and thus has the potential for self-compaction.

The mixture of SCC is strongly dependent on the composition and characteristics of its constituents in the fresh state. The properties of SCC in its fresh state have a great effect on its properties in the hardened state. Therefore it is critical to understand its flow behaviour in the fresh state. As the SCC is essentially defined in terms of its flow-ability, the characterisation and control of its rheology is crucial for its successful production. This is even more relevant if the fibres are added to SCC. Self-compacting high and ultra-high performance fibre reinforced concretes (SCHPFRC/SCUHPFRC) must maintain their flow-

ability and passing ability despite the presence of a large volume fraction of fibres. This presents a challenge which makes the control of rheology crucial for the successful production of SCHPFRC/SCUHPFRC.

The flow of all SCCs with or without fibres is best described by the Bingham constitutive model (Dufour and Pijauder-Cabot, 2005). This model contains two material properties, namely the yield stress and the plastic viscosity. It is known however that the yield stress of SCC mixes is low in comparison with normal vibrated concretes and remains nearly constant over a large range of plastic viscosities. The viscosity of a homogenous viscous fluid such as the cement paste can be measured accurately which cannot be said of any SCC.

1.2 Research objectives

The objectives of this thesis are as follows:

- To produce high and ultra high performance self-compacting concretes with and without short steel fibres, which exhibit good flow-ability, good cohesiveness and passing ability.

- To predict the plastic viscosity of the high and ultra high performance self-compacting concretes with or without steel fibres from the knowledge of the plastic viscosity of the paste alone using appropriate micromechanical models and to validate these predictive models by comparing with real test data available in the literature.

- To model the flow behaviour of high and ultra high performance self-compacting concretes with and without short steel fibres in two standard test configurations, namely the slump flow and L-box tests using appropriate computational strategies.

- To provide guidance for proportioning the mixes of the high and ultra high performance self-compacting concretes with or without steel fibres that have both flow and passing ability using the computational flow modelling technique at the mix design stage.

1.3 Research methodology

To achieve the above objectives research is undertaken in four stages:

- First, high and ultra high performance self-compacting concrete mixes with and without short steel fibres are developed by trial and error. For the SCC mixes without steel fibres the fulfilment of the flow and cohesiveness criteria is checked for each trial mix design by the slump flow test. The design of SCC trial mixes with steel fibres is additionally tested to meet the passing ability criterion.

- Second, the plastic viscosity of the mixes with and without steel fibres is estimated from the known plastic viscosity of the cement paste. For this, concrete is regarded as a two-phase suspension of solid and liquid phases. The liquid matrix phase consists of cement paste, i.e. cement and/or any superplasticiser or viscosity modifying agent (VMA). The plastic viscosity of this liquid matrix phase is assumed to be known, as it can be measured accurately. The increase in the plastic viscosity due to the addition of a solid phase (i.e. any cement-replacement materials, fine and coarse aggregates) to this matrix is predicted from a two-phase model. The model is applied in several stages. The plastic viscosity of the viscous concrete consisting of the liquid and solid phases is further increased if steel fibres are added to it. This increase is quantified using a micromechanical model.

- Third, a Lagrangian particle-based technique, the so-called smooth particle hydrodynamics (SPH) method, is chosen for simulating the flow of SCC with or without steel fibres. An incompressible SPH method is applied to simulate the flow of these non-Newtonian fluids whose behaviour is described by a Bingham-type model. The plastic viscosity of the SCC is predicted using the procedures described above. The basic equations solved in the SPH are the incompressible mass conservation and Navier-Stokes equations. The results of the numerical simulation are benchmarked against actual slump flow tests carried out in the laboratory.

- Fourth, the SPH simulation technique is used at the mix design stage to provide guidance for proportioning the mixes of high and ultra high performance self-compacting concretes, which meet the flow and passing ability requirements and have the desired plastic viscosity.

1.4 Outline of the thesis

The contents of this thesis are organised into eight chapters, followed by bibliographical references. For clarity of presentation, each chapter is divided into sections and sub-sections, as required. In order not to interrupt the flow of the text in the main body of the thesis, all details have been relegated to appendices. A brief overview of the contents of various chapters follows:

Chapter 2 gives a general overview of SCC and its basic properties, materials used in its production and their influence on its characteristics in the fresh and hardened states and of the relevant workability tests on the fresh SCC. Also, some practical examples of structures made with SCC will be presented.

Several tools which are available to address the workability of SCC are reviewed in Chapter 3. These tools can be classified into two main groups: an empirical group, e.g. tools that model the flow of SCC, and the second based on the measurement of the concrete flow. Both sets of tools will be reviewed. The rheology of cement paste, SCC and the methods of measurement of their rheological characteristics will be briefly discussed. Different methods of the simulation of the flow of SCC which are available in the literature will be reviewed.

Chapter 4 describes the steps taken to develop self-compacting high and ultra-high performance concretes with and without steel fibres. In the design of such concretes, the flow-ability, good cohesiveness and passing ability criteria must be met. An extensive investigation will be carried out on the proportions of solids and liquids, the type of superplasticiser, and the steel fibres needed in order to produce SCC mixes with the right flow and passing ability.

Chapter 5 describes micromechanical constitutive models used to predict the plastic viscosity of the high and ultra-high performance self-compacting concretes with or without steel fibres from the measured plastic viscosity of the paste. The concrete is regarded as a suspension in which the solid phase is suspended in a viscous liquid phase. The liquid matrix phase consists of cement, water and any viscosity modifying agent (VMA) to which the solids (fine and coarse aggregates and fibres) are added in succession. The predictions will be correlated with the available experimental data. Comments will be made on the practical usefulness of the predicted plastic viscosity in simulating the flow of SCC.

Chapter 6 is devoted to the simulation of the flow of high and ultra-high performance self-compacting concretes with or without steel fibres. An incompressible SPH methodology is adopted. The formulations relating to incompressible SPH and coupling of SPH formulation with a suitable Bingham model to represent the rheological behaviour of SCC will be briefly discussed and numerical results for SCCs flow with and without steel fibres will be compared with some available experimental observations. The basic equations solved in the SPH are the incompressible mass conservation and Navier-Stokes equations.

Chapter 7 uses the SPH simulation technique as a practical aid in the proportioning of the mixes of high and ultra-high performance self-compacting concretes with or without steel fibres.

Chapter 8 summarises the main conclusions on the basis of the research work embodied in chapters 4 to 7, inclusive and also makes recommendations for future research.

The thesis concludes with an alphabetical list of references to the works in the literature, cited in the text, and appendices. Some of the work described in this thesis has been published or is in the process of publication. For easy reference, the publications are listed below.

1. Ghanbari A, Karihaloo B L. Prediction of the plastic viscosity of self-compacting steel fibre reinforced concrete, *Cement and Concrete Research* 2009;39(12):1209-1216.

2. Kulasegaram S, Karihaloo B L, Ghanbari A. Modelling the flow of self-compacting concrete, *International Journal for Numerical and Analytical Methods in Geomechanics* 2011 (in press) DOI: 10.1002/nag.924.

3. Deeb R, Ghanbari A, Karihaloo B L. Development of Self-Compacting High and Ultra High Performance Concretes with and without Steel Fibres, *Cement and Concrete Composites* 2011 (submitted).

4. Karihaloo B L, Kulasegaram S, Ghanbari A. Modelling the flow of self-compacting concrete, *ECCM* 2010, Paris, CD-ROM Paper 59.

5. Kulasegaram S, Karihaloo, B L, Ghanbari A. Modelling the flow of self-compacting fibre-reinforced concrete, Proc 5th *SPHERIC workshop*, Manchester,U.K., June 2010, pp. 69-75.

6. Ghanbari A, Karihaloo B L, Kulasegaram S. Prediction of the plastic viscosity of self-compacting steel fibre reinforced concrete, Proc *CONMOD2010*, Lausanne June 2010, pp 61-64.

Chapter 2

Self-Compacting Concrete

2.1 Introduction

The production of high strength concrete has always been one of the main objectives of concrete technologists. For over 20 years now, concretes with compressive strength of 50-130 MPa have been used worldwide in tall buildings and bridges with long spans or in buildings in aggressive environments. Building elements made of such concretes are usually densely reinforced. The small spacing between the reinforcing bars may lead to defects in concrete (Dietz and Ma, 2000). Normally, vibration is used to achieve the required compaction, reduce the porosity and the air entrapped in the concrete. However, vibration of densely reinforced concretes is not an easy job even for skilled workers.

The lack of good vibratory compaction directly affects the mechanical characteristics of the concrete in its hardened state. Insufficient compaction will lead to the inclusion of voids, which not only results in a reduction in the compressive strength but also strongly influences the natural physical and chemical protection of the embedded steel reinforcement afforded by the concrete (Gaimster and Dixon, 2003).

If such a high compressive strength concrete is self-compacting (SCC), the production of densely reinforced elements would be an easier task, thanks to the high homogeneity of SCC.

The self-compacting concrete is a type of concrete which can fill the whole mould completely with a minimum of defects and which compacts under its own self-weight without vibration. The concrete so produced is sufficiently cohesive and flows without segregation or bleeding. The self-compacting concrete was first developed in Japan (Ozawa et al., 1989) in the late 1980s to be mainly used for highly congested reinforced structures in seismic regions (Bouzoubaa and Lachemib, 2001).

The hardened SCC is dense, homogeneous and can have the same engineering properties and durability as the traditional vibrated concrete.

This chapter gives a general overview of SCC and its basic properties, materials used in its production and their influence on its characteristics in the fresh and hardened states. It also reviews the workability tests relevant to the fresh SCC. Also some examples of structures made with SCC will be presented.

2.2 Historical development of self-compacting concrete

Research undertaken into underwater placement technology in the mid-1980s in the UK, North America and Japan led to the production of concrete mixes with a high degree of washout resistance. This, in turn, led to the development of SCC with the concept being first initiated in Japan in the mid-1980s (Gaimster and Dixon, 2003). It was recognised that the reduction in the number of skilled workers in the Japanese construction industry was leading to a reduction in the quality of construction work with subsequent knock-on effects on the concrete durability (Okamura et al., 1998).

A prototype of SCC was proposed in 1986 at the Tokyo University. The first model for proportioning SCC mixes was developed in 1988 using constituent materials readily used in conventional concrete (Ozawa et al., 1989). These mixes were to be used mainly for highly congested reinforced structures in seismic regions (Bouzoubaa and Lachemi, 2001).

The main aims were to shorten the construction time, to avoid vibrating the confined zones which are rather difficult to reach, and to eliminate vibration noise especially at concrete product plants. The proportioning model performed satisfactorily with regard to the fresh properties and also to the long-term hardened properties, such as the shrinkage.

The self-compacting concrete technology spread to Europe through Holland and Sweden in the 1990s (Bennenk, 2005, Billberg 1999). In the beginning of the 21st century, the SCC started to be of interest in the USA (Ouchi et al., 2003). However, the annual production of SCC indicates that challenges still need to be overcome (Thrane, 2007). The ways of producing SCC are quite different in various countries depending on the traditions and materials available. In the last two decades, the SCC has been developed further, utilizing various materials such as condensed silica fume (CSF), ground granulated blast furnace slag (GGBS) and pulverized-fuel ash (PFA). Today, the SCC is an important topic among researchers and industries in the field of concrete, although the overall production is still relatively small compared to the conventional vibrated concrete. The self-compacting concrete amounted for less than 1% of the ready mix concrete production in Europe in 2004 (ermco.org, 2005). However, the SCC is now well established in a number of countries, such as Sweden and the USA.

2.3 Definitions of self-compacting concrete

Researchers have defined SCC in several ways; some of these are listed below.

Khayat et al. (1999): a highly flow-able, yet stable concrete that can spread readily into place and fill the formwork without any consolidation and without undergoing any significant segregation.

Bartos and Marrs (1999): self-compacting concrete is a type of concrete which flows under its own weight, can fill any part of formwork without vibration (even in the presence of highly dense reinforcing bars) and maintains its homogeneity.

Ozawa et al. (1989): self-compacting concrete must have the following properties: Filling ability, i.e. without vibrating the concrete, the SCC has to fill any space within the formwork passing ability, i.e. a homogenous distribution of the components of SCC in the vicinity of obstacles; and resistance to segregation, i.e. the resistance of the components of SCC to migration or separation. Figure 2.1 shows how this definition is incorporated in a rational design model (Okamura et al., 2000).
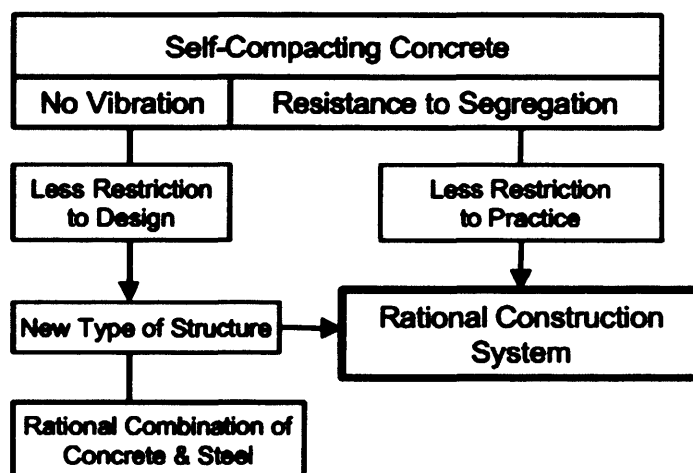
Figure 2.1: Proposed rational model of Ozawa (After Ouchi, 1999)

2.4 Basic properties of self-compacting concrete

Many workers involved in the development of SCC (Domone and Chai, 1998; Okamura, 1999; Ozawa et al., 1990) have recognised that there are three fundamental factors that govern the fresh concrete properties:

(i) Properties of the mortar;

(ii) Volume of coarse aggregate in the mix;

(iii) Use of a superplasticiser to enhance workability.

The properties of the paste and mortar have important effects on the SCC properties, as with conventional vibrated concrete. The water to binder ratio primarily determines the workability of the mix, as will the proportion of sand in the mortar (Okamura, 1999). The volume content of coarse aggregate in the concrete not only affects the workability but plays a major role in the segregation resistance of the mix. Okamura and Ozawa (1995) have employed three key procedures to attain self-compacting ability: limited coarse aggregate content, low water to powder ratio, and use of superplasticiser. Today, the new generation of superplasticisers, the polycarboxylate ethers (see Section 2.7), gives improved workability retention to the cementitious mix. These superplasticisers disperse the cement by steric stabilization, which is more powerful compared to the electrostatic repulsion of older types of plasticisers (Yamada et al., 2000, Flatt, 2004a).

Figure 2.2 shows a typical comparison of mix proportioning for SCC and normal vibrated concrete. As can be seen the cementitious component of the SCC is larger than that in the conventional concrete with a consequent reduction in the volume fraction of the coarse aggregate.

Normal Vibrated Concrete

10%	18%		25%	45%
Cement	**Water**	**Air**	**Fine Aggregate**	**Coarse Aggregate**
			Fines	
10%	18%	8%	26%	36%

2%

2%

Self-Compacting Concrete
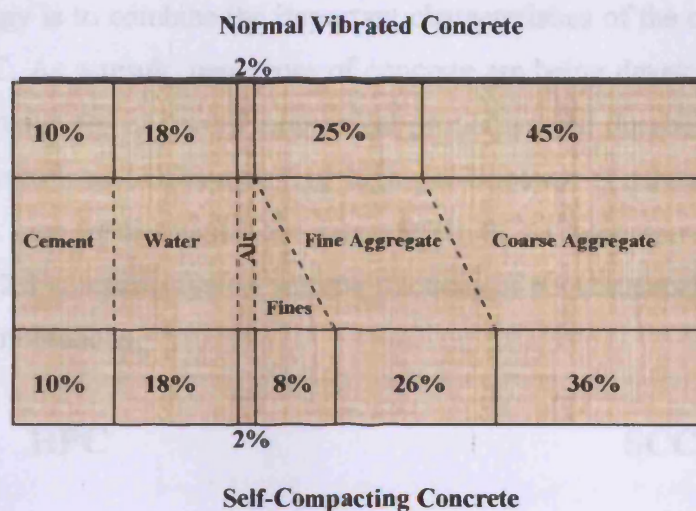
Figure 2.2: A typical mix proportioning of SCC and normal vibrated concrete

The self-compacting concrete offers many important advantages in comparison with a conventional vibrated and high performance concrete. It can fill all the formwork spaces without internal vibration, reducing labour time and improving the surface finish. The use of SCC leads to an overall cost reduction with improvements in the quality of the structure and construction environment.

To be self-compactable a concrete should have a paste with high deformability for ease of flow around rebars, as well as resistance to segregation between the coarse aggregate and the paste during the flow (Okamura and Ouchi, 2003a). These requirements may seem to be contradictory because for high deformability, a high water content would seem necessary, resulting in a paste with low viscosity and hence a concrete prone to segregation. The self-compacting concrete is able to flow under its own weight and achieve full compaction, even in the presence of congested reinforcement such as in mat foundations and moment-resisting frames. The hardened concrete is dense, homogeneous and can have the same engineering properties and durability as the traditional vibrated concrete. The self-compacting concrete improves the efficiency at the construction sites, enhances the working conditions and the quality and the appearance of concrete. The key difference in the production of SCC in comparison to other types of high performance concrete (HPC) is the use of a superplasticiser and/or a viscosity modifying agent and cement replacement materials in its composition to effectively stabilise the rheological properties of SCC. An alternative in the advancement of

concrete technology is to combine the important characteristics of the conventional vibrated HPC and the SCC. As a result, new types of concrete are being developed in order to meet the increasing demand for improved mechanical properties and durability. These new types of concrete are known as self-compacting high performance concrete (SCHPC) and self-compacting ultra high performance concrete (SCUHPC) (compressive strengths of 150-200MPa). Figure 2.3 compares typical volume fractions of constituents in conventional HPC, SCC and their combinations.

HPC

SCC

SCHPC

SCUHPC
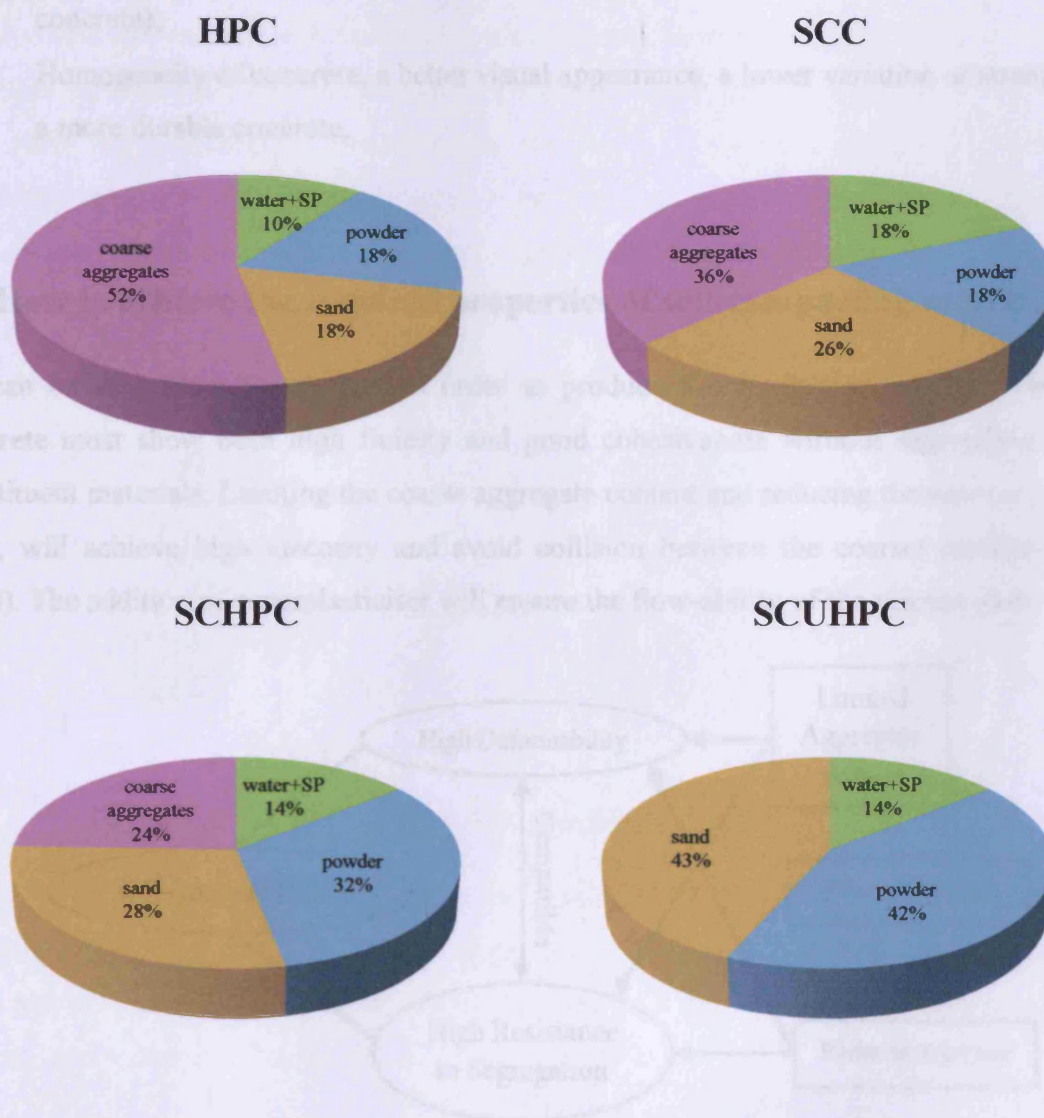
Figure 2.3: Typical volumes of constituents in normal HPC and SCCs

The application of SCC has benefits related to:

- Productivity, i.e. lower production costs, and a higher casting rate;

- Working conditions due to the reduced noise and dust emissions;

- Casting conditions, i.e. casting of densely-reinforced sections and remote casting;

- Environment-friendly production, e.g. the filler and aggregates can be waste/recycled materials;

- Elimination of the effect of vibration (which affects the quality of normal vibrated concrete);

- Homogeneity of concrete, a better visual appearance, a lower variation of strength and a more durable concrete.

2.5 How to achieve the required properties of self-compacting concrete?

As can be seen from Figure 2.4, in order to produce a non-vibrated concrete, the fresh concrete must show both high fluidity and good cohesiveness without segregation of the constituent materials. Limiting the coarse aggregate content and reducing the water to powder ratio, will achieve high viscosity and avoid collision between the coarser particles (Utsi, 2008). The addition of superplasticiser will ensure the flow-ability of the viscous paste.
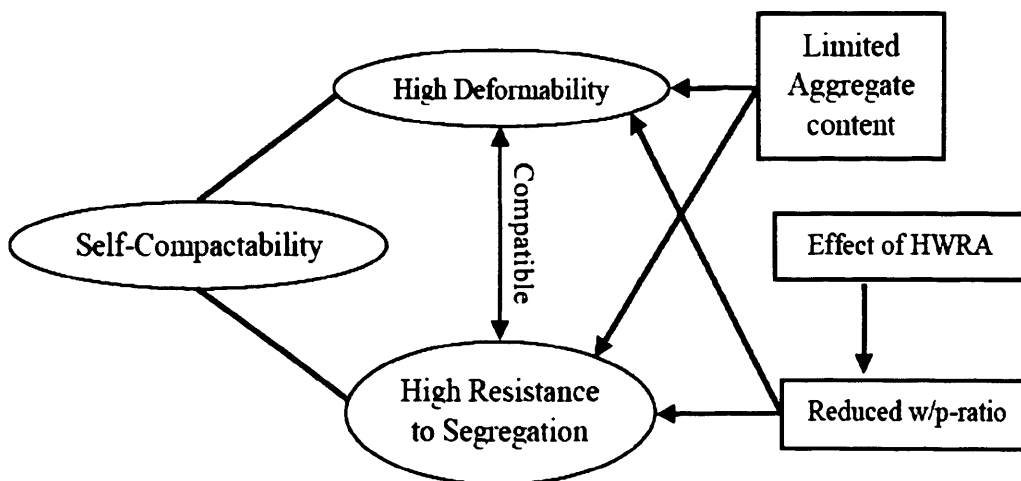
Figure 2.4: Methods to achieve self-compacting ability (After Ouchi et al., 1996)

To achieve self-compacting ability of concrete, different design approaches are followed in different countries. These approaches aim to optimize three aspects of the fresh concrete. Firstly, the paste content; by introducing a superplasticiser that significantly affects the structure of the powders by dispersing the cement grains and reducing the water to binder ratio. Secondly, the aggregate skeleton; in order to obtain higher packing density, the maximum aggregate size is decreased and crushed aggregates are replaced with round ones. Thirdly, some cement is replaced by viscosity modifying agents and/or fillers to fill the interstices of the granular skeleton thereby increasing the viscosity of the mix and reducing the cost of concrete. The self-compacting concrete can be distinguished on two levels: first, all solids (powders and aggregates) are suspended by water and superplasticiser and second, aggregates are lubricated by cement paste. An excess of the fluid reduces the friction by separating the solids with a small layer of either water or cement paste. Figure 2.5 shows the formation of layers of cement paste around aggregates. The thickness of the paste layer can be best related to the diameter of the aggregates (Oh et al., 1997).
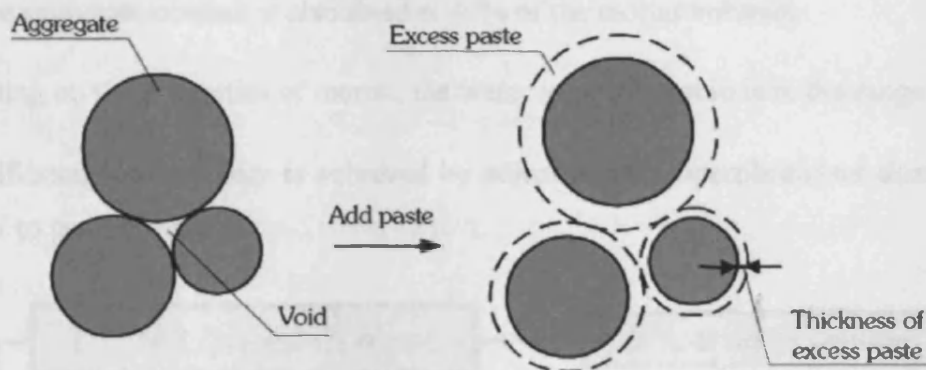
Figure 2.5: Excess paste layer around aggregates (After: Oh et al., 1997)

Self-compacting concrete mixtures are usually designed with higher volumes of paste than vibrated concrete mixtures. An excess of paste has to be added to keep the solid particles apart and to reduce the friction between the aggregates. The cement paste thus has a filling, a binding, and a smearing role in the SCC (Ma et al., 2003).

2.6 Different mix designs of self-compacting concrete

Three different types of SCC can be distinguished depending on the method of providing viscosity.

1. **Powder-type SCC.** This was the first proposed prototype of SCC. It is characterized by a high powder content and low water to powder ratio. The requirements for this type are (i) increasing the plastic viscosity by limiting the free water content, and (ii) using a superplasticiser to provide consistence. Because of the high powder content, powder-type SCC mixes are sensitive to changes in the constituent materials. Usually cement replacement materials are used to control the strength and heat of hydration. Due to the low water to powder ratio, such SCCs are predicted to have a high strength and shrinkage, and low permeability.

Okamura and Ozawa (1995) proposed a simple mix proportioning system for this type of SCC (Figure 2.6). According to their method, the coarse and fine aggregate contents are fixed and the self-compacting ability can be obtained by adjusting the water to powder ratio and the amount of superplasticiser. A typical procedure is

1) The coarse aggregate content is fixed at 50% of the solid volume;

2) The fine aggregate content is also fixed at 40% of the mortar volume;

3) Depending on the properties of mortar, the water to powder ratio is in the range of 0.9-1.0.

4) The self-compacting ability is achieved by adjusting the superplasticiser dosage and the final water to powder ratio.
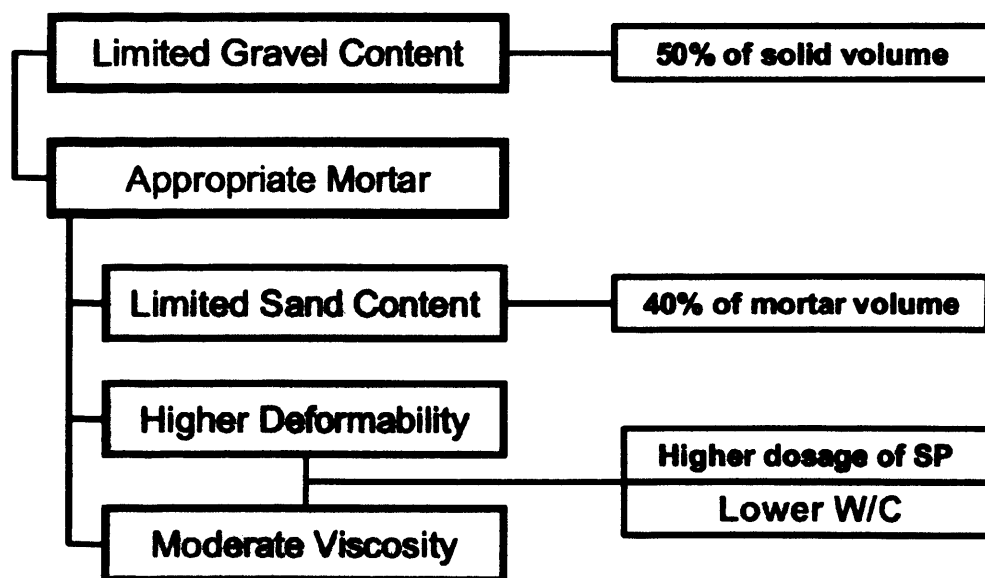
Figure 2.6: A typical mix design of SCC based on the Okamura and Ozawa procedure (Brite, 2000)

2. **VMA-type SCC** is characterized by a high dosage of a viscosity modifying agent (VMA), which is added primarily for increasing the plastic viscosity. Compared with the powder-type SCC, the VMA-type SCC requires a higher superplasticiser dosage or water to powder ratio to obtain the required filling ability. The powder content is less because the viscosity is controlled by the addition of VMA.

3. **Combined-type SCC** was developed to improve the robustness of powder-type SCC by adding a small amount of VMA. In such mixes, the VMA content is less than that in the VMA-type SCC and the powder content and water to powder ratio are less than those in the powder-type SCC. The viscosity is provided by the VMA along with the powder. This type of SCC was reported to have high filling ability, high segregation resistance and improved robustness (Rozie`re et al., 2007).

2.7 Superplasticiser

The demand for a high level of workability, together with good stability of the mix for SCC has led to the use of a number of admixtures. The advent of superplasticisers and the developments in the admixture technology have made the production of SCC easier, and as a result a variety of materials may be used. There are mainly four categories of superplasticiser, namely the sulfonated melamine formaldehyde condensates (plasticiser), sulfonated naphthalene formaldehyde condensates, modified lignosulfonates, and carboxylated acrylic ester co-polymers or poly-carboxylic ethers (Kong et al., 2003). Figure 2.7 shows the progression in the development of admixture technology.
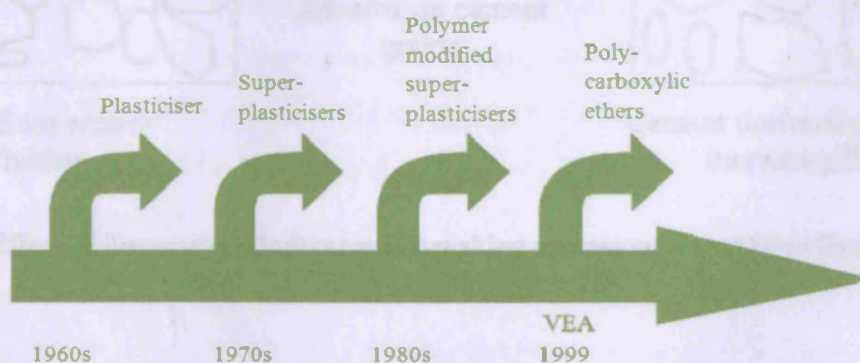
Figure 2.7: Development in admixture technology (After Dransfield, 2003)

The advances in admixture technology have played a vital part in the development of SCC. Modern superplasticisers (based on poly-carboxylic ethers) promote good workability retention and can be added at any stage of the batching cycle. They contribute to the achievement of denser packing and lower porosity in concrete by increasing the flow-ability and improving the hydration through greater dispersion of the cement particles, and thus assisting in producing SCCs of high strength and good durability.

2.7.1 Action of superplasticisers

The use of superplasticisers improves the flow-ability of SCC by their liquefying and dispersing actions. In addition, a superplasticiser deflocculates the cement particles and frees the trapped water by their dispersing action and hence enhances the flow-ability of SCC. Due to the dispersing action, the inter-particle friction and, thus, the flow resistance are also decreased, thus improving the flow-ability of concrete. As stated by Dransfield (2003), "this is analogous to the situation where people are walking both ways along a narrow pavement. If groups of people walking in one direction hold hands, then it is hard for people walking the other way to pass, especially if they are also holding hands. If everyone stops holding hands and walking in groups, then it is easy for people going in opposite directions to move round each other and pass". Admixtures adsorb on to the cement surfaces and break up the flocs, leaving individual cement grains, which can pass each other easily, making the mix more fluid (Figure 2.8).

Dispersing admixture

Adsorbs on cement grains

Cement flocs reduce fluidity

Cement uniformly dispersed increasing fluidity
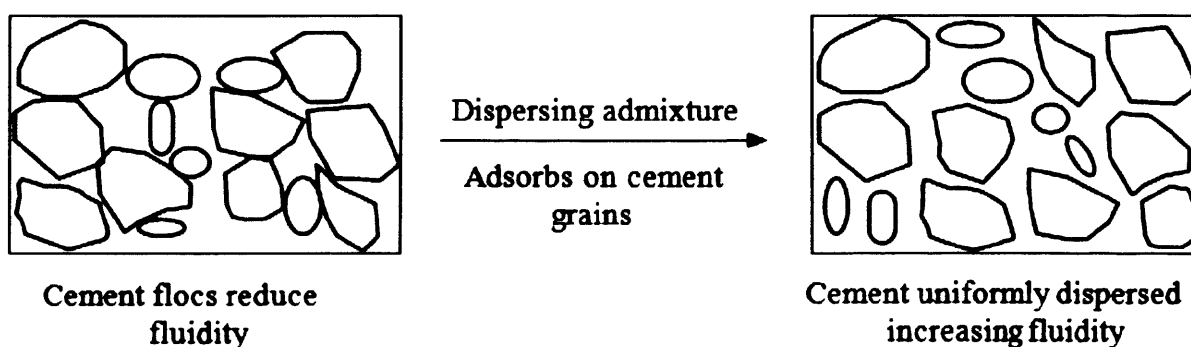
Figure 2.8: Effect of dispersing admixtures in breaking up cement flocs (After Dransfield, 2003)

2.8 Cement replacement materials and micro-silica

2.8.1 Cement replacement materials

A self-compacting concrete requires a high amount of flow-ability that can easily be achieved by the addition of a superplasticiser to the concrete mixture, as stated earlier. However, for such a concrete to remain cohesive during the flow, special attention has to be paid to mix proportioning. To avoid segregation following the addition of a superplasticiser, a simple approach is to increase the sand content, whilst at the same time to decrease the coarse aggregate content. But the reduction in the coarse aggregate content results in the use of a high volume of cement which has the disadvantage related to a higher temperature rise during hydration and an increase in the cost. An alternative approach is to incorporate a viscosity-modifying admixture to enhance the stability, i.e. cohesiveness (Khayat and Guizani, 1997). Chemical admixtures are, however, expensive, and their use may increase the cost of concrete. Although savings in labour cost might offset the increased material cost, the use of cement replacement materials (CRM) or mineral admixtures in SCC is a better way to impart high workability to the mix, as well as to reduce the total cost of SCC.

Cement replacement materials, sometimes also called mineral admixtures, are added to concrete as part of the total cementitious system. They enhance self-compacting ability, fluidity, cohesiveness, segregation resistance and limit heat generation during hydration. The CRMs may be used in addition to, or as a partial replacement of, Portland cement in concrete depending on the properties of the materials and the desired effect on concrete (Mindess et al., 2003).

The mineral admixtures are generally industrial by-products and have therefore economic and environmental benefits. The slow rate of setting and hardening associated with the incorporation of CRMs in concrete is advantageous, if durability is the primary interest. The CRMs are less reactive than cement and can reduce problems resulting from the loss of fluidity of a rich concrete.

Two of the most commonly used CRMs are the ground granulated blast furnace slag (GGBS) and pulverised fuel ash or fly ash (FA). These additives can be used as binary, ternary (two CRMs in a single mix) and quaternary mixtures.

2.8.1.1 Ground granulated blast furnace slag

The ground granulated blast furnace slag is one of the CRMs widely used in the production of SCC. It is a by-product from the blast furnaces used to make iron. It is classified by EN 15167-1 and EN 15167-2 (or BS 6699) according to its level of reactivity.

The powder is about 10% less dense than Portland cement. For equal mass of the total binder (i.e. cement plus GGBS) content in the concrete, the GGBS will produce a larger volume of the binder paste increasing the segregation resistance and making the concrete easier to work, pump, place and compact. Finer particles in the GGBS (compared with the Portland cement) can also reduce bleeding.

The use of GGBS as a CRM in SCC has benefits related to the protection against both sulphate and chloride attack.

However a SCC made with GGBS sets more slowly. The setting time depends on the amount of GGBS used. The SCC containing GGBS gains strength over a longer period of time; this results in a lower heat of hydration and a lower temperature rise.

Depending on the desired properties, the amount of GGBS can be as high as 50 per cent by mass of the total cementitious material content (Ramachandran et al., 1981). The use of GGBS lowers concrete permeability, thereby reducing the rate of chloride ion diffusion (Russell, 1997). A proper combination of the Portland cement and GGBS can eliminate the need to use low alkali or sulphate-resistant cements. As reported by Russell (1997), replacing the Portland cement by 20 to 30 per cent of GGBS by mass can enhance the strength gain when the concrete is older than 28 days. Sobolev (1999) studied the effect of adding up to 50% by mass GGBS to the cementitious material and reported that it resulted in an increase of chemical and thermal resistance. A high proportion of GGBS may affect the stability of SCC resulting in reduced robustness with problems of consistence control, while slower setting can also increase the risk of segregation (EU Guidelines for SCC, 2005).

Druta (2003) reported no visible destruction in concrete samples containing GGBS after 140 cycles of freezing and thawing and also a high resistance to elevated temperatures.

2.8.1.2 Fly ash

Fly ash (also known as pulverised fuel ash) is a by-product of coal-fired electricity generating plants. The ash is produced during the combustion of ground or powdered coal. Due to its pozzolanic properties, the fly ash can be used as a replacement for some of the Portland cement content in SCC.

The fly ash for use in Portland cement concrete conforms to the requirements of ASTM C 618, standard specification.

According to the type of coal used in the power station, there are two classes of fly ash, i.e. class C fly ash and class F fly ash.

The class C fly ash is produced from the burning of younger lignite or sub-bituminous coal. This class generally contains more than 20% lime (CaO). The class C fly ash is preferable in the green building application.

The class F fly ash is obtained from the burning of harder, older anthracite and bituminous coal. This fly ash is pozzolanic in nature and contains less than 20% lime (CaO).

The use of fly ash as a partial replacement for Portland cement is generally limited to Class F fly ash. It can replace up to 30% by mass of Portland cement, and can add to the final strength of the SCC and also increase its chemical resistance and durability.

Due to the spherical shape of fly ash particles, they can also increase the workability of SCC mixtures, while reducing the water demand. The fly ash reduces segregation and bleeding and lowers the heat of hydration.

Concrete mixes containing the fly ash reach their maximum strength more slowly than concretes made with only Portland cement.

The investigations by Bouzoubaa and Lachemib (2001) show that the use of fly ash and blast furnace slag in SCC reduces the dosage of superplasticiser needed to obtain slump flow spread comparable to that of the concrete made with Portland cement only (Yahia et al., 1999). Also, the use of fly ash improves the rheological properties and reduces the thermal cracking of concrete due to the heat of hydration (Kurita and Nomura, 1998). Kim et al. (1996) studied the properties of super-flowing concrete containing fly ash and reported that the replacement of 30% cement by fly ash resulted in excellent workability and flow-ability.

Chindaprasirt et al. (2005) reported that the use of fly ash increased both the initial and final setting times of fly ash-cement pastes due to the smaller surface area of fly ash particles (adsorbing less free water from the mixture). Due to the higher free water content, the powder concentration decreases. The addition of lime powder (LP) enhances the rate of hydration. A ternary mixture of fly ash and lime powder showed better flow-ability and deformability/workability compared to brick powder and kaolinite. The lime powder is the finest and the fly ash is the coarsest admixture. An increase of 5% in the LP content reduces the flow time and increases the relative spread of the mix. An increase of LP content beyond 50% is not advantageous as the compressive strength begins to decrease sharply. A partial replacement of cement by fly ash results in a higher volume of paste due to the lower density of FA. This increase in the volume of the paste reduces the friction at the fine aggregate-paste interfaces, and improves the plasticity and cohesiveness of the mix, leading to increased workability. Therefore, the fineness of the CRMs is not the only parameter to improve the workability.

2.8.2 Micro-silica

Micro-silica (MS) or silica fume (SF) is a by-product of the manufacture of silicon metal and ferrosilicon alloys. It is a very fine almost pure silica (SiO_2) powder collected from the exhaust gases consisting mainly of spherical particles or microspheres of mean diameter about 0.15 microns.

Each microsphere is on average 100 times smaller than an average cement grain. At a typical dosage of 10% by mass of cement, there will be 50,000–100,000 micro-silica particles per cement grain.

Because of its extreme fineness and high silica content, micro-silica is a very effective pozzolanic material. Standard specifications for micro-silica used in cementitious mixtures are given in ASTM C1240 and EN 13263.

Micro-silica is one of the most effective and widely used fines that is added to SCC to improve its properties, in particular its compressive strength, bond strength, and abrasion resistance. It also significantly reduces the concrete permeability by blocking the capillary channels.

Micro-silica increases the yield stress of a SCC mix thus decreasing the slump flow and segregation (Carlsward et al., 2003). It also reduces the ionic strength of the pore solution leading to a reduced consistence loss (Bonen and Sarkar, 1995). In the case of Portland cement, 18% micro-silica (by weight of cement) is theoretically enough for the total consumption of calcium hydroxide (Papadakis, 1999) produced during the primary reaction of cement with water. However, as the small micro-silica particles also physically fill the pores, more than 25% micro-silica should be added to concrete to get the densest granular mixture (Richard and Cheyrezy, 1995). An excessive use of micro-silica in the SCC can be counterproductive because of the difficulty in attaining the desired workability (Hassan et al., 2010).

Khayat et al. (1997) have studied the influence of micro-silica blended with cement on some of the properties of fresh and hardened concretes. The properties studied were bleeding, slump loss, compressive strength and setting time. A total of 26 mixtures were developed. One half of the mixtures were air-entrained and had water-cement ratios ranging from 0.3 to 0.6. The remaining half contained non air-entrained mixtures and the water-cement ratios varied between 0.45 and 0.7. Their study revealed that the addition of small percentages of micro-silica, usually less than 10%, and of a proper amount of high range water reducing admixture (superplasticiser) could decrease the viscosity of the paste, thus reducing the water demand and the risk of bleeding. The small particles of micro-silica can displace some of the water present among flocculated cement particles and fill some of the voids between the coarser particles, which otherwise can be occupied by some of the mix water. This causes some gain in workability and in the densification of the fresh paste. Concrete mixtures made with blended micro-silica cement exhibited substantially less bleeding than those made with type I Portland cement. In addition, mixtures made with blended micro-silica cement showed 15 to 20 mm greater loss of slump than concretes without micro-silica.

In general, concrete mixtures made with type I Portland cement and blended micro-silica cement exhibited initial times of setting that were within one hour apart. When 15% of micro-silica was added with a high dosage of superplasticiser, initial and final times of setting were delayed by approximately 1 and 2 hours, respectively (Liu, 2009). Regarding the compressive strength, Khayat et al. (1997) found out that after three days of curing, no effect of cement type was observed on the development of compressive strength for concretes. However, starting with the seventh day, mixtures containing blended micro-silica cement exhibited

greater strength than those made with type I Portland cement. After 28 days, in non-air-entrained concretes, the use of blended micro-silica cement resulted in approximately 20% better strength gain compared with mixtures containing only Portland cement. Similar results were obtained in air-entrained concrete.

Duval and Kadri (1998) studied the influence of micro-silica on the workability and compressive strength of concretes. The concretes that have been investigated had low water-cement ratios (0.25 to 0.40). The type I Portland cement was replaced by 10-30% by mass micro-silica, and superplasticiser was added. It was found that micro-silica increased the compressive strength at most by 25%, but the workability of concretes was best when its content was between 4 and 8%. Duval and Kadri also found out that if micro-silica exceeds 15% of the cementitious material, both compressive and tensile strengths are reduced.

Carlsward et al. (2003) observed a decrease of slump flow with an increase in the micro-silica content in all of their workability tests. Regarding the rheological parameters, the general tendency was an increase in the yield stress with an increase in the micro-silica content.

Vikan and Justnes (2003) also observed the same effect on the yield stress.

2.8.3 Benefits of CRMc

In summary, the benefits of CRMs to concrete (besides the obvious economic and environmental ones) are as follows:

- The placing and compaction are made easier thus giving better workability;
- The durability of concrete is increased because of the retardation in the early setting time with a better long term strength;
- The risk of thermal cracking in large pours is reduced, because of lower early-age temperature rise due to hydration;
- The resistance to attack by sulphate and other chemicals is increased;
- The risk of reinforcement corrosion is reduced.

2.9 Effect of fibres on the behaviour of fresh self-compacting concrete

The modern development of steel fibre reinforced concrete may have begun around the early 1960s. Polymeric fibres came into commercial use in the late 1970s; glass fibres experienced

widespread use in the 1980s, and the carbon fibres attracted much attention in 1990s. The main application of steel fibre reinforced concrete (SFRC) is in structures subjected to potentially damaging concentrated and dynamic loads. The steel fibre reinforced concrete has been used in several areas of infrastructure and industrial applications such as airport pavements, industrial floors, overlays, and channel linings, where laboratory tests and field applications have shown SFRC to be more durable than plain concrete subjected to high velocity water flow (Aydin, 2007).

Fibres can be used in the SCC to extend the range of its application and to overcome its drawbacks, namely the brittleness, as well as the volume changes which occur during the hardening of the material, i.e. the autogenous shrinkage. Such fibre reinforced SCCs are called self-compacting (high or ultra-high performance) fibre reinforced concrete (SCFRC). Fibres bridge cracks and retard their propagation. They contribute to an increased energy absorption compared with plain SCC. In the past, steel fibres have been used to replace bar reinforcement, to decrease the width of cracks and to improve the tensile strength or the post-cracking behaviour (e.g. Benson and Karihaloo, 2005a,b).

Both metallic and polymeric fibres have been used in the production of SCC, but they may reduce flow and passing ability. Trials are therefore needed to establish the optimum type, length and quantity of the fibre to give all the required properties to both the fresh and hardened SCFRC.

Steel and long polymer structural fibres are used to modify the ductility/toughness of hardened SCFRC. Their length L_f and quantity V_f are selected depending on the maximum size of the aggregate and structural requirements. The higher the aspect ratio (L_f/d_f) and the volume fraction of the fibres, the better is the performance of the mix in the hardened state. On the other hand, the higher the fibre factor ($V_f L_f/d_f$) the more the slump flow is decreased. Before the addition of fibres the slump flow spread should be larger than 700mm. If the fibres are used as a substitute for normal reinforcement, the risk of blockage is reduced but it should be emphasised that using SCFRC in structures with normal reinforcement significantly increases the risk of blockage (European Guidelines for SCC, 2005).

2.9.1 Characteristics of the fibres

The mixture composition of fibre reinforced SCC is a compromise between the requirements in the fresh and the hardened states. The shape of the fibres differs from that of the

aggregates; due to the long elongated shape and/or a higher surface area, the workability of SCC is affected. The practical fibre content is limited; a sudden decrease of workability occurs at a certain fibre content, which depends on the mixture composition and the fibre type used. To optimise the performance of a single fibre, fibres need to be homogeneously distributed; clustering of fibres has to be counteracted (EU Guideline for SCC, 2005).

The steel fibre is the most common fibre type in the building industry; plastic, glass and carbon fibres contribute to a smaller part to the market. Also polymer fibres are mainly used to improve the stability of SCC, as they help prevent settlement and cracking due to plastic shrinkage of the concrete. In high and ultra high performance SCCFRC, polymer fibres maybe additionally needed as sacrificial fibres to achieve the required fire rating in these very dense mixes.

The size of the fibres relative to that of the aggregates determines their distribution. To be effective in the hardened state it is recommended to choose fibres not shorter than the maximum aggregate size. Usually, the fibre length is 2-4 times that of the maximum aggregate size (Groth, 2000). The effect of aggregate size on the fibre distribution is shown in Figure 2.9.
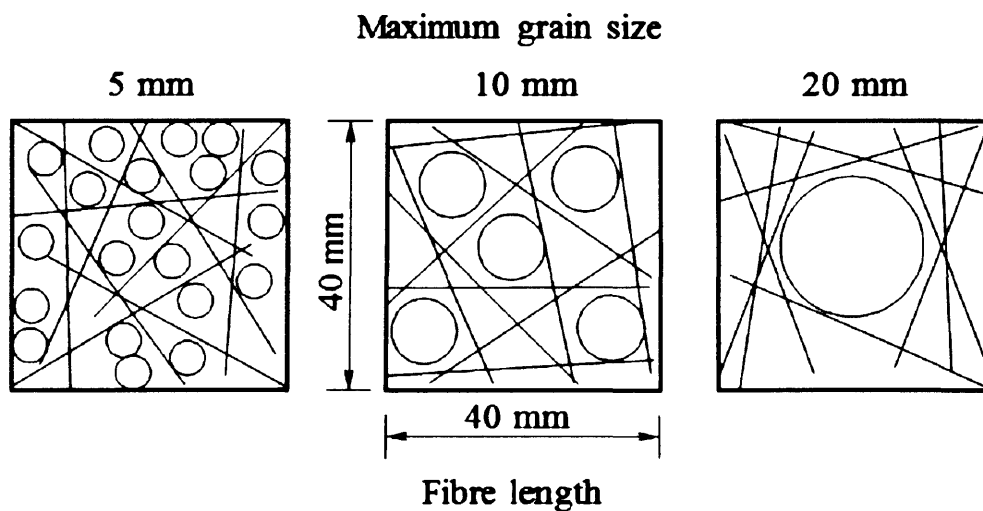
Figure 2.9: Effect of aggregate size on fibre distribution (After Johnston, 1996)

The self-compacting fibre reinforced concrete can maintain its flow-ability in spite of the addition of fibres. The slump flow decreases with the addition of fibres, also increasing the T_{500} time. The degree to which the steel fibres affect the slump flow and T_{500} depends on the

composition of the SCC mix (Saak et al., 2001). The effect of two types of polypropylene fibres on the characteristics of SCC in the fresh state was studied by Grünewald & Walraven (2003); these two were a monofilament and a fibrillated type. The self-compacting concrete remained self-compacting with the fibrillated type; the slump flow decreased from 710 to 620 mm. The monofilament type, on the other hand significantly decreased the slump flow to 440 mm due to the higher surface area.

The effect of fibres on the workability of SCC is summarised below:

- The shape of the fibres is more elongated compared with the aggregates; the surface area at the same volume is higher;

- Stiff fibres change the structure of the granular skeleton, while flexible fibres fill the space between them. Stiff fibres push apart particles that are relatively large compared with the fibre length (i.e. the porosity of the granular skeleton increases);

- Surface characteristics of fibres differ from that of cement and aggregates, e.g. polymer fibres might be hydrophilic or hydrophobic;

- Steel fibres often are deformed (e.g. have hooked or crimped ends or are wave-shaped) to improve the anchorage between the fibre and the surrounding matrix. The friction between hooked-end steel fibres and aggregates is higher compared with straight steel fibres.

2.10 Properties of fresh self-compacting concrete

The self-compacting concrete differs from conventional concrete in that its fresh properties are vital in determining whether or not it can be placed satisfactorily (Jacobs and Hunkeler, 1999). All the aspects of workability need to be fully controlled to ensure that its ability to be placed remains acceptable. These include the flowing ability, the passing ability, and the segregation resistance. Driven by its own weight, the concrete has to fill a mould completely without leaving entrapped air even in the presence of dense steel bar reinforcement. The components have to be homogeneously distributed during the flow and at rest. Clustering of the aggregates in the vicinity of reinforcement (blocking) and separation of water or paste affect the characteristics of SCC in the hardened state.

2.10.1 Flowing ability

Without vibrating the concrete, the SCC has to fill any space within the formwork; it has to flow in horizontal and vertical directions without keeping air entrapped inside the concrete or at the surface. The driving forces of this process are the weight of the concrete and the casting energy. To achieve high flowing ability, it is necessary to reduce inter-particle friction among solid particles (coarse aggregates, sand and powder) in the concrete by using a superplasticiser and a lower coarse aggregate content (Khayat, 1999, Sonebi and Bartos, 2005). Adding more water could improve flowing ability by decreasing inter-particle friction, but it also reduces viscosity, thus leading to segregation. Too much water also leads to undesirable influences on the strength and durability. Unlike water addition, which reduces both the yield stress and viscosity, the incorporation of a superplasticiser not only reduces the inter-particle friction by dispersing the cement particles but also maintains the deformation capacity and viscosity. It also impairs the hardened properties less than does additional water. The particle size distribution also affects the flowing ability. Inter-particle friction can be reduced by using continuously graded materials, aggregates and powder (Khayat, 1999, Sonebi et al., 2001).

2.10.2 Passing ability

Passing ability is required to guarantee a homogenous distribution of the components of SCC in the vicinity of obstacles. The minimum bar distance to avoid blocking depends on the flowing ability of the SCC, on the maximum aggregate size, the paste content and the distribution and the shape of the aggregates (Khayat and Roursel, 2000). Blocking results from the interaction among aggregate particles and between the aggregate particles and reinforcement; when concrete approaches a narrow space, the different flowing velocities of the mortar and coarse aggregate lead to a locally increased content of coarse aggregate (Noguchi et al., 1999, Okamura and Ouchi, 2003b). Some aggregates may bridge or arch at small openings which block the rest of the concrete, as shown in Figure 2.10.
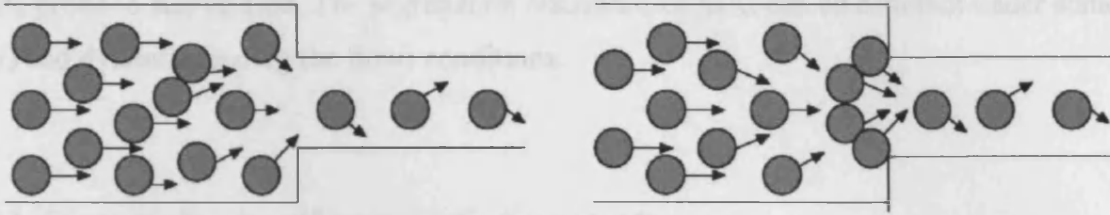
Figure 2.10: Schematic of blocking (After RILEM TC 174 SCC, 2000)

A reduction in the coarse aggregate content and in its size are both effective in preventing blocking. The paste volume of the concrete is also an important factor in blocking (Billberg et al., 2004). Blocking depends mainly on the yield stress, whereas the plastic viscosity does not influence the passing ability of the SCC. However, a paste with sufficient viscosity also prevents local increases in coarse aggregate volume, and hence blocking is avoided. As shown in Figure 2.11, the passing ability is therefore achieved by a reduction in the coarse aggregate size and content and by the use of VMA or by a proper selection of the powder.
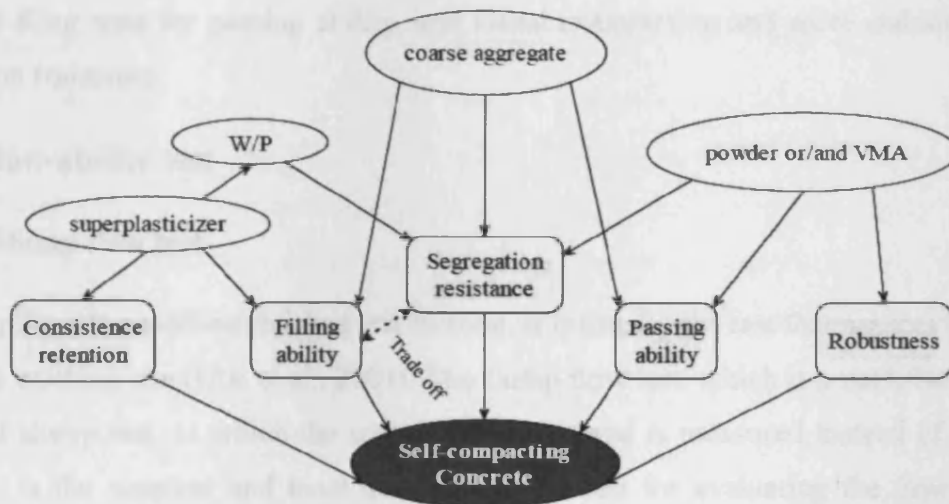
Figure 2.11: Schematic of ways to achieve SCC (After Liu, 2009)

2.10.3 Segregation resistance

The segregation resistance is the resistance of the components of SCC to migration or separation. Particles having a relatively high density or a low surface to volume ratio are

more prone to segregation. The segregation resistance of SCC can be different under static (at rest) and dynamic (during the flow) conditions.

2.11 Tests on fresh self-compacting concrete

The rheological tests can be performed on a SCC mix using rheometers of different types. However these tests suffer for some drawbacks; they are not suited for use at the working site, and they can be rather time-consuming (Utsi et al., 2003). Therefore, it is important to find suitable workability test methods for continuous use outside the laboratory, and to calibrate them with rheological parameters. For the SCC, a number of empirical workability tests (slump flow test, V-Funnel, L-Box test, U-Box test, J-Ring, wet sieve stability and surface settlement tests) have been proposed and established in practice (Wu et al., 2009). Two aspects of SCC, the deformation capacity and deformation velocity, are evaluated by the workability tests. In this section, the workability tests which are recommended by the EN standard (EN 206-9:2010) are discussed, namely the slump flow test for flowing ability, L-box and J-Ring tests for passing ability, and visual examination and sieve stability tests for segregation resistance.

2.11.1 Flow-ability test

2.11.1.1 Slump flow test

The slump flow is a well-established test method. It is usually the test that accepts or rejects a mix at the working site (Utsi et al., 2003). The slump flow test, which is a modification of the traditional slump test, in which the spread of the material is measured instead of the height reduction, is the simplest and most commonly used test for evaluating the flow-ability of SCC (Pashias et al., 1996). The slump flow test evaluates the deformation capacity of SCC under its own weight without external forces against the friction of the base plate. As shown in Figure 2.12, the slump flow is the diameter of the concrete flowing over a level plate after a slump cone is lifted. The larger the slump flow spread, the greater the deformation capacity of the concrete provided that no segregation occurs. T_{500}, the time from lifting of the cone to the concrete spreading to a 500 mm diameter, is used to indicate the deformation rate. The higher the T_{500} value, the lower the deformation rate of the concrete. T_{500} varies from 2-7 seconds in the case of fresh SCC (Neophytou et al., 2010). However the T_{500} value can be

difficult to measure especially the small values for the very flow-able concrete (Carlsward et al., 2003).
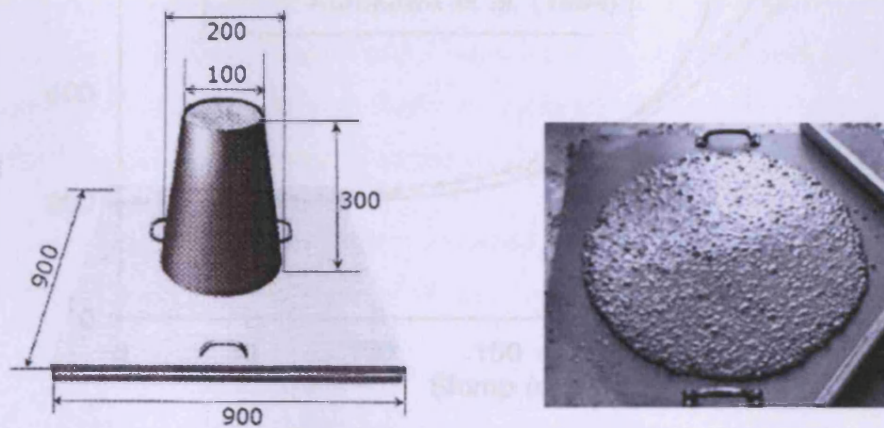
Figure 2.12: Apparatus for Slump Flow test (After David and Shah, 2004). All dimensions in mm

Segregation can be visually evaluated by observing the flowing process and the edge of the spread after the concrete stops. The occurrence of unevenly distributed coarse aggregate is considered as an indication of segregation, which demonstrates that the concrete segregates during the test and may segregate after placing. However the lack of segregation during the slump flow test cannot ensure that the mix is resistant to segregation. It is therefore insufficient to detect segregation by visual observation only.

The slump flow test in some respects is similar to the slump test performed on normal vibrated concrete except that no compaction is involved. Researchers have found a relationship between the slump and slump flow tests. However as shown in Figure 2.13, the best-fit relationship diverges at higher slumps.
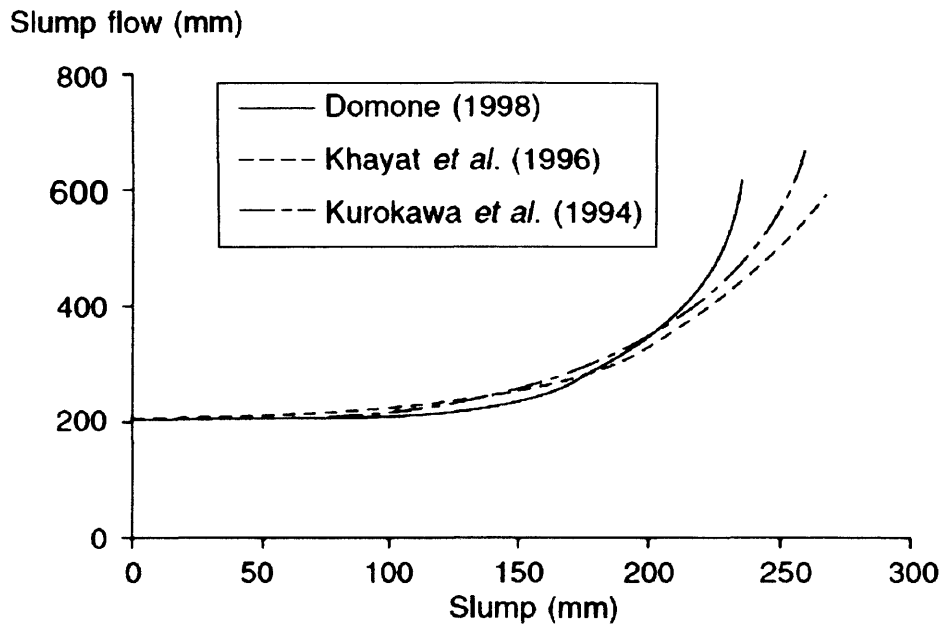
Figure 2.13: The relationship between slump and slump flow measurements (After Domone, 2003)

Bouzoubaa and Lachemi (2001) have reported that the slump flow is determined primarily by the superplasticiser dosage; the water to powder ratio and the fly ash replacement content have only a secondary effect. However, Sonebi (2004) showed that the water to binder (cement+ fly ash) ratio had the greatest effect on the slump flow for SCC incorporating fly ash.

2.11.1.2 Is there any relationship between rheological characteristics of self-compacting concrete and slump flow test measurements?

In the slump flow test, the concrete stops flowing when the shear stress of the sample becomes equal to or smaller than the yield stress. This confirms that the yield stress must be the dominant factor that governs the slump flow spread.

Several researchers have investigated the possibility that there exists a relationship between the rheological characteristics (yield stress and plastic viscosity) of a self-compacting concrete and measured parameters in the slump flow test (namely, the diameter of slump flow spread and T_{500}) (e.g. Thrane, 2007; Grunewald, 2004). The yield stress is defined as the critical shear stress required to initiate the deformation (flow), while the plastic viscosity

describes the resistance to flow once the yield stress is exceeded (more details of these two rheological parameters will be given in Chapter 3). In general, both the yield stress and the plastic viscosity increase with time, as the concrete hardens (de Castro and Liborio, 2006).

Roussel et al. (2005) found an analytical correlation between the slump flow spread and the yield stress of cement pastes. Roussel and Coussot (2005), and Roussel (2006) performed three-dimensional simulations of the flow of concrete in different slump tests. They concluded that slump flow depends only on the yield stress and the density of the SCC mix.

Grunewald (2004) obtained a correlation between the slump flow and yield stress for different mixes of self-compacting fibre reinforced concrete (Figure 2.14).

Yield value (Pa)
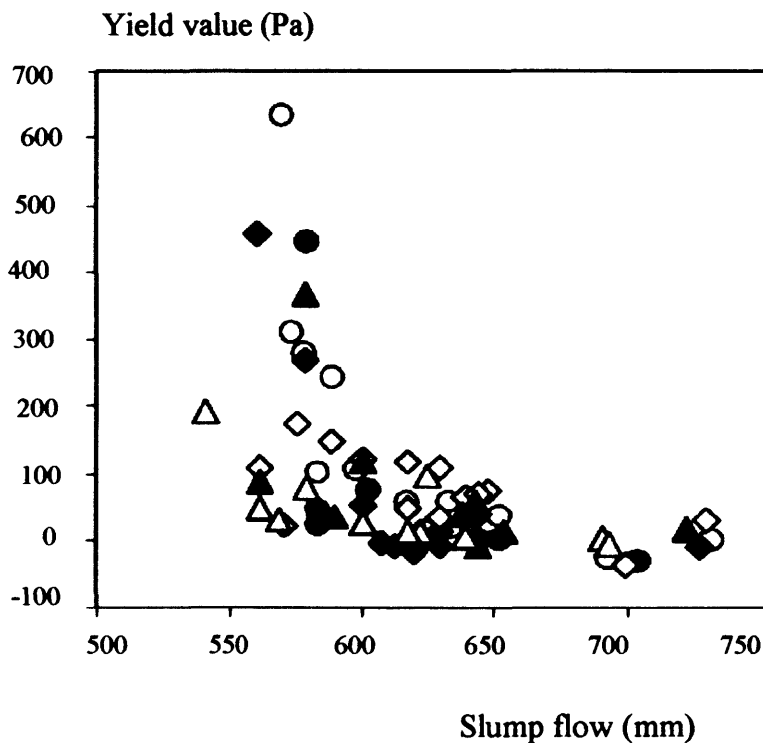
Slump flow (mm)

Figure 2.14: A typical relationship between slump flow diameter and yield stress for different mixes of self-compacting concrete (After Grunewald, 2004)

Carlsward et al. (2003) concluded that the slump flow is dependent on both the yield stress and the plastic viscosity of the mix.

Various concrete mixtures have been examined by Utsi et al., (2003) to find the possible relations between workability and rheology. The yield stress was found to be correlated to the

slump flow spread for stiff mixes (spread less than 600 mm) but not for mixes with flow spread in excess of this value.

However, Esping (2007) carried out a set of tests on SCCs and found that the slump flow spread is not a unique function of the yield stress, but rather a more complex function of both the yield stress and plastic viscosity. The results of Tregger et al., (2008) also suggest that the slump flow spread is a not unique function of the yield stress. Another study by Tregger et al., (2007) revealed that the plastic viscosity of SCC is linked to the time required for slump flow test to reach its final spread but no reliable correlations were found.

Roussel (2007a) showed that there is no correlation between the Bingham parameters (i.e. the yield stress and plastic viscosity) and the slump flow test and suggested alternate test methods.

Reinhardt and Wustholz (2006) concluded that the plastic viscosity also affected the slump flow but the influence can be negligible compared to that of the yield stress and concrete density. Moreover they have stated that other factors such as the surface tension can also affect the measurements and should not be ignored. T_{500} has a good correlation with the plastic viscosity ($R^2 > 0.70$) provided there is no segregation (Figure 2.15), but rather a poor correlation with the yield stress (R^2 below 0.4) (The EU guidelines for SCC).
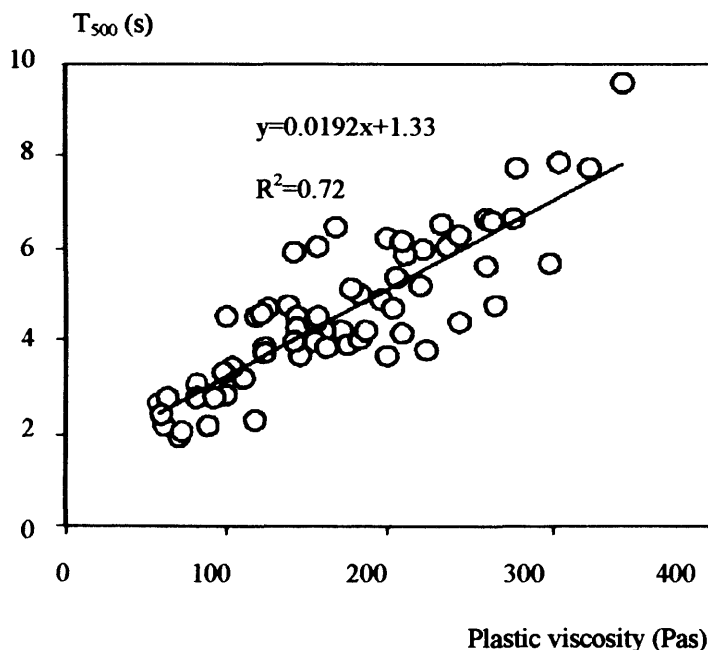
Figure 2.15: A typical relationship between flow time (T_{500}) and plastic viscosity of SCC (After Grunewald, 2004)

Utsi et al., (2003) also obtained a correlation between T_{500} and the plastic viscosity for their stiffer mixes with slump flows below 600mm.

Thrane (2007) has reported that Kurokawa et al. (1994) used the visco-plastic finite element method (VFEM; see Chapter 3) and obtained a relation between the T_{500} and the plastic viscosity.

From their experiments, Neophytou et al., (2010) conclude that T_{500} can only be used to estimate the plastic viscosity of a mixture with a constant yield stress, while the slump flow can be used to estimate the yield stress with constant plastic viscosity.

There have been many attempts to correlate the rheological parameters of SCC to empirical test data. However correlations of this type are highly dependent on the choice of materials and the devices for measuring the rheological parameters (i.e. different types of rheometers) and therefore it is not certain whether a relationship can be easily generalised.

From the above literature review, it can be concluded that the T_{500} time can be related to the plastic viscosity but that the slump flow spread is a function of both the yield stress and the density of SCC.

2.11.2 Passing ability tests

2.11.2.1 L-box test

The L-box test evaluates the passing ability of SCC in a confined space. The apparatus (Figure 2.16) consists of a long rectangular trough with a vertical column/hopper at one end. A gate is fitted to the base of the column allowing discharge of SCC into the horizontal trough. Adjacent to the gate is an arrangement of bars which permits assessment of the blocking potential to be made.
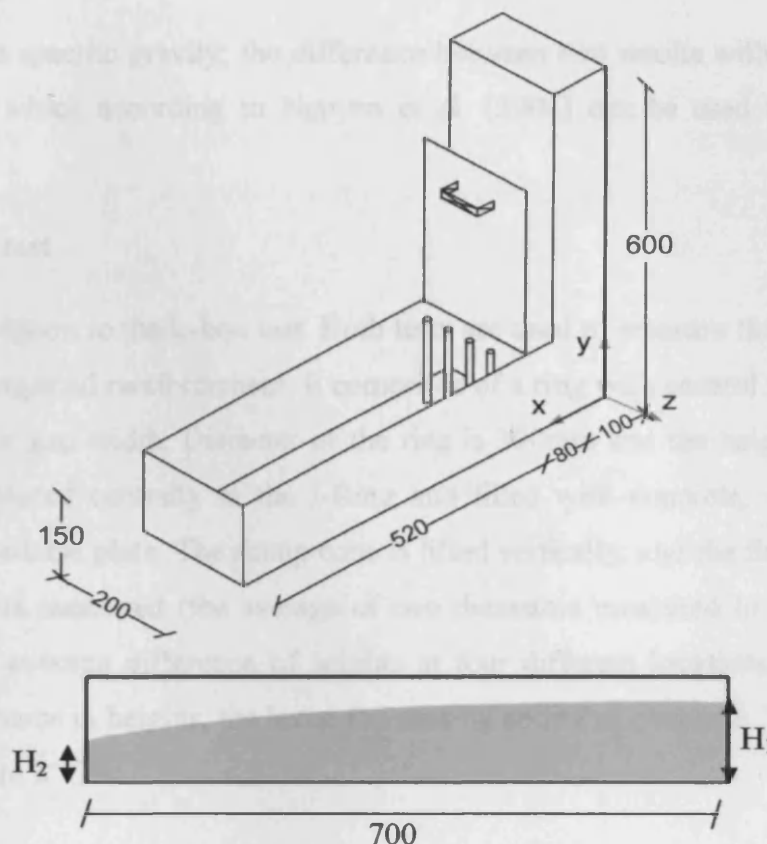
Figure 2.16: Schematic of L-box (top), (After Thrane, 2007), with heights at either end of horizontal trough (bottom). All dimensions in mm

The heights at either end of the horizontal trough (H_1 and H_2) can be measured to determine the levelling ability. The ratio of H_1 to H_2 is called the blocking ratio. If the SCC has perfect fresh properties, the blocking ratio is equal to 1. Conversely, the blocking ratio is equal to 0 if the concrete is too stiff or segregated.

An expression for the H_2/H_1 ratio can be obtained if the inertia is neglected and the gate in the L-box is lifted slowly (Thrane, 2007; Thrane et al., 2004).

Also the flow speed can be measured by the time taken to reach the distance of 200 mm (T_{200}) or 400 mm (T_{400}) from the gate. L-boxes of different sizes with different reinforcing bars and gaps were used by Bui et al. (2002), and Petersson (2003). Investigations have showed that the L-box was sensitive to blocking and that it was more difficult for concrete to pass three rather than two bars (Sedran and De Larrard, 1999). The test depends on the operator, for example, in regard to the lifting speed of the gate (Nguyen et al., 2006); if the gate was lifted slowly and there was no segregation, the final shape of the concrete was determined by the yield stress and there were correlations between blocking ratio to the ratio

of yield stress to specific gravity; the difference between two results with and without steel bars was small which according to Nguyen et al. (2006) can be used to detect dynamic segregation.

2.11.2.2 J-Ring test

This test is a variation to the L-box test. Both tests are used to measure the passing ability of SCC through congested reinforcement. It comprises of a ring with several reinforcement bars with an adaptable gap width. Diameter of the ring is 300mm and the height is 100mm. The slump cone is placed centrally in the J-Ring and filled with concrete, while pressing the slump cone to the base plate. The slump cone is lifted vertically, and the final diameter of the concrete spread is measured (the average of two diameters measured in two perpendicular directions). The average difference of heights at four different locations is calculated; the greater the difference in heights, the lesser the passing ability of concrete. The test equipment is shown in Figure 2.17.
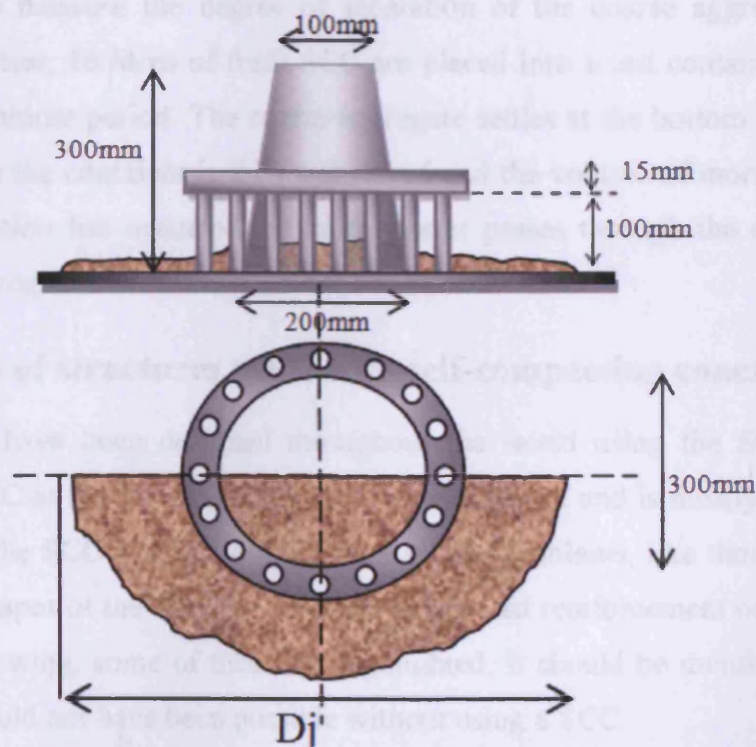
Figure 2.17: J-Ring apparatus

2.11.3 Segregation tests

Several empirical tests have been proposed to evaluate static segregation (i.e. at rest). However, no methods have yet been proposed for dynamic segregation (i.e. during flow).

2.11.3.1 Visual examination

The visual examination method (PCI-TR, 2003) is carried out by inspecting the periphery of the concrete after measuring the slump flow spread and rating it from 0 to 3. However it is an inadequate method because it relies on the experience of the performer and fails to evaluate segregation quantitatively.

2.11.3.2 Sieve stability test

The potential for static segregation can be evaluated by a simple sieve stability test, which measures the amount of grains passing through a 5 mm sieve after a standard period, which is called sieve segregation or segregation index. The GTM Stability Sieving test (Cussigh, 1999) is used to measure the degree of separation of the coarse aggregates and mortar fractions. In this test, 10 litres of fresh SCC are placed into a test container and allowed to settle over a 15 minute period. The coarse aggregate settles at the bottom and the upper part of the concrete in the container is then wet sieved and the volume of mortar calculated. The more the segregation has occurred the more mortar passes through the sieve, indicating a higher risk of segregation after the placement of SCC.

2.12 Examples of structures made with self-compacting concrete

Many structures have been designed throughout the world using the SCC. However the application of SCC at the building site is not yet widespread and is mostly limited to special structures. With the SCC it is possible to solve special problems, like those occurring in the case of special shapes of the concrete elements, congested reinforcement or casting in remote areas. In the following, some of these are highlighted. It should be mentioned that some of these projects would not have been possible without using a SCC.

Akashi-Kaikyo (Straits) Bridge (Figure 2.18): It is a suspension bridge with the longest span in the world (1,991 meters). The volume of the cast concrete in the two anchorages amounted to 290,000 m^3. The concrete was mixed at the batching plant beside the site, and was pumped out to the place. It was transported 200 meters through pipes to the casting site,

where the pipes were arranged in rows 3 to 5 meters apart. In the final analysis, the use of SCC shortened the construction period by 20% (Ouchi and Hibino-Nagaoka, 2000).

Figure 2.18: Akashi- Kaikyo (Straits) Bridge (After Ouchi and Hibino-Nagaoka, 2000)

Midsummer place in London (Figure 2.19): The structure contains elliptical columns (8.5m to 10m high) with a highly dense reinforcement. This project reduced the construction period and expenses by 40% and 10%, respectively in comparison with normal concrete.

Figure 2.19: Midsummer place in London (After Goodier, 2003)

Other examples are an immersed tunnel in Kobe Japan (Goodier, 2003), Bunkers Hill in Calgary, Canada (Nmai and Violetta, 1996), and Landmark tower in Minato Mirai in Yokohama ,Japan (Billberg, 1999).

2.13 Concluding remarks

The self-compacting concrete homogenously fills moulds of different shapes and geometry under its own weight, without any additional compaction energy. Building elements made of high strength concrete are usually densely reinforced. The small distance between reinforcing bars may lead to defects in concrete. If the high strength concrete is self-compacting, the production of densely reinforced building element from high strength concrete with high homogeneity would ease the task (Ma et al., 2003).

The use of SCC offers great opportunity for automated pre-cast production. Not only will it reduce the unhealthy tasks for workers, it can also reduce the technical costs of in situ cast concrete constructions, due to improved casting cycle, quality, durability, surface finish and reliability of concrete structures and eliminate some of the potential for human error (Esping, 2007).

However, the annual production of SCC indicates that challenges still need to be overcome. According to the European Ready Mixed Concrete Organization, SCC amounted for less than 1% of the ready mix concrete production in Europe in 2004 (ermco.org 2005).

This chapter gave a general overview of SCC and the basic principles involved in its design. Different mix designs of SCC were introduced, i.e. powder-type SCC, VMA-type SCC and combined-type SCC.

The influence of cement replacement materials on the characteristics of SCC was discussed with the emphasis on the fresh state of SCC. It was concluded that CRMs enhance self-compacting ability, fluidity, cohesiveness, segregation resistance and limit heat generation during hydration.

Tests to examine the workability of SCC, i.e. flowing ability, passing ability and segregation resistance of SCC were described, along with the possibility that relationships exist between the rheological characteristics (the yield stress and the plastic viscosity) of self-compacting concrete and parameters measured in these empirical tests (such as the diameter of slump flow and T_{500}). It was however observed that there is as yet no consensus on such relationships.

The effect of fibres on the SCC was reviewed. Fibres bridge cracks and retard their propagation. They contribute to an increase in the energy absorption compared with plain

concrete. The addition of fibres to SCC will lead to benefits in the fresh state and an improved performance in the hardened state, although the fibres greatly impair the workability of SCC because of their elongated shape and large surface area. In order to make the best use of the fibres, they need to be homogeneously distributed in the mix without clustering.

It was noted that the development of SCC has been closely related to the development of superplasticisers. The latter have a profound effect on the high level of workability of the SCC together with the good stability of the mix through liquefying and dispersing actions. Nowadays, the new generation of superplasticisers - the polycarboxylate ethers - give improved workability retention to the cementitious mix (Thrane, 2007). These superplasticisers disperse the cement by steric stabilisation, which is more powerful than the electrostatic repulsion of older types of plasticisers (Yamada et al., 2000, Flatt 2004a).

In the next Chapter, we shall review the rheology of SCC, and in particular introduce the Bingham model for describing its constitutive behaviour. We shall also review the computational techniques that are used to simulate the flow of SCC which is a non-Newtonian fluid.

Chapter 3

An Introduction to the Rheology of Self-Compacting Concrete and Methods of Simulating its Flow

3.1 Introduction

Over the past few decades, self-compacting concrete (SCC) technology has advanced in a similar manner to many other aspects of concrete technology. Workable SCC mixes at lower water to binder ratios have been achieved through the use of superplasticisers, thus increasing their compressive strength. The principles of rheology can be applied in the field of workability to explain the development and use of test methods which give a more complete understanding of the behaviour of the SCC. Several tools are available to address the workability of SCC. These tools can be classified into two main groups: empirical group e.g. tools that model the flow of SCC, and the second based on the measurement of concrete flow. Both sets of tools will be reviewed in this chapter. The field of fluid mechanics that studies the relation between the applied stress and the resulting deformation of a fluid is called by the Greek word Rheology. The rheology of cement paste, SCC and methods of measurement of their rheological characteristics will be briefly discussed. Different computational methods of simulation of the flow of SCC which are available in the literature will be reviewed and the equations used in the general flow simulation will be introduced.

3.2 Classification of workability

The workability of concrete can be studied at three levels as follows (Tattersall, 1991):

- Qualitative: studying the general behaviour of concrete without trying to quantify it, e.g. workability, flow-ability, pump-ability, etc.

- Quantitative empirical: dealing with a simple quantitative behaviour, e.g. slump flow test, L-box test, etc.

- Quantitative fundamental: studying the rheological characteristics, such as plastic viscosity, yield stress, fluidity, etc.

The first two classes have been dealt with in Chapter two. In the following, the third class will be examined in more detail.

3.3 Rheological characteristics of self-compacting concrete

The mixture of self-compacting concrete is strongly dependent on the composition and characteristics of its constituents in the fresh state. The properties of SCC in its fresh state have a great effect on its hardened state. Therefore it is critical to understand its flow behaviour in the fresh state. As the SCC is essentially defined in terms of its workability, the

characterisation and control of rheology is crucial for the successful production of this type of concrete. However the measuring techniques in its fresh state have not changed significantly in the last two decades. The slump flow has for a long time been considered to be a unique function of the yield stress of a Bingham fluid, without being influenced by its plastic viscosity (Wallevik, 2006). But, as we have seen in the previous Chapter, this is still an unresolved question. In fact, concretes with the same slump spread may flow differently and have different workability (Ferraris, 2000); this is because concrete flow cannot be described by a single parameter. For a normal concrete, researchers have found that the flow of concrete can be defined reasonably well by using the Bingham constitutive model. This constitutive model is a linear representation of the flow using two parameters, namely the shear stress (response of the considered concrete) against shear rate. This relationship involves two main parameters, i.e. the yield stress and the plastic viscosity.

3.4 Measuring the rheological parameters

The instruments that measure the relationship between the shear stress and strain rate are called rheometers or viscometers. To obtain the rheological characteristics of general viscous liquids (such as cement pastes) and solid-liquid suspensions (such as self-compacting concretes), a rheometer is to be used. Several types of this instrument have been proposed to evaluate the plastic viscosity and yield stress of cementitious materials. Empirical techniques have also been proposed. The most basic type is the cup method, where the time that it takes to empty a cup with a defined hole in the bottom gives a measure of the viscosity. Other types use a penetration rod, ball, etc., where a falling object with a defined density penetrates the sample. These types of kinematic viscometers are only appropriate for making comparative studies, as the shear rate is not fully controllable (Esping, 2007) and they are therefore excluded from this review.

3.4.1 Rheology of cement paste

For testing viscous liquids (such as cement pastes) in which the maximum particle size is about 100 μm, the rheometer used is the so-called coaxial cylinder rheometer. In this type of rheometer the annular gap between the inner and outer cylinders can be of the order of few millimetres. A BML rheometer is the most common type for measuring the rheological

properties of cement paste. As shown in Figure 3.1, the inner cylinder is rotated and the torque imposed on the stationary outer cylinder is measured; other rotating and measuring arrangements are possible.
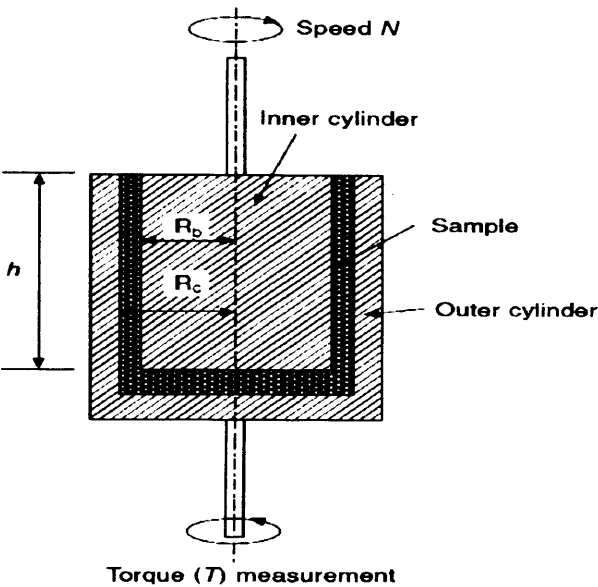
Figure 3.1: A coaxial cylinder rheometer (After Domone, 2003)

Let us consider the simplest mixture of cement and water; both the yield stress and plastic viscosity of this mixture reduce with increasing water content. Figure 3.2 shows a fan-shaped family of flow curves. As a result the extent of changes in both the yield stress and plastic viscosity are comparable.
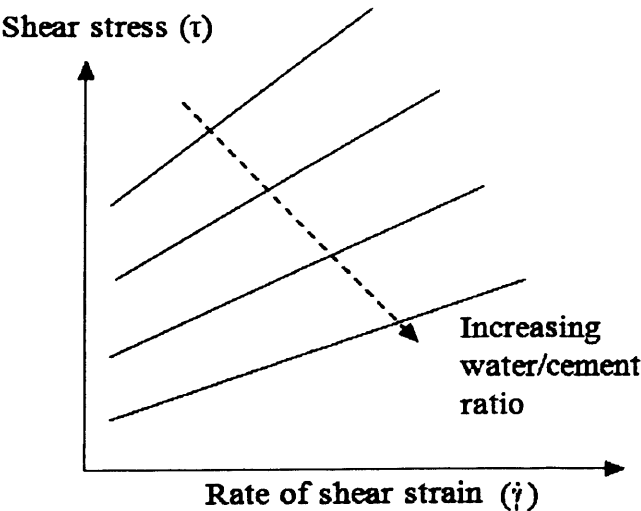
Figure 3.2: Fan-shaped curves for different water-cement ratio (After Domone, 2003)

Figure 3.3 shows a typical effect of water-cement ratio on the Bingham constants for cement paste which confirms that adding or subtracting water leads to similar changes in both properties.
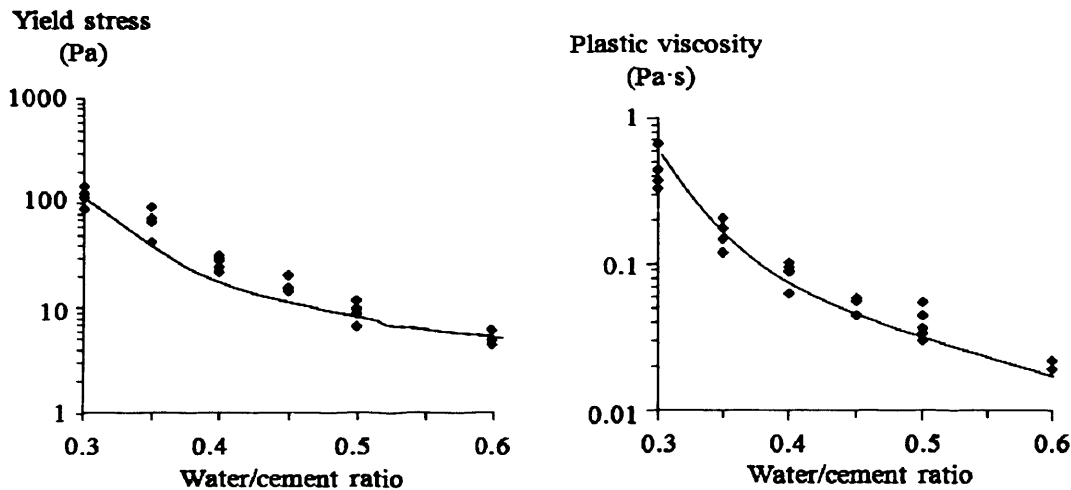
Figure 3.3: Typical effect of water-cement ratio on Bingham constants for cement paste (After Domone and Thurairatnam, 1988)

However when superplasticisers are added, the behaviour is somewhat different. Domone and Thurairatnam (1988) have used naphthalene formaldehyde superplasticisers in pastes with three different water-cement ratios. As shown in Figure 3.4, increasing the dosage of superplasticiser leads to a reduction in both the plastic viscosity and the yield stress, however the reduction in the plastic viscosity is much less than that in the yield stress.
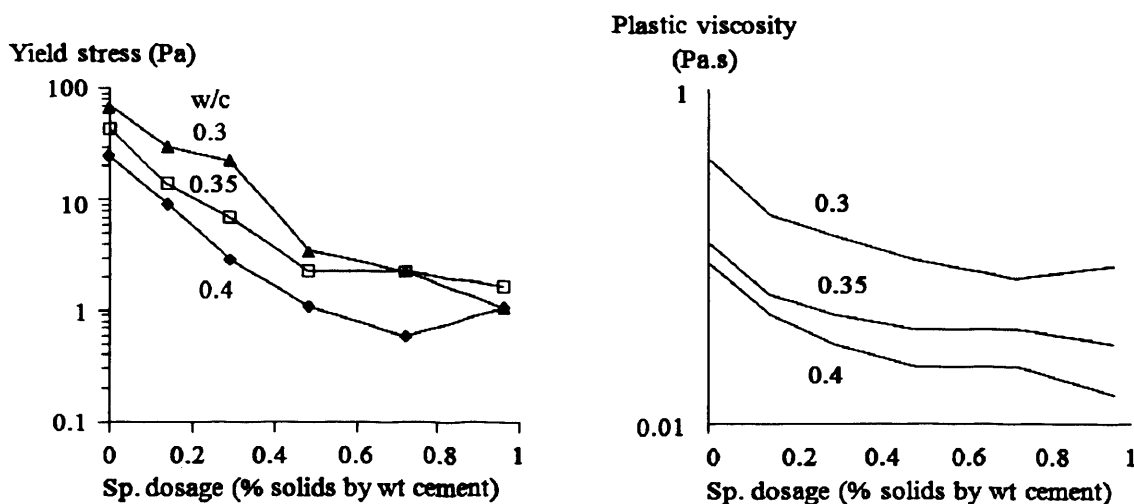
Figure 3.4: Typical effect of superplasticiser on Bingham constants for cement paste (After Domone and Thurairatnam, 1988).

Domone (2003) combined the data in Figures 3.3 and 3.4 into a single diagram, shown in
Figure 3.5.
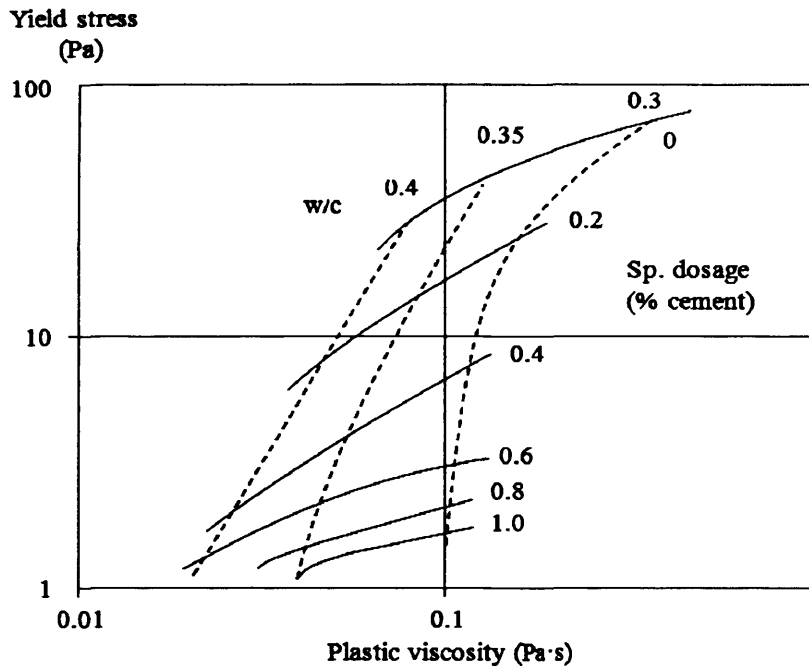
Figure 3.5: Yield stress vs. plastic viscosity for cement paste with different water-cement ratios
and superplasticiser dosage (After Domone, 2003)

3.4.2 Rheology of self-compacting concrete

A SCC mix has some special characteristics that should be considered when choosing a
rheometer. These are the size of aggregate (smaller than in conventional vibrated concrete),
time-dependence of flow properties, the presence of yield stress, moderate plastic viscosity,
the potential for segregation and the high sensitivity to small changes in materials and their
proportions. However it should be noted that at the present time not a single rheometer exists
that can take into account all of the characteristics of the SCC mentioned above. Normally
there are two main types of rheometer, namely those that impose a controlled shear rate on
SCC and measure its shear stress and those that do the opposite. A wide range of rheometers
is commercially available, as described below.

3.4.2.1 Coaxial cylinder rheometers

A coaxial cylinder rheometer consists of two cylinders with one cylinder rotating relative to
the other. In order to ensure a homogeneous test sample, the distance between outer and inner

cylinders must be much greater than the maximum aggregate size. Depending on the range of rotation speeds, the material rheological properties, and the ratio of outer to inner cylinder radii, a certain portion of the material in the annulus of a coaxial cylinder rheometer may be subjected to a stress below the yield stress. Figure 3.6 is a BML coaxial rheometer. It consists of concentric ribbed cylinders to prevent slippage at the cylinder surfaces.
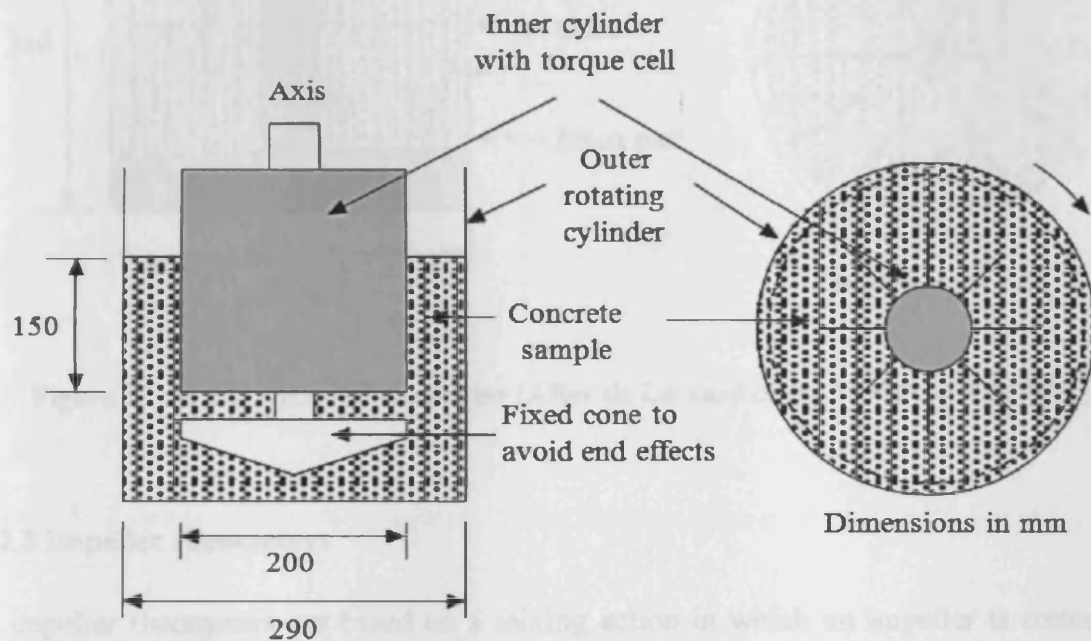
Figure 3.6: A BML rheometer (After Wallevik and Gjorv, 1990; RILEM, 2002)

3.4.2.2 Parallel plate rheometers

A parallel plate rheometer consists of two horizontal plates with one plate rotating relative to the other. This device permits testing a small sample and the direct analytical calculation of its rheological parameters in fundamental units. The complicated part is the calculation of rheological parameters related to the slippage that occurs at the vertical side walls.

A BT RHEOM rheometer is shown in Figure 3.7. A cylindrical sample of concrete is sheared between two circular parallel plates.
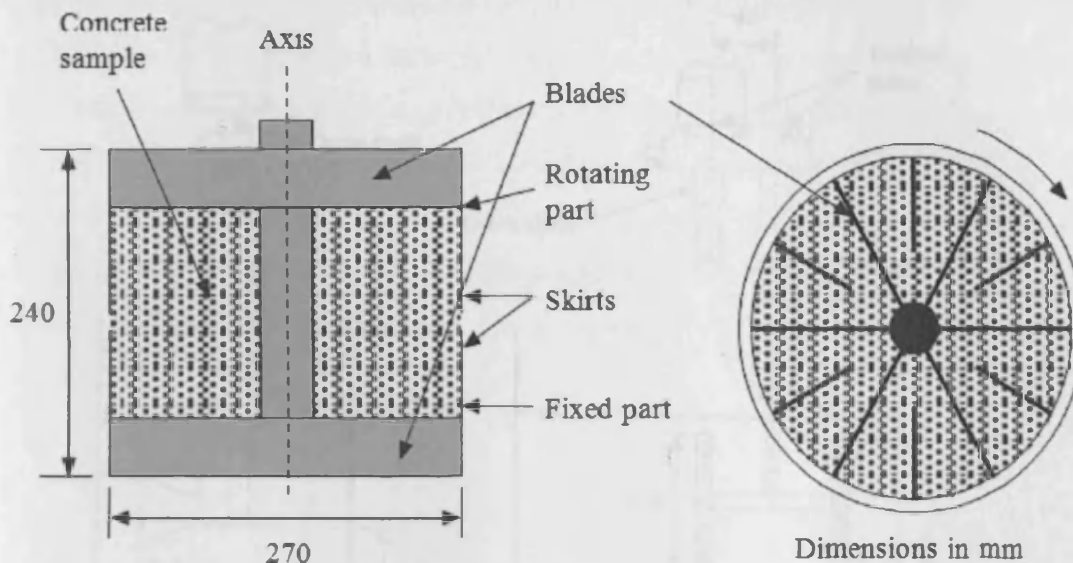
Figure 3.7: A BT RHEOM rheometer (After de Larrard et al., 1997; RILEM 2002)

3.4.2.3 Impeller rheometers

The impeller rheometers are based on a mixing action in which an impeller is rotated in a bowl of concrete. They are also known as the Tattersall rheometers (after their developer) or two-point workability testing equipment. These devices are simple to use; however, the shear rate and shear stress in the material around the impeller cannot be measured. Also the fundamental rheological parameters cannot be directly evaluated. Calibration procedures have been suggested to relate the torque versus rotation speed plot to the yield stress and plastic viscosity; however these procedures are still not universally accepted.

Figure 3.8 shows two alternative impeller types that can be found in the literature: the MH system (left) and the LM system (right) for medium to high and medium to low workability mixes, respectively.
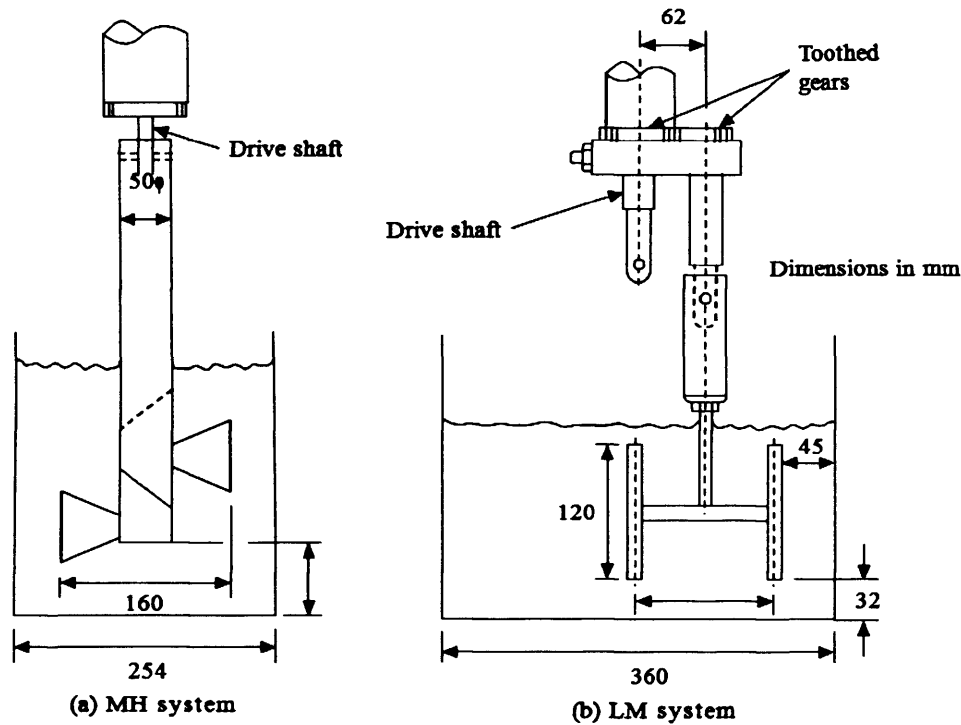
Figure 3.8: Two systems for the impeller rheometer (After Domone, et al., 1999; RILEM, 2002)

3.5 Mathematical description of self-compacting concrete rheology

All the above tests give a flow curve in the form of a relationship between the applied torque (T) and speed of rotation of the moving part (N). For most concrete mixes, a straight-line relationship of the form T=g+h.N fits the data well. Concrete and other cement-based materials, such as self-compacting concretes, are usually considered to be a Bingham fluid, i.e. their behaviour under shear depends on the shear stress and shear rate. Considering a Bingham model, g is the yield term and h the plastic viscosity term.

The relationships between g and the yield stress (τ_y) and between h and the plastic viscosity (η) depend on factors such as the rheometer size, the flow pattern and geometry, which are all obviously different for each rheometer. By assuming a laminar uniform flow, simple relationships have been proposed for the BML and BT RHEOM rheometers. However for the impeller rheometer, the analytical relationships are far more complex.

3.5.1 Is there any consistency in the rheological properties of concrete?

The yield stress and plastic viscosity are the fundamental properties of a Bingham fluid. Logically for a given concrete mix, any rheometer should give the same values of these two

fundamental parameters. But in practice that is not the case. As reported by Domone (2003), to quantify and to try to resolve these differences, a series of comparative tests was carried out in 2000, in which all three instruments were taken to the same laboratory and used simultaneously to test a series of fresh concrete mixes with a wide range of rheological characteristics (Banfill et al., 2001). The results confirmed that the instruments did indeed give differing values of the yield stress and plastic viscosity for the same mix. Figure 3.9 is an example of how two different rheometers gave totally different responses for one and the same mix.

Shear stress (Pa)
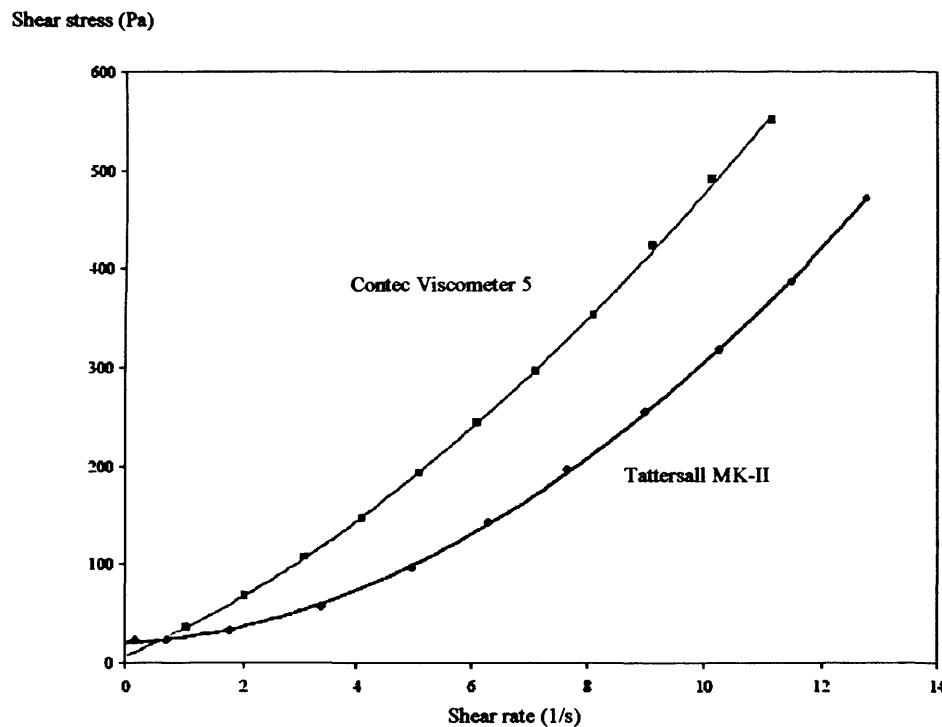
Figure 3.9: Two different responses for a single SCC mix tested by two rheometers (After Feys, 2007)

3.5.2 Effect of concrete constituents on the Bingham constants

The effect of the paste content, water, superplasticiser and cement replacement materials on the yield stress and plastic viscosity of a concrete mix are discussed here. Similar to what has been observed in the cement paste, the addition of water to a concrete mix decreases both its yield stress and the plastic viscosity. Superplasticisers normally reduce the yield stress but seem to have a different effect on the plastic viscosity. Solid-based superplasticisers like naphthalene-based, lead to an increase in the plastic viscosity, while the liquid-based

superplasticisers such as Gelenium ACE 333 have the opposite effect. Replacing some cement by Pulverized-Fuel Ash (PFA) or Ground Granulated Blast Furnace Slag (GGBS) reduces the yield stress, but leads to a decrease, and an increase, in the plastic viscosity, respectively. Also, using more paste increases the plastic viscosity but decreases the yield stress. All these effects are summarised in Figure 3.10.
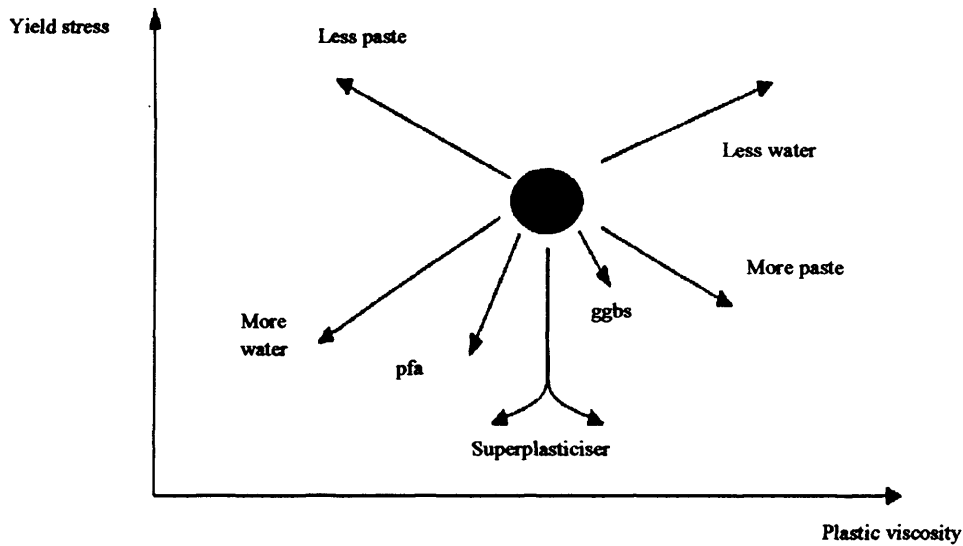
Figure 3.10: The effect of mix constituents on Bingham constants (After Domone, 2003)

As stated by Carlsward et al. (2003) regarding the influence of constituents on rheology, air and crushed aggregates primarily decrease and increase the plastic viscosity, respectively, while the addition of silica fume predominantly increases the yield stress. Addition of water also decreases both the yield stress and plastic viscosity (see Figure 3.11).
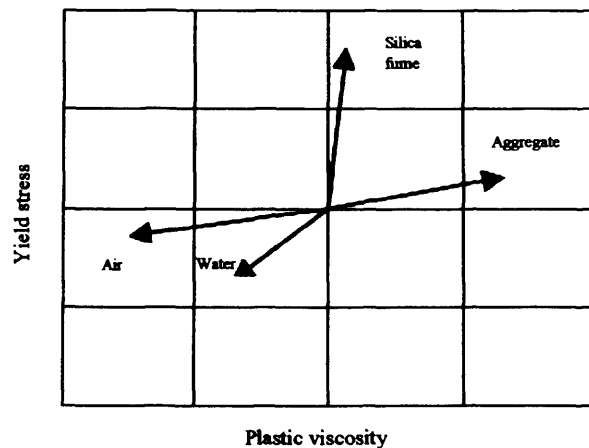
Figure 3.11: Effect of some constituents on the rheological characteristics of SCC (After Dietz and Ma, 2000)

All these effects, although typical, will not necessarily occur with all mixes, and the behaviour can vary according to the type and source of component materials (particularly admixtures) and the properties of the initial mix, i.e. the starting point in Figure 3.10.

Also, it is difficult to predict the interactive effects of two or more variables; an example of this is shown in Figure 3.12 for mixes containing varying cement and microsilica contents. Small amounts of microsilica reduce the plastic viscosity, with almost no effect on the yield stress; however, above a threshold level of microsilica, which depends on the cement content, there is a substantial increase in the yield stress, followed by an increase in the plastic viscosity.
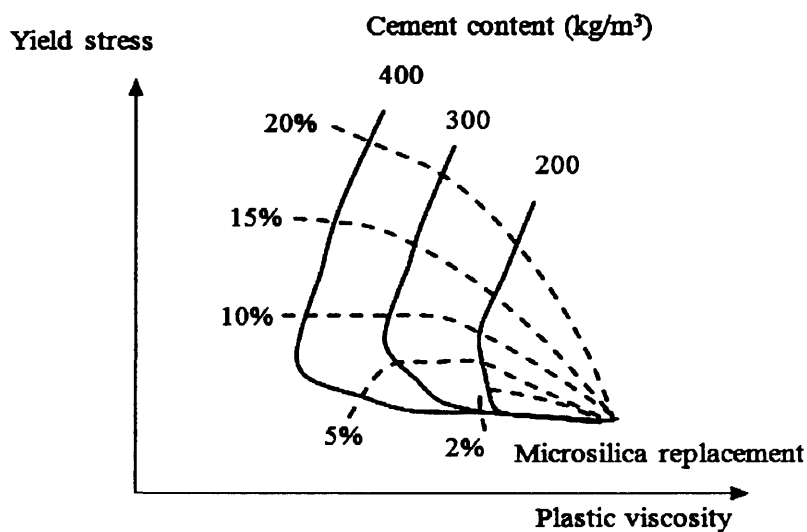
Figure 3.12: Bingham constants for mixes containing various amount of microsilica (After Gjorv, 1997)

3.6 Basic terms and equations used in the general flow simulation

Fluid dynamics uses the concept of fluid particles whose motion is described by Newton's second law of motion. In continuum mechanics, the mathematical relations are written in the form of conservation equations. The basic governing equations of motion for a fluid particle are the equations of mass, momentum, and energy conservation. However in the absence of heat flux in a continuum, the energy can be assumed to be identically conserved (see Section 3.7). In this Section we will derive the mass and momentum conservation equations in the Lagrangian frame of reference that employ the material derivative (a combination of local

and convective derivatives). Normally the derivations use either the finite control volume or an infinitesimal fluid element concept.

3.6.1 Finite control volume

Consider a finite region of a flow field shown in Figure 3.13. Let us assign a control volume V and a control surface S to this region. The control volume can be fixed in space and the flow pass through it or it may move with the flow in such a way that a constant number of fluid particles is always inside it. The fundamental physical principles are applied to the fluid inside the control volume to derive the equations in an integral form. The integral equations are then converted to partial differential equations. If the concept of a fixed control volume is used, the equations so obtained are called the conservation form of the governing equations, while the concept of a moving control volume gives the non-conservation form of the governing equations (Wendt, 1992).
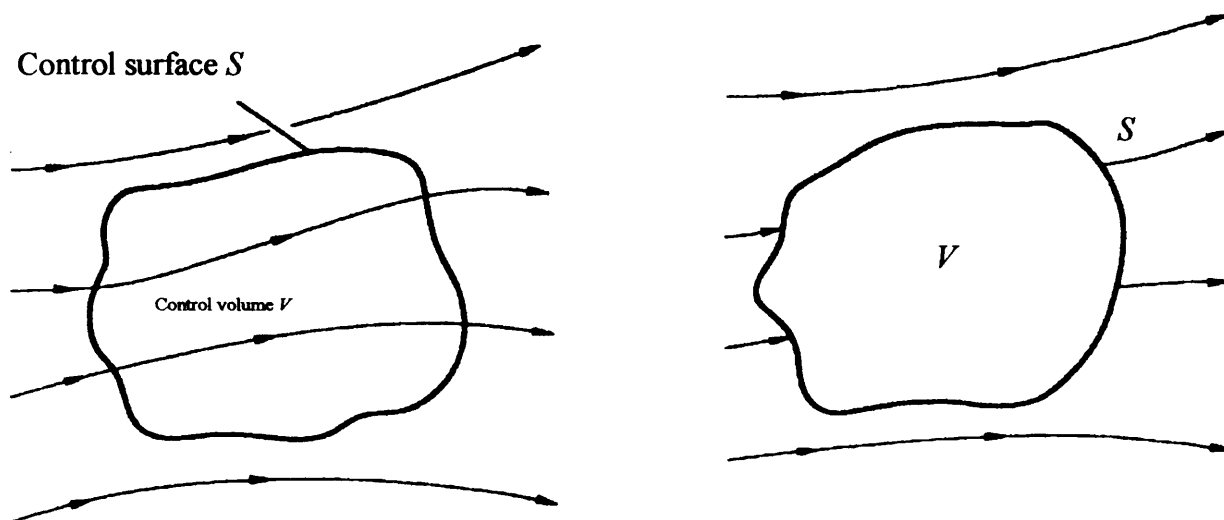
Figure 3.13: Finite control volume approach with fixed control volume (left) and moving control volume (right) (After Wendt, 1992)

3.6.2 Infinitesimal fluid element

Let us consider a general flow field shown in Figure 3.14. On the one hand, the fluid element should be small to be considered as a differential volume dV for the purpose of the modelling and on the other this volume has to be sufficiently large to contain a very large number of molecules in order to regard it as a continuous medium. Again the fluid element can be fixed in space and the flow pass through it or it may move with the flow in such a way that a constant number of fluid particles is always inside it. This approach gives the partial

differential equations directly. These equations are obtained based on the fixed or moving
fluid elements which yield the conservation and non-conservation forms of the equations,
respectively.
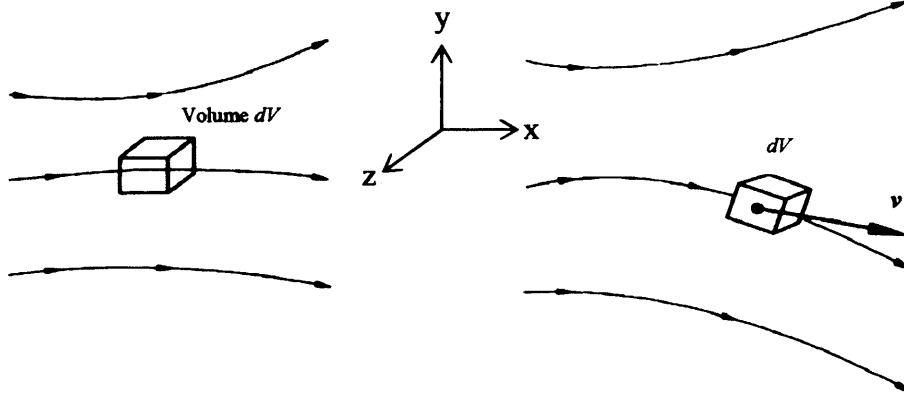
**Figure 3.14: Infinitesimal fluid element approach with fixed control element (left) and moving
control element (right)**

3.6.3 Material derivative

The substantial derivative or the total time derivative is an important physical concept in fluid
dynamics. Let us consider the infinitesimal fluid cell moving with the flow (right side of
Figure 3.14) at two time instants, t_1 and t_2. The scalar density field at time t_1 is given by;

$$\rho_1 = \rho(x_1, y_1, z_1, t_1) \tag{3.1}$$

At a later time, t_2 this field becomes:

$$\rho_2 = \rho(x_2, y_2, z_2, t_2) \tag{3.2}$$

The function (3.2) is expanded in a Taylor's series around the first point t_1 (Wendt, 1992) to
give

$$\rho_2 = \rho_1 + \left(\frac{\partial \rho}{\partial x}\right)_1 (x_2 - x_1) + \left(\frac{\partial \rho}{\partial y}\right)_1 (y_2 - y_1) + \left(\frac{\partial \rho}{\partial z}\right)_1 (z_2 - z_1)$$

$$+ \left(\frac{\partial \rho}{\partial t}\right)_1 (t_2 - t_1) + \text{(higher order terms)} \tag{3.3}$$

Dividing both sides of (3.3) by $(t_2 - t_1)$ gives

$$\frac{\rho_2 - \rho_1}{t_2 - t_1} = \left(\frac{\partial \rho}{\partial x}\right)_1 (\frac{x_2 - x_1}{t_2 - t_1}) +$$

$$\left(\frac{\partial \rho}{\partial y}\right)_1 (\frac{y_2 - y_1}{t_2 - t_1}) + \left(\frac{\partial \rho}{\partial z}\right)_1 (\frac{z_2 - z_1}{t_2 - t_1}) + \left(\frac{\partial \rho}{\partial t}\right)_1 \qquad (3.4)$$

The left hand side of (3.4) is physically the average time rate of change in density of the fluid element as it moves from point 1 to point 2. If t_2 approaches t_1, then

$$\lim_{t_2 \to t_1} \left(\frac{\rho_2 - \rho_1}{t_2 - t_1}\right) \equiv \frac{D\rho}{Dt} \qquad (3.5)$$

Examining (3.5), it can be realized that in a physical sense $\frac{D\rho}{Dt}$ is the time rate of change of the fluid element, i.e. the change of density as it moves through point one as opposed to $\left(\frac{\partial \rho}{\partial t}\right)_1$ which is the time rate of change of density at the fixed point 1. By taking the limit of the right hand side of (3.4) as t_2 approaches t_1, we have

$$\lim_{t_2 \to t_1} (\frac{x_2 - x_1}{t_2 - t_1}) \equiv v_x$$

$$\lim_{t_2 \to t_1} (\frac{y_2 - y_1}{t_2 - t_1}) \equiv v_y \qquad (3.6)$$

$$\lim_{t_2 \to t_1} (\frac{z_2 - z_1}{t_2 - t_1}) \equiv v_z$$

Therefore (3.4) becomes

$$\frac{D\rho}{Dt} \equiv v_x \frac{\partial \rho}{\partial x} + v_y \frac{\partial \rho}{\partial y} + v_z \frac{\partial \rho}{\partial z} + \frac{\partial \rho}{\partial t} \qquad (3.7)$$

By considering (3.7), a general expression can be obtained for a material derivative

$$\frac{D}{Dt} \equiv \frac{\partial}{\partial t} + v_x \frac{\partial}{\partial x} + v_y \frac{\partial}{\partial y} + v_z \frac{\partial}{\partial z} \qquad (3.8)$$

Denoting

$$\nabla \equiv \vec{i}\,\frac{\partial}{\partial x} + \vec{j}\,\frac{\partial}{\partial y} + \vec{k}\,\frac{\partial}{\partial z} \qquad\qquad (3.9)$$

(3.8) can be written as

$$\frac{D}{Dt} \equiv \frac{\partial}{\partial t} + (\mathbf{v}\cdot\nabla) \qquad\qquad (3.10)$$

$\mathbf{v}\cdot\nabla$ is called the convective derivative, which in physical terms defines the time rate of change as the fluid element moves from one location to another in the flow field. The substantial derivative can be used for any flow field variables, e.g. pressure.

3.6.4 Physical meaning of $\nabla \cdot \mathbf{v}$

The divergence of the velocity is a term that appears frequently when dealing with fluid dynamics problems. Consider a moving control volume in a flow field (right side of Figure 3.13); this control volume contains the same particles as it moves through the flow. As the control volume moves to a different location of the fluid, its volume V and control surface S will change because at its new position a different value of ρ might exist. The moving control volume with a constant mass is continuously changing its volume and shape depending on the characteristics of the flow. Consider an infinitesimal element moving at the local velocity $\mathbf{v}$, with surface dS and volume ΔV. Figure 3.15 shows the change in the volume of the control volume ΔV over a time increment Δt.
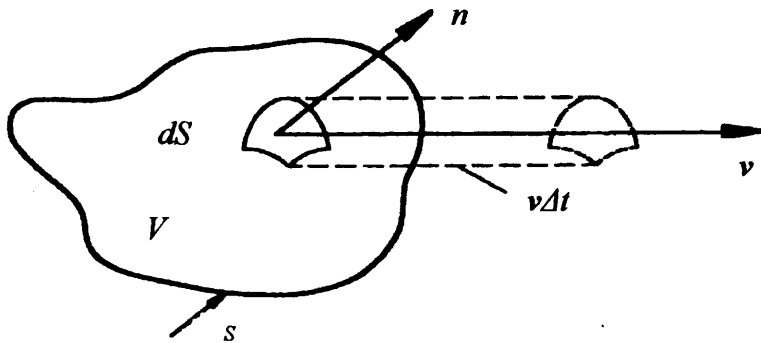
Figure 3.15: Physical meaning of the divergence of velocity (After Wendt, 1992)

From Figure 3.15, the change in volume is equal to the volume of the cylinder with base area dS and height $(\mathbf{v}\Delta t)\cdot\mathbf{n}$, where $\mathbf{n}$ is a unit vector perpendicular to the surface. This change in volume is equal to

$$\Delta V = [(\mathbf{v}\Delta t)\cdot\mathbf{n}]dS \tag{3.11}$$

The total volume change of the entire control volume is the integral over the control surface S

$$\Delta V = \int_S \mathbf{v}\Delta t \cdot \mathbf{n}dS \tag{3.12}$$

Dividing both sides of (3.12) by Δt and applying the divergence theorem yields

$$\frac{\Delta V}{\Delta t} = \int_V \nabla \cdot \mathbf{v}dV \tag{3.13}$$

where ∇ is the divergence operator (3.9).

Note that the left side of (3.13) is the material derivative of V, because this case is dealing with the time rate of change of the control volume as the volume moves with the flow.

If the control volume is shrunk to an infinitesimal fluid element with volume dV, (3.13) becomes

$$\frac{\Delta(\delta V)}{\Delta t} = (\nabla \cdot \mathbf{v})\int_V d(\delta V) = (\nabla \cdot \mathbf{v})\delta V \tag{3.14}$$

Finally, the velocity divergence is given by;

$$\nabla \cdot \mathbf{v} = \frac{1}{\delta V}\frac{D(\delta V)}{Dt} \tag{3.15}$$

The RHS of (3.15) explains physically the divergence of the velocity. It expresses the fact that $\nabla \cdot \mathbf{v}$ is the time rate of change of the volume of a moving fluid element per unit volume.

3.6.5 The continuity equation

Consider a moving fluid element with a fixed mass δm and volume δV then

$$\delta m = \rho\delta V \tag{3.16}$$

The continuity equation is based on the conservation of mass. It implies that the time rate of change of the mass of the fluid element is zero as the element moves along with the flow. Physically, this means that the substantial derivative of the infinitesimal mass is zero, i.e.

$$\frac{D(\delta m)}{Dt} = 0 \tag{3.17}$$

The substantial derivative of (3.17) reads

$$\frac{D(\delta m)}{Dt} = \frac{D(\rho \delta V)}{Dt} = \delta V \frac{D\rho}{Dt} + \rho \frac{D(\delta V)}{Dt} = 0 \tag{3.18}$$

Rearranging (3.18) gives

$$\frac{D\rho}{Dt} + \rho \frac{1}{\delta V} \frac{D(\delta V)}{Dt} = 0 \tag{3.19}$$

The second term in (3.19) is the divergence of the velocity (see (3.15)). Therefore

$$\frac{D\rho}{Dt} + \rho \nabla \cdot \mathbf{v} = 0 \tag{3.20}$$

(3.20) is the continuity equation or the mass conservation equation in the Lagrangian form.

3.6.6 The momentum equations

The momentum equations are based on the conservation of momentum. The physical principle here is Newton's second law, i.e. the total force on a fluid element equals to its mass times the acceleration of the considered fluid element. Let us consider a moving fluid element as shown in Figure 3.14. The fluid element with the components of the force in the x direction is shown in more detail in Figure 3.16.
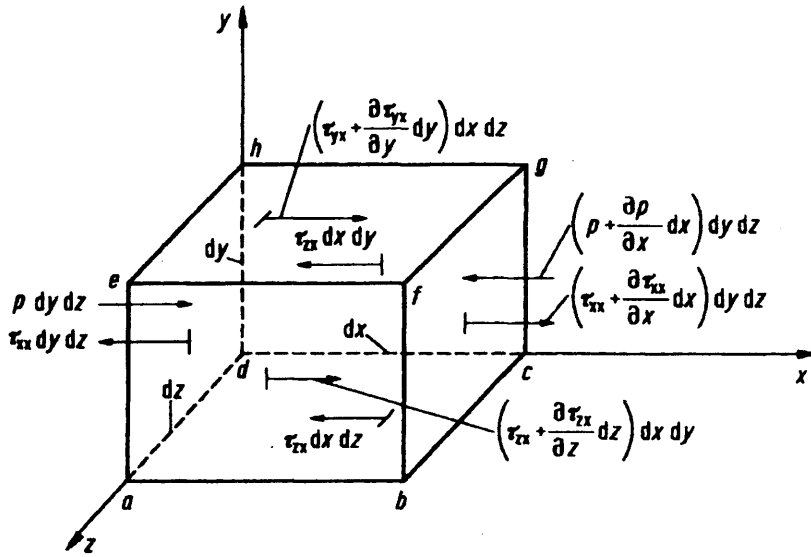
Figure 3.16: A fluid element with components of the force in the x direction (After Wendt, 1992)

The acceleration of the fluid element is $\dfrac{Dv_x}{Dt}, \dfrac{Dv_y}{Dt}$ and $\dfrac{Dv_z}{Dt}$, in x, y and z directions respectively; where v_x, v_y and v_z are the components of the velocity in the same directions.

The net force acting on this element follows from two sources: the body force and the surface force.

- Body forces act directly on the volumetric mass of the fluid; examples of this kind of force are the gravitational, electric and magnetic forces;

- Surface forces act on the surface of the fluid element and are divided into two sub-categories, i.e. the pressure imposed by the outside fluid surrounding the fluid element, and the shear and normal stress distributions related to the time rate of change of the deformation of the element which result in a shear deformation and volume change, respectively.

The face *dhgc* may be called as the negative face of *x* and the face *aefb* as the positive face of *x* since the x value for face *dhgc* is less than that for the face *aefb*. Similarly, the face *abcd* is the negative face of y and *ehgf* is positive face of *y*. Negative and positive faces of z are *hgcd* and *efab*. Note that the stress on the positive face is equal to the stress on the negative face plus the rate of change of that stress multiplied by the distance between the faces. The

convention will be used here that a stress is positive when it is on the positive face in the positive direction or on the negative face in the negative direction. Also, the shear stress τ_{ij} denotes a stress in the j-direction exerted on a plane perpendicular to the i-axis.

Both the shear and normal stresses depend on the velocity gradients in the flow. In most viscous flows, the normal stresses (e.g. τ_{xx}) are much smaller than the shear stresses and are neglected; however when the normal velocity gradients (e.g. $\partial v_y / \partial x$) are very large, the normal stresses have to be taken into account (such as inside a shock wave).

With the above in mind, in the x direction, all the forces acting on the infinitesimal fluid element are:

$$-[(P + \frac{\partial P}{\partial x}dx) - P]dydz + [(\tau_{xx} + \frac{\partial \tau_{xx}}{\partial x}dx) - \tau_{xx}]dydz +$$

$$[(\tau_{yx} + \frac{\partial \tau_{yx}}{\partial y}dy) - \tau_{yx}]dxdz + [(\tau_{zx} + \frac{\partial \tau_{zx}}{\partial z}dz) - \tau_{zx}]dxdy \qquad (3.21)$$

$$= -\frac{\partial P}{\partial x}dxdydz + \frac{\partial \tau_{xx}}{\partial x}dxdydz + \frac{\partial \tau_{yx}}{\partial y}dxdydz + \frac{\partial \tau_{zx}}{\partial z}dxdydz$$

where P is the pressure from the surrounding fluid.

If the body force in the x direction is F_x, then according to Newton's second law;

$$m\frac{dv_x}{dt} = \rho dxdydz\frac{dv_x}{dt} = -\frac{\partial P}{\partial x}dxdydz +$$

$$\frac{\partial \tau_{xx}}{\partial x}dxdydz + \frac{\partial \tau_{yx}}{\partial y}dxdydz + \frac{\partial \tau_{zx}}{\partial z}dxdydz +$$

$$F_x(\rho dxdydz)$$

(3.22)

And hence the momentum equation in the x direction is given by

$$\rho\frac{Dv_x}{Dt} = -\frac{\partial P}{\partial x} + \frac{\partial \tau_{xx}}{\partial x} + \frac{\partial \tau_{yx}}{\partial y} + \frac{\partial \tau_{zx}}{\partial z} + \rho F_x \qquad (3.23)$$

Similarly, the y and z components can be obtained as

$$\rho\frac{Dv_y}{Dt} = -\frac{\partial P}{\partial y} + \frac{\partial \tau_{xy}}{\partial x} + \frac{\partial \tau_{yy}}{\partial y} + \frac{\partial \tau_{zy}}{\partial z} + \rho F_y \qquad (3.24)$$

$$\rho\frac{Dv_z}{Dt} = -\frac{\partial P}{\partial z} + \frac{\partial \tau_{xz}}{\partial x} + \frac{\partial \tau_{yz}}{\partial y} + \frac{\partial \tau_{zz}}{\partial z} + \rho F_z \qquad (3.25)$$

Equations (3.23) to (3.25) are called the Navier-Stokes equations in honour of M. Navier and G. Stokes, who obtained the equations independently in the first half of the nineteenth century.

If only the gravitational force on a particle is considered, the momentum equations (3.23) to (3.25) may be written in a compact form as

$$\frac{D\mathbf{v}}{Dt} = \frac{1}{\rho}\frac{\partial \sigma_{ij}}{\partial x_j} + \mathbf{g} \tag{3.26}$$

Note that, in (3.26) the first term in the right hand side is the total stress tensor, which is made up of two parts: the isotropic pressure P and the viscous stress τ as

$$\sigma_{ij} = -P\delta_{ij} + \tau_{ij} \tag{3.27}$$

Therefore, in summary the momentum conservation equations become

$$\frac{D\mathbf{v}}{Dt} = -\frac{1}{\rho}\nabla P + \frac{1}{\rho}\nabla.\tau + \mathbf{g} \tag{3.28}$$

3.7 Disregarding energy conservation equations

In the case of an incompressible flow ($\nabla.\mathbf{v} = 0$), $i{=}CT$, where i is the sum of internal energy and C is the specific heat. Therefore the energy conservation equations reduce to temperature equations. In these equations if the differences between the surface and free stream temperatures are small so that the fluid properties such as its density and viscosity in the conservation equations are not affected by temperature, the conservation equations for energy can be ignored.

3.8 Fluid classifications

Fluids may be classified in two different ways according to their response to (i) shear rate, in which case they are called Newtonian or non-Newtonian, and (ii) pressure, in which case they are called compressible or incompressible.

3.8.1 Newtonian and Non-Newtonian fluids

Consider a simple shear flow as shown in Figure 3.17. The fluid is held between two parallel plates separated by a distance Δy and a force F is applied to the top plate.
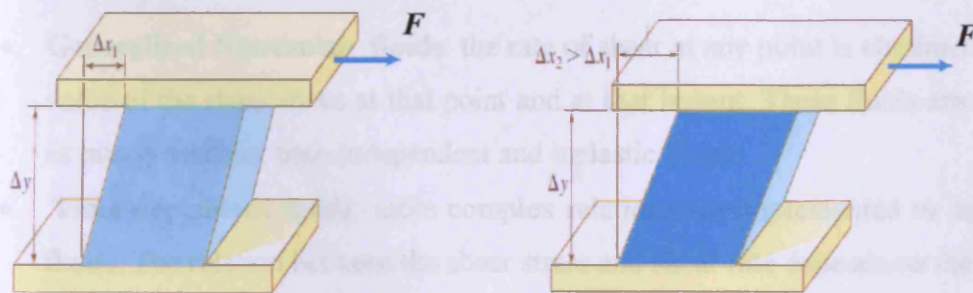
Figure 3.17: Fluid sample as tested by a parallel plate device at two time instant, t_1 (left) and $t_2 > t_1$ (right)

As a result of the force F, the lower plate moves at a constant velocity v_1 and upper plate moves at a constant velocity $v_1 + dv_1$. Assuming no-slip condition at the solid boundary, the velocity of the fluid particles close to each plate is the same as the plate velocity. The remaining fluid particles move with an intermediate velocity between v_1 and $v_1 + dv_1$. It can be assumed that there is a linear velocity distribution in the gap between the plates as shown in Figure 3.18.
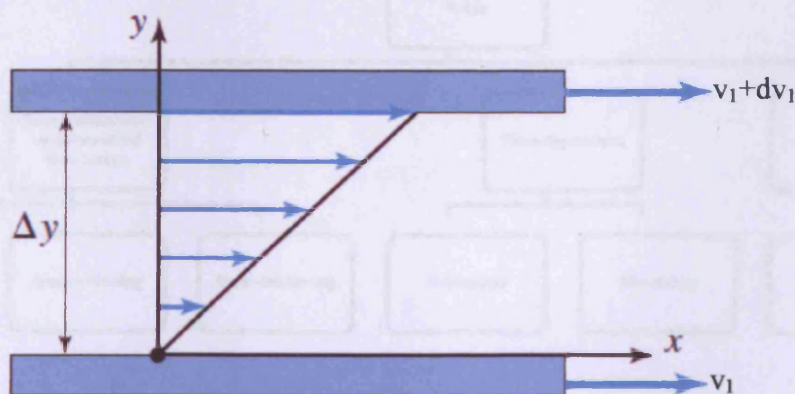
Figure 3.18: The fluid velocity profile varies linearly

For this simple case, the force is constant and is proportional to the velocity gradient, $\dot{\gamma}$. Therefore

$$F / A = \tau_{yx} = \eta \dot{\gamma}_{yx} \qquad (3.29)$$

The first subscript represents the direction normal to the shearing surface, while the second subscript indicates the direction of the force (or flow).

If the ratio $\tau / \dot{\gamma}$ is constant, the fluid is Newtonian, otherwise it is non-Newtonian. The non-Newtonian fluids can be grouped into three categories as follows:

- **Generalized Newtonian fluids**: the rate of shear at any point is obtained only by the value of the shear stress at that point and at that instant. These fluids are also known as purely viscous, time-independent and inelastic fluids.

- **Time-dependent fluids**: more complex relations are implemented to describe such fluids. The relation between the shear stress and shear rate depends on the duration of shearing and their kinematic history.

- **Visco-elastic fluids**: demonstrate properties of both ideal fluids and elastic solids. These fluids show partial elastic recovery after deformation.

These categories of fluids may be further subdivided, as shown in Figure 3.19.
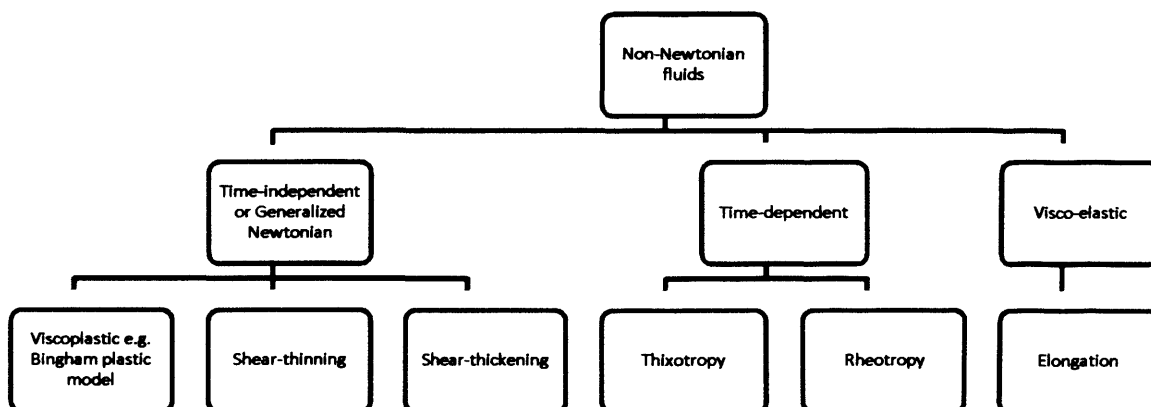
Figure 3.19: Subdivision of non-Newtonian fluids

The most common type of flow behaviour observed is generalized Newtonian or time-independent non-Newtonian. Figure 3.20 shows sets of qualitative flow curves on linear scales for the above three types of non-Newtonian fluid behaviour.
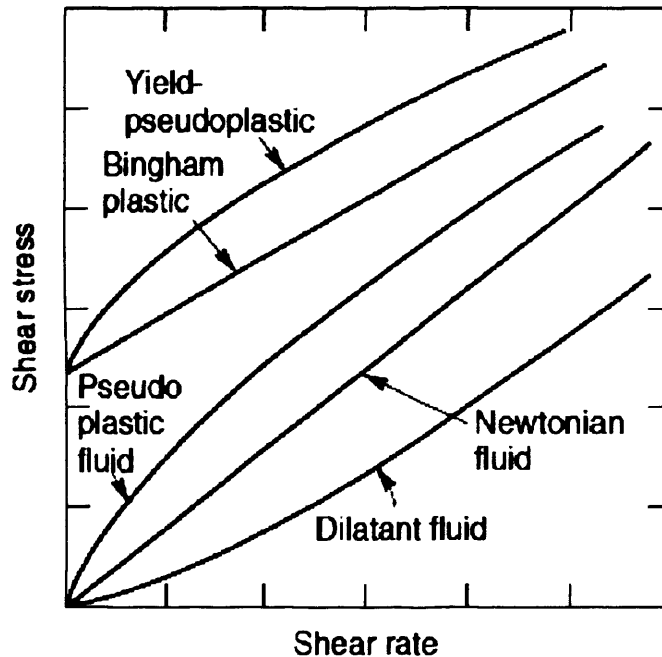
Figure 3.20: Types of generalized non-Newtonian flow behaviour (After Chhabra and Richardson, 2008)

Among these three, the most common type of flow behaviour is the visco-plastic one, characterized by the existence of a yield stress (τ_y) which must be exceeded in order for a fluid to flow.

The viscosity of a fluid can be a decreasing or an increasing function of $\dot{\gamma}$; such fluids are called shear thinning and shear thickening, respectively. Figure 3.21 shows these behaviours in relation to Bingham and Newtonian fluids.
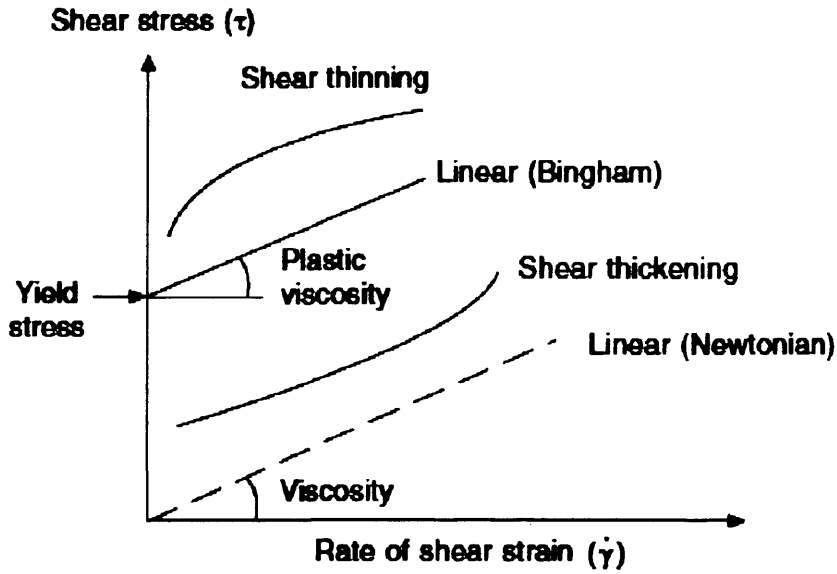
Figure 3.21: Behaviour of shear thinning and shear thickening fluids in relation to viscoplastic fluids behaviour (After Domone, 2003)

Once the shear stress reaches this yield value, the flow curve (shear stress vs. shear rate) may be linear or non-linear which do not pass through the origin. Over the years, some empirical equations have been proposed. The three commonly used models are described below.

3.8.1.1 Bingham plastic model

The Bingham plastic model or simply the Bingham model is the simplest relation to show the behaviour of a fluid having a yield stress τ_y. It is written as

$$\begin{aligned} \tau &= \tau_y + \eta\dot{\gamma} & \tau > \tau_y \\ \dot{\gamma} &= 0 & \tau < \tau_y \end{aligned} \qquad (3.30)$$

3.8.1.2 Herschel-Bulkley model

This model is a generalization of the Bingham model in such a way that, upon deformation, the viscosity can be shear thinning or shear thickening (see Figure 3.21). The constitutive equation is

$$\begin{aligned} \tau &= \tau_y + m\dot{\gamma}^n & \tau > \tau_y \\ \dot{\gamma} &= 0 & \tau < \tau_y \end{aligned} \qquad (3.31)$$

For $n<1$, the fluid exhibits shear thinning properties

$n=1$, the fluid shows Bingham behaviour

$n>1$, the fluid shows shear thickening behaviour

In equation (3.31), m and n are two empirical curve-fitting parameters and are known as the fluid consistency coefficient and the flow behaviour index, respectively. For a shear thinning fluid, the index may have any value between 0 and 1. The smaller the value of n, the greater is the degree of shear thinning. For a shear thickening fluid, the index n will be greater than unity.

3.8.2 Compressible and incompressible fluids

As previously mentioned, one can divide the flows based on their response to an external pressure. Physically, a fluid which is not reduced in volume by an increase in pressure is called an incompressible fluid, whereas the opposite is true for a compressible fluid. In an incompressible flow the ratio of the material speed to the speed of sound in the fluid is very low (normally around 0.1); this ratio is called the Mach number. In computational fluid dynamics this classification is of prime importance in order to solve the conservation equations (see Sections 3.6.5 and 3.6.6 above). A problem that occurs in solving the conservation equations is introduced by the pressure term, which only appears in the momentum conservation equations (3.28) and needs to be coupled with the velocity field in the mass conservation equations (3.20). In compressible flows, this problem can be solved by adopting a suitable equation of state $P = P(\rho,T)$ which gives the pressure based on density and temperature; this means that the continuity equations are used as a transport for density. However, if the flow is incompressible, the density is constant and by definition has no link to pressure. The main aim in solving an incompressible fluid flow problem is to apply the correct pressure field in the momentum equations in order to have a continuous velocity field, i.e. divergence free velocity ($\nabla \cdot \mathbf{v} = 0$). As we shall be solving an incompressible flow problem later in Chapter 6, we shall review briefly how the pressure-velocity linkage is affected through either the concept of artificial compressibility or the pressure-Poisson (projection or pressure correction) equation.

3.8.2.1 Artificial compressibility

As stated before, the main difficulty with the solution of the incompressible fluid flow equations is due to the decoupling of the mass and momentum conservation equations due to the absence of the pressure (or density) term from the continuity (or mass conservation) equations. Chorin (1968) proposed an approach to overcome this problem. He introduced an

artificial compressibility term into the continuity equations. In the absence of external forces and the deviatoric part in the momentum conservation equations, using this method the conservation equations become

$$\frac{1}{\beta}\frac{DP}{Dt} + \nabla.\mathbf{v} = 0$$

$$\frac{D\mathbf{v}}{Dt} = -\frac{1}{\rho}\nabla P$$

(3.32)

β is a factor which enables the conservation equations to have a divergence free solution, i.e. to satisfy the incompressibility requirement. The artificial compressibility gives sets of equations which are hyperbolic and hyperbolic-parabolic and whose solution is often less computationally expensive than that of elliptic equations (used in the pressure-Poisson method; see below).

3.8.2.2 Pressure-Poisson equation

The basic idea of this method is to formulate a Poisson's equation for the pressure correction. The pressure and velocity fields are updated until they reach a divergence free state. Taking the divergence of the momentum conservation equations in the absence of a deviatoric stress gives

$$\nabla^2 P = -\rho\nabla.(\nabla\mathbf{v})$$

(3.33)

In order to use the pressure-Poisson's equation, a projection formulation introduced by Chorin (1968) is implemented in such a way that the pressure field is applied to enforce a divergence-free velocity. The basic idea of projection method is to introduce a vector field (here velocity or velocity gradient), $\mathbf{v} = (v^x, v^y, v^z)$ neglecting the divergence of the velocity field, and then to recover the incompressible nature of the flow through projection. The operation is

$$\mathbf{v}^d = P(\mathbf{v})$$

(3.34)

where $\mathbf{v}^d$ is a desired solenoidal vector field i.e. $\nabla.\mathbf{v} = 0$.

The projection methods in turn are divided into exact and approximate projections. In the exact projection, the discrete divergence of a vector field is intended to be identically zero after applying the projection to a vector field. In the approximate projection, the discrete

divergence is a function of the truncated error of the scheme. In Chapter 6, we shall be using the pressure-Poisson equation in order to impose exactly the incompressibility requirement.

3.9 Simulation of the flow of concrete

This section briefly provides a general overview of the present computational strategies available in the literature to model the flow of fresh concrete. From the modelling point of view, the fresh concrete can be considered as a fluid when a particular degree of flow-ability is achieved, e.g. the slump is at least 100 mm (Ferraris et al., 2001a) and when the concrete is homogeneous. Due to its extreme flow-ability, the SCC in general satisfies the flow and cohesiveness requirements and can thus be modelled as a Bingham fluid (Vasilic et al., 2010). In most numerical simulations, only the steady-state of the flow is considered, i.e. thixotropy is not taken into account. Therefore the loss of workability of concrete during the flow is not modelled. However, sometimes the viscosity increases with the shear rate which means the SCCs exhibit a shear thickening behaviour (e.g. in mixing and pumping). This behaviour can be modelled by a generalization of the Bingham model, the so-called Herschel-Bulkley model (see equation (3.31)).

Computational modelling of flow could be used in three main ways; first, for the simulation of mould filling behaviour; second, a potential tool for understanding the rheological behaviour of concrete; and third, a tool for mix proportioning. The numerical simulation of the SCC flow could allow us to determine the minimum workability of the fresh concrete that would ensure the proper filling of a given mould.

The computational modelling techniques based on the finite element method (FEM) are used to deal with the concrete particles. In the literature, these mesh-based FEM modelling techniques may be divided into two main families: homogeneous fluid simulation and non-homogeneous fluid simulation. An alternative to modelling the concrete particles is to use methods which are based on the mesh-less methodology, such as the smooth particle hydrodynamics (SPH) method.

3.9.1 FEM modelling techniques

3.9.1.1 Homogeneous fluid simulation

The homogenous fluid approach has mostly been used to model the flow of fresh concrete. It refers to the simulation of ideal fluids without particle inclusions and is included in the overall framework of computational fluid dynamics (CFD) (Wendt, 1992). A numerical solution method is applied to obtain the flow characteristics by solving the governing equations of mass, momentum and energy conservation.

The important assumptions are that the segregation of the coarse particles during the flow (dynamic segregation) does not take place and that the blocking of concrete caused by particle interactions, e.g. by their interaction with the reinforcement bars, at any stage of flow is avoided. Also the smallest characteristic dimension of the flow (size of the mould or the spacing between the bars) must be large compared to the size of the largest particle (five times larger) (Spangenberg et al., 2010). Otherwise, other simulation methods must be used.

In this approach a single fluid characteristic is assigned during the flow, such as the yield stress and the plastic viscosity. The Bingham model is the most common model used. The discretization methods comprise the finite volume method, the finite element method, and the finite difference method (Wendt 1992). In the past researchers have mainly used two models to simulate the fluidity tests of fresh concrete, namely the visco-plastic finite element method (VFEM) (e.g. Mori and Tanigawa, 1992), and the visco-plastic divided element method (VDEM) (e.g. Kurokawa et al., 1996).

Both methods assume that concrete can be described as a homogeneous fluid with single rheological properties. As reported by Roussel et al. (2007), in the VFEM, the fresh concrete is divided into elements in which the deformation is calculated, and the flow is described by the displacement of the nodal points. In the VDEM, the domain is divided into elements and cells, which are either empty or full, and the flow is described by the displacement of virtual markers.

A few studies have been carried out on the process of casting cementitious materials using the homogeneous fluid approach. For the SCC, Thrane (2007) registered consistency between the experimental and simulated flow behaviour for the slump flow test, the L-box test, and

the form filling tests and found reasonable agreement between the rheological parameters determined in the viscometer and those applied to simulate the flow (Bakker et al., 2010).

Although these models provide the fastest way to simulate the flow of concrete, the main numerical difficulty in connection with these kinds of simulations is the free surface displacement because fresh concrete displaying a moving free boundary requires a clear definition of the boundary conditions. Also the homogeneous fluid approach does not simulate particle blocking or dynamic segregation; therefore additional tools are needed to assess under which flow conditions there is a risk of blocking and dynamic segregation (Thrane, 2007).

3.9.1.2 Non-homogeneous fluid simulation

The aim of this method is to carry out detailed studies of the movement, trajectory, rotation, and interaction of particles (Thrane, 2007). This type of simulation considers the difference in physical properties of liquid and granular components used in the concrete and their effect on the flow. Based on this analogy, the flow of concrete can be dominated by either a fluid-like or a solid-like behaviour. In the case of SCC, normally the coarse aggregate is limited therefore it is reasonable to assume that it behaves as a fluid suspension. For normal concrete, the solid-like behaviour might be dominant. In this category, the standard discrete element method (DEM) is mainly used. This method divides the calculations into two steps: obtaining the contact forces between the solids, and determining the motion of each solid using Newton's second law. Noor and Uomoto (1999) used a 3D DEM developed by Chu et al. (1996) to simulate the flow of SCC in slump flow test, L-box test and V-funnel test. They divided the material into mortar and coarse aggregate larger than 7.5mm. As stated by Roussel et al. (2007) the result of Noor and Uomoto (1999) gave the qualitative behaviour in fresh concrete. Martys (2005) used another method called the dissipative particle dynamics (DPD) method in the field of cementitious materials which allowed for much larger time steps, as opposed to DEM.

The advantages of implementing the non-homogeneous simulation are as follows: the ability to carry out detailed studies of the particle flow and thereby to simulate the heterogeneous flow phenomena (Thrane, 2007), the scale of observation could match the size of real materials that are dealt with, and, as opposed to an homogeneous simulation, the moving free

surface of the concrete can be more easily modelled. In summary, the non-homogeneous method aims at simulating both the macroscopic and local behaviour of granular materials and suspensions (Thrane, 2007). A limited number of studies has been performed on the form filling ability and flow patterns, but the relation between the simulations and experiments is not clear (Bakker et al., 2010). The main disadvantage of this method is related to the physical meaning, i.e. it is difficult to define physically a direct contact between solid particles that are representing the mortar phase and coarsest grains.

3.9.1.3 Disadvantages of mesh-based numerical simulations

Mesh-based numerical simulation suffers from some inherent difficulties in many aspects, which limit their application to concrete simulation. In mesh-based methods, the mesh generation for the problem domain is a condition for the numerical simulations.

In Eulerian mesh-based methods, such as the finite difference method (FDM), making grids (meshes) for complex or irregular geometry is a difficult task which usually involves additional complex mathematical transformation that could be even more expensive than solving the problem itself. Other difficulties in the fixed Eulerian grid are determining the precise locations of the inhomogeneities, free surfaces, etc.

In Lagrangian methods such as the finite element method (FEM), mesh generation is a prerequisite for the problem being modelled. The construction of mesh usually takes a significant portion of the computational effort. The treatment of large deformation is an important issue in a Lagrangian grid-based method. It usually requires special techniques like rezoning. Mesh rezoning, however, is a formidable and time consuming task which can lead to additional inaccuracy.

In the whole process of concrete simulation there exist special features such as large deformations, large inhomogeneities and free surfaces. These special features pose great challenges to numerical simulations using grid-based methods.

3.9.2 Mesh-less particle based simulation

Due to the Lagrangian nature of the SCC flow and due to the fact that an SCC mix is essentially an aggregate of particles of different sizes and shapes, the use of meshless particle-based Lagrangian numerical techniques to simulate such flows is both more appropriate and simpler than the traditional mesh-based methods (e.g. Petersson, 2003,

Dufour and Pijaudier-Cabot, 2005 and Roussel et al., 2007) reviewed above. An example of this category is the smooth particle hydrodynamics (SPH) method. The SPH is a mesh-less Lagrangian approach that offers considerable potential as a numerical method for modelling problems involving large deformations. Its simplicity and Lagrangian nature have been exploited in the past to model many free-surface fluid flows and related engineering problems (e.g. Kulasegaram et al., 2004, Cummins and Rudman, 1999 and Monaghan, 1992). The following section is devoted to a brief explanation of SPH method and its essential properties.

3.10 Introduction to smooth particle hydrodynamics (SPH)

The smooth particle hydrodynamics (SPH) was first introduced by Lucy (1977) and Gingold and Monaghan (1977) to solve astrophysical problems in three-dimensional open space. The SPH has been extensively studied and extended to fluid flow with large deformations (e.g. Bonet and Kulasegaram, 2000; Shao and Lo, 2003). Applications of the SPH method are very wide, ranging from computational fluid mechanics to computational solid mechanics, from micro-scale to macro-scale and to astronomical scale, and from discrete to continuum systems (Liu and Liu, 2003).

3.10.1 Key characteristics of SPH method

The SPH method has the following key characteristics:

1. **Mesh free**: The problem and boundary domains are represented by a set of arbitrarily distributed particles. No connection between these particles is needed.

2. **Integral representation**: All field variables such as the density, velocity, energy, etc. are represented by integral functions. The so-called kernel function is used to approximate these integral functions.

3. **Compact support**: The kernel approximation is then further approximated using particles. This process is called the particle approximation. It is done by replacing the integration in the integral representation of the field function and its derivatives with summations over all the corresponding values at the neighbouring particles in a local domain called the support domain (see section 6.3.3 below).

4. Lagrangian: The particle approximations are performed on all terms related to field variables to produce a set of ordinary differential equations in a discretized form with respect to time only.

In the following all the technical terms used above are discussed in detail.

3.10.2 Nodes or particles in SPH

As with other mesh-less methods, SPH use a set of nodes scattered within the problem domain as well on the boundaries to represent (not discretize) the configuration of the problem (Figure 3.22).
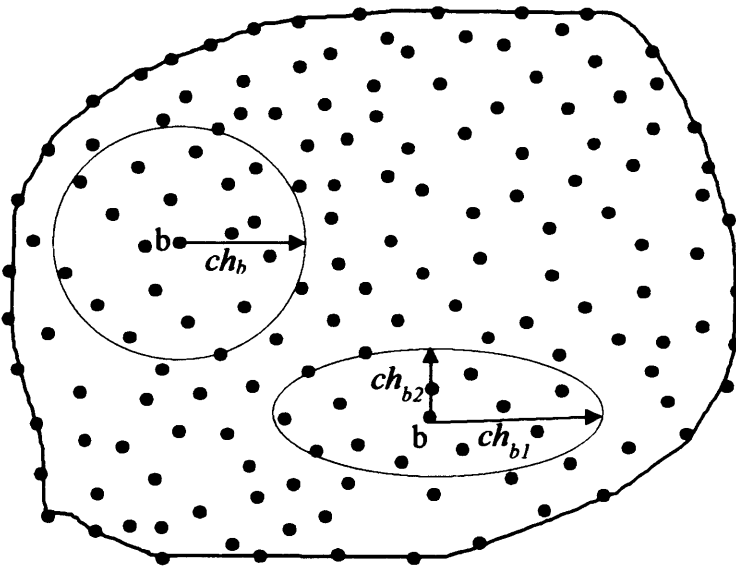
Figure 3.22: Scattered nodes to represent the problem and boundary domains with two shapes of the support domain

3.10.3 Support domain

The SPH method approximates field variables only on the particles. Each particle in the SPH method has a support domain. The support domain for a field point $x=(x, y, z)$ is the domain where the information for all the points inside this domain is used to determine the information at the point x.

The support domain in mesh-free methods can be global or local. For global support domain, the entire problem domain is considered; therefore it is computationally expensive. A local support domain is usually preferred, in which only the nodes or particles that are within a local region of finite dimensions of a point are used for the approximations of the field variables at that point.

The dimensions and shape of the support domain can be different. As shown in Figure 3.22 the most commonly used support domain shapes are elliptic (preferably circular). The support domain is usually taken to be symmetric, especially for points near the boundary.

The concepts of support domain for a particle are closely related to the smoothing length h of that particle. The smoothing length h multiplied by a factor c determines the size of support domain in which the smoothing function applies (the terms c and h will be defined later). Therefore the support domain of a particle is governed by the region of size ch for that particle (Figure 3.22).

3.10.4 Essential formulation of SPH

The formulation of SPH is divided into two key stages, namely the integral representation (or the so-called kernel approximation of field functions) and the particle approximation. In the following these two stages will be examined in more detail.

3.10.4.1 Integral representation

The smooth particle hydrodynamics uses the following identity to represent an arbitrary function $\phi(\mathbf{x})$ in an integral form

$$\phi(\mathbf{x}) = \int_{\Omega} \phi(\mathbf{x}') \delta(\mathbf{x} - \mathbf{x}') d\mathbf{x}' \tag{3.35}$$

where the integral is taken over the volume Ω and $\delta_{\mathbf{x}\mathbf{x}'}$ is the Kronecker delta

$$\delta(\mathbf{x} - \mathbf{x}') = \begin{cases} 1 & \mathbf{x} = \mathbf{x}' \\ 0 & \mathbf{x} \neq \mathbf{x}' \end{cases} \tag{3.36}$$

The Kronecker delta can be replaced by a function W, so that the integral representation of ϕ becomes

$$\phi(\mathbf{x}) = \int_\Omega \phi(\mathbf{x}')W(\mathbf{x}-\mathbf{x}',h)d\mathbf{x}' \qquad (3.37)$$

where W is the so-called kernel or smoothing function.

In the smoothing function, h is the smoothing length defining the domain of influence of the smoothing function W. It is worth noting that the kernel function gives only an approximation of the original function as long as it is not equal to the Kronecker delta.

The kernel W has the following properties:

1. Normalization or unity condition that states

$$\int_\Omega W(\mathbf{x}-\mathbf{x}',h)d\mathbf{x}' = 1 \qquad (3.38)$$

2. Kronecker delta property that is observed when the smoothing length approaches zero

$$\lim_{\mathbf{x}\to\mathbf{x}'} W(\mathbf{x}-\mathbf{x}',h) = \delta_{\mathbf{x}\mathbf{x}'} \qquad (3.39)$$

3. Compact condition

$$W(\mathbf{x}-\mathbf{x}',h) = 0 \quad \text{if} \quad |\mathbf{x}-\mathbf{x}'| > ch \qquad (3.40)$$

where c is a scaling factor to normalise the kernel function. It is a parameter to define the effective non-zero of the smoothing function. This effective area is called the support domain (see Figure 3.22) and is given by

$$|\mathbf{x}-\mathbf{x}'| \le ch \qquad (3.41)$$

Here, the length parameter h has a similar interpretation to the element size in the finite element method.

3.10.4.1.1 Kernel function

The kernel or interpolation or smoothing function usually has a bell shape with a compact support. The most commonly used kernel function in the SPH is a cubic spline

$$W\left(\mathbf{x}-\mathbf{x}',h\right)=\frac{c}{h^{d}}\begin{cases}1-\dfrac{3}{2}\xi^{2}+\dfrac{3}{4}\xi^{3} & \text{if } \xi \leq 1\\[2mm]\dfrac{1}{4}\left(2-\xi\right)^{3} & \text{if } 1<\xi \leq 2\\[2mm]0 & \text{if } \xi > 2\end{cases}\quad ; \quad \xi=\frac{\left\|\mathbf{x}-\mathbf{x}'\right\|}{h} \qquad (3.42)$$

where d is the number of dimensions of the problem.

3.10.4.2 Particle approximation

In the SPH method, the entire problem domain is divided into a finite number of particles that carry individual mass and occupy individual space. The continuous integral (3.35) can be converted to a discretized form of summation over all the particles in the support domain shown in Figure 3.23.
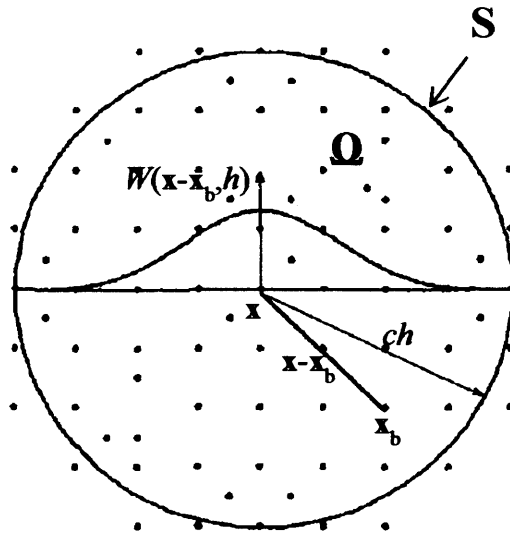
Figure 3.23: Particle approximations using particles within the support domain of the smoothing function W for a particle at centre

The process of particle approximation in the SPH is as follows. The infinitesimal volume $d\mathbf{x}'$ in the above integrations at the location of particle b (as shown in Figure 3.23) is replaced by the finite volume of the particle V_b. The particle b is a generic particle in the set $1, 2, ..., N$ in which N is the number of particles within the support domain. Therefore the continuous

integral in (3.35) can be expressed by the following form of discretized particle approximation

$$\phi(\mathbf{x}) = \sum_{b=1}^{N} V_b \phi_b W(\mathbf{x} - \mathbf{x}_b, h) \tag{3.43}$$

or

$$\phi(\mathbf{x}) = \sum_{b=1}^{N} V_b \phi_b W_b(\mathbf{x}) \tag{3.44}$$

where the assumed mass of particle b is given by

$$m_b = V_b \rho_b \tag{3.45}$$

Note that $W_b(\mathbf{x})$ has the unit of the inverse of volume and that

$$W_b(\mathbf{x}) = W(\mathbf{x} - \mathbf{x}_b, h) \tag{3.46}$$

Similar to (3.44), the differential of the function $\phi(\mathbf{x})$ is given by

$$\nabla\phi(\mathbf{x}) = \sum_{b=1}^{N} V_b \phi_b \otimes \nabla W_b(\mathbf{x}) \tag{3.47}$$

Equations (3.44) and (3.47) state that the value of a function (or its differential) at any position is approximated using the average of those values of the function at all the particles within the support domain (particles $b=1$, 2, ..., N) of that particle weighted by the smoothing function $W_b(\mathbf{x})$.

The approximation of the arbitrary function $\phi(\mathbf{x})$ in terms of the kernel function $W_b(\mathbf{x})$ is shown in Figure 3.24.
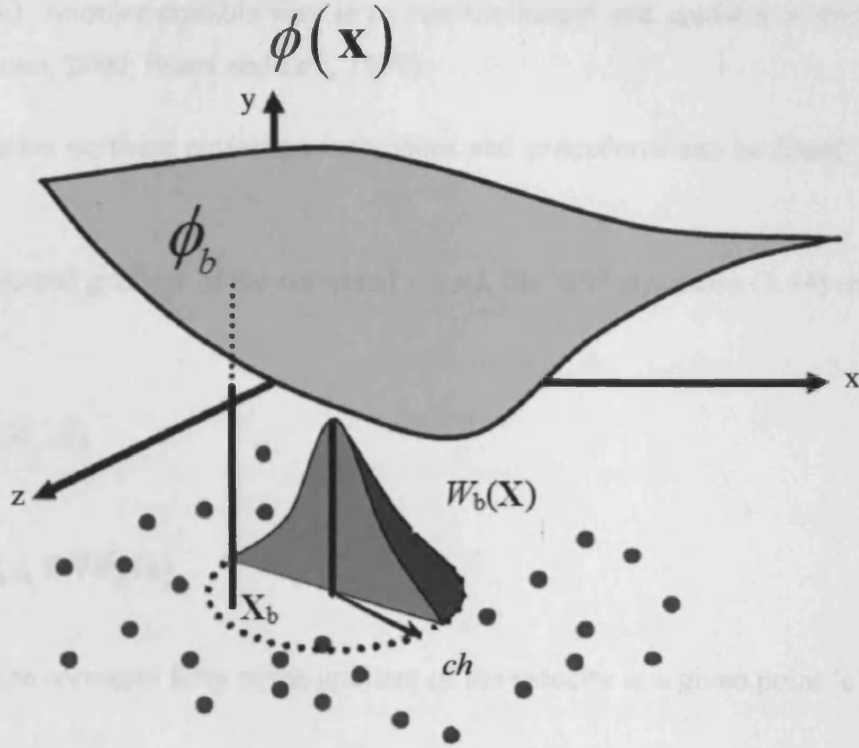
Figure 3.24: Approximation of an arbitrary function $\phi(\mathbf{x})$ in terms of kernel function $W_b(\mathbf{x})$

(After Kulasegaram et al., 2002)

The application of equation (3.44) to compute the approximate value for the density of a continuum leads to the classical SPH equation

$$\rho(\mathbf{x}) = \sum_{b=1}^{N} m_b W_b(\mathbf{x}) \tag{3.48}$$

3.10.5 Corrected SPH integration

The basic SPH approximations as given by equation (3.44) or (3.47) do not accurately reproduce or approximate the function $\phi(\mathbf{x})$ and $\nabla\phi(\mathbf{x})$. Therefore, in the past, corrected SPH equations were developed to address these issues (Bonet and Lok, 1999; Bonet and Kulasegaram, 2000). The main aim of the correction techniques is to satisfy the conservation of angular momentum which, unlike the linear momentum, is not automatically satisfied.

In order to correct the SPH algorithms, some work was done on the gradient of the kernel directly (Bonet and Lok, 1999), whereas others have modified the kernel function itself (Li

and Liu, 1996). Another possible way is to mix the kernel and gradient corrections (Bonet and Kulasegaram, 2000; Bonet and Lok, 1999).

More information on these correction techniques and procedures can be found in Appendix A.

Using the corrected gradient of the corrected kernel, the SPH equations (3.44) and (3.47) can be rewritten as

$$\phi(\mathbf{x}) = \sum_{b=1}^{N} V_b \phi_b \tilde{W}_b (\mathbf{x}) \tag{3.49}$$

$$\nabla\phi(\mathbf{x}) = \sum_{b=1}^{N} V_b \phi_b \otimes \tilde{\nabla} \tilde{W}_b (\mathbf{x}) \tag{3.50}$$

For instance, the corrected form of the gradient of the velocity at a given point 'a' is given by,

$$\nabla\mathbf{v}_a = \sum_{b=1}^{N} V_b \mathbf{v}_b \otimes \tilde{\nabla} \tilde{W}_b (\mathbf{x}) \tag{3.51}$$

where $\tilde{W}$ indicates that the kernel function is corrected to satisfy the consistency conditions, and b is the neighbouring particle within the support domain of particle a. Further, $\tilde{\nabla}$ above indicates that the gradient is corrected to reproduce linear consistency. The gradient correction used here is adopted from the mixed kernel and gradient correction.

To simulate the SCC flow, an incompressible SPH methodology will be adopted in this thesis (Chapter 6). A Bingham model suitable to represent the rheological behaviour of SCC with and without fibres is developed in Chapter 5 from micromechanical principles. The formulations relating to the incompressible SPH and its coupling with the Bingham constitutive model are used in Chapter 6 to simulate the flow of SCC with and without steel fibres.

3.10.6 Incompressibility in SPH

In the original simulation of incompressible flows by SPH, incompressibility was imposed through an equation of state so that the fluid was considered to be weakly compressible. In this situation, normally a large speed of sound in the medium has to be assumed so that the corresponding density fluctuations can be kept small.

However, the artificial compressibility can cause problems with sound wave reflection at the boundaries and the high speed of sound can lead to a stringent time step constraint (Shao and Lo, 2003).

As stated before, in this research a strictly incompressible SPH model will be used to simulate the flow of SCC mixes. By implementing the fully incompressible state, the time step can be larger and it can be chosen based on the fluid velocity field rather than the speed of sound. The disadvantage of this method is that the pressure is not an explicit thermodynamic variable obtained through an equation of the state, but obtained by solving a pressure Poisson equation which might be numerically time consuming.

3.11 Concluding remarks

The fundamental quantification of the workability of self-compacting concrete was discussed. The techniques for measuring the rheology of the paste and the SCC using different types of rheometers were presented. The general rheological parameters of a viscous fluid were more deeply examined. Fluids were classified into two broad categories, i.e. their response to shear rate and to pressure. The former gave two classes; Newtonian and non-Newtonian, whereas the later resulted in compressible and incompressible fluids. According to the response to shear rate, the SCC can be regarded as a generalized non-Newtonian incompressible fluid. It is stated that the rheology of SCC is best describe by the Bingham model which contains two material properties, namely the yield stress τ_y and the plastic viscosity η. The governing equations of the flow of concrete, i.e. conservation of mass and momentum which will be used in the flow simulations were derived. Different methods available in the literature to simulate the flow of fresh concrete, along with some of their advantages and disadvantages were briefly reviewed. It was argued that owing to the Lagrangian nature of the SCC flow and due to the fact that an SCC mix is essentially an aggregate of particles of different sizes and shapes, the use of mesh-less particle-based Lagrangian numerical techniques to simulate such flows is both more appropriate and simpler than the traditional mesh-based methods.

Chapter 4

Development of Self-Compacting High and Ultra High Performance Concretes with and without Steel Fibres

4.1 Introduction

The ideal design of a self-compacting concrete (SCC) mix is a compromise between two conflicting objectives. On the one hand, the SCC has to be as fluid as possible to ensure that it will fill the formwork under its own weight, but on the other, it has to be a stable mixture to prevent segregation of solids during the flow (Spangenberg et al., 2010, Su et al., 2004, Roussel, 2007b). The former is ensured by using superplasticiser and/or viscosity modifying admixtures, while the latter is achieved through the selection of the right amount and type of powders, i.e. cement and cement replacement materials (CRM) and by striking the right balance between the solids and liquids in the mix.

Steel fibres can be added to the SCCs mixes to improve the mechanical properties and the durability of the mixes in much the same manner as in vibrated concrete. However, the fibres greatly impair the workability of the SCC because of their elongated shape and large surface area. The amount of fibre that can be added to a SCC mix is therefore limited and depends on the fibre type used and the composition of the SCC mix. The maximum amount of fibre needs to be determined in such a way as to cause the least decrease in the workability, whilst maintaining good flow and passing ability. In order to make the best use of the fibres, they need to be homogeneously distributed in the mix without clustering (Grünewald and Walraven, 2003).

This chapter reports on the development of self-compacting high and ultra high performance concrete (SCHPC/SCUHPC) mixes with and without steel fibres (SCHPFRC/SCUHPFRC). The aim is to investigate how the proportions of solids and liquids, the type of superplasticiser, and the steel fibres need to be selected in order to produce SCHPFRC/SCUHPFRC mixes with the right flow and passing ability. It is found that for the mixes without steel fibres the fulfilment of the flow and cohesiveness criteria is sufficient for the mix design. However, for the design of SCC mixes with steel fibres, they must additionally meet the passing ability criterion. The major part of this chapter has been submitted for publication to the journal Cement and Concrete Composites (see publication 3 in the list in Chapter 1).

4.2 Development of Self-Compacting High-Performance Fibre-Reinforced Concrete (SCHPFRC)

The original goal of this part of the investigation was to develop a self-compacting version of a high-performance vibrated concrete (with a nominal characteristic compressive strength of 100 MPa) which has been produced regularly in the same laboratory over many years using naphthalene sulfonate-based superplasticiser. The mix proportions of this standard vibrated mix are shown in Table 4.1. The binder refers to cement plus micro-silica.

Table 4.1: Mix proportions (kg) of a standard vibrated high-performance mix

		Mix 1
Constituents (kg)	Cement	500
	Microsilica	55
	Limestone	0
	Sand < 2 mm	660
	Coarse aggregates < 10 mm	1105
	Water	161
	Superplasticiser	9
	Fibres	0
Ratios	Water/binder	0.29
	SP/water	0.06

4.2.1 Mix preparation

The trial mixes were prepared in a planetary mixer by mixing the coarsest constituent (coarse aggregate) and the finest one (micro-silica), followed by the next coarsest (sand) and next finest constituent (cement), and so on. Before each addition, the constituents were mixed for 2 minutes. To fluidise the dry mix, two-thirds of the superplasticiser (SP) was added to the water. One-half of this water-SP mixture was added to the dry constituents and mixed for two minutes. One-half of the remaining water-SP mixture was then added and mixed for two minutes. This process was continued until all water-SP mixture was added. The remaining one-third of the SP was added and mixed for two minutes just before transferring the SCC mix into the slump cone or placing it in the moulds.

4.2.2 Flow-ability test

The slump flow test was performed on trial mixes to obtain a mix with the maximum flow-ability and homogeneity. The horizontal spread up to 500 mm was timed. If it was different from 3 sec, or any segregation was visible, the mix proportions were judiciously altered. This trial process was continued until the mix met the flow-ability criterion (horizontal spread T_{500} of 500 mm in 3 sec) and was homogeneous with no visible segregation.

4.2.2.1 SCHPC and SCHPFRC mixes

To achieve a self-compacting version of the Mix 1 in Table 4.1, several trial mixes were made and tested. Table 4.2 gives the composition of these mixes and their corresponding slump flow test results. It should be noted that these mix proportions will lead to slightly different yields in terms of volume.

Table 4.2: Composition of SCHPC and SCHPFRC mixes (kg) with naphthalene sulfonate-based superplasticiser

		Mix 2	Mix 3	Mix 4	Mix 5
Constituents (kg)	Cement	500	500	500	500
	Microsilica	72	72	72	72
	Limestone	225	225	232	232
	Sand < 2 mm	680	648	648	648
	Coarse aggregates < 10 mm	880	797	797	797
	Water	166	166	166	166
	Superplasticiser	18.5	18.5	18.5	18.5
	Fibres	0	0	0	39
Ratios	Water/binder	0.29	0.29	0.29	0.29
	SP/water	0.11	0.11	0.11	0.11
Slump	Slump flow spread (mm)	---	540	600	560
	T_{500} (sec)	---	4	3	3

Comments on the contents of Table 4.2 follow:

In Mix 2, the coarse aggregate content was decreased by 20% (relative to Mix 1) in order to reduce the inter-particle friction. Limestone dust was added to increase the paste volume and to lubricate the aggregate particles. The micro-silica content was increased by up to 30%. The

superplasticiser to water ratio was increased from 0.06 to 0.11. The sand content was increased by 3%. The water to binder ratio was held unchanged at 0.29. It was observed that the mix was too stiff without any horizontal flow at all.

In Mix 3, the sand and coarse aggregate contents were decreased by 5% and 9%, respectively, while the SP-water ratio and water-binder ratio were kept constant at 0.11 and 0.29, respectively. The horizontal slump flow of the mix was 540 mm but T_{500} was 4 sec, i.e. more than the required 3 sec.

In the next mix (Mix 4), the paste volume was increased by adding 3% more limestone dust. This mix met the T_{500} criterion, and there was no visible segregation (Figure 4.1). However, the compression test on specimens made out of this mix at the age of 3 days suggested that it would fall short of the 28-day target compressive strength of 100 MPa. This is a consequence of the reduction in the coarse aggregate content by nearly 28% (relative to Mix 1) in order to achieve the desired flow-ability and cohesiveness of the mix.

Figure 4.1: Horizontal spread of SCHPC mix 4

The simplest way to increase the compressive strength of this SCHPC mix without having to alter any other mix proportions was to add a small amount of steel fibres to the mix.

In the present study, 30 mm long Z560 Dramix fibres with crimped ends (Figure 4.2) were used. The fibres are supplied by the manufacturer as small flat packs containing more than 40 fibres temporarily held together by water-solvable glue. 0.5% by volume of these fibres were
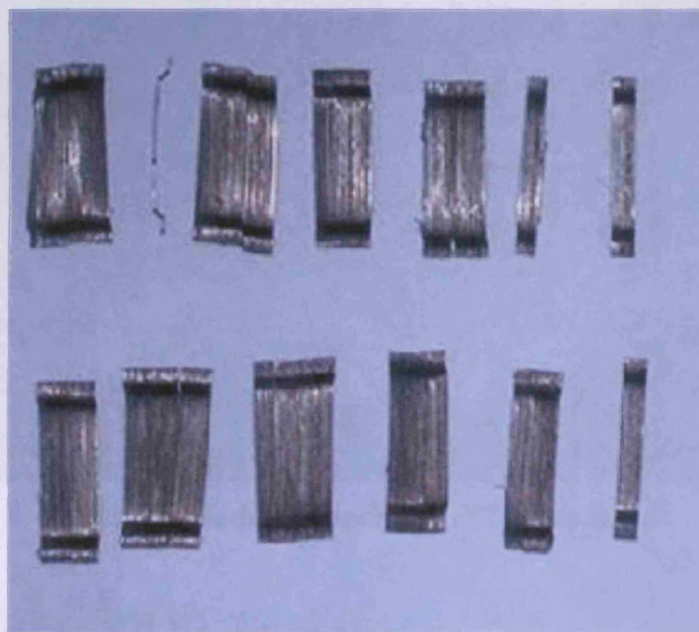
Figure 4.2: 30 mm long glued steel fibres

added to Mix 4 to create Mix 5 (Table 4.2). The fibres were added progressively to the wet SCHPC mix (i.e. after all the water-SP mixture had been added and mixed; see section 4.2.1) and mixed until the glue had dissolved and the fibres had dispersed uniformly in the mix. The remaining one-third of the SP was added and mixed for two minutes just before transferring the fibre-reinforced mix into the slump cone. The horizontal spread up to 500 mm was timed at 3 sec, as required, although the final spread was slightly less than that of the SCHPC without fibres (560 mm against 600 mm). This self-compacting high-performance fibre-reinforced concrete (SCHPFRC) met the flow-ability criterion and was very homogeneous with no visible segregation (Figure 4.3).

Figure 4.3: Horizontal spread of SCHPFRC mix 5

4.2.3 Influence of the type of superplasticiser

It has been reported (Flatt, 2004b) that polycarboxylate ether-based superplasticisers, e.g. Glenium ACE 333, which disperse particles by steric stabilisation result in better workability than do the naphthalene sulfonate-based superplasticisers, which disperse particles by electrostatic repulsion. For this reason the naphthalene sulfonate-based superplasticiser was replaced by an equal amount of Glenium ACE 333. Table 4.3 shows the compositions of the SCHPC and SCHPFRC mixes using this SP.

Table 4.3: Composition of SCHPC and SCHPFRC mixes (kg) with Glenium ACE 333 superplasticiser

		Mix 6	Mix 7	Mix 8	Mix 9	Mix 10
Constituents (kg)	Cement	500	500	500	500	500
	Microsilica	72	72	75	75	75
	Limestone	232	232	243	243	243
	Sand < 2 mm	648	648	680	680	680
	Coarse aggregates < 10 mm	797	810	850	850	850
	Water	166	143	117	127	127
	Superplasticiser	18.5	10	12	18.5	18.5
	Fibres	0	0	0	0	39
Ratios	Water/binder	0.29	0.25	0.20	0.22	0.22
	SP/water	0.11	0.07	0.10	0.15	0.15
Slump	Slump flow spread (mm)	855	800	745	780	770
	T_{500} (sec)	2	3	5	3	3

Comments on the trial mixes of Table 4.3 follow:

In Mix 6, the naphthalene sulfonate-based superplasticiser of Mix 4 was replaced by an equal amount of Glenium ACE 333. The resulting mix was found to have a very low viscosity with a horizontal spread in excess of 850 mm and clear bleeding. This meant that either the liquid content could be decreased or the solid content could be increased.

Accordingly, in Mix 7, the water-binder ratio and SP-water ratio were reduced from 0.29 to 0.25 and from 0.11 to 0.07, respectively. Despite obtaining the horizontal slump flow of 800 mm and T_{500} of 3 sec, the mix was rejected because of bleeding.

In a further attempt to reduce the bleeding (Mix 8), all the solid contents (except the cement) were modestly increased (by 5%), while the SP-water ratio was increased to 0.10. The slump flow was 745 mm but T_{500} was equal to 5 sec.

In the next trial mix (Mix 9), the SP-water and the water-binder ratios were increased to 0.15 and 0.22, respectively. This mix had the required flow-ablility (slump flow of 780mm and T_{500} equal to 3 sec) and was cohesive.

In the trial Mix 10, 0.5% by volume of 30 mm long Z560 Dramix fibres was used. The mix so produced satisfied both the flow-ability (the horizontal slump flow was only marginally smaller i.e. 770 mm against 780 mm) and cohesiveness criteria.

4.2.4 Passing ability test

The trial Mixes 9 and 10 (without and with fibres) that satisfied the flow-ability criterion and showed no signs of segregation i.e. were highly cohesive, were subjected to the passing ability test to ensure that they were able to pass through narrow gaps that exist between reinforcing bars in a real reinforced concrete structural element. For this test, a 300 mm diameter J-Ring apparatus with 16 steel rods (each of diameter 16 mm) was used, as recommended by The European Federation of National Trade Associations (EFNRC) (efnarc.org, 2005) (see Figure 2.17 in chapter 2).

This test showed that there was some blocking in the SCHPFRC Mix 10 with the bulk of the fibres and coarse aggregates lumped in the centre of flow spread. It was therefore necessary to adjust the mix proportions. Table 4.4 gives the various trial mixes of SCHPC with steel fibres which have been tested for passing ability in J-Ring apparatus.

Table 4.4: Composition of SCHPC mixes (kg) with 0.5% steel fibres for the J-Ring test

		Mix 11	Mix 12	Mix 13
Constituents (kg)	Cement	500	500	500
	Microsilica	75	75	75
	Limestone	243	243	222
	Sand < 2 mm	680	680	680
	Coarse aggregates < 10 mm	850	850	850
	Water	143	133	133
	Superplasticiser	18.5	18.5	18.5
	Fibres	39	39	39
Ratios	Water/binder	0.25	0.23	0.23
	SP/water	0.13	0.14	0.14
Slump	Slump flow spread (mm)	740	730	740
	T_{500} (sec)	5	5	3

In the first attempt (Mix 11) to meet the passing ability requirement, the water to binder ratio was increased from 0.22 to 0.25 and the SP to water ratio was correspondingly decreased to 0.13. Most of the fibres and the coarse aggregate were still clustered in the middle of flow spread.

Therefore, in the next trial Mix 12 the water to binder ratio was decreased to 0.23 but the SP to water ratio was correspondingly increased from 0.13 to 0.14. This mix too failed to meet the passing ability requirement.

It was therefore decided to reduce the amount of powder, while keeping the amount of liquids constant. Thus in Mix 13, the amount of limestone dust was reduced by about 10%. The result was a much improved mix with only a slight segregation in the middle of flow spread.

In the next trial mix (Mix 14 in Table 4.5) the limestone dust content was further reduced by 10%. The coarse aggregate content was also slightly decreased, with a corresponding increase in the fine aggregate (sand). The SP-water ratio was kept constant, while the water-binder ratio was increased to 0.24. This mix (Mix 15 in Table 4.5) met the passing ability criterion based on both the EFNRC (2005) and PCI (2003) recommendations.

Table 4.5: SCHPC and SCHPFRC mixes (kg) that met both flowability and passing ability tests

		Mix 14	Mix 15
Constituents (kg)	Cement	500	500
	Microsilica	75	75
	Limestone	200	200
	Sand < 2 mm	700	700
	Coarse aggregates < 10 mm	833	833
	Water	138	138
	Superplasticiser	20	20
	Fibres	0	39
Ratios	Water/binder	0.24	0.24
	SP/water	0.14	0.14
Slump	J-Ring flow spread Dj(mm)	805	760
	T_{500j} (sec)	3	3

It should be mentioned that although the trial Mix 10 had satisfied both the flow-ability and the passing ability tests and thus did not require re-designing, it was the aim of this study to

develop a SCHPFRC mix from the same base SCHPC mix. This led to the development of Mix 14 which differs from Mix 15 only by the absence of steel fibre. The mixes 14 and 15 (Figures 4.4 and 4.5) of Table 4.5 were flow-able, homogeneous, and reached the target compressive strength 100 MPa.

Figure 4.4: Flow and passing ability of SCHPC Mix 14

Figure 4.5: Flow and passing ability of SCHPFRC Mix 15

It should be mentioned that the slump and J-Ring tests can be performed by using an upright or an inverted cone. In this study both orientations were used and it was observed that in the inverted orientation the flow time T_{500j} is slightly increased when large coarse aggregates are present. There was no discernible difference when such aggregates were absent, as in the mixes to be described below.

4.3 Development of Self-Compacting Ultra High-Performance Fibre-Reinforced Concrete (SCUHPFRC)

In this section, the development of a SCUHPFRC will be described. The base mix is CARDIFRC mix I (Benson and Karihaloo, 2005a, b and Benson et. al., 2005). As can be seen from Table 4.6 this mix contains a total of 6% by volume of two types of fibre: 6mm (5% by volume) and 13mm (1% by volume) long steel fibres (diameter 0.15mm). It is a very dense and highly viscous mix and is meant for vibratory compaction. However, the mix without the fibres is highly flow-able and thus has the potential for self-compaction.

Table 4.6: Original CARDIFRC mix I (kg/m³)

			CARDIFRC Mix I
Constituents (kg/m³)		Cement	855
		Micro-silica	214
		Quartz Sand 9-300 μm	470
		250-600 μm	470
		Water	188
		Superplasticiser	28
		Fibres 6 mm	390
		Fibres 13mm	78
Ratios		Water/binder	0.18
		SP/water	0.15

In the present development, the 6% by volume brass-coated thin fibres of the original CARDIFRC mix I was replaced by 2.5% by volume of the cheaper 30 mm long steel Z560 Dramix fibres with 0.55 mm diameter. It was expected that such a replacement will lead to a reduction in the compressive (200 MPa) and indirect tensile (25 MPa) strengths of the original CARDIFRC mix I, but not to its toughness because the main impact of the long

fibres lies in enhancing the toughness of the composite. However, as 85% of the cost of the original CARDIFRC mix I is attributable to the expensive thin brass-coated fibres, the cost of the self-compacting version using the much cheaper Dramix fibres will be substantially reduced, thus making it a highly competitive advanced cement-based construction material which can be used in many situations in which steel is currently the preferred option.

4.3.1 Flow-ability test

Trial mixes were prepared from the original CARDIFRC mix I without fibres. The slump flow test was performed on the trial mixes to obtain a mix with the maximum flow-ability and homogeneity and least segregation. For the preparation of each mix the mixing procedure used for CARDIFRC was followed (see section 4.2.1). Based on the experience with the SCHPFRC mix 15 (Table 4.5) reported above, which contained only 0.5% by volume of the same type of fibres as envisaged in the present SCUHPFRC, it was planned to achieve a slump flow of 900 mm for mixes without steel fibres. Then 2.5% of 30 mm long steel Z560 Dramix fibres with 0.55 mm diameter were added to the mix and its flow-ability was checked again using the slump flow test. With the addition of steel fibres it was planned to achieve a slump of at least 500 mm and the flow time T_{500} of 3 sec.

4.3.1.1 SCUHPC and SCUHPFRC

4.3.1.1.1 Self-compacting ultra-high performance concrete (SCUHPC)

The constituents of CARDIFRC mix I without fibres were modified. Various water to binder ratios (0.18-0.20) and SP to water ratios (0.15-0.22) were tried to obtain highly flow-able trial mixes. A part of the cement was replaced by ground granulated blast furnace slag (GGBS). GGBS maintains the cohesion of the SCCs mixes and hence prevents the segregation. It also reduces the heat of hydration and the cost of the mixes. These trial mixes were then tested for flowing ability using the slump flow test.

The trial mixes were prepared in both a planetary mixer (with a capacity of 81 kg) and a standard pan/liner drum mixer (with a capacity of 163 kg) to check the consistency in the results for the mixes in larger quantities. Figure 4.6 shows the procedure used to create a flow-able SCUHPC.

```
        ┌─────────────────┐
        │      Start      │
        └─────────────────┘
                 │
                 ▼
        ╱─────────────────╲
       ╱  CARDIFRC Mix I    ╲
       ╲  without fibres    ╱
        ╲─────────────────╱
                 │
                 ▼
        ┌─────────────────┐
        │ Change SP-water │◄──────────────┐
        │ ratio and/or    │               │
        │ GGBS            │               │
        └─────────────────┘               │
                 │                         │
                 ▼                         │
        ┌─────────────────┐               │
        │ Start trial     │               │
        │ mixing in       │               │
        │ planetary mixer │               │
        └─────────────────┘               │
                 │                         │
                 ▼                         │
           ◇─────────────◇                │
          ╱ Is the slump  ╲     NO         │
          ╲ flow spread   ╱───────────────┘
           ◇ >900 mm?    ◇
                 │
                Yes
                 │
                 ▼
           ◇─────────────◇
     Yes  ╱ Is there any  ╲
    ┌─────╲ segregation?  ╱
    │      ◇─────────────◇
    │            │
    │           No
    │            ▼
    │      ◇─────────────◇
    │ No  ╱ Are the       ╲
    └─────╲ results        ╱
          ◇ consistent    ◇
           ╲ with those of╱
            ◇ Pan mixer? ◇
                 │
                Yes
                 ▼
        ╱─────────────────╲
        ╲     SCUHPC       ╱
         ╲───────────────╱
                 │
                 ▼
        ┌─────────────────────┐
        │ Add fibres (see     │
        │ Figure 4.8)         │
        └─────────────────────┘
```
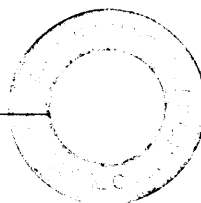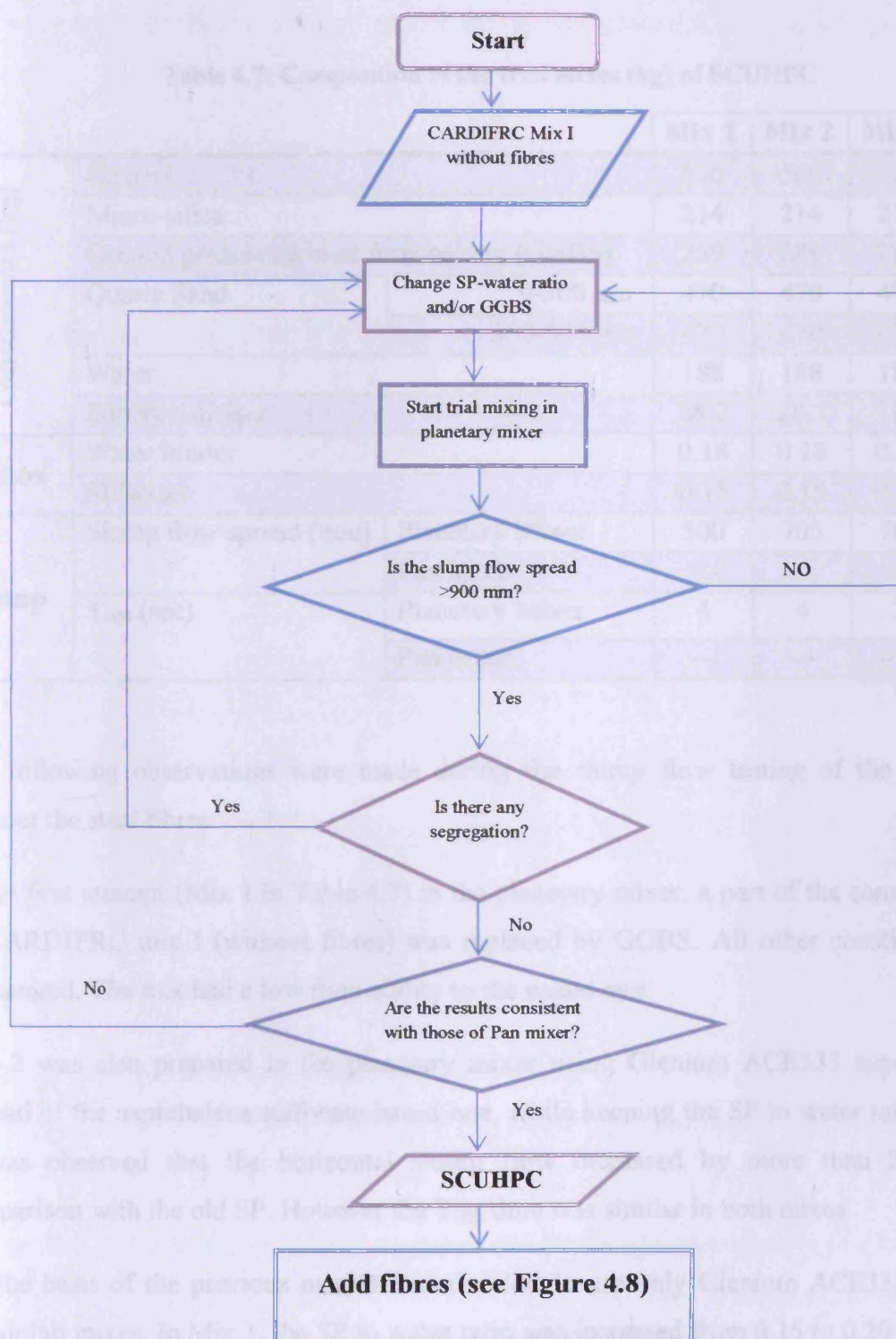
Figure 4.6: Procedure to create a flow-able SCUHPC

Table 4.7 gives the composition of the trial mixes and the slump flow test results.

Table 4.7: Composition of the trial mixes (kg) of SCUHPC

			Mix 1	Mix 2	Mix 3	Mix 4
Constituents (kg)	Cement		566	566	566	543.5
	Micro-silica		214	214	214	214
	Ground granulated blast furnace slag (GGBS)		289	289	289	311.5
	Quartz Sand	9-300 µm	470	470	470	470
		250-600 µm	470	470	470	470
	Water		188	188	188	188
	Superplasticiser		28.2	28.2	37.6	37.6
Ratios	Water/binder		0.18	0.18	0.18	0.18
	SP/water		0.15	0.15	0.20	0.20
Slump	Slump flow spread (mm)	Planetary Mixer	500	705	768	905
		Pan Mixer	---	---	---	772
	T_{500} (sec)	Planetary Mixer	4	4	3	2
		Pan Mixer	---	---	---	4

The following observations were made during the slump flow testing of the trial mixes without the steel fibres:

In the first attempt (Mix 1 in Table 4.7) in the planetary mixer, a part of the cement (33.8%) in CARDIFRC mix I (without fibres) was replaced by GGBS. All other constituents were unchanged. The mix had a low flow-ability to the naked eye.

Mix 2 was also prepared in the planetary mixer using Glenium ACE333 superplasticiser instead of the naphthalene sulfonate-based one, while keeping the SP to water ratio constant. It was observed that the horizontal slump flow increased by more than 200 mm in comparison with the old SP. However the T_{500} time was similar in both mixes.

On the basis of the previous mix, it was decided to use only Glenium ACE333 SP in the remaining mixes. In Mix 3, the SP to water ratio was increased from 0.15 to 0.20 which gave a spread of 768 mm.

In the next mix (Mix 4), the GGBS content was increased by 8% while the cement content was decreased by 4%. It gave a slump flow spread of 905 mm when mixed in the planetary mixer. To check whether it would give a similar result if mixed in large quantities this mix was prepared again in the standard pan mixer. It was observed that the slump spread was reduced.

Table 4.8 gives the composition of SCUHPC mixes with a constant amount of solid constituents and a variable amount of a viscosity modifying admixture (VMA).

Table 4.8: Composition of SCUHPC mixes (kg) with a constant amount of solid constituents

			Mix 5	Mix 6	Mix 7	Mix 8	Mix 9
Constituents (kg)	Cement		543.5	543.5	543.5	543.5	543.5
	Micro-silica		214	214	214	214	214
	Ground granulated blast furnace slag (GGBS)		311.5	311.5	311.5	311.5	311.5
	Quartz Sand	9-300 µm	470	470	470	470	470
		250-600 µm	470	470	470	470	470
	Water		188	188	188	188	188
	Superplasticiser		37.6	37.6	41.33	41.33	41.33
	Viscosity modifying admixture (VMA)		1.1	27.2	27.2	1.1	2.2
Ratios	Water/binder		0.18	0.18	0.18	0.18	0.18
	SP/water		0.2	0.2	0.22	0.22	0.22
Slump	Slump flow spread (mm)	Planetary Mixer	---	660	---	---	855
		Pan Mixer	785	---	780	835	775
	T_{500} (sec)	Planetary Mixer	---	4	---	---	2
		Pan Mixer	3	---	4	3	2

In Mix 5, to increase the slump flow spread, 0.1% of VMA (Glenium 2006L) by weight of cement was added to the mix in a standard pan mixer. This resulted in only a slight increase in the slump flow spread (785 mm against 772 mm).

The amount of VMA was increased further to 5% by weight of cement in trial mix 6 which was mixed in a planetary mixer. But this step resulted in further reduction of the slump flow.

Mix 7 was prepared in the standard pan mixer. The superplasticiser to water ratio was increased to 0.22, while the VMA content was held constant. But the slump spread did not reach the target value of 900 mm.

In mixes 8 and 9, with new SP to water ratio held constant at 0.22, the content of VMA was changed to 0.1% and 0.2% by weight of cement. In both mixes, it was observed that the increase in the VMA content led to a decrease in the slump flow spread. Hence it was concluded that, the version of SCUHPC based on CARDIFRC mix I prepared in the laboratory did not require the addition of a VMA. The reasons might be as follows:

- **Quantity of the mix**: the quantity prepared in the laboratory is much smaller than that on an actual construction site;
- **Water-binder ratio**: on a construction site, the water to binder ratio can be high and VMA is required to thicken the paste, i.e. to enhance the plastic viscosity of the paste;
- **Weather conditions**: the mixes were prepared and tested at room temperature (around 21 degree Celsius) when the evaporation of the liquids is practically negligible, whereas at higher temperatures, VMA may need to be added to compensate for evaporation.

The VMA constituent was therefore discarded and it was decided to vary the water to binder ratios and SP to water ratios (Table 4.9) to reach the target slump flow spread of 900 mm.

Table 4.9: Effect of the variation of the water-binder and SP-water ratios on the flow-ability of SCUHPC

			Mix 10	Mix 11	Mix 12
Constituents (kg)	Cement		543.5	543.5	543.5
	Micro-silica		214	214	214
	Ground granulated blast furnace slag (GGBS)		311.5	311.5	311.5
	Quartz Sand	9-300 µm	470	470	470
		250-600 µm	470	470	470
	Water		214	188	188
	Superplasticiser		41.33	41.33	41.33
Ratios	Water/binder		0.20	0.18	0.18
	SP/water		0.22	0.20	0.22
Slump	Slump flow spread (mm)	Planetary Mixer	---	950	---
		Pan Mixer	940	820	905
	T_{500} (sec)	Planetary Mixer	---	2	---
		Pan Mixer	2	3	3

The detailed comments on the SCUHPC mixes presented in Table 4.9 follow:

In the trial Mix 10 prepared in the standard pan mixer, the water to binder ratio was increased from 0.18 to 0.20 which gave a slump spread of 940 mm. This was due to the increase in the water quantity which is not desirable in practice. Therefore this mix was ignored and it was decided to change the SP to water ratio, while keeping the water to binder ratio constant.

For Mix 11, the SP to water ratio of 0.20 and water-binder ratio of 0.18 were used. The slump flow spreads for the mixes prepared in the planetary and standard pan mixer were 950 mm and 820 mm, respectively. However the mix was rejected because of the large difference in the flow spreads.

In Mix 12, the SP to water ratio was increased to 0.22. A slump of 905 mm with T_{500} equal to 3 sec was obtained for the mix prepared in the standard pan mixer. The horizontal spread in the slump flow cone test is shown in Figure 4.7.
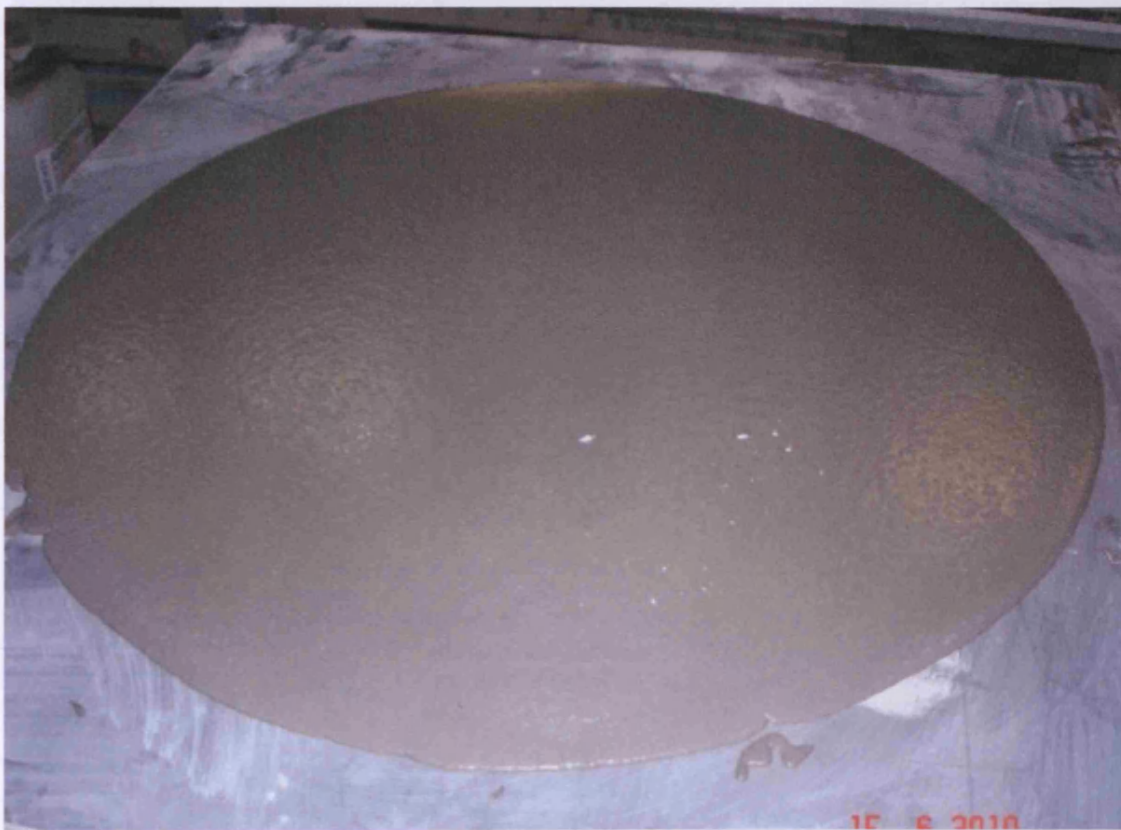
Figure 4.7: Horizontal spread of SCUHPC mix 12

4.3.1.1.2 Self-compacting ultra-high performance fibre reinforced concrete (SCUHPFRC)

Mix 12 was selected as the starting mix to which 2.5% by volume of steel fibres were added. Figure 4.8 shows the procedure for achieving the SCUHPFRC.
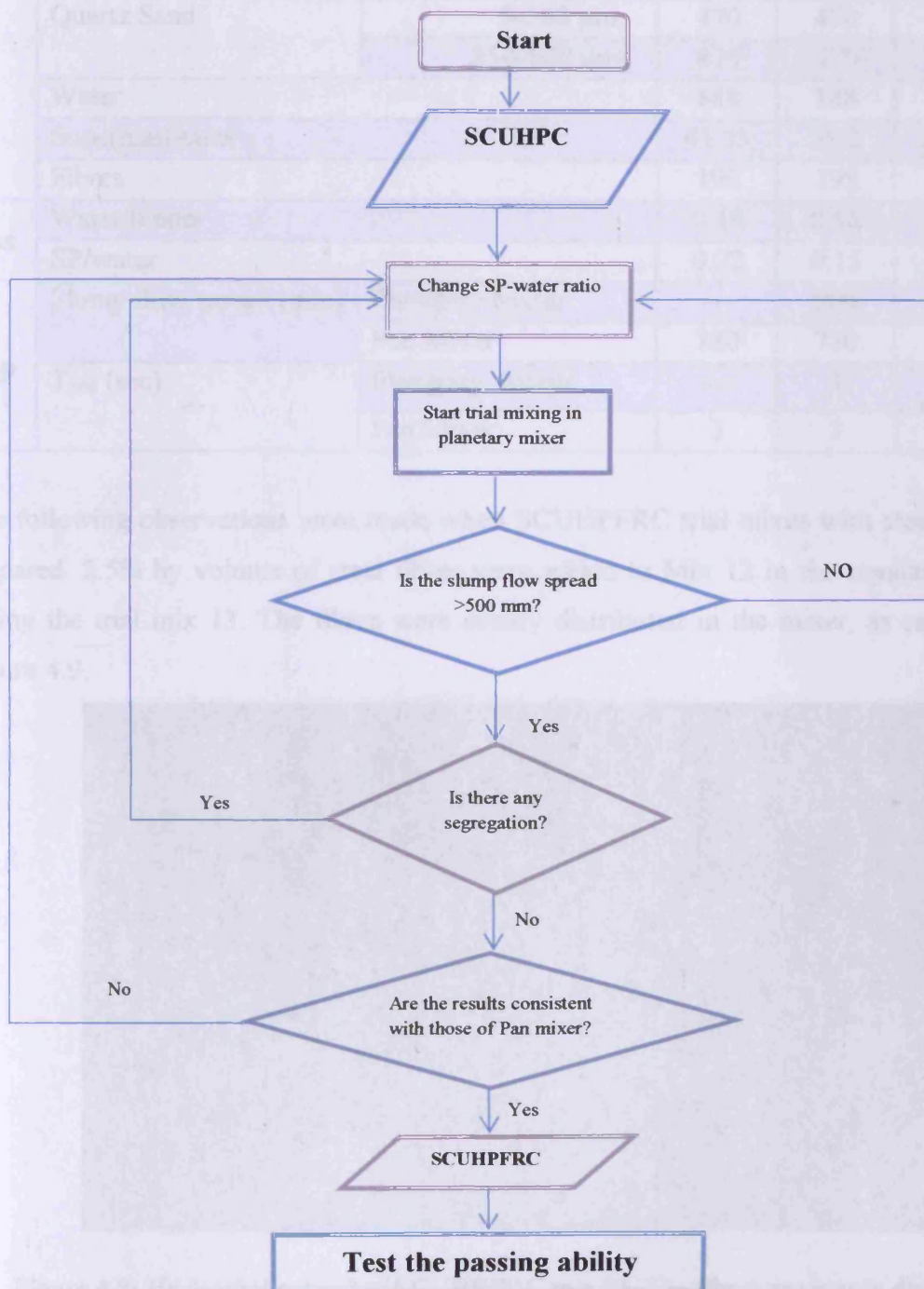
Figure 4.8: Procedure for achieving the SCUHPFRC

Table 4.10 gives the composition of the SCUHPFRC trial mixes with steel fibres.

Table 4.10: Composition of SCUHPFRC mixes (kg) with steel fibres

			Mix 13	Mix 14	Mix 15	Mix 16
Constituents (kg)	Cement		543.5	543.5	543.5	543.5
	Micro-silica		214	214	214	214
	Ground granulated blast furnace slag (GGBS)		311.5	311.5	311.5	311.5
	Quartz Sand	9-300 µm	470	470	470	470
		250-600 µm	470	470	470	470
	Water		188	188	188	188
	Superplasticiser		41.33	28.2	20.83	19.17
	Fibres		195	195	195	195
Ratios	Water/binder		0.18	0.18	0.18	0.18
	SP/water		0.22	0.15	0.11	0.10
Slump	Slump flow spread (mm)	Planetary Mixer	---	900	---	---
		Pan Mixer	780	750	750	700
	T_{500} (sec)	Planetary Mixer	---	3	---	---
		Pan Mixer	3	3	3	3

The following observations were made when SCUHPFRC trial mixes with steel fibres were prepared. 2.5% by volume of steel fibres were added to Mix 12 in the standard pan mixer giving the trial mix 13. The fibres were evenly distributed in the mixer, as can be seen in Figure 4.9.

Figure 4.9: Horizontal spread of SCUHPFRC mix 13. The fibres are evenly distributed

From this trial Mix 13 it became clear that the mix did not lose its workability even after the addition of 2.5% by volume fibres. The slump flow was expected to reduce by about 300-400 mm after the addition of fibres but in actual fact it reduced by only 100 mm. This showed that the final mix had very good workability and the target initial slump flow of 900 mm had been overestimated. Thus a flow-able mix with fibres would be possible to make even after reducing the SP to water ratio below 0.20.

Therefore in the next trial mix i.e. Mix 14 the SP to water ratio was reduced to 0.15 and a slump flow of 900 mm and 750 mm were achieved on mixes made in the planetary and standard pan mixers, respectively.

In Mix 15, the SP to water ratio was further reduced to 0.11 which gave a slump flow of 750 mm with very good distribution of fibres, even at the edges of the slump flow. In this mix the SP to water ratio was initially chosen to be 0.1 during the mixing process. Additional superplasticiser (0.01) was added at the end to increase the workability on the basis of visual observation.

The SP to water ratio was further reduced to 0.10 in Mix 16 which was made in the standard pan mixer. A slump flow of 700 mm and T_{500} equal to 3 sec were achieved. But as can be seen from Figure 4.10, the SCUHPFRC seems drier than Mix 13 (Figure 4.9) although it is still workable.

Figure 4.10: Horizontal spread of SCUHPFRC mix 16

The segregation resistance of the SCUHPC/SCUHPFRC mixes was judged by visual inspection of concrete in the mixer and after the slump flow test. However as can be seen from Figures 4.7, 4.9 and 4.10, no segregation of particles occurred during the tests. This is due to the fact that CARDIFRC mix I is a highly optimised mix with excellent homogeneity because of the absence of coarse aggregates (as can be seen from Table 4.5, the maximum size of the fine aggregates used is only 600 μm).

4.3.2 Passing ability test

As before, the mixes of SCUHPFRC were subjected to the passing ability test in the J-Ring apparatus, with the cone in the inverted orientation for it could not be placed in the ring in the upright position because of the lifting lugs attached to its base. The Mix 12 without fibres easily and smoothly flowed through the gaps between the steel rods reaching a spread of 900 mm, with the spread T_{500j} timed at 3 sec (Figure 4.11).
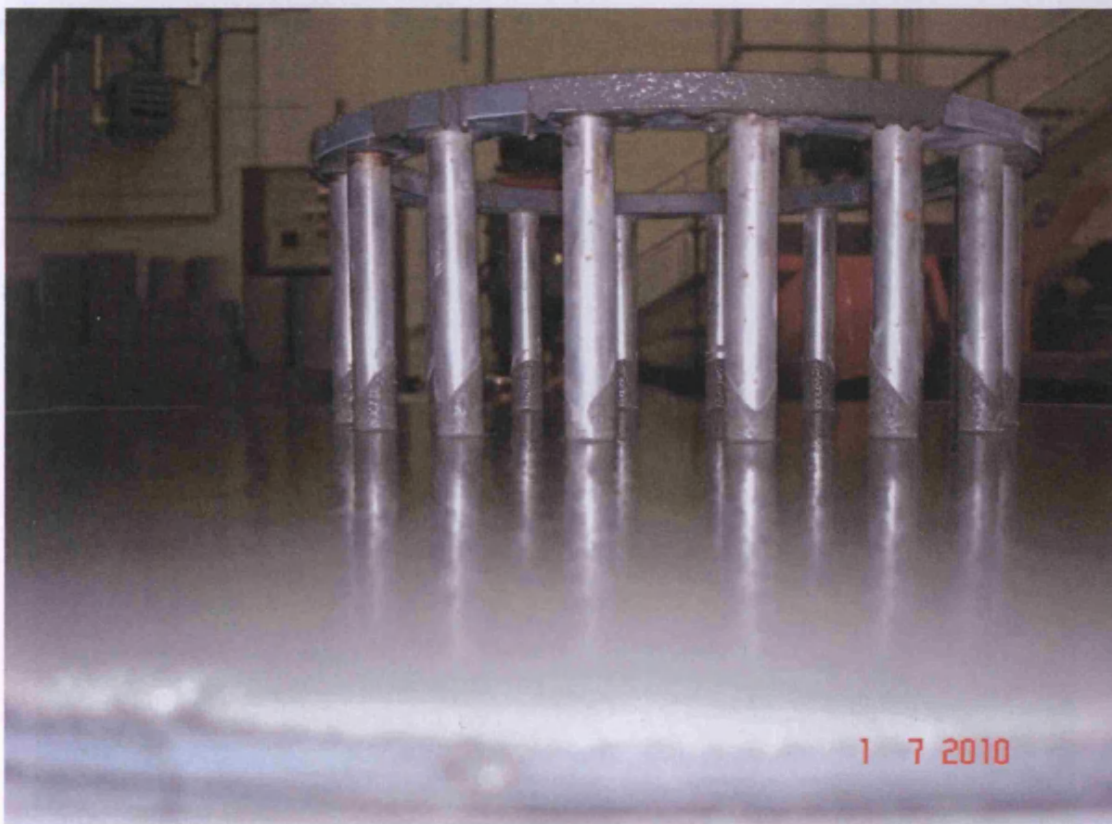
Figure 4.11: SCUHPC mix 12 flows smoothly through the gaps between the steel rods

Mix 16 could not meet the passing ability criterion as it has a lower SP to water ratio. The
steel fibres block the spaces between the rods and prevent the SCC mix to pass through them.

The J-Ring test was repeated with a SCUHPFRC mix that had a higher amount of SP. Mix 13
was selected with a SP to water ratio of 0.22. The Mix 13 also did not satisfy the passing
ability test. Some fibres nested around the steel bars, preventing the remaining fibres to pass
through the gaps (Figure 4.12). It was therefore necessary to improve the passing ability of
this mix by increasing the superplasticiser content. However, the superplasticiser content was
also increased by the same amount in the base mix 13 without fibres in order to maintain
commonality between the SCUHPC mixes with and without fibres. The SP-water ratio had to
be increased from 0.22 of mixes 12 and 13 to 0.28 in order to satisfy the passing ability test
(Figures 4.13 and 4.14). The mix proportions of these mixes, designated SCUHPC mix 17
and SCUHPFRC mix 18 are given in Table 4.11. The compressive strength of SCUHPFRC
mix 18 was measured at 162 MPa after 7 days of hot curing at 90°C. As expected, it is less
than the compressive strength (200 MPa) of the original CARDIFRC mix I because of the
reduced fibre content.

**Figure 4.12: SCUHPFRC mix 13 did not satisfy the passing ability test. The fibres are nested
around the steel rods**

Table 4.11: Mix proportions of SCUHPC and SCUHPFRC mixes (kg) meeting the flow-ability, cohesiveness and passing ability criteria

			SCUHPC Mix 17	SCUHPFRC Mix 18
Constituents (kg)	Cement		543.5	543.5
	Micro-silica		214	214
	Ground granulated blast furnace slag (GGBS)		311.5	311.5
	Quartz Sand	9-300 µm	470	470
		250-600 µm	470	470
	Water		188	188
	Superplasticiser		52.64	52.64
	Fibres		---	195
tios	Water/binder		0.18	0.18
	SP/water		0.28	0.28
mp	J-Ring slump flow Dj(mm)	Planetary Mixer	---	---
		St. Pan Mixer	910	830
	T_{500j} (sec)	Planetary Mixer	---	---
		St. Pan Mixer	3	3
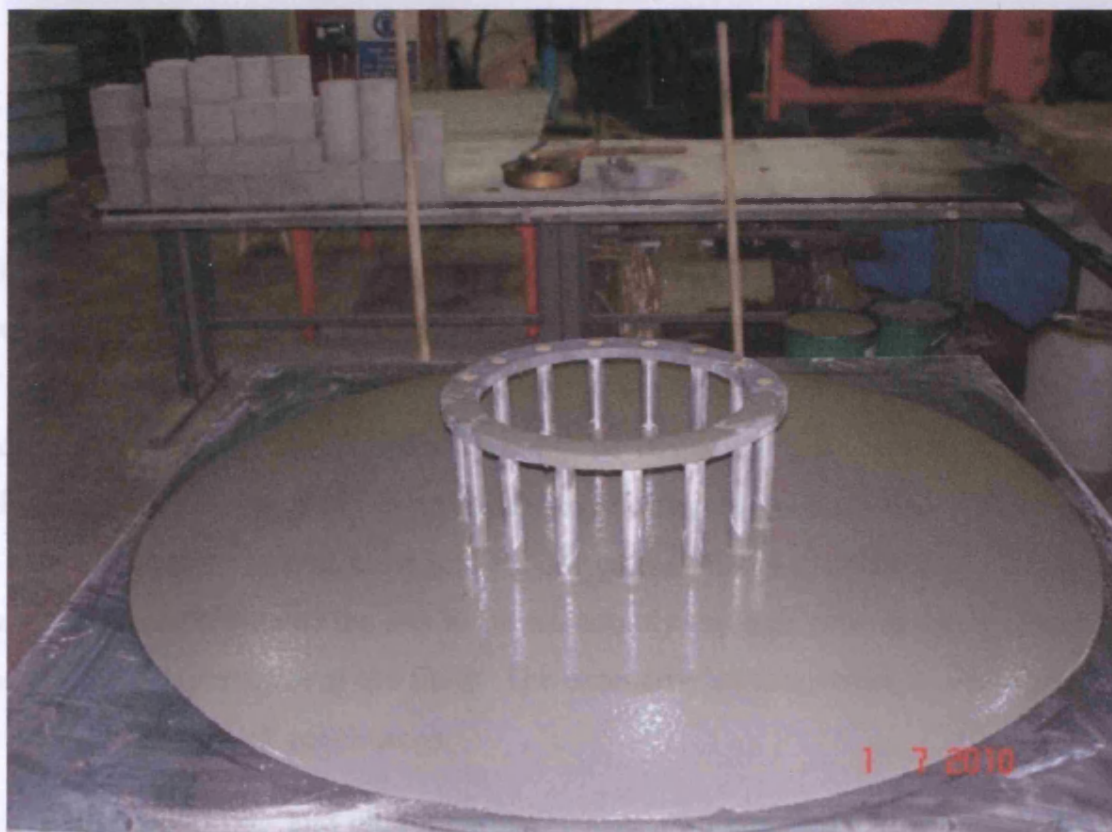
Figure 4.13: Flow and passing ability of SCUHPC mix 17
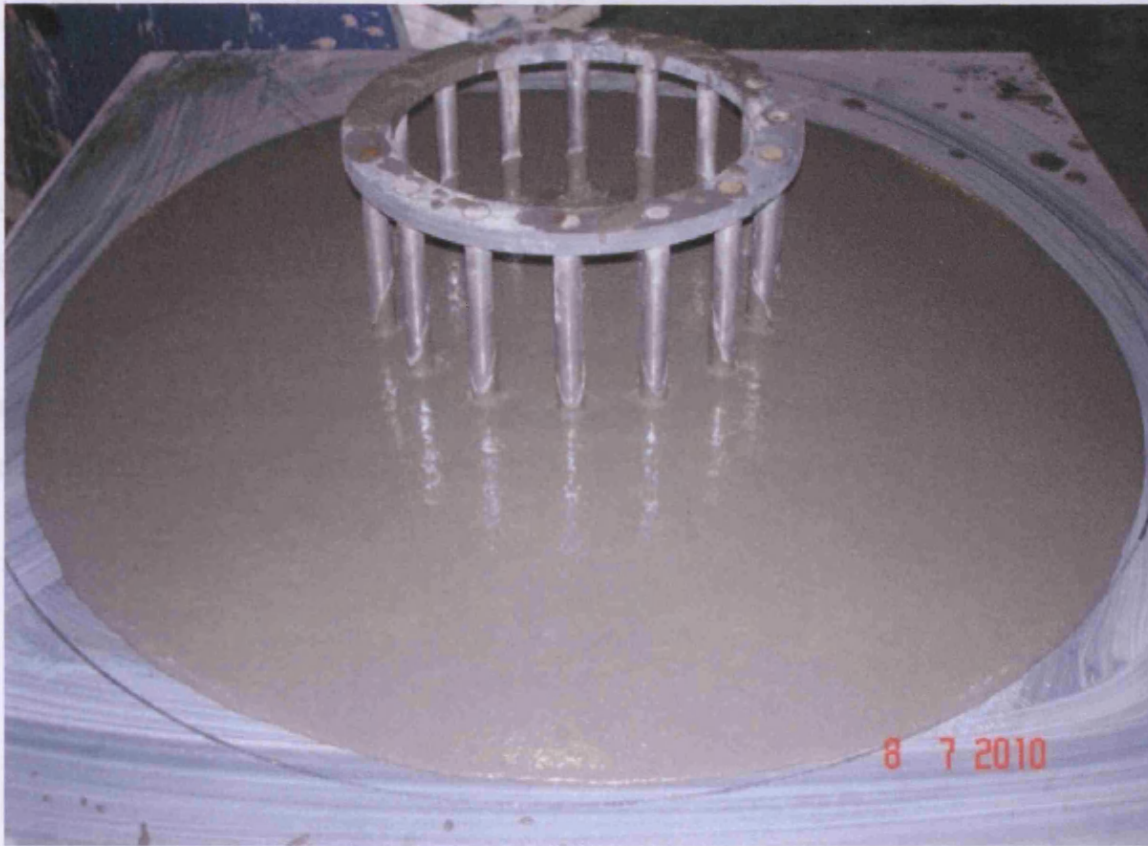
Figure 4.14: Flow and passing ability of SCUHPFRC mix 18

4.4 Concluding remarks

The development of self-compacting high-performance and ultra high-performance concrete mixes is a complex process requiring the resolution of conflicting demands of flow-ability and non-segregation. Whilst these demands can be reconciled by increasing the paste content and decreasing the large aggregate volume, the resulting self-compacting mixes may not reach the target compressive strength. The easiest way to meet the strength requirement is to include steel fibres in the mix. This can however compromise the ability of the mix to flow smoothly through gaps in the reinforcement and to cause segregation of the fibres. The extensive investigations in this chapter led to the following major conclusions.

Self-compacting high- and ultra high-performance concrete mixes without fibres may be designed to satisfy only the flow-ability and cohesiveness criteria using the slump flow test. However, when long steel fibres are present in the mixes, it is additionally

necessary to check that the mixes meet the passing ability criterion using the J-Ring apparatus. It can be concluded that although the mixes with fibres meet the flow-ability and cohesiveness criteria, as judged by the slump flow test, they may not meet the passing ability criterion. These mixes need to be more flow-able than required by the slump flow test, in order to satisfy the passing ability test.

In the next Chapter we shall develop micromechanical models for estimating the plastic viscosity of SCC mixes. In particular, we shall estimate the plastic viscosity of the SCHPC/SCHPFRC and SCUHPC/SCUHPFRC mixes developed above.

Chapter 5

Prediction of the Plastic Viscosity of

Self-Compacting

High and Ultra High

Performance Concretes

With and Without

Steel Fibres

5.1 Introduction

The rheological study of concrete is of prime importance for the construction industry because concrete is placed in its plastic state. This is even more relevant when dealing with a self-compacting concrete (SCC) (Heirman et al., 2008; Petit et al., 2007). However, there is as yet no systematic coverage of this topic in the literature. Part of the reason for this may be the various ranges of particle size used in the concrete industry (as seen in Chapters 2 and 4) and the different devices used (as seen in Chapter 3) to measure the plastic viscosity (Laskar and Talukdar, 2008; Kuder et al., 2007; Westerholm et al., 2008) of the heterogeneous concrete mix.

The plastic viscosity, together with the yield stress of the SCC mix, is needed to study the flow of concrete. The flow of SCC with or without fibres is best described by the Bingham constitutive model. As stated in Chapter 3, this model contains two material properties, namely the yield stress τ_y and the plastic viscosity η. It is known, however, that the yield stress of SCC mixes is very low in comparison with normal concretes. Moreover, the yield stress of SCC mixes remains nearly constant over a large range of plastic viscosities (Dransfield, 2003).

The aim of this chapter is to develop a micromechanical basis for determining the plastic viscosity of self-compacting high and ultra-high performance concretes (SCHPC/SCUHPC) with and without steel fibres (developed in Chapter 4) from the knowledge of the plastic viscosity of the paste alone. The latter can be measured with a reasonable degree of confidence, whereas the measurement of the plastic viscosity of the concrete mix is fraught with many difficulties and inaccuracies, especially when steel fibres are present.

The plastic viscosity of the mixes with and without steel fibres will be estimated from the known plastic viscosity of the cement paste using micromechanical relations. The predictions of this micromechanical approach are shown to correlate very well with available experimental data. Comments will be made on the practical usefulness of the predicted plastic viscosity in simulating the flow of SCCs.

The major part of this Chapter has been published in a journal (see publication 1 in the list in Chapter 1) and also reported at an International Conference (publication 6 in the list).

5.2 Methodology

Micromechanical constitutive models are used to predict the plastic viscosity of self-compacting high and ultra-high performance concretes with and without steel fibres from the measured plastic viscosity of the paste. The viscosity of a homogeneous viscous fluid such as the cement paste can be measured accurately, which cannot be said about non-homogeneous viscous fluids such as SCHPFRC and SCUHPFRC.

The concrete is regarded as a two-phase suspension in which the solid phase is suspended in a viscous liquid phase. The liquid matrix phase consists of cement, water and any viscosity modifying agent (VMA) to which the solids (fine and coarse aggregates and fibres) are added in succession.

The plastic viscosity of this liquid matrix phase is assumed to be known. The increase in plastic viscosity due to the addition of a solid phase (i.e. any cement-replacement materials, fine and coarse aggregates) to this matrix is predicted from the two-phase suspension model. The model is applied in stages; in the first stage, the solid phase is the finest solid material which could be the cement-replacement material in the viscous fluid (cement paste). In the next stage, when the second finest solid (it could be the fine aggregate) is added, the suspension from the first stage is regarded as the continuous fluid matrix phase. This procedure is continued until all the solid phase constituents have been added to make the SCC.

The plastic viscosity of the viscous concrete consisting of the liquid and solid phases is further increased if steel fibres are added to it. The volume fraction of steel fibres is usually small, so that the dilute approximation is sufficient. In order to estimate the effect of the addition of steel fibres, these are treated by the rigid slender-body approximation in a viscous medium (Russel, 1973; Phan-Thien and Huilgol, 1980). The main assumption in this approximation is that the fibres undergo only a rigid body motion in the viscous flow, i.e. translation and rotation, but no elastic deformation (i.e. no bending).

Figure 5.1 shows the hierarchy of these two-phase liquid-solid suspensions used in the estimation of the plastic viscosity of SCC mixes based on the viscosity of the cement paste

used in them. At each stage, the suspension consists of a continuous liquid phase in which is suspended a discrete solid phase.

CRM (S)
Paste (L)

$$\eta_{C1} = \eta_{paste} f_1(\phi_1)$$

Fine sand (S)
Paste+CRM (L)

$$\eta_{C2} = \eta_{C1} f_2(\phi_2)$$

Coarse sand (S)
Paste+CRM+ FS (L)

$$\eta_{C3} = \eta_{C2} f_3(\phi_3)$$

Coarse Aggregate (S)
Paste+CRM+ FS+CS (L)

$$\eta_{C4} = \eta_{C3} f_4(\phi_4)$$

Fibres (S)
Visous concrete (L)

$$\eta = \eta_{C4} f_5(\phi_5)$$
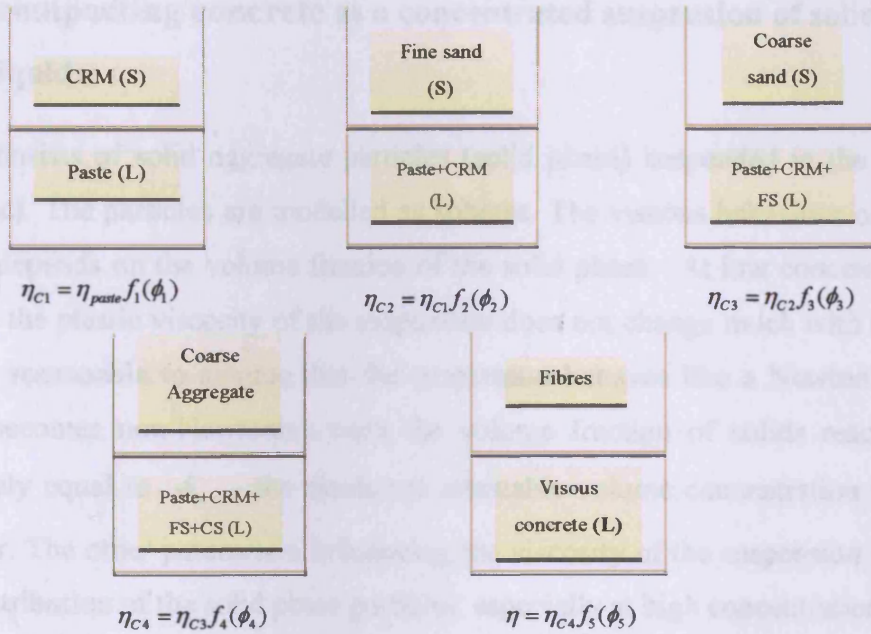
Figure 5.1: Hierarchy of two-phase liquid-solid suspensions constituting a SCC mix with fibres, showing the liquid (L) and solid (S) phases in each suspension

The plastic viscosity of the i-th liquid-solid suspension can be estimated from the plastic viscosity of the preceding $(i-1)$-th phase as follows

$$f_i(\phi_i) = \eta_r = \eta_{Ci} / \eta_{Ci-1} \tag{5.1}$$

with $\eta_{C0} = \eta_{Paste}$ being the known plastic viscosity of the cement paste. For instance, with reference to Figure 5.1, the cement replacement materials form the solid phase in the viscous cement paste in the first liquid-solid suspension. The viscosity of this suspension is calculated from the known viscosity of the cement paste. This process is repeated until all the ingredients of SCC have been accounted for. In the final fluid-solid suspension, the increase in the viscosity induced by a dilute concentration of long steel fibres is estimated. In the following sections the relative viscosity, $f_i(\phi_i)$ (or η_r) which is a function of the volume fraction of solid phase ϕ_i, will be discussed.

5.3 Plastic viscosity of self-compacting concrete without steel fibres

5.3.1 Self-compacting concrete as a concentrated suspension of solid particles in a viscous liquid

The SCC consists of solid aggregate particles (solid phase) suspended in the viscous paste (liquid phase). The particles are modelled as spheres. The viscous behaviour of the resulting suspension depends on the volume fraction of the solid phase. At low concentrations of the solid phase, the plastic viscosity of the suspension does not change much with the shear rate, so that it is reasonable to assume that the suspension behaves like a Newtonian fluid. The behaviour becomes non-Newtonian once the volume fraction of solids reaches a critical value, roughly equal to ϕ_m - the maximum attainable volume concentration which will be defined later. The other parameters influencing the viscosity of the suspension are the shape, size, and distribution of the solid phase particles, especially at high concentrations.

5.3.1.1 Low concentration ($\phi_i < 0.1$)

A low concentration of solid phase is also called dilute, in the sense that the particles are sufficiently far apart from one another, so that the relative motion of the fluid near one particle is unaffected by the presence of the others and the hydrodynamic interaction of the particles can be neglected (Batchelor, 1971). Einstein (see, e.g. Struble and Sun, 1995) was the first to derive the viscosity of a dilute suspension of rigid spheres. He showed that the addition of second phase to a suspension leads to an increase in the bulk viscosity proportional to volume fraction of particles:

$$f_i(\phi_i) = 1 + [\eta]\phi_i \qquad (5.2)$$

$f_i(\phi_i)$ is the relative viscosity, i.e. ratio of viscosity of the suspension (mortar or concrete) to that of the liquid phase (cement paste), ϕ_i is the volume concentration of particles, and $[\eta]$ is the intrinsic viscosity which is a measure of the effect of individual particles on the viscosity (Struble and Sun, 1995).

$$[\eta] = \lim_{\phi_i \to 0} \frac{f_i(\phi_i) - 1}{\phi_i} \qquad (5.3)$$

A value of $[\eta] = 2.5$ is adopted when the particles are rigid and packed randomly in a hexagonal arrangement, and the distance between them compared to the mean particle diameter is large. It is also important that the movement of the particles is sufficiently slow so that their kinetic energy can be neglected.

Einstein's equation has been widely used by other researchers in this field even at higher volume concentrations of particles. Ford (as stated by Shenoy, 1999) modified Einstein's equation using a binomial expression:

$$f_i(\phi_i) = (1 - [\eta]\phi_i)^{-1} \tag{5.4}$$

As reported by Utracki (2003), Simha (1952) modified Einstein's relation to read $f_i(\phi_i) = 1 + 2.5 f(a_1)\phi_i$, where $f(a_1)$ is the so-called shielding factor, by using a cage model and a reduced volume fraction, ϕ_i / ϕ_m, where ϕ_m is the maximum packing fraction. In this model each solid spherical particle of radius a is placed inside a spherical enclosure (cage) of radius b. A simplified version of the resulting equation for a low volume concentration can be written as:

$$f_i(\phi_i) = 1 + 2.5\phi_i \left[1 + \frac{25}{32}\left(\frac{\phi_i}{\phi_m}\right) - \frac{21}{64}\left(\frac{\phi_i}{\phi_m}\right)^{\frac{5}{3}} + \frac{625}{128}\left(\frac{\phi_i}{\phi_m}\right)^2 + \ldots \right] \tag{5.5}$$

Based on the Simha calculation for concentrated suspensions, Thomas arrived at the following relation for dilute suspensions (as cited by Shenoy, 1999):

$$f_i(\phi_i) = 1 + 2.5\phi_i \left(1 + \frac{25\phi_i}{4a_1^3} \right) \tag{5.6}$$

For low volume fractions, $a_1 = 1.111$.

5.3.1.2 High concentration $(0.1 < \phi_i < \phi_m)$

At higher volume concentrations of particles, the volume fraction is not the only parameter that influences the viscosity. It is now necessary to consider the size and type of particles used and their hydrodynamic interaction. The general expression of the viscosity can be written as

(Shenoy, 1999; Utracki, 2003; Barnes et al., 1993; Mittal and Kumar, 1999; Gupta, 2000; Willis and Acton, 1976)

$$f_i(\phi_i) = 1 + [\eta]\phi_i + B\phi_i^2 + C'\phi_i^3 + \dots \tag{5.7}$$

where B (in some references this is called Huggins coefficient) and C are very sensitive to the structure of suspension. Tables 5.1 and 5.2 give the values of constants B and C that have been reported in the literature (Shenoy, 1999; Willis and Acton, 1976; Batchelor, 1977; Guth and Simha, 1936; Vand, 1948; Saito, 1950).

Table 5.1: Different values for parameter B available in the literature

Reference	Shenoy, 1999	Shenoy, 1999	Willis and Acton, (1976)	Batchelor, (1977)	Guth and Simha, (1936)	Vand, (1948)	Saito, (1950)	de Kruif, (1985)
B value	10.05	6.25	4.84	6.2	14.1	7.35	12.6	6

Table 5.2: Different values for parameter C available in the literature

Reference	Shenoy, 1999	Vand, (1948)	de Kruif, (1985)
C value	15.7	16.2	35

The variation in the cited values of parameters B and C is the result of taking into account one or several effects appearing due to the increase in solid concentration.

Thomas (as stated by Mittal and Kumar, 1999) suggested that the C term in (5.7) could be replaced by an exponential term

$$f_i(\phi_i) = 1 + 2.5\phi_i + 10.05\phi_i^2 + 0.00273 \exp(16.6\phi_i) \tag{5.8}$$

because the resulting expression fits the experimental data very well in the range of $\phi_i = 0.15 - 0.60$.

In view of the uncertainties in the parameters B and C, Krieger and Dougherty (1959), and others, have used the concept of maximum packing fraction, ϕ_m for a better description of the suspensions. ϕ_m corresponds to the situation in which the particles have the minimum possible separation, i.e. the void fraction (porosity) is the least and the viscosity is infinite.

The value is 0.74 for hexagonal closed packing, 0.637 for random hexagonal packing and 0.524 for cubic packing (Shenoy, 1999).

Krieger and Daugherty (1959) proposed a generalized version of Einstein's equation; they used the maximum packing volume fraction and intrinsic viscosity parameter to a non-Newtonian suspension of rigid spheres. Ball and Richmond (as stated by Barnes et al., 1993) used the results of Krieger and Dougherty but simplified their complex mathematics conceptually based on Einstein's equation.

It starts from an averaging technique such that the effect of all the particles in a concentrated suspension is the sum of the effects of particles added successively. Therefore the Einstein equation (5.2) can be written in a differential form as:

$$df_i(\phi_i) = [\eta]d\phi_i \tag{5.9}$$

They have pointed out that this neglects the correlations between spheres due to their finite size. This means that when a particle is added to a relatively concentrated suspension it requires more space than its volume $d\phi_i$, due to packing difficulties. Therefore $d\phi_i$ has to be replaced by $d\phi_i/(1-K\phi_i)$, where K is the so-called crowding factor.

The viscosity of the final suspension is then obtained by integrating the phase volume between 0 and ϕ_i. This gives:

$$f_i(\phi_i) = (1-K\phi_i)^{-[\eta]K} \tag{5.10}$$

From this equation it can be seen that the viscosity becomes infinite when $\phi_i = 1/K$. Thus one can replace $1/K$ by the maximum packing fraction ϕ_m. The Krieger-Dougherty equation is:

$$f_i(\phi_i) = \left(1 - \frac{\phi_i}{\phi_m}\right)^{-[\eta]\phi_m} \tag{5.11}$$

ϕ_m is strongly dependent on the particle size distribution. Also, the intrinsic viscosity $[\eta]$ and ϕ_m depend upon the shear rate; the former tends to decrease with increasing shear rate whereas the latter shows the opposite trend. However $[\eta]$ and ϕ_m change in such a way that

an increase in the one leads to a decrease in the other, but the product of the two changes remains practically the same and equal, on average, to 1.92 for rigid spheres (de Kruif et al., 1985).

It should be noted that the Krieger and Dougherty equation (5.11) has been successfully tested by Struble and Sun (1995) on cement paste.

Frankel and Acrivos (1967) derived theoretically an equation for the viscosity of a very high concentration of solid spheres in suspension, i.e. when $\phi_i \to \phi_m$:

$$f_i(\phi_i) = \frac{9}{8} \left(\frac{(\phi_i / \phi_m)^{\frac{1}{3}}}{1 - (\phi_i / \phi_m)^{\frac{1}{3}}} \right) \tag{5.12}$$

As reported by Shenoy (1999), their aim was to derive an expression to complement Einstein's equation for dilute suspension. This equation fits the experimental data for high volume fraction of solid particles rather well:

Chong et al. (1971) obtained a single expression to cover the entire range of volume concentrations from $\phi_i \to 0$ to $\phi_i \to \phi_m$ which fits the experimental data well

$$f_i(\phi_i) = \left(1 + \frac{[\eta]\phi_m}{2} \left[\frac{\phi_i / \phi_m}{1 - (\phi_i / \phi_m)} \right] \right)^2 \tag{5.13}$$

They added direct Brownian contribution to the viscosity in the range of $\phi_i / \phi_m \le 0.7$ because it leads to a slight increase in the relative viscosity. However, it should be mentioned that the Brownian contribution can be neglected at higher volume fractions, as confirmed theoretically by Ball and Richmond (as stated by Barnes et al., 1993). Equation (5.13) reduces to Einstein's equation (5.2) at low volume fractions.

The drawbacks of applying the ϕ_m based relations to predict the plastic viscosity of concrete are twofold; firstly, due to the difficulties faced in the measurement of viscosity when ϕ_i is large ($\phi_i \to \phi_m$). Secondly, it is difficult to determine the maximum volume fraction accurately because of the swelling in particles, adsorbed surface, etc (e.g. Ball & Richmond in Barnes et al., 1993).

5.3.2 Are the expressions for the viscosity of a suspension of solid particles in a viscous fluid applicable to cement paste?

The theoretical expressions discussed in the previous Section are generally applicable to a suspension of solid particles in a viscous fluid at low shear rates. As previously mentioned the Krieger and Dougherty equation (5.11) has been used successfully on Portland cement paste and fits the data well (Struble and Sun, 1995). If the concrete in its fresh state is assumed to be an isotropic material then the theory applicable at low shear rates has been demonstrated experimentally by Barnes et al. (1993) to be applicable also at high shear rates. They have combined the data from Krieger (1959) and de Kruif et al. (1985) for zero and infinite shear rates and fitted these data to (5.11) as shown in Figure 5.2.
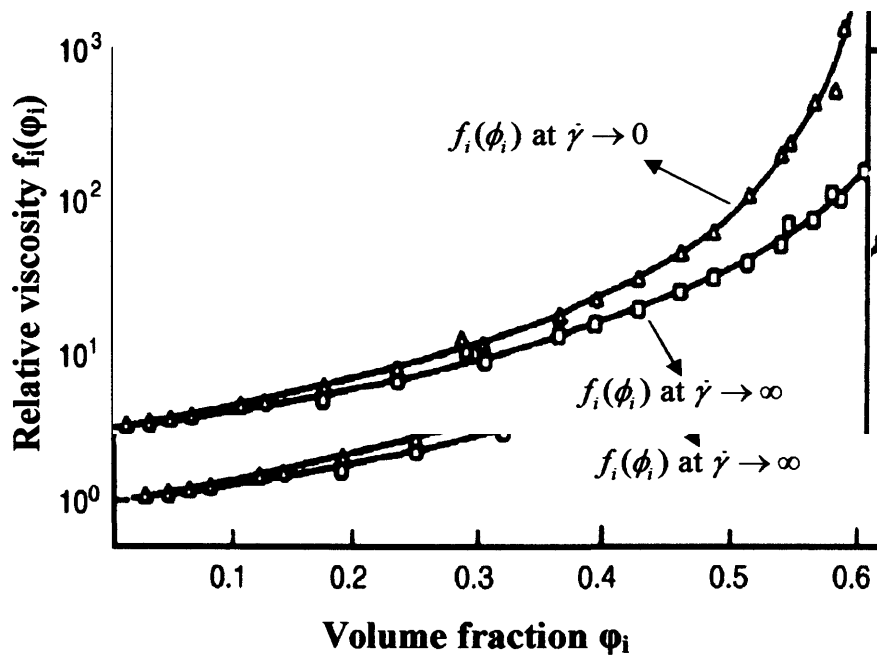
Figure 5.2: Dependency of relative viscosity on the shear rate in a suspension at zero and infinite shear rates and fit to the Krieger and Dougherty equation (After Struble and Sun, 1995)

The effect of shear rate is to alter the packing arrangement. Thus, whilst the packing is random hexagonal at low shear rates, it becomes more and more like closed hexagonal at high rates. The densification of packing at high shear rates is associated with shear thinning such that the product $[\eta]\phi_m$ is constant and equal to about 1.92. It is clear however from Figure 5.2 that the shear rate has little influence for volume fractions less than $\phi_i = 0.4$. However, for

comparison with test data which have been obtained at high shear rates, the values of $[\eta]$ and

ϕ_m corresponding to the lower curve in Figure 5.2 will be used later.

All the above mentioned equations for high volume fraction of particles have been the subject
of experimental verification, some of them even on cement-based materials (e.g. Struble and
Sun, 1995). They give similar predictions in the range of $0.1 < \phi_i < 0.4$ with only the Frankel
and Acrivos (1967) equation deviating slightly from the rest (Figure 5.3).
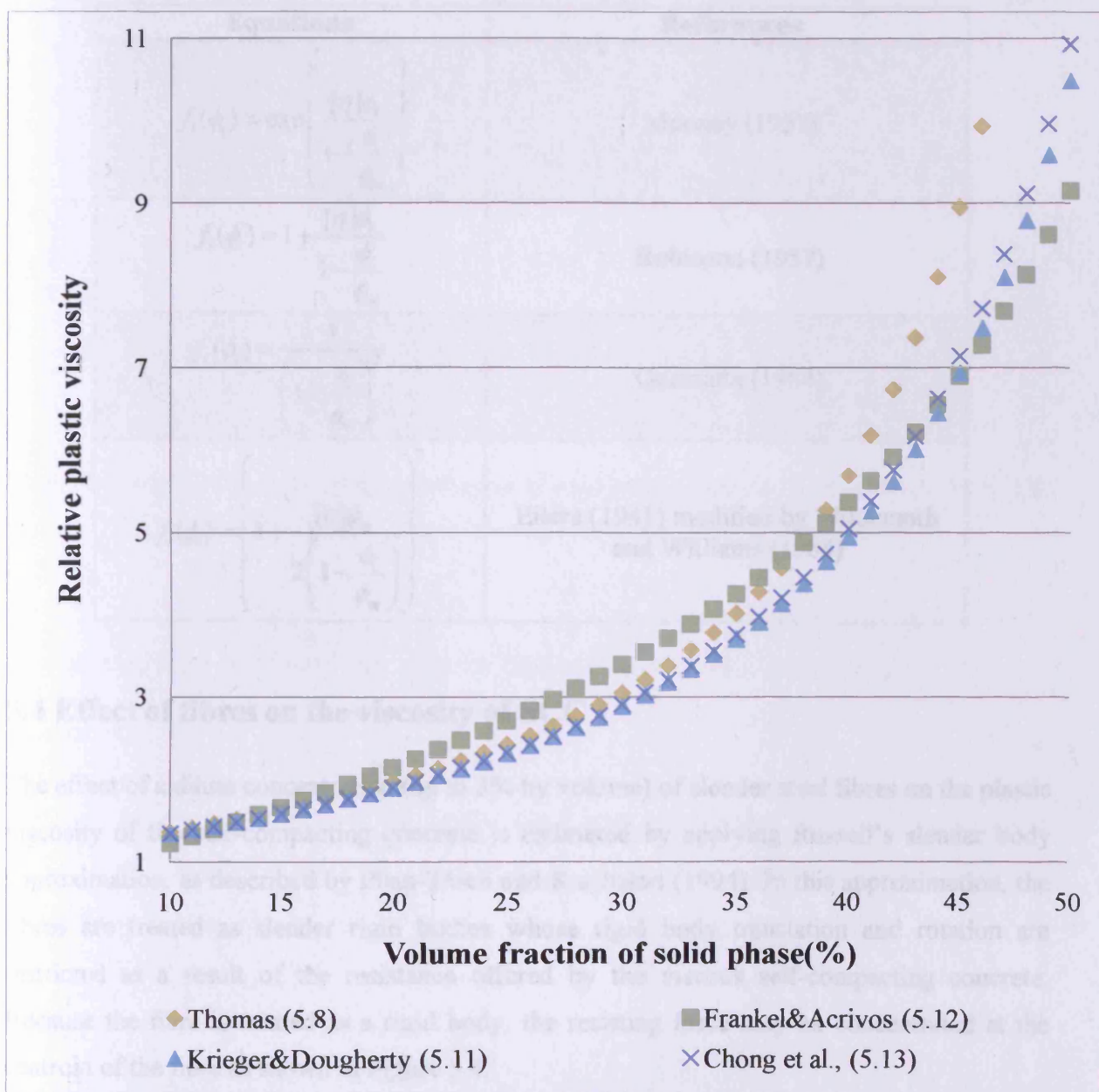
Figure 5.3: Comparison of different formulas for high volume fraction of spherical particles
with ϕ_m=0.708 and $[\eta]$=2.71

Other attempts to derive the viscosity of suspensions based on volume concentration of solid particles are summarised in Table 5.3.

Table 5.3: Equations of the viscosity of suspensions based on volume concentration of solid particles

Equations	References
$f_i(\phi_i) = \exp\left(\dfrac{[\eta]\phi_i}{1 - \dfrac{\phi_i}{\phi_m}}\right)$	Mooney (1957)
$f_i(\phi_i) = 1 + \dfrac{[\eta]\phi_i}{1 - \dfrac{\phi_i}{\phi_m}}$	Robinson (1957)
$f_i(\phi_i) = \dfrac{1}{\left(1 - \dfrac{\phi_i}{\phi_m}\right)^2}$	Quemada (1984)
$f_i(\phi_i) = \left(1 + \dfrac{[\eta]\phi_m}{2\left(1 - \dfrac{\phi_i}{\phi_m}\right)}\right)^2$	Eilers (1941) modified by Wildemuth and Williams (1984)

5.4 Effect of fibres on the viscosity of SCC

The effect of a dilute concentration (up to 3% by volume) of slender steel fibres on the plastic viscosity of the self-compacting concrete is estimated by applying Russell's slender body approximation, as described by Phan-Thien and Karihaloo (1994). In this approximation, the fibres are treated as slender rigid bodies whose rigid body translation and rotation are restricted as a result of the resistance offered by the viscous self-compacting concrete. Because the fibre is treated as a rigid body, the resisting force may be concentrated at the centroid of the fibre as shown in Figure 5.4.
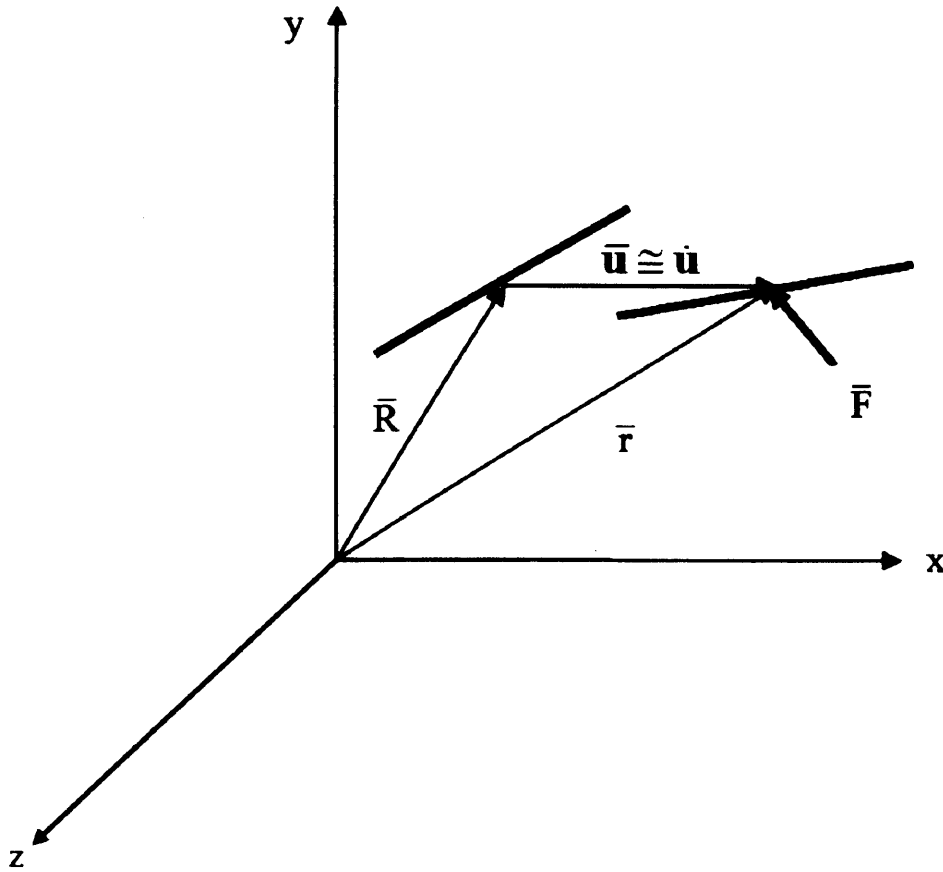
Figure 5.4: Rigid body translation and rotation of a single fibre resisted by the viscous SCC. The resistive concentrated force (F) is shown at the centroid of the fibre

The resisting force components are given by (Phan-Thien and Karihaloo, 1994)

$$F_i = \zeta \dot{u}_i \tag{5.14}$$

where $\dot{u}_i$ are the components of the displacement rate (i.e. velocity) of the fibre centroid in the x, y and z directions, and ζ depends on the viscosity of concrete, the length of fibre and its aspect ratio. It is given by:

$$\zeta = \frac{2\pi\eta l}{\ln(2l_d)} \tag{5.15}$$

where η is the plastic viscosity of the mix without fibres, and l is the length of the fibre with l_d its aspect ratio.

The effective stress tensor of a dilute suspension can be written as the contribution from the matrix and the fibre fabric tensor. The fibre fabric tensor depends upon the number of fibres. The effective stress tensor of the viscous suspension with matrix designated m and fibre f is:

$$\langle \sigma_{ij} \rangle = (1 - \phi_f)\langle \sigma_{ij} \rangle_m + \langle \sigma_{ij} \rangle_f \qquad (5.16)$$

where ϕ_f is the volume fraction of fibres and the angular brackets represent the ensemble average.

5.4.1 Replacing ensemble average by volume average

For a statistically homogeneous and random distribution of a dilute concentration of fibres in the viscous matrix such that the fibres are unlikely to overlap (Figure 5.5), the ensemble average can be replaced by the volume average over a representative volume element (RVE). Therefore, the ensemble average used in (5.16) can be replaced by its equivalent volume average, so that the bulk stress for a representative volume element is changed to:

$$\langle \sigma_{ij} \rangle = \frac{1}{V} \int_V \sigma_{ij} dv \qquad (5.17)$$
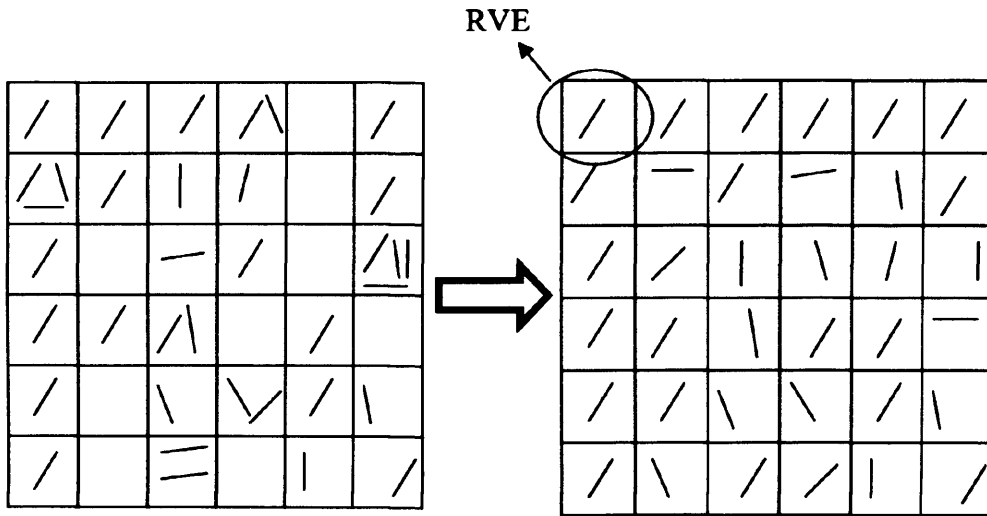
Figure 5.5: The ensemble average can be replaced by volume average if the fibres are homogeneously and randomly distributed

Equation (5.17) consists of two parts, i.e. the matrix part

$$\langle \sigma_{ij} \rangle_m = \frac{1}{V} \int_{V_m} \sigma_{ij} dv$$

and the fibre part

$$\langle \sigma_{ij} \rangle_f = \frac{1}{V} \int_{V_f} \sigma_{ij} dv.$$

If volume of a single fibre is V_α, then $V_f = \sum_\alpha V_\alpha$. Therefore, the fibre contribution to the stress tensor can be written as

$$\langle \sigma_{ij} \rangle_f = \frac{1}{V} \sum_\alpha \int_{V_\alpha} \sigma_{ij} dv \tag{5.18}$$

With reference to Figure 5.4, if the body force and inertia effects are neglected then it can be shown that

$$\sigma_{ij} = \left(\sigma_{ik} x_j \right)_{,k} \tag{5.19}$$

where a comma denotes the covariant derivative. Therefore, (5.18) can be rewritten as

$$\langle \sigma_{ij} \rangle_f = \frac{1}{V} \sum_\alpha \int_{V_\alpha} \left(\sigma_{ik} x_j \right)_{,k} dv \tag{5.20}$$

Applying the divergence theorem (Gauss theorem) on (5.20) yields

$$\langle \sigma_{ij} \rangle_f = \frac{1}{V} \sum_\alpha \int_{A_\alpha} x_j \sigma_{ik} n_k dA \tag{5.21}$$

The integral is taken over the fibre surface area and the sigma sign represents the summation over the total number of fibres in the statistically homogeneous volume V. By definition, $x_j \sigma_{ik} n_k$ is traction force and it can be written as $\overline{Fr}$. Therefore (5.21) becomes

$$\langle \sigma_{ij} \rangle_f = \frac{1}{V} \sum_\alpha \int_{A_\alpha} \overline{Fr} ds \tag{5.22}$$

where A_α, $\overline{\mathbf{F}}$ and $\overline{\mathbf{r}}$ denote the fibre surface area, the traction force and the position vector of the centroid of the fibre in the deformed configuration (distance from origin of xyz coordinate system, Figure 5.4), respectively.

There is no guarantee that the fibre tractions are symmetric, i.e. $F_i r_j \neq r_i F_j$, therefore, the fibre fabric tensor is averaged over the total number of fibres

$$\langle \sigma_{ij} \rangle_f = \frac{N}{2} \langle F_i r_j + r_i F_j \rangle \qquad (5.23)$$

where N is the number of fibres, r_i are the components of the position vector of the centroid in the deformed configuration (see Figure 5.4), and angular brackets denote volume average.

5.4.2 Random distribution of fibres

Let us consider two fibres with unit vectors p_i and p_j along their length, and require that the product be

$$p_i p_j = A \delta_{ij} \qquad (5.24)$$

where δ_{ij} is the Kronecker delta. This requirement is consistent with the assumption of a dilute suspension of fibres i.e. $\phi_f \ll 1$ so that at no instant is there a situation when two fibres overlap each other.

In order to find the value of the constant A, let us set $i = j$, then the left hand side of (5.24) is equal to one, because it is a multiplication of a matrix by its transpose. Thus, $A = 1/3$. Finally for a random distribution of fibres

$$\langle p_i p_j \rangle = \frac{1}{3} \delta_{ij} \qquad (5.25)$$

This ensures that the fibre contribution is isotropic.

5.4.3 Calculation of the fibre fabric tensor

If components of the traction forces applied on the fibres are known (i.e. $F_i r_j$ or $r_i F_j$) then the fibre fabric tensor can be determined using (5.23). First, note that the displacement rate components ($\dot{u}_i$) in (5.14) can be written as

$$\dot{u}_i = l \dot{\varepsilon}_{ij} p_j \qquad (5.26)$$

where $\dot{\varepsilon}_{ij}$ is the strain rate tensor. Also from Figure 5.4

$$r_i = \dot{u}_i + R_i \qquad (5.27)$$

Because $p_i = \delta_{ij} p_j$ and $R_i = l p_i$, (5.27) can be rearranged using (5.26) as

$$r_i = l \left(\delta_{ij} + \dot{\varepsilon}_{ij} \right) p_j \qquad (5.28)$$

Substitution of (5.15) into (5.14) and the application of (5.28) gives the components of (5.23)

$$F_i r_j = \frac{2\pi \eta l^3}{\ln(2 l_d)} \dot{\varepsilon}_{ik} p_k p_j \qquad (5.29)$$

$$F_j r_i = \frac{2\pi \eta l^3}{\ln(2 l_d)} \dot{\varepsilon}_{jk} p_k p_i \qquad (5.30)$$

Substituting (5.29) and (5.30) into (5.23) yields

$$\left\langle \sigma_{ij} \right\rangle_f = \frac{N \pi \eta l^3}{\ln(2 l_d)} \left\langle \dot{\varepsilon}_{ik} p_k p_j + \dot{\varepsilon}_{jk} p_k p_i \right\rangle \qquad (5.31)$$

By definition, the volume fraction of fibres is

$$\phi_f = N a l \qquad (5.32)$$

where a is the fibre cross-sectional area and l its length.

Also, the aspect ratio can be estimated as

$$l_d = \frac{l}{\sqrt{a}} \qquad (5.33)$$

Therefore (5.32) gives

$$Nl^3 = \phi_f l_d^2 \tag{5.34}$$

Finally, (5.31) can be written as

$$\left\langle \sigma_{ij} \right\rangle_f = \frac{\pi \eta \phi_f l_d^2}{\ln(2l_d)} \left\langle \dot{\varepsilon}_{ik} p_k p_j + \dot{\varepsilon}_{jk} p_k p_i \right\rangle \tag{5.35}$$

As demonstrated by (5.25) for random distribution of fibres $\left\langle p_i p_j \right\rangle = \frac{1}{3} \delta_{ij}$, (5.35) can be simplified as

$$\left(\sigma_{ij} \right)_f = \frac{\pi \eta \phi_f l_d^2}{3\ln(2l_d)} \left(\dot{\varepsilon}_{ji} + \dot{\varepsilon}_{ij} \right) \tag{5.36}$$

$\left(\dot{\varepsilon}_{ji} + \dot{\varepsilon}_{ij} \right)$ can be replaced by the equivalent "engineering" shear rate $\dot{\gamma}_{ij}$, giving

$$\left(\sigma_{ij} \right)_f = \frac{\pi \eta \phi_f l_d^2}{3\ln(2l_d)} \dot{\gamma}_{ij} \tag{5.37}$$

Thus the effective stress tensor (5.16) of the viscous suspension can be written as

$$\left(\sigma_{ij} \right) = \left(1 - \phi_f\right)\left(\sigma_{ij} \right)_m + \frac{\pi \eta \phi_f l_d^2}{3\ln(2l_d)} \dot{\gamma}_{ij} \tag{5.38}$$

The above tensor is isotropic. In particular, the shear stress components are related to the shear rates. In view of isotropy, we can, for example, write

$$\sigma_{xy} \equiv \tau = \left(1 - \phi_f\right)\eta \dot{\gamma}_{xy} + \frac{\pi \eta \phi_f l_d^2}{3\ln(2l_d)} \dot{\gamma}_{xy} \tag{5.39}$$

The other two shear stress components are likewise related to the corresponding shear rates. We may therefore drop the suffixes and write the effective viscosity of the suspension with fibres, $\tau / \dot{\gamma}$ as

$$\eta_e = \eta \left\{ \left(1 - \phi_f\right) + \frac{\pi \phi_f l_d^2}{3\ln(2l_d)} \right\} \tag{5.40}$$

The second term on the right hand side is the contribution of the fibres to the plastic viscosity of the mix without fibres. It is clear that this contribution increases linearly with the volume fraction of fibres. The effect of the aspect ratio on this contribution is more complex, as will be demonstrated below.

5.5 Comparison of the proposed formulae with test results

Extensive experimental work has been done on self-compacting fibre reinforced concretes by Grünewald and Walraven (2003) who used a BML rheometer to measure the viscosity of many mixes. Here only the first seven optimised series (OS) of their mixes have been used and their measured plastic viscosity compared with the predictions. The mix proportions can be found in Appendix B. Some of the main parameters were as follows: the size of coarse aggregate varied from 4 to 16mm and that of sand from 0.125 to 4mm, paste volume from 34 to 39%, paste solid content from 53 to 55.7%, water to cement ratio from 0.42 to 0.47. Four types of Dramix steel fibre (RC and RL types) were used with aspect ratios of 46.3, 64.9, 78.5 and 85.7 in concentrations of 80, 100, 120 and 140 kg/m^3 in the mix. The fibres replaced the aggregates so that the ratio of sand to total aggregate remained constant.

5.5.1 Plastic viscosity of cement paste

The plastic viscosity of the paste used in each of the seven SCC mixes (Grünewald and Walraven, 2003) is estimated from the data available in the literature that most closely approximates the actual paste used in the mix. It should be mentioned that the plastic viscosity of cement paste is affected by the type and dosage of superplasticiser (Lachemi et al., 2004; Mikanovic and Jolicoeur, 2008; Cyr et al., 2000), type of cement additives (Cyr et al., 2000; Ferraris et al., 2001b), mixing sequence and time (Aiad et al., 2002; Fernàndez-Altable and Casanova, 2006; Williams et al., 1999), besides the main factors, i.e. the water to cement ratio and amount of superplasticiser in relation to cement and water used. It appears that there is a threshold to the amount of superplasticiser beyond which the plastic viscosity of the paste actually drops. The plastic viscosity of the paste has been estimated from the data in the literature (Lachemi et al., 2004; Chindaprasirt et al., 2008; Sun et al., 2006; Grzeszczyk and Lipowski, 1997; Nehdi and Rahman, 2004; Zhang and Han, 2000); the estimated plastic viscosity of the paste is shown in Table 5.4, based on the paste content, paste solid content (%) and water to cement ratio.

In view of the fact that the main factors that control the viscosity of the cement paste, enumerated above, vary only marginally in the seven mixes, it is not surprising that the plastic viscosity of the pastes also varies marginally.

Table 5.4: Estimated plastic viscosity of the paste. The superplasticiser to water ratio is 0.02 (0.03 for Mix3) and the superplasticiser to cement ratio is 0.01

Paste property	Mix1	Mix2	Mix3	Mix4	Mix5	Mix6	Mix7
Paste content (%)	36.5	39.0	36.5	39.0	34.0	36.5	39.0
Paste solid content (%)	53.0	53.7	53.0	53.7	54.5	55.1	55.7
Water/cement	0.42	0.44	0.43	0.44	0.46	0.47	0.47
Plastic viscosity (Pas)	0.44	0.43	0.43	0.43	0.39	0.40	0.41

5.5.2 Plastic viscosity of self-compacting fibre reinforced concrete

Once the plastic viscosity of the paste has been estimated, the increase in the plastic viscosity due to the addition of a solid phase (i.e. cement-replacement materials, fine and coarse aggregates) to this paste is predicted from the above two-phase suspension model. The model is applied in stages (see Figure 5.1); in the first stage, the solid phase is the finest solid material which is the cement-replacement material in the viscous fluid (cement paste). In the next stage when the second finest solid (i.e. fine aggregate) is added, the suspension from the first stage is regarded as the continuous fluid matrix phase. This procedure is continued to until all the constituents used in the aforementioned SCC mixes have been taken into account. The plastic viscosity increase in SCC relative to the fluid phase without fibres is thus:

$$f_i(\phi_i) = f_1(\phi_1) f_2(\phi_2) \dots f_n(\phi_n) \tag{5.41}$$

$$\phi_i = \frac{v_i}{v_i + v_0} \tag{5.42}$$

where

n: total number of solid phases in the mix, such as coarse aggregate, sand, and cement additives;

v_i: volume of solid phase i;

v_0: volume of the continuous matrix phase in which the solid phase i is suspended;

$f_i(\phi_i)$: one of the several two-phase relations introduced in Section 5.3.1.

Finally, to obtain the plastic viscosity of SCC with steel fibres, the result of the application of (5.41) to the SCC mix is used in (5.40). Here, the Krieger and Dougherty equation (5.11) will be used as the function $f_i(\phi_i)$ in (5.41) because it has been found to be the most suitable for cement-based mixes (Struble and Sun, 1995). The values of $[\eta] = 2.5$ and $\phi_m = 0.63$ were

used in this study. There are in fact thirty seven different mix combinations formed from the seven basic mixes (Grünewald, 2004), depending upon the fibre type, fibre content and aspect ratio, as shown in Table 5.5 below. We have also introduced two fibre parameters, $\phi_f l_d^2$ and $1/\ln(2l_d)$ as they appear in (5.40).

Table 5.5: Mix combinations based on the seven base mixes and the first and second fibre parameters; $\phi_f l_d^2$ and $1/\ln(2l_d)$

Mix Designation	No.	Sub-mixes by fibre type, content (kg/m³) and aspect ratio	$\phi_f l_d^2$	$1/\ln(2l_d)$	Measured plastic viscosity (Pas)	Predicted plastic viscosity (Pas)	Error (%)
OS 1-57.0/36.5 (Mix1)	1	D-45/30,80,46.3	21.99	0.22	109.90	99.85	10.1
	2	D-45/30,100,46.3	27.48	0.22	137.50	119.39	15.2
	3	D-80/30 BP,40,78.5	31.60	0.20	116.80	126.67	-7.8
	4	D-80/30 BP,60,78.5	47.40	0.20	167.80	179.64	-6.6
	5	D-80/60 BP,40,85.7	37.66	0.19	122.90	145.53	-15.6
OS 2-57.0/39.0 (Mix2)	6	D-80/30 BP,60,78.5	47.40	0.20	171.10	149.24	14.6
	7	D-80/30 BP,80,78.5	63.20	0.20	223.20	192.39	16.0
	8	D-80/60 BP,40,85.7	37.66	0.19	98.60	120.83	-18.4
	9	D-80/60 BP,60,85.7	56.50	0.19	159.90	172.49	-7.3
OS 3-68.0/36.5 (Mix3)	10	D-80/30 BP,40,78.5	31.60	0.20	143.10	146.80	-2.5
	11	D-80/30 BP,60,78.5	47.40	0.20	199.30	207.85	-4.1
	12	D-80/60 BP,40,85.7	37.66	0.19	124.30	154.58	-19.6
OS 4-68.0/39.0 (Mix4)	13	D-45/30,120,46.3	32.98	0.22	117.50	128.08	-8.3
	14	D-45/30,140,46.3	38.48	0.22	145.70	145.27	0.3
	15	D-45/30,160,46.3	43.97	0.22	176.10	162.05	8.7
	16	D-65/40,100,64.9	54.00	0.21	182.40	189.69	-3.8
	17	D-65/40,120,64.9	64.80	0.21	221.10	222.05	-0.4
	18	D-80/30 BP,60,78.5	47.40	0.20	156.50	166.40	-6.0
	19	D-80/30 BP,80,78.5	63.20	0.20	245.30	214.27	14.5
	20	D-80/60 BP,80,85.7	75.33	0.19	199.70	248.43	-19.6
OS 5-68.0/34.0 (Mix5)	21	D-45/30,100,46.3	27.48	0.22	245.30	206.67	18.7
	22	D-45/30,120,46.3	32.98	0.22	280.30	239.05	17.3
	23	D-80/30 BP,40,78.5	31.60	0.20	195.80	221.20	-11.5
	24	D-80/30 BP,60,78.5	47.40	0.20	326.20	312.77	4.3
OS 6-68.0/36.5 (Mix6)	25	D-45/30,120,46.3	32.98	0.22	211.50	181.26	16.7
	26	D-80/30 BP,60,78.5	47.40	0.20	266.80	236.21	12.9
	27	D-80/30 BP,80,78.5	63.20	0.20	344.20	303.85	13.3
	28	D-80/60 BP,40,85.7	37.66	0.19	182.80	191.67	-4.6
	29	D-80/60 BP,60,85.7	56.50	0.19	301.80	273.01	10.5
OS 7-68.0/39.0 (Mix7)	30	D-45/30,120,46.3	32.98	0.22	157.10	147.71	6.4
	31	D-45/30,140,46.3	38.48	0.22	204.40	171.23	19.4
	32	D-65/40,80,64.9	43.20	0.21	155.20	180.56	-14.0
	33	D-65/40,100,64.9	54.00	0.21	206.10	218.77	-5.8
	34	D-80/30 BP,60,78.5	47.40	0.20	209.10	191.94	8.9
	35	D-80/30 BP,80,78.5	63.20	0.20	306.10	255.68	19.7
	36	D-80/60 BP,60,85.7	56.50	0.19	224.80	221.84	1.3
	37	D-80/60 BP,80,85.7	75.33	0.19	233.10	286.55	-18.7

5.5.3 Comparison of the predicted and measured plastic viscosity with respect to first fibre parameter $\phi_f l_d^2$

Figure 5.6 compares the measured and predicted variation of the plastic viscosity of SCFRC as a function of the first fibre parameter, $\phi_f l_d^2$ for all the seven base mixes (Grünewald, 2004).

Figure 5.6: Continued

Mix 3

Mix 4

Figure 5.6: Continued

Mix 5

Mix 6
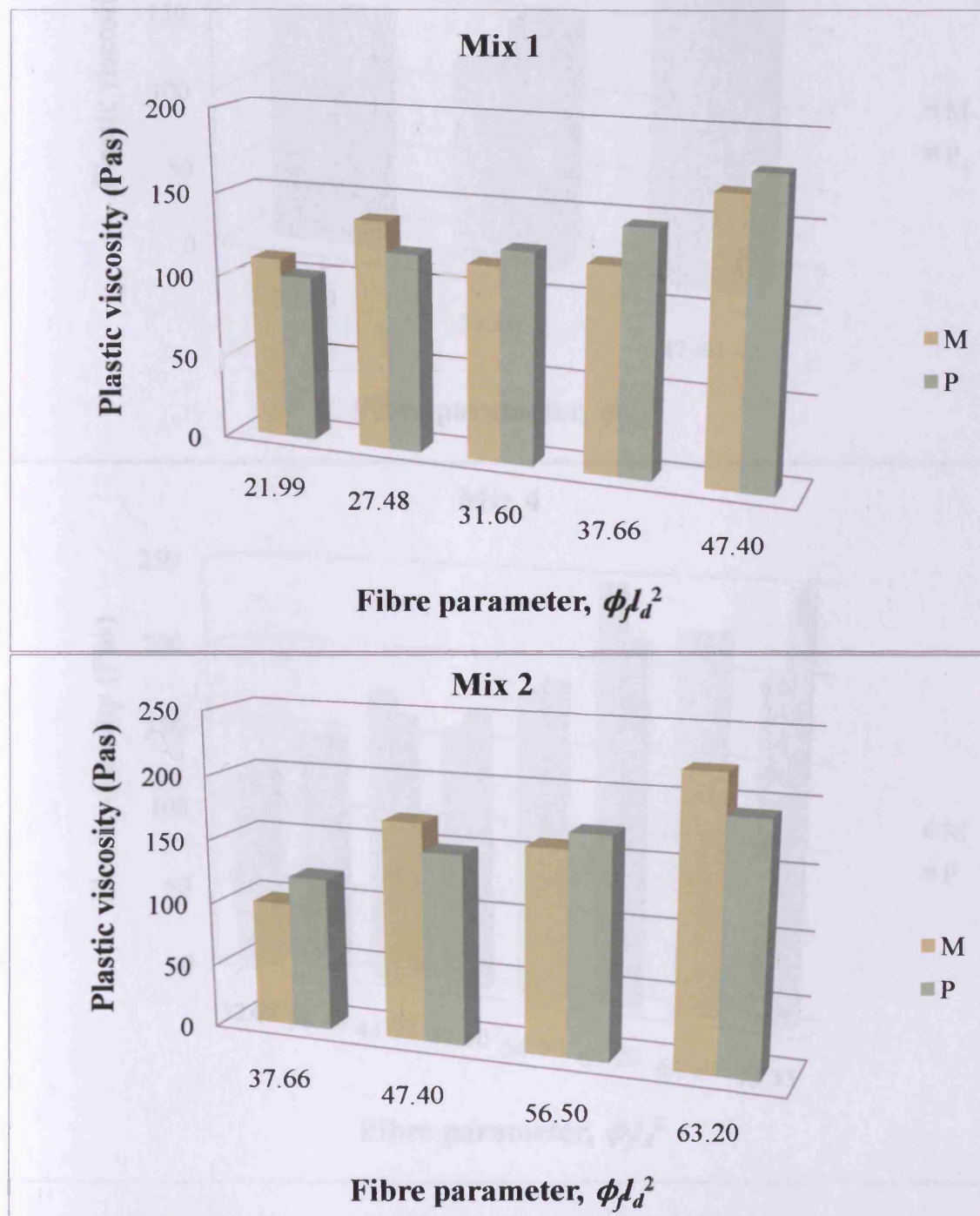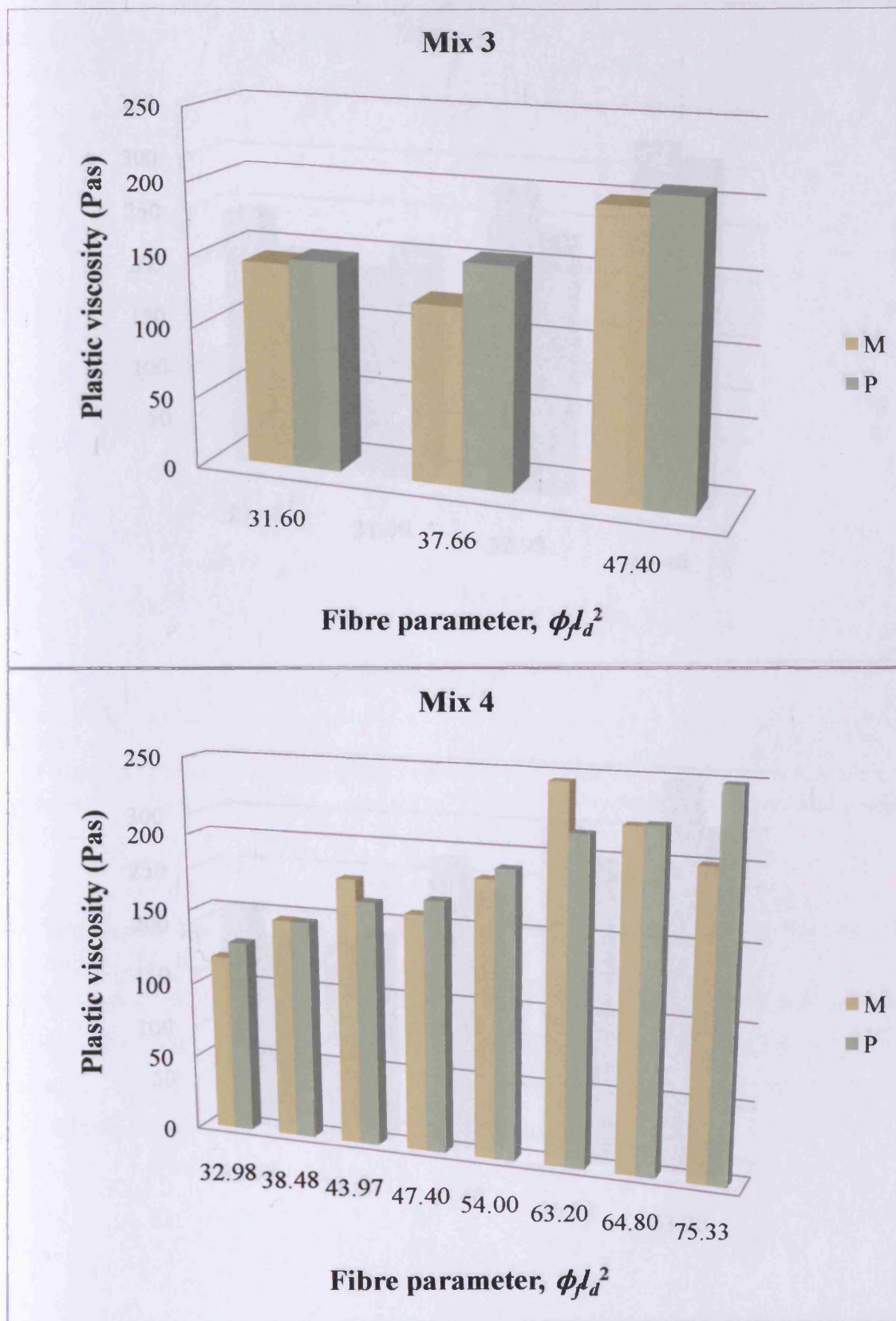
Figure 5.6: Continued
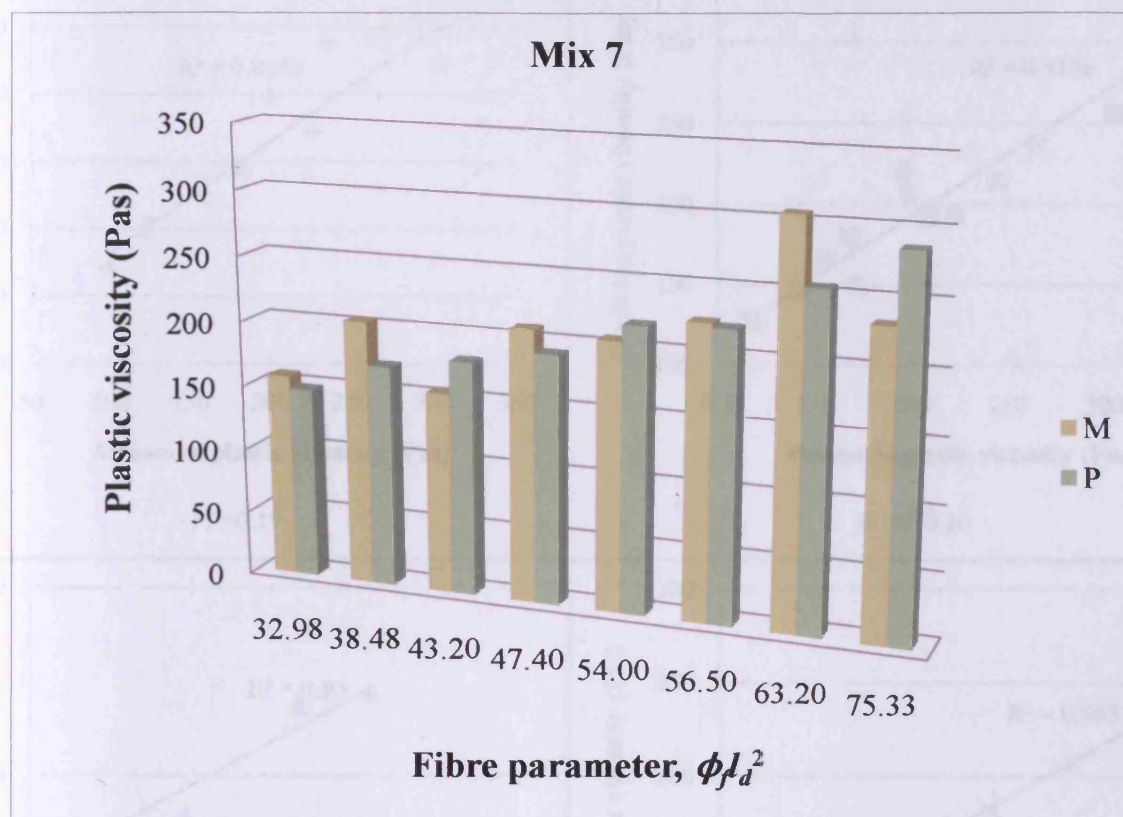
**Figure 5.6: Comparison of the plastic viscosity with experimental results vs. first fibre
parameter, ϕl_d^2 for the seven main mixes with "M" and "P" indicating measured and predicted
plastic viscosity**

5.5.4 Predicted vs. measured plastic viscosity with respect to second fibre parameter $1/\ln(2l_d)$

It can be seen from Figure 5.7 that the predicted plastic viscosity is in very good agreement
with the experimental data. The trend line has a high correlation with the second fibre
parameter: R^2 factors are 0.96, 0.93, 0.92 and 0.85 for fibre parameter values 0.22, 0.21,
0.20 and 0.19, respectively.
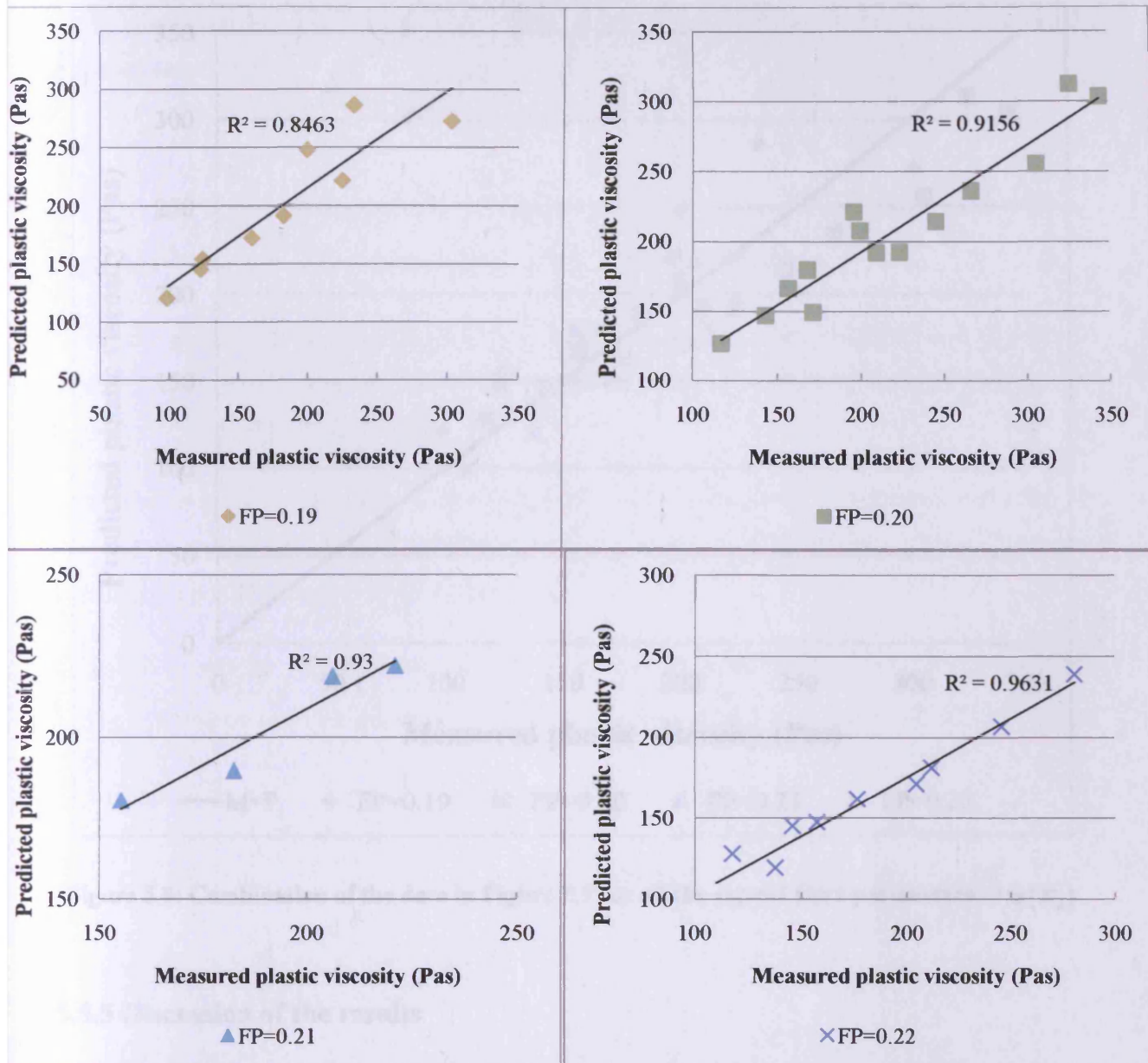
Figure 5.7: Predicted vs. experimental plastic viscosity as a function of the second fibre parameter $1/\ln(2l_d)$ **for the seven main mixes**

The data in Figure 5.7 can be combined into a single diagram, shown in Figure 5.8.
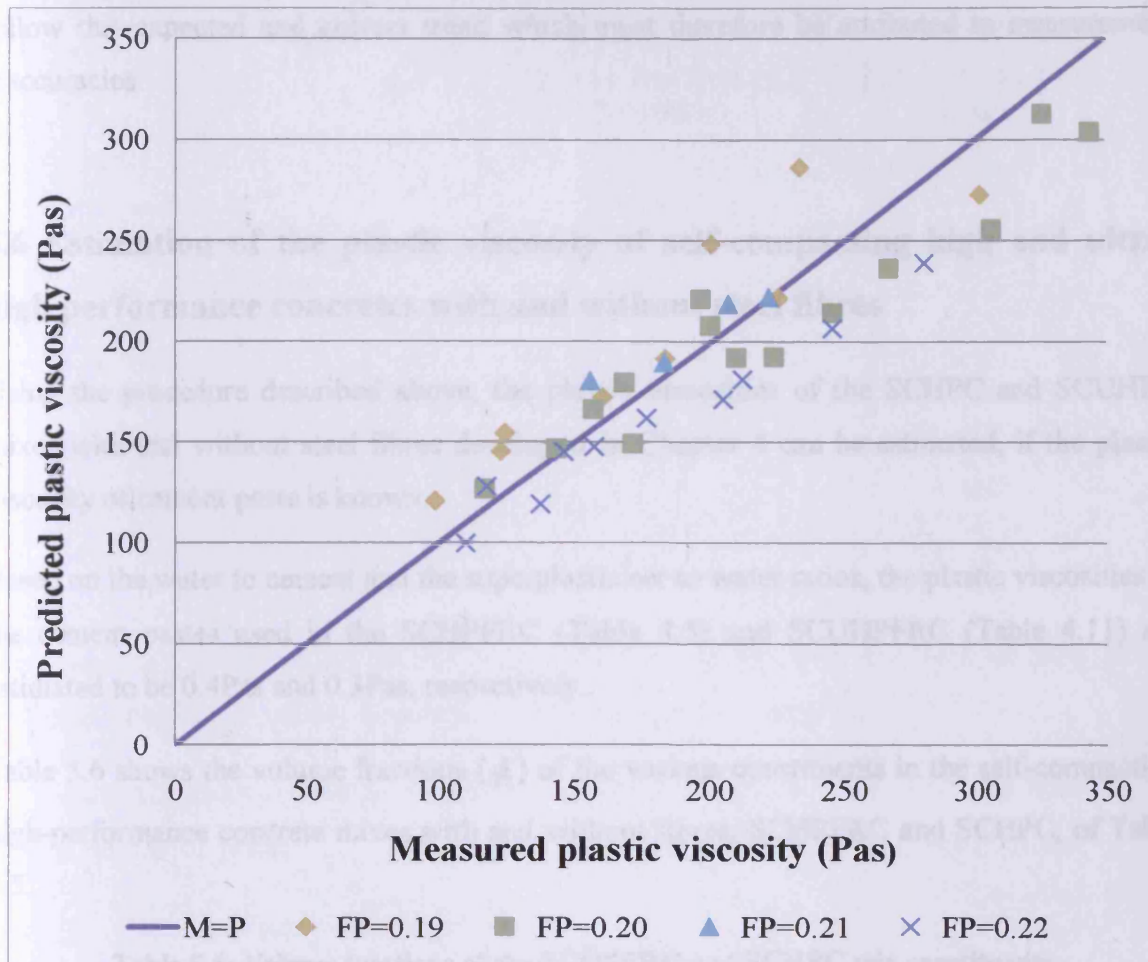
Figure 5.8: Combination of the data in Figure 5.7 for all the second fibre parameters $1/\ln(2l_d)$

5.5.5 Discussion of the results

It is clear from Figures 5.6 and 5.7 that the proposed micromechanical relations are able to predict reasonably accurately the plastic viscosity of SCC mixes once the plastic viscosity of the cement paste is known. The accuracy of the predictions is all the more remarkable given that the plastic viscosity of the paste was not measured but only estimated from similar pastes in the literature. It is quite likely that the predictions would be even more accurate when the viscosity of the paste is measured. The predicted trend, namely that the viscosity increases with increasing fibre parameters $\phi_f l_d^2$ and $1/\ln(2l_d)$ is consistent with experience which shows that the flow-ability of SCC with fibres is impaired both when the fibre volume fraction and/or the aspect ratio of the fibre are increased. Some of the measured values however do not

follow this expected and correct trend which must therefore be attributed to measurement inaccuracies.

5.6 Estimation of the plastic viscosity of self-compacting high and ultra-high performance concretes with and without steel fibres

Using the procedure described above, the plastic viscosities of the SCHPC and SCUHPC mixes with and without steel fibres developed in Chapter 4 can be estimated, if the plastic viscosity of cement paste is known.

Based on the water to cement and the superplasticiser to water ratios, the plastic viscosities of the cement pastes used in the SCHPFRC (Table 4.5) and SCUHPFRC (Table 4.11) are estimated to be 0.4Pas and 0.3Pas, respectively.

Table 5.6 shows the volume fractions (ϕ_i) of the various constituents in the self-compacting high-performance concrete mixes with and without fibres, SCHPFRC and SCHPC, of Table 4.5.

Table 5.6: Volume fractions of the SCHPFRC and SCHPC mix constituents

Constituents	Volume fraction in SCHPFRC	Volume fraction in SCHPC
Cement	0.169	0.170
Microsilica	0.034	0.034
Limestone	0.083	0.084
Sand < 2 mm	0.264	0.265
Coarse aggregates < 10 mm	0.298	0.299
Water	0.138	0.139
Superplasticiser	0.019	0.019
Fibres	0.005	---

Table 5.7 shows the volume fractions (ϕ_i) of the constituents of in the self-compacting ultra high-performance concrete mixes with and without fibres, SCUHPFRC and SCUHPC, of Table 4.11.

Table 5.7: Volume fractions of the SCUHPFRC and SCUHPC mix constituents

Constituents	Volume fraction in SCUHPFRC	Volume fraction in SCUHPC
Cement	0.184	0.189
Micro-silica	0.097	0.100
Ground granulated blast furnace slag (GGBS)	0.130	0.133
Quartz Sand 9-300 µm 250-600 µm	0.177 0.177	0.182 0.182
Water	0.188	0.193
Superplasticiser	0.049	0.050
Fibres	0.025	---

The plastic viscosities of the SCHPC and SCUHPC mixes with and without steel fibres predicted using the procedure developed above are given in Table 5.8.

Table 5.8: Plastic viscosities of SCHPC and SCUHPC mixes with and without fibres

Plastic viscosity (Pas)	Without fibres	With fibres
SCHPC (Mixes 14 and 15 in Table 4.5)	9.9	42.7
SCUHPC (Mixes 17 and 18 in Table 4.11)	3.1	54.4

5.7 Practical usefulness of the proposed micromechanical model

This section will briefly discuss the practical usefulness of the proposed model for predicting the plastic viscosity of SCC mixes with and without fibres. As stated before, the constitutive flow behaviour of SCC is best described by the Bingham fluid model which requires the plastic yield stress τ_y besides the plastic viscosity. It is known however that the yield stress of SCC mixes is low (around 200 Pa) in comparison with normal concretes (thousands of Pascal) and remains nearly constant over a large range of plastic viscosities (Figure 5.9).
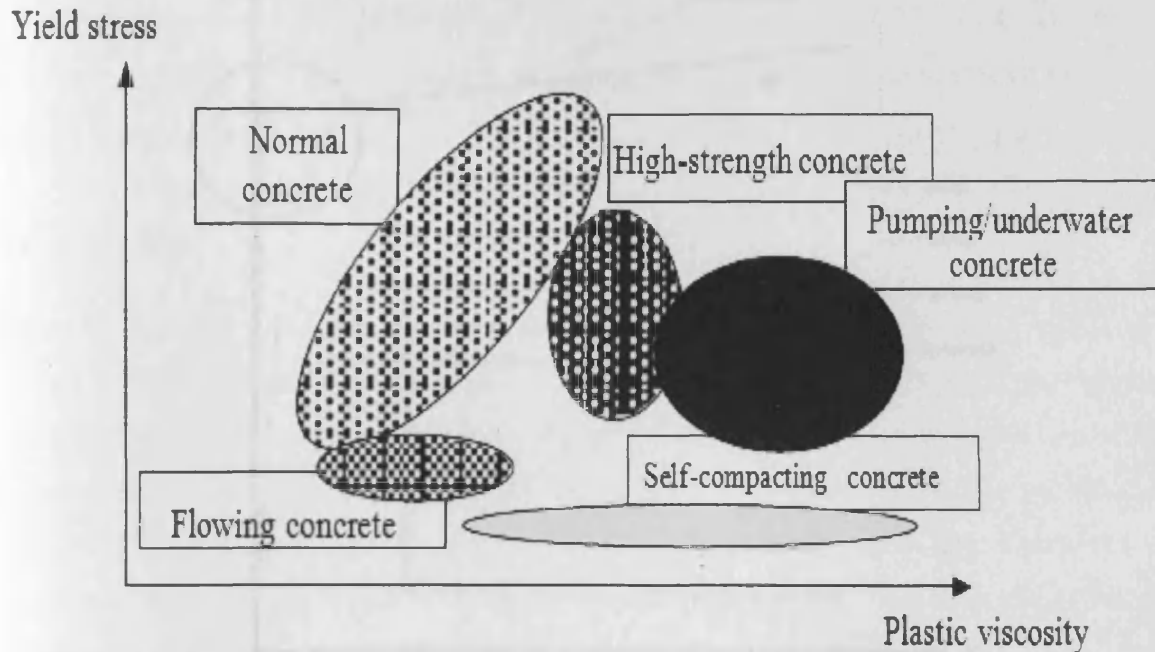
Figure 5.9: The yield stress of SCC mixes is nearly constant over a large range of plastic viscosity. (After Dransfield, 2003)

Thus, the constitutive relation of a SCC mix as a Bingham fluid can be immediately written once its effective plastic viscosity which depends on the mix composition and fibre parameters, and the plastic yield stress which depends only on the paste are known. From a practical point of view, it is expedient to represent the bilinear Bingham model with its associated discontinuity at zero shear rate by a continuous function (Papanastasiou, 1987)

$$\tau = \eta\dot{\gamma} + \tau_y\left(1 - e^{-m\dot{\gamma}}\right) \tag{5.43}$$

where m is a very large number. It can be seen from Figure 5.10 that the continuous function (5.43) approaches the bi-linear function for large m.
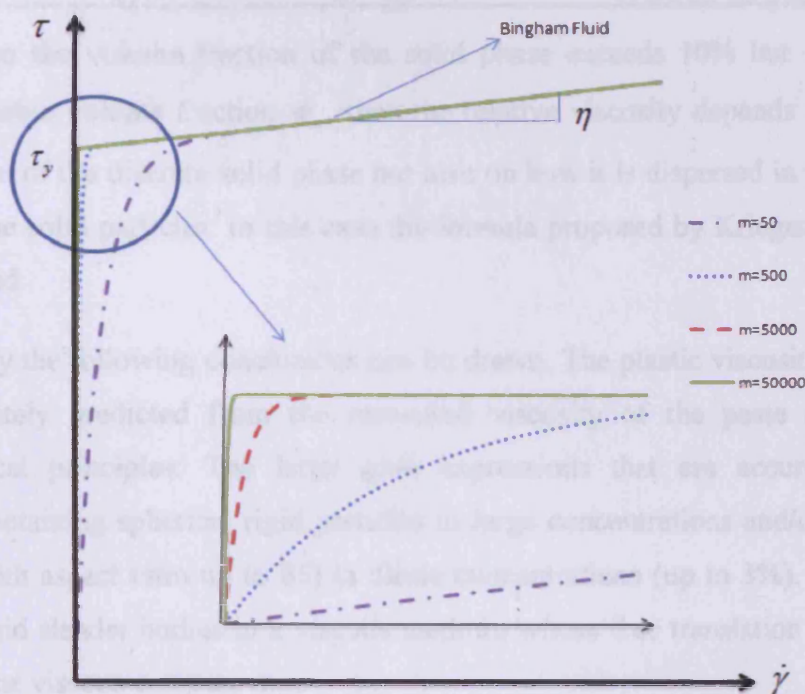
**Figure 5.10: A bilinear Bingham fluid constitutive model replaced by the continuous function
(5.43). On the scale of the figure, the discontinuity at τ_y cannot be distinguished for m=5,000
and 50,000. However, at a magnification of 100 on the horizontal scale as shown in the inset, it is
clear that the continuous approximation is better for m=50,000.**

5.8 Concluding remarks

The micromechanical procedure developed in this Chapter estimates the plastic viscosity of
SCC mixes with or without steel fibres from the knowledge of the plastic viscosity of cement
paste alone or of the cement paste with SP and/or VMA. The plastic viscosity of the SCC
mixes developed in Chapter 4 was estimated by this procedure. In this procedure, the SCC
mix is regarded as a succession of two-phase suspensions- solid and liquid phases.

It was noted that the influence of the discrete solid phase on the plastic viscosity of the
continuous liquid phase depends only on the volume fraction of the solid phase ϕ_i, if it is less
than 10%. This influence was captured by the Einstein equation (or many of its later
modifications) which contains the intrinsic viscosity $[\eta]$. A value of 2.5 was adopted in this
study because the particles are considered as rigid spheres with a large separation between the
neighbouring particles compared to the mean particle diameter.

However, when the volume fraction of the solid phase exceeds 10% but is less than the maximum possible volume fraction ϕ_m, then the relative viscosity depends not only on the volume fraction of the discrete solid phase but also on how it is dispersed in the fluid and on the shape of the solid particles. In this case the formula proposed by Krieger and Dougherty (1959) was used.

From this study the following conclusions can be drawn. The plastic viscosity of SCC mixes can be accurately predicted from the measured viscosity of the paste alone based on micromechanical principles. The latter give expressions that are accurate for viscous suspensions containing spherical rigid particles in large concentrations and/or needle-shaped steel fibres (with aspect ratio up to 85) in dilute concentrations (up to 3%). The fibres were regarded as rigid slender bodies in a viscous medium whose free translation and rotation are restrained by the viscous concrete mix.

However for steel fibres in larger concentrations and/or larger aspect ratios, the assumptions that the fibres are rigid and that they are statistically homogeneously distributed in the mix need to be re-examined.

The plastic viscosity, together with the yield stress of the SCC mixes with or without fibres, is needed to simulate the flow both at the mix design stage, e.g. to simulate the flow in a slump flow cone or an L-box test, and at the industrial use stage to simulate the flow in the formwork. For this simulation, it is of course necessary to use computational tools. In Chapter 6 we have used the relation (5.43) to simulate the flow of SCHPFRC/SCUHPFRC in the cone and L-box tests using the mesh-less smooth particle hydrodynamics method (Bonet and Kulasegaram, 2000) and have compared the results with actual measurements.

Chapter 6

Modelling the Flow of

Self-Compacting

High and Ultra High

Performance Concretes

With and Without

Steel Fibres

6.1 Introduction

In recent years, the self-compacting concrete (SCC) is increasingly replacing conventional concrete in the construction industry. The need for very high durability structures demands excellent flow-ability of SCC into the formwork. The filling behaviour of SCC is even more difficult to predict in the presence of reinforcing steel and in formworks of complex shape. Therefore, in order to produce high quality SCC structures it is vital to understand fully the flow characteristics of SCC. The most cost-effective way to gain such an understanding is by performing numerical simulations. These will not only enable us to understand the filling behaviour but will also provide insight into how the fibres will orientate themselves during the flow of SCC containing fibres.

However, in reality it is not easy to model SCC or any such heterogeneous material flow due to their very constitutive properties. Any computational model for SCC flow should be able to describe accurately the rheological behaviour of SCC and to follow the large deformation and Lagrangian nature of the flow.

A brief overview of various computational techniques used in the past to model concrete flow and their advantages and disadvantages was given in Chapter 3. The computational strategies that have been attempted in the past are mesh-based numerical simulations. However, in the simulation of the flow of fresh concrete one has to take into account special features such as large deformations, large inhomogeneities and free surfaces. These special features pose great challenges to the numerical simulation using the grid-based methods.

In this chapter, a Lagrangian particle-based technique, the so-called smooth particle hydrodynamics (SPH) method is chosen for simulating the flow of self-compacting high and ultra-high performance concretes (SCHPC/SCUHPC) with or without short steel fibres (developed in Chapter 4).

An incompressible SPH method is implemented to simulate the flow of these non-Newtonian fluids whose behaviour is described by a Bingham-type model, in which the kink in the shear stress vs shear strain rate diagram is first appropriately smoothed out (as described in Chapter 5). The viscosity of the self-compacting concrete mixes is predicted from the measured viscosity of the paste using micromechanical models in which the second phase aggregates are treated as rigid spheres and the short steel fibres as slender rigid bodies (see Chapter 5).

The basic equations solved in the SPH are the incompressible mass conservation and Navier-Stokes equations ((3.20) and (3.28)). The solution procedure uses prediction-correction fractional steps with the temporal velocity field integrated forward in time without enforcing incompressibility in the prediction step. The resulting temporal velocity field will be used in mass conservation equation (3.20) to satisfy incompressibility through a pressure Poisson equation derived from an approximate pressure equation (3.33). The results of the numerical simulation are benchmarked against actual slump tests carried out in the laboratory. The numerical results are in excellent agreement with test results, thus demonstrating the capability of SPH and a proper rheological model to predict self-compacting concrete flow behaviour.

The major part of this Chapter has been published in a journal (see publication 2 in the list in Chapter 1) and also reported at two International Conferences (publications 4 and 5).

6.2 Governing Equations

Self-compacting concrete is assumed to have the characteristics of a viscous non-Newtonian fluid, described by a bi-linear Bingham-type rheological model in which the fluid flow only initiates once the shear stress has reached a critical value called the yield stress τ_y. Thereafter, the shear stress varies linearly with the shear rate $\dot{\gamma}$, the slope being equal to the plastic viscosity η of the SCC mix. In Chapter 5, it was demonstrated how to predict the plastic viscosity η of self-compacting concretes with and without short steel fibres from the measured viscosity of the paste alone using micromechanical models in which the second phase aggregates are treated as rigid spheres and the short steel fibres as slender rigid bodies. It was also argued that the yield stress τ_y of SCC mixes is practically unchanged over a very large range of plastic viscosities (see Figure 5.9). From a computational point of view, it is expedient to approximate the bilinear Bingham constitutive relation with a kink at $\dot{\gamma} = 0$ by a smooth function with a continuous first derivative. As shown in Chapter 5, this function is given by

$$\tau = \eta\dot{\gamma} + \tau_y\left(1 - e^{-m\dot{\gamma}}\right) \tag{6.1}$$

in which m is a very large number. Experience has showed that when $m > 10^5$ the smooth function (6.1) is practically indistinguishable from the original bi-linear constitutive relation (Figure 5.10).

The isothermal, Lagrangian form of the mass and momentum conservation equations derived in Chapter 3 are repeated here:

$$\frac{1}{\rho}\frac{D\rho}{Dt} + \nabla \cdot \mathbf{v} = 0 \tag{6.2}$$

$$\frac{D\mathbf{v}}{Dt} = -\frac{1}{\rho}\nabla P + \frac{1}{\rho}\nabla.\tau + \mathbf{g} \tag{6.3}$$

In equations (6.1), (6.2) and (6.3), ρ, t, v, P, g and τ represent the fluid particle density, time, particle velocity, pressure, gravitational acceleration and shear stress, respectively.

Equation (6.1) determines the shear stress that influences the viscous force during the fluid flow as described by equation (6.3).

The three-dimensional (3D) and cylindrical forms of the vector equations (6.2) and (6.3) are given below.

6.2.1 3D discretisation of mass and momentum conservation equations

6.2.1.1 Mass conservation equation

Multiplying both side of (6.2) by ρ and noting that the substantial derivative (or total time derivative) of density ($\frac{D\rho}{Dt}$) can be decomposed into the normal derivative ($\frac{\partial\rho}{\partial t}$) and the advective derivative ($\mathbf{v}.\nabla\rho$) (see (3.10)) we can write

$$\left(\frac{\partial\rho}{\partial t}\right) + \mathbf{v}.\nabla\rho + \rho\nabla.\mathbf{v} = \left(\frac{\partial\rho}{\partial t}\right) + \nabla.(\rho\mathbf{v}) \tag{6.4}$$

For a steady-state flow, ρ does not change with respect to time hence the term $\frac{\partial\rho}{\partial t}$ vanishes. Therefore, in Cartesian coordinates (6.4) can be rewritten as

$$\frac{\partial(\rho v_x)}{\partial x} + \frac{\partial(\rho v_y)}{\partial y} = 0 \tag{6.5}$$

When additionally the flow is incompressible, ρ is constant and does not change with respect to space, (6.5) is further simplified to

$$\frac{\partial v_x}{\partial x} + \frac{\partial v_y}{\partial y} = 0 \qquad (6.6)$$

6.2.1.2 Momentum conservation equations

Multiplying both sides of (6.3) by ρ and noting that the material derivative (or total time derivative) of velocity ($\frac{Dv}{Dt}$) can be decomposed into the normal derivative ($\frac{\partial v}{\partial t}$) and the convective derivative ($v.\nabla v$) (see (3.10)), we can write

$$\rho\left(\frac{\partial v}{\partial t}\right) + \rho\left(v.\nabla v\right) = -\nabla P + \rho g + \nabla.\tau \qquad (6.7)$$

In Cartesian coordinates, (6.7) can be written explicitly as

$$\rho\left(\frac{\partial v_x}{\partial t} + v_x\frac{\partial v_x}{\partial x} + v_y\frac{\partial v_x}{\partial y} + v_z\frac{\partial v_x}{\partial z}\right) = -\frac{\partial P}{\partial x} + \rho g_x + \eta_{\mathit{eff}}\left(\frac{\partial^2 v_x}{\partial x^2} + \frac{\partial^2 v_x}{\partial y^2} + \frac{\partial^2 v_x}{\partial z^2}\right) \qquad (6.8)$$

$$\rho\left(\frac{\partial v_y}{\partial t} + v_x\frac{\partial v_y}{\partial x} + v_y\frac{\partial v_y}{\partial y} + v_z\frac{\partial v_y}{\partial z}\right) = -\frac{\partial P}{\partial y} + \rho g_y + \eta_{\mathit{eff}}\left(\frac{\partial^2 v_y}{\partial x^2} + \frac{\partial^2 v_y}{\partial y^2} + \frac{\partial^2 v_y}{\partial z^2}\right) \qquad (6.9)$$

$$\rho\left(\frac{\partial v_z}{\partial t} + v_x\frac{\partial v_z}{\partial x} + v_y\frac{\partial v_z}{\partial y} + v_z\frac{\partial v_z}{\partial z}\right) = -\frac{\partial P}{\partial z} + \rho g_z + \eta_{\mathit{eff}}\left(\frac{\partial^2 v_z}{\partial x^2} + \frac{\partial^2 v_z}{\partial y^2} + \frac{\partial^2 v_z}{\partial z^2}\right) \qquad (6.10)$$

where η_{eff} is the effective viscosity of the fluid such that $\tau = \eta_{\mathit{eff}}(\dot{\gamma})\dot{\gamma}$. In the case of a Newtonian fluid it is constant.

To obtain η_{eff} for a Bingham fluid, both sides of (6.1) are divided by $\dot{\gamma}$ to give

$$\frac{\tau}{\dot{\gamma}} = \eta + \frac{\tau_y\left(1 - e^{-m\dot{\gamma}}\right)}{\dot{\gamma}} \qquad (6.11)$$

The right hand side of (6.11) is η_{eff}.

$\dot{\gamma}$ is the shear rate which is defined as

$$\dot{\gamma} = \sqrt{\frac{1}{2}\left(tr\dot{\varepsilon}^2\right)} \qquad (6.12)$$

(6.12) states that $\dot{\gamma}$ is the second invariant of the rate of deformation $\dot{\varepsilon}$, given by

$$\dot{\varepsilon} = \frac{1}{2}\left(\nabla \mathbf{v} + \nabla \mathbf{v}^{T}\right); \qquad \nabla \mathbf{v} = \nabla \otimes \mathbf{v} \tag{6.13}$$

where $\nabla \mathbf{v}$ is the velocity gradient and superscript T denotes transpose. $\dot{\varepsilon}$ in explicit form is

$$\dot{\varepsilon}_{xy} = \frac{1}{2}\left(\begin{bmatrix} \dfrac{\partial v_x}{\partial x} & \dfrac{\partial v_x}{\partial y} & \dfrac{\partial v_x}{\partial z} \\[2mm] \dfrac{\partial v_y}{\partial x} & \dfrac{\partial v_y}{\partial y} & \dfrac{\partial v_y}{\partial z} \\[2mm] \dfrac{\partial v_z}{\partial x} & \dfrac{\partial v_z}{\partial y} & \dfrac{\partial v_z}{\partial z} \end{bmatrix} + \begin{bmatrix} \dfrac{\partial v_x}{\partial x} & \dfrac{\partial v_y}{\partial x} & \dfrac{\partial v_z}{\partial x} \\[2mm] \dfrac{\partial v_x}{\partial y} & \dfrac{\partial v_y}{\partial y} & \dfrac{\partial v_z}{\partial y} \\[2mm] \dfrac{\partial v_x}{\partial z} & \dfrac{\partial v_y}{\partial z} & \dfrac{\partial v_z}{\partial z} \end{bmatrix}\right) \tag{6.14}$$

6.2.2 Discretisation of mass and momentum conservation equations in the cylindrical co-ordinate system

6.2.2.1 Mass conservation equation

A change of variables from the Cartesian equations gives the following mass conservation equation in the cylindrical co-ordinates r, ϕ, and z

$$\frac{1}{r}\frac{\partial}{\partial r}(rv_r) + \frac{1}{r}\frac{\partial v_\phi}{\partial \phi} + \frac{\partial v_z}{\partial z} = 0 \tag{6.15}$$

6.2.2.2 Momentum conservation equations

Similar to (6.15), the momentum conservation equations are given by

r component:
$$\rho\left(\frac{\partial v_r}{\partial t} + v_r\frac{\partial v_r}{\partial r} + \frac{v_\phi}{r}\frac{\partial v_r}{\partial \phi} + v_z\frac{\partial v_r}{\partial z} - \frac{v_\phi^2}{r}\right) =$$
$$-\frac{\partial P}{\partial r} + \eta_{eff}\left[\frac{1}{r}\frac{\partial}{\partial r}\left(r\frac{\partial v_r}{\partial r}\right) + \frac{1}{r^2}\frac{\partial^2 v_r}{\partial \phi^2} + \frac{\partial^2 v_r}{\partial z^2} - \frac{v_r}{r^2} - \frac{2}{r^2}\frac{\partial v_\phi}{\partial \phi}\right] + \rho g_r \tag{6.16}$$

ϕ component:
$$\rho\left(\frac{\partial v_\phi}{\partial t} + v_r\frac{\partial v_\phi}{\partial r} + \frac{v_\phi}{r}\frac{\partial v_\phi}{\partial \phi} + v_z\frac{\partial v_\phi}{\partial z} - \frac{v_r v_\phi}{r}\right) =$$
$$-\frac{\partial P}{\partial \phi} + \eta_{eff}\left[\frac{1}{r}\frac{\partial}{\partial r}\left(r\frac{\partial v_\phi}{\partial r}\right) + \frac{1}{r^2}\frac{\partial^2 v_\phi}{\partial \phi^2} + \frac{\partial^2 v_\phi}{\partial z^2} + \frac{2}{r^2}\frac{\partial v_r}{\partial \phi} - \frac{v_r}{r^2}\right] + \rho g_\phi \tag{6.17}$$

z component: $\rho\left(\dfrac{\partial v_z}{\partial t}+v_r\dfrac{\partial v_z}{\partial r}+\dfrac{v_\phi}{r}\dfrac{\partial v_z}{\partial \phi}+v_z\dfrac{\partial v_z}{\partial z}\right)=$

$$-\dfrac{\partial P}{\partial r}+\eta_{eff}\left[\dfrac{1}{r}\dfrac{\partial}{\partial r}\left(r\dfrac{\partial v_z}{\partial r}\right)+\dfrac{1}{r^2}\dfrac{\partial^2 v_z}{\partial \phi^2}+\dfrac{\partial^2 v_z}{\partial z^2}\right]+\rho g_z$$

(6.18)

In modelling the flow of SCC mixes, in order to reduce the computational cost, the two-dimensional (2D) and axisymmetric configurations are used here which are reduced versions of 3D and cylindrical coordinates, respectively. The discretisation of the governing equations is given below.

6.2.3 2D discretisation of mass and momentum conservation equations

To derive the governing equations, the z components of (6.8), (6.9), (6.10) and (6.14) is set equal to zero. Therefore (6.6), (6.8), (6.9) and (6.14) become (6.19), (6.20), (6.21) and (6.22), respectively.

$$\dfrac{\partial v_x}{\partial x}+\dfrac{\partial v_y}{\partial y}=0$$

(6.19)

$$\rho\left(\dfrac{\partial v_x}{\partial t}+v_x\dfrac{\partial v_x}{\partial x}+v_y\dfrac{\partial v_x}{\partial y}\right)=-\dfrac{\partial P}{\partial x}+\eta_{eff}\left(\dfrac{\partial^2 v_x}{\partial x^2}+\dfrac{\partial^2 v_x}{\partial y^2}\right)$$

(6.20)

$$\rho\left(\dfrac{\partial v_y}{\partial t}+v_x\dfrac{\partial v_y}{\partial x}+v_y\dfrac{\partial v_y}{\partial y}\right)=-\dfrac{\partial P}{\partial y}+\rho g_y+\eta_{eff}\left(\dfrac{\partial^2 v_y}{\partial x^2}+\dfrac{\partial^2 v_y}{\partial y^2}\right)$$

(6.21)

$$\dot\varepsilon_{xy}=\dfrac{1}{2}\left(\begin{bmatrix}\dfrac{\partial v_x}{\partial x}&\dfrac{\partial v_x}{\partial y}\\[2mm]\dfrac{\partial v_y}{\partial x}&\dfrac{\partial v_y}{\partial y}\end{bmatrix}+\begin{bmatrix}\dfrac{\partial v_x}{\partial x}&\dfrac{\partial v_y}{\partial x}\\[2mm]\dfrac{\partial v_x}{\partial y}&\dfrac{\partial v_y}{\partial y}\end{bmatrix}\right)$$

(6.22)

6.2.4 Axisymmetric discretisation of mass and momentum conservation equations

A flow is axisymmetric, if the displacement takes place along the r and z axes but is independent of the ϕ direction. Therefore any derivative with respect to ϕ in the cylindrical co-ordinates vanishes. Furthermore in this case due to the irotational nature of the flow the

velocity in ϕ direction (v_ϕ) is also set equal to zero. Therefore (6.15), (6.16) and (6.18) become (6.23), (6.24) and (6.25), respectively.

$$\frac{1}{r}\frac{\partial}{\partial r}(rv_r)+\frac{\partial v_z}{\partial z}=0 \tag{6.23}$$

r component:
$$\rho\left(\frac{\partial v_r}{\partial t}+v_r\frac{\partial v_r}{\partial r}+v_z\frac{\partial v_r}{\partial z}\right)=$$
$$-\frac{\partial P}{\partial r}+\eta_{\textit{eff}}\left[\frac{1}{r}\frac{\partial}{\partial r}\left(r\frac{\partial v_r}{\partial r}\right)+\frac{\partial^2 v_r}{\partial z^2}-\frac{v_r}{r^2}\right]+\rho g \tag{6.24}$$

z component:
$$\rho\left(\frac{\partial v_z}{\partial t}+v_r\frac{\partial v_z}{\partial r}+v_z\frac{\partial v_z}{\partial z}\right)=$$
$$-\frac{\partial P}{\partial r}+\eta_{\textit{eff}}\left[\frac{1}{r}\frac{\partial}{\partial r}\left(r\frac{\partial v_z}{\partial r}\right)+\frac{\partial^2 v_z}{\partial z^2}\right]+\rho g \tag{6.25}$$

$\eta_{\textit{eff}}$ is obtained from (6.11) after replacing x and y by r and z, respectively.

6.3 Numerical solution procedure

To track the Lagrangian non-Newtonian flow, a fully incompressible method is used. However, equation (6.2) is for a general compressible flow. As shown in Chapter 3, the strict enforcement of incompressibility results in a Poisson's equation for pressure correction. In order to use this pressure-Poisson equation, a projection formulation introduced by Chorin (1968) and Cummins and Rudman (1999) is implemented. In this way the pressure and velocity fields are updated until they reach a divergence free state. This predictor-corrector time stepping scheme is described below.

6.3.1 Prediction step

The first, prediction step is an explicit integration in time without enforcing incompressibility. Only the viscous stress and gravity terms in equation (6.3) are considered and an intermediate velocity and position are obtained by integration

$$\mathbf{v}^*_{n+1}=\mathbf{v}_n+\left(\mathbf{g}+\frac{1}{\rho}\nabla\cdot\tau\right)\Delta t \tag{6.26}$$

where

$$\mathbf{v}_{n+1}^* = \mathbf{v}_n + \Delta\mathbf{v}_{n+1}^* \tag{6.27}$$

$$\mathbf{x}_{n+1}^* = \mathbf{x}_n + \mathbf{v}_{n+1}^*\Delta t \tag{6.28}$$

Here, $\mathbf{v}_n$ and $\mathbf{x}_n$ are the particle velocity and position vectors at time t, $\mathbf{v}_{n+1}^*$ and $\mathbf{x}_{n+1}^*$ are the intermediate particle velocity and position vectors, and $\Delta\mathbf{v}_{n+1}^*$ is the change in the particle velocity vector during the time increment Δt.

6.3.2 Correction step

A corrective step is next applied to enforce the incompressibility condition prior to incrementing the time. The correction step is performed by considering the pressure term in (6.3)

$$\frac{\mathbf{v}_{n+1} - \mathbf{v}_{n+1}^*}{\Delta t} = -\left(\frac{1}{\rho}\nabla P_{n+1}\right) \tag{6.29}$$

where $\mathbf{v}_{n+1}$ is the corrected particle velocity vector at the time level $n+1$. As the particle density remains constant during the flow, the mass conservation (6.2) imposes the following incompressibility condition on the corrected velocity

$$\nabla \cdot \mathbf{v}_{n+1} = 0 \tag{6.30}$$

Taking the divergence of (6.29) and noting the above incompressibility condition gives

$$\nabla \cdot \left(\frac{1}{\rho}\nabla P_{n+1}\right) = \frac{\nabla \cdot \mathbf{v}_{n+1}^*}{\Delta t} \tag{6.31}$$

which can be rewritten as

$$\nabla^2 P_{n+1} = \frac{\rho}{\Delta t}\nabla \cdot \mathbf{v}_{n+1}^* \tag{6.32}$$

Once the pressure is obtained from the Poisson equation (6.32), the particle velocity is updated by the computed pressure gradient (see equation (6.29)):

$$\mathbf{v}_{n+1} = \mathbf{v}_{n+1}^* - \left(\frac{1}{\rho}\nabla P_{n+1}\right)\Delta t \tag{6.33}$$

Finally, the instantaneous particle position can be updated using the corrected velocity

$$\mathbf{x}_{n+1} = \mathbf{x}_n + \mathbf{v}_{n+1}\Delta t \tag{6.34}$$

6.4 SPH discretisation of the governing equations

There are three terms in the mass and momentum conservation equations that need to be defined in the SPH formulation, namely the divergence of velocity in the mass conservation (6.2), the gradients of pressure and viscosity terms in the momentum conservation (6.3), and the Laplacian term $\nabla^2 P_{n+1}$ resulting from the enforcement of incompressibility. In following, these terms will be discretised in the SPH sense.

6.4.1 Gradient of pressure

The gradient of pressure in the Navier-Stokes equations can be obtained by identifying $\phi(\mathbf{x})$ in (3.51) (see Chapter 3) with the pressure term P to give

$$(\nabla P)_a = \sum_{b=1}^{N} V_b P_b \otimes \tilde{\nabla}\tilde{W}_b(\mathbf{x}) \tag{6.35}$$

where a and b are the reference particle and its neighbour, respectively. $\tilde{\nabla}\tilde{W}$ is the corrected gradient of the corrected kernel (see Chapter 3 and Appendix A).

6.4.2 Divergence of velocity

Similarly, the divergence of the velocity field can be calculated from

$$(\nabla \cdot \mathbf{v})_a = \sum_{b=1}^{N} V_b \mathbf{v}_b \cdot \tilde{\nabla}\tilde{W}_b(\mathbf{x}) \tag{6.36}$$

6.4.3 Laplacian

The Laplacian in the pressure Poisson equation (6.32) can be formulated using the divergence and gradient operators of the SPH formulation to give

$$\sum_{b=1}^{N} V_b V_a \nabla P_b \cdot \nabla \tilde{W}_b(\mathbf{x}) = \frac{\rho_a}{\Delta t} \sum_{b=1}^{N} V_b \mathbf{v}_b \cdot \tilde{\nabla} \tilde{W}_b(\mathbf{x}) \qquad (6.37)$$

6.4.4 Viscosity

The viscosity term, $\dfrac{1}{\rho}\nabla \cdot \boldsymbol{\tau}$ in the momentum conservation equation can be written in a

similar manner to (6.36) as

$$\left(\frac{1}{\rho}\nabla \cdot \boldsymbol{\tau}\right)_a = \sum_{b=1}^{N} \frac{m_b}{\rho_b^2}\boldsymbol{\tau}_b \cdot \tilde{\nabla}\tilde{W}_b(\mathbf{x}) \qquad (6.38)$$

where the shear stress is given by (6.1).

6.5 Time step

The time step Δt is chosen based on the relevant stability conditions for the given problem. In the case of a Bingham-type SCC fluid flow, the time step is primarily controlled by the plastic viscosity. The time step size is generally decided by (Shao and Lo, 2003)

$$\Delta t = \min\left(\frac{\alpha_1 r_0}{v_{\max}}, \frac{\alpha_2 r_0^2 \rho \dot{\gamma}}{\tau_y + \eta \dot{\gamma}}\right) \qquad (6.39)$$

where r_0 is the initial particle spacing, $v_{\max}$ is the maximum particle velocity, and α_1 and α_2 are coefficients usually in the order of 0.1. These coefficients depend on the choice of SPH kernel functions and the nature of the engineering application. Note that the term $\left(1 - e^{-m\dot{\gamma}}\right)$ was excluded from (6.39) because its value is close to one when m is a very large number.

6.6 Numerical simulation results

In this Section, a number of numerical tests are presented to investigate the flow-ability and filling behaviour of the SCC mixes with and without fibres. In the case of flow of the SCC with fibres, the numerical results are compared with laboratory slump flow tests.

The SCC mixes studied are the self-compacting high and ultra-high performance concretes with and without fibres developed in Chapter 4 (see Tables 4.5 and 4.11). From the micromechanical model developed in Chapter 5, the plastic viscosities of the SCC mixes with and without fibres were calculated from the known plastic viscosity of the cement paste and the volume fractions of the various fine aggregates and fibre (see Table 5.8). As mentioned previously, the yield stress of SCC is low and practically constant over a wide range of plastic viscosities (see Figure 5.9). For the present mixes τ_y was chosen to be 200 Pa.

The numerical simulations of SCC flow in two different geometrical configurations are carried out. Firstly, a slump flow test is carried out on SCC mixes with and without fibres. The key difference in the model parameters between SCC mixes with and without fibres is the plastic viscosity, which, as we have seen, increases significantly in the presence of needle-like short steel fibres. However, as the volume fraction of the fibres in the SCC mixes is usually small (0.5% and 2.5% in the present simulations) the density is only marginally increased with the addition of fibres.

The slump flow test is first simulated in an axisymmetric configuration, followed by a simulation in a 2D approximation along a vertical plane of symmetry. Finally, the flow of SCC with and without fibres is simulated in an L-box configuration.

6.6.1 Slump flow test

6.6.1.1 Initial configuration and boundary conditions

Figure 6.1 illustrates the initial configuration of the slump cone for which numerical simulations of the flow of SCC mixes with and without fibres was carried out in both the axisymmetric and two-dimensional configurations.
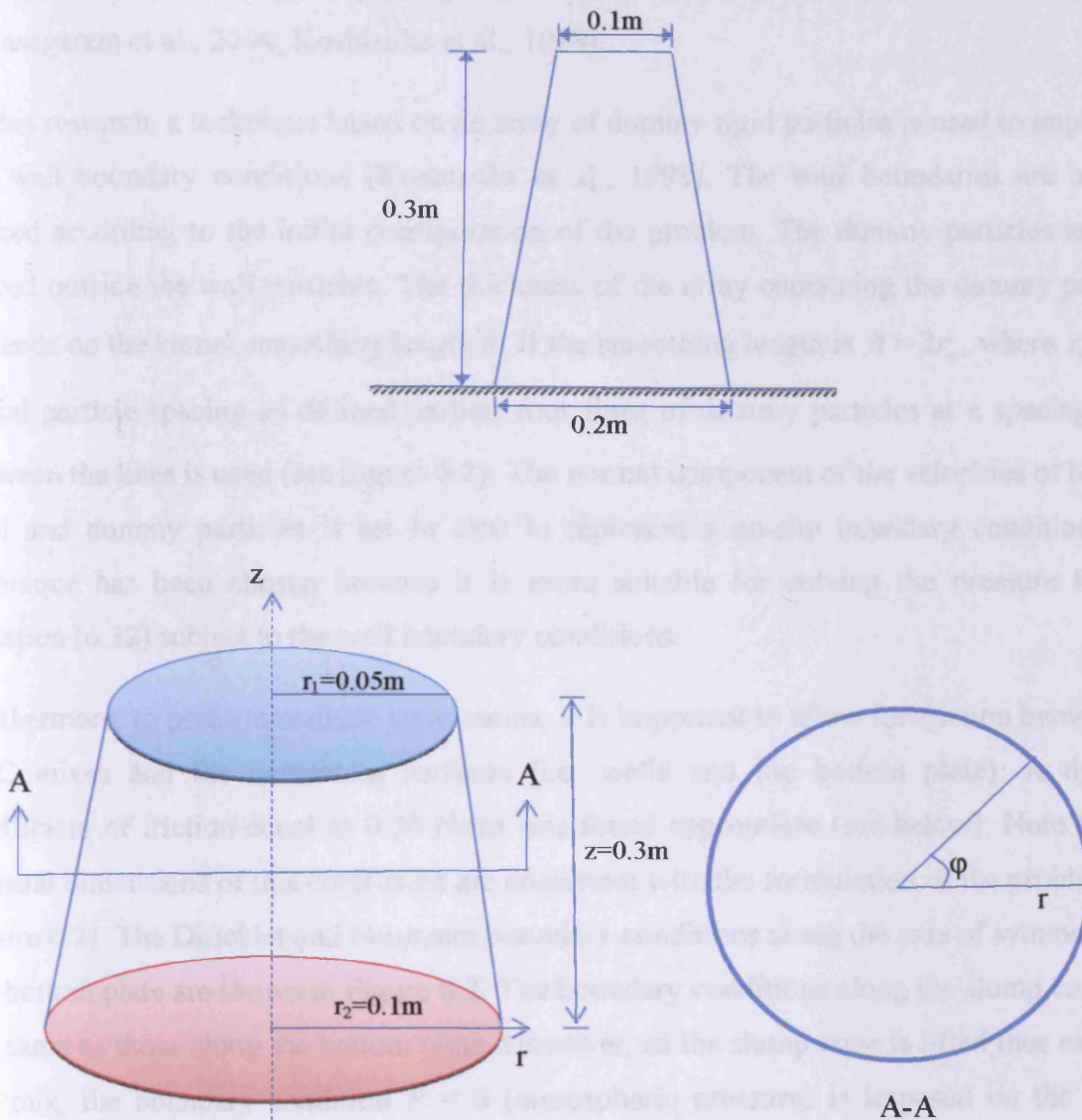
Figure 6.1: Initial configuration of the Slump Test in the two-dimensional (Top) and axisymmetric configurations (Bottom).

The governing equations have to be supplemented by proper boundary conditions. On a free-surface, a zero pressure condition (i.e. atmospheric pressure) has to be met. At a wall and on the bottom plate a Dirichlet (or first-type) boundary condition has to be imposed on the normal component of the velocity field, while Neumann (or second-type) conditions have to be imposed on pressure. In the SPH method, the implementation of boundary conditions is not as straightforward as in the traditional mesh-based methods. A number of techniques have been developed in the past to treat the boundary conditions in SPH applications (Monaghan,

1994; Bonet and Kulasegaram, 2000; Bonet and Lok, 1999; Cummins and Rudman, 1999; Kulasegaram et al., 2004; Koshizuka et al., 1998).

In this research, a technique based on an array of dummy rigid particles is used to implement the wall boundary conditions (Koshizuka et al., 1998). The wall boundaries are initially spaced according to the initial configuration of the problem. The dummy particles are then placed outside the wall particles. The thickness of the array containing the dummy particles depends on the kernel smoothing length h. If the smoothing length is $h = 2r_o$, where r_0 is the initial particle spacing as defined earlier, four lines of dummy particles at a spacing of r_0 between the lines is used (see Figure 6.2). The normal component of the velocities of both the wall and dummy particles is set to zero to represent a no-slip boundary condition. This technique has been chosen because it is more suitable for solving the pressure Poisson equation (6.32) subject to the wall boundary conditions.

Furthermore, to perform realistic simulations, it is important to allow for friction between the SCC mixes and the contacting surfaces (i.e. walls and the bottom plate). A dynamic coefficient of friction equal to 0.56 Ns/m was found appropriate (see below). Note that the unusual dimensions of this coefficient are consistent with the formulation of the problem (see Figure 6.2). The Dirichlet and Neumann boundary conditions along the axis of symmetry and the bottom plate are shown in Figure 6.2. The boundary conditions along the slump cone wall are same as those along the bottom plate. However, as the slump cone is lifted thus exposing the mix, the boundary condition $P = 0$ (atmospheric pressure) is imposed on the newly-formed free surfaces. The friction boundary condition is imposed on the bottom plate and on the slump cone wall when it is still in contact with the mix. The effect of friction boundary condition depends on the relative tangential velocity between the wall and the fluid flow and ensures that slip with friction boundary condition is enforced along the tangential direction of the wall.

• Dummy boundary particles
• Material particles

$P = 0$

$v_n = 0,$

$\dfrac{\partial P}{\partial n} = 0$

$\dfrac{\partial P}{\partial n} = 0,$

$v_n = 0,$

$F_t = c_f v_t$

$v_n = 0,$

$\dfrac{\partial P}{\partial n} = 0$

$P{=}0$

$\dfrac{\partial P}{\partial n} = 0,$

$v_n = 0,$

$F_t = c_f v_t$

$P = 0$

$\dfrac{\partial P}{\partial n} = 0, v_n = 0 \ \text{and} \ F_t = c_f v_t$

$\dfrac{\partial P}{\partial n} = 0, v_n = 0 \ \text{and} \ F_t = c_f v_t$

Figure 6.2: Boundary conditions for the slump cone (*P*- pressure, v_n- normal velocity, v_t -

tangential velocity and c_f- dynamic coefficient of friction)

6.6.1.2 Numerical test results

For the numerical simulation of the slump flow test approximately 2000 SPH particles were used to model one half of the cone configuration shown in Figure 6.2.

Figures 6.3 and 6.4 show the various stages during the numerical simulation of slump flow test of SCUHPC mixes without fibres and with fibres, respectively. It is evident from these

results that the fluidity of the flow without fibres is much higher than that of SCC with fibres. It can also be noted in both cases that the initial profiles of the free surfaces are influenced by the motion of the steel cone during its quick removal. For the purposes of comparison, the SCC mix with fibres was simulated using both the axisymmetric (Figures 6.4) and 2D (Figure 6.6) configurations. It can be noted from the figures that 2D flow approximation is slower than the real axisymmetric flow. Figure 6.5 shows the slump flow circles at different heights (z) along the axis of symmetry in the axisymmetric configuration.

t=0.1 sec

t=0.5 sec

t=1 sec

t=2 sec
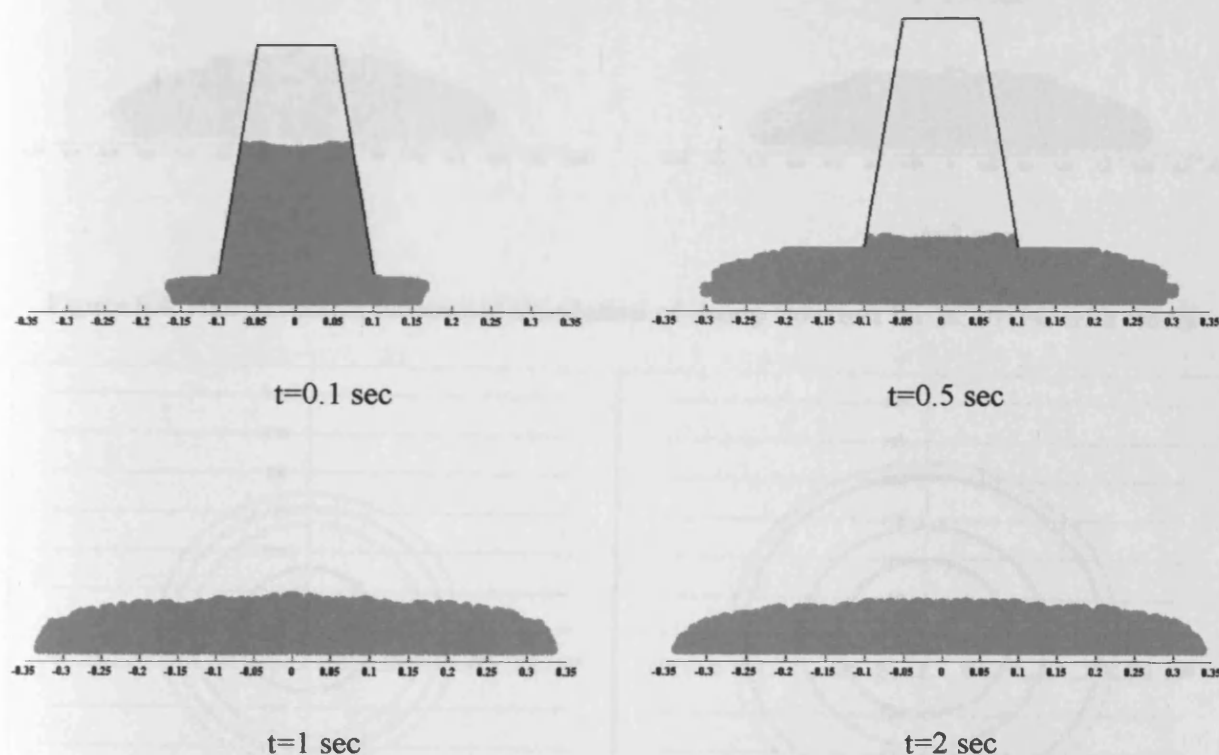
Figure 6.3: Axisymmetric numerical simulation of slump flow test for SCUHPC without fibres

t=0.5 sec

t=1.5 sec

t=2 sec

t=3 sec
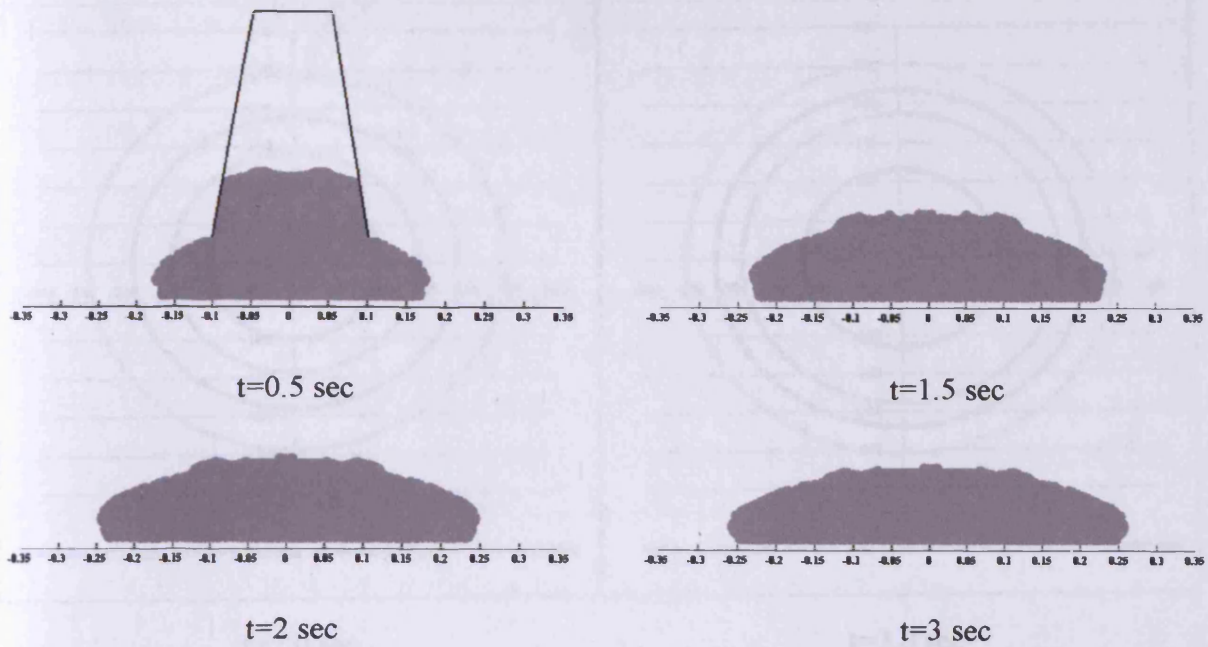
Figure 6.4: Axisymmetric numerical simulation of slump flow test for SCUHPC with fibres
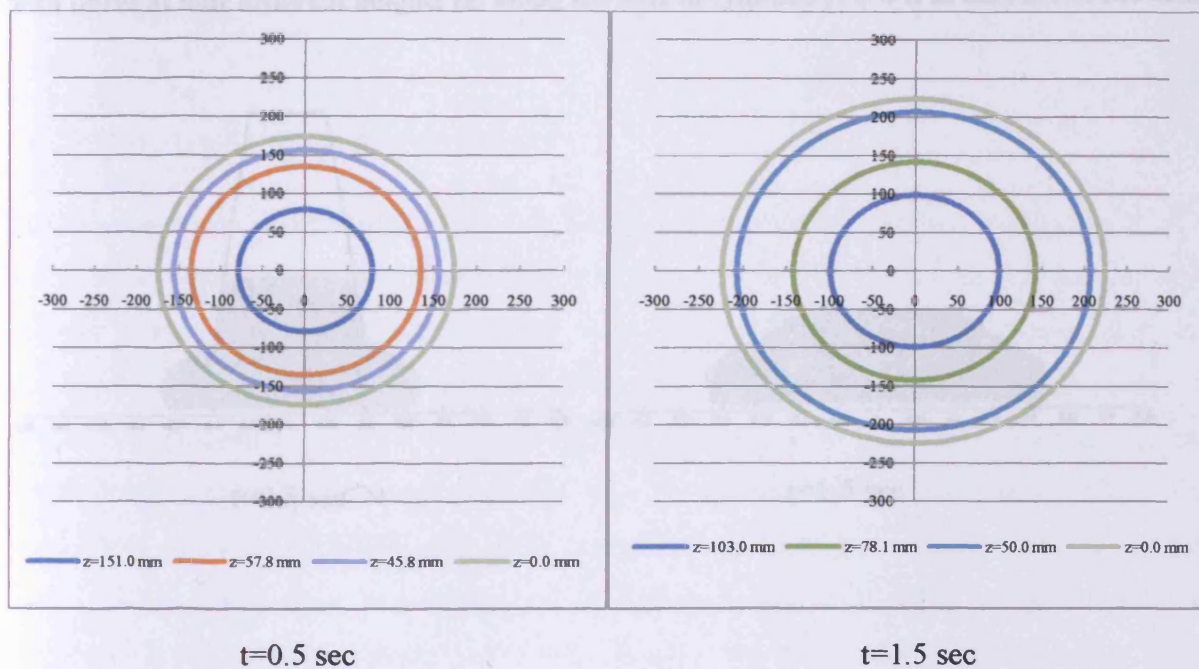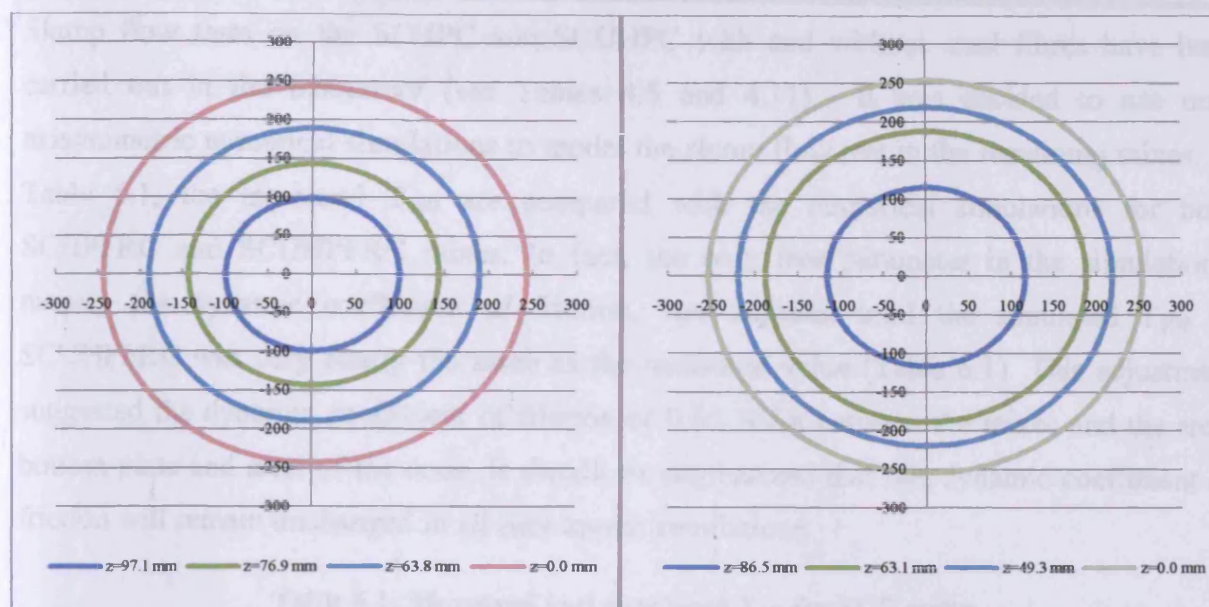
t=0.5 sec

t=1.5 sec

t=2.0 sec   t=3.0 sec

**Figure 6.5: Plan view of axisymmetric numerical simulation of slump flow test for SCUHPC
with fibres at four different heights (z) along the axis of symmetry. z=0 is at the base of the cone.**
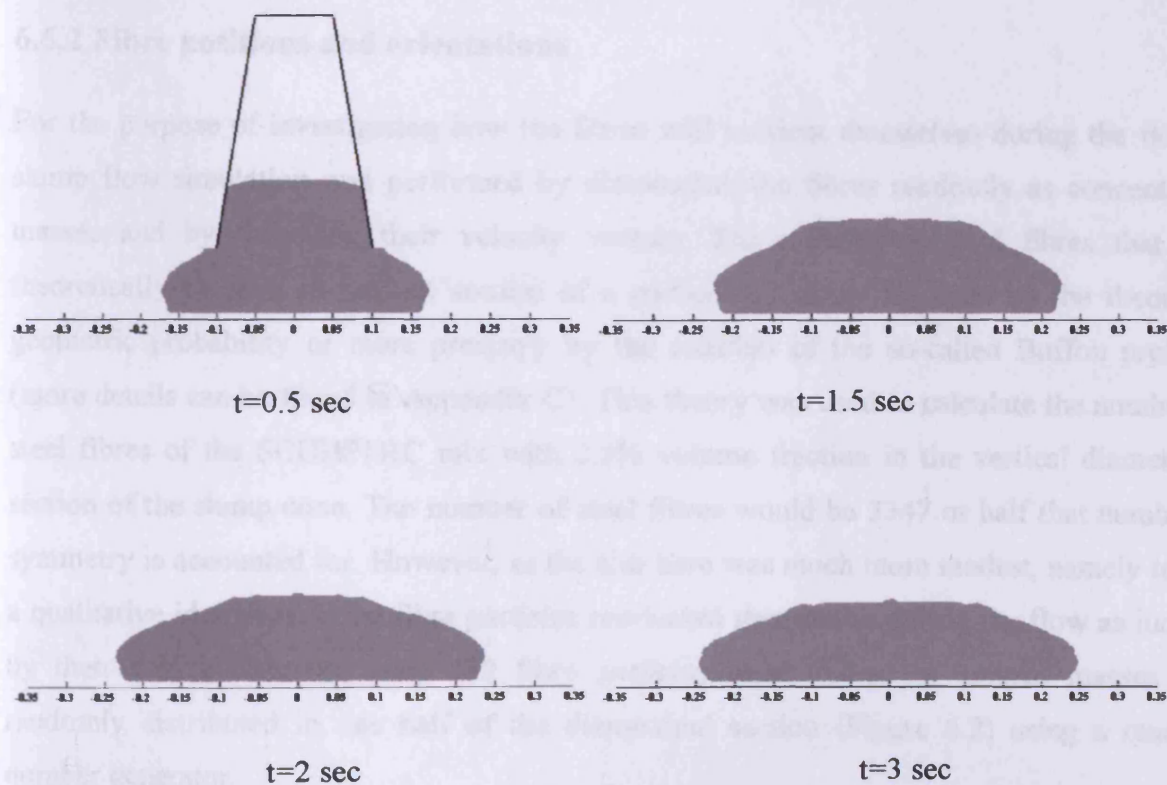
t=0.5 sec   t=1.5 sec

t=2 sec   t=3 sec

**Figure 6.6: Numerical simulation of slump flow test for SCUHPC with fibres in 2D
approximation**

Slump flow tests on the SCHPC and SCUHPC with and without steel fibres have been carried out in the laboratory (see Tables 4.5 and 4.11). It was decided to use only axisymmetric numerical simulations to model the slump flow test in the remaining mixes. In Table 6.1, the measured T_{500} are compared with the numerical simulations for both SCHPFRC and SCUHPFRC mixes. In fact, the only free parameter in the simulations, namely the dynamic coefficient of friction, was adjusted until the simulated T_{500} of SCUHPFRC was very nearly the same as the measured value (Table 6.1). This adjustment suggested the dynamic coefficient of friction of 0.56 Ns/m between the mixes and the steel bottom plate and steel of the cone. It should be emphasized that this dynamic coefficient of friction will remain unchanged in all subsequent simulations.

Table 6.1: Measured and simulated T_{500} for SCC mixes

SCC type	Volume fraction of steel fibres (%)	Measured T_{500} (sec)	Simulated T_{500} (sec)	Error (%)
SCHPFRC	0.5	3.0	2.8	7.1
SCUHPFRC	2.5	3.0	2.9	3.4

6.6.2 Fibre positions and orientations

For the purpose of investigating how the fibres will reorient themselves during the flow, a slump flow simulation was performed by distributing the fibres randomly as concentrated masses and by following their velocity vectors. The number of steel fibres that will theoretically be seen in the cut section of a particular volume is given by the theory of geometric probability or more precisely by the solution of the so-called Buffon problem (more details can be found in Appendix C). This theory was used to calculate the number of steel fibres of the SCUHPFRC mix with 2.5% volume fraction in the vertical diametrical section of the slump cone. The number of steel fibres would be 3347 or half that number if symmetry is accounted for. However, as the aim here was much more modest, namely to get a qualitative idea of how the fibre particles reoriented themselves during the flow as judged by their velocity vectors, only 112 fibre particles were treated as lumped masses and randomly distributed in one half of the diametrical section (Figure 6.2) using a random number generator.

The random distribution of this limited number of lumped masses representing the fibre
particles and their associated velocity vectors at various times during the flow are shown in
Figure 6.6.

t=0.1 sec   t=0.5 sec

t=1.5 sec   t=3 sec
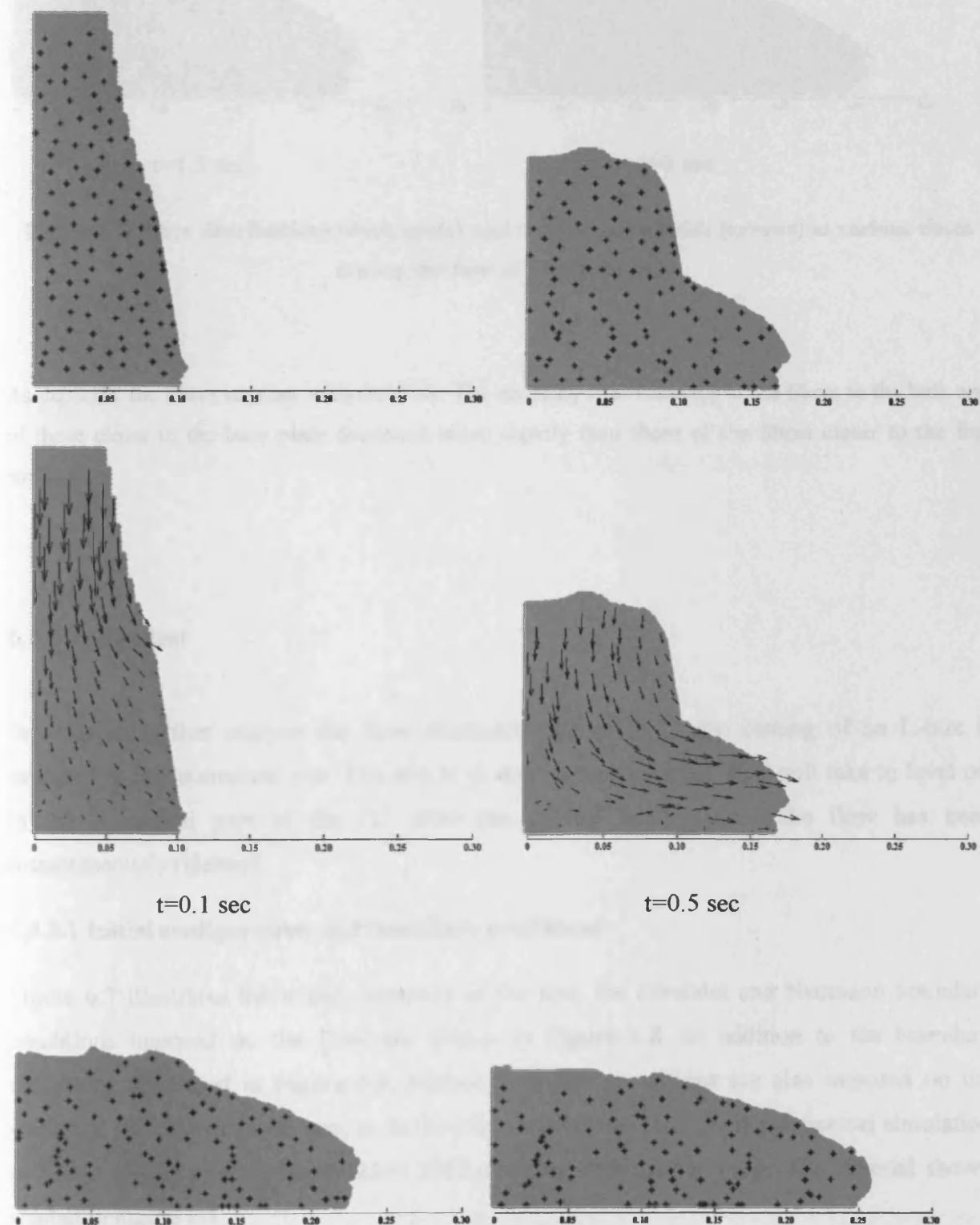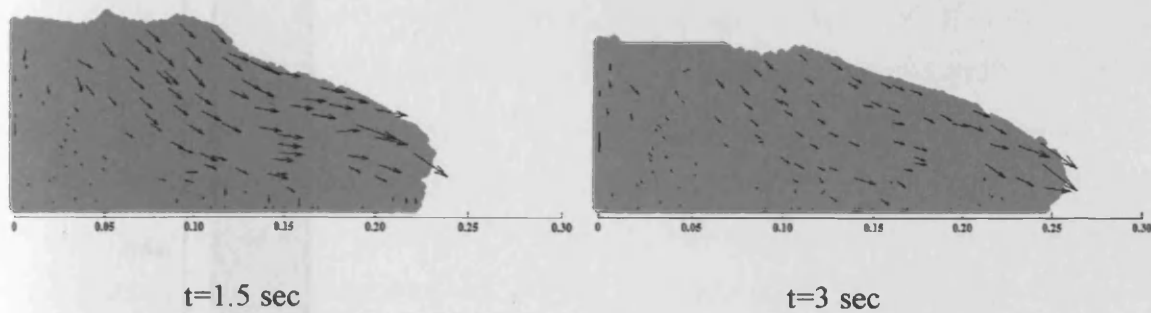
Figure 6.7: Fibre distributions (dark spots) and their velocity fields (arrows) at various times during the flow of SCUHPFRC

As expected the fibres reorient with the flow. The mobility (i.e. velocity) of the fibres in the bulk and of those closer to the base plate decreases more rapidly than those of the fibres closer to the free surfaces.

6.6.3 L-box test

In order to further analyse the flow characteristics of SCC, the casting of an L-box is explored in this numerical test. The aim is to record how long the SCC will take to level off in the horizontal part of the 'L' after the shutter holding back the flow has been instantaneously released.

6.6.3.1 Initial configuration and boundary conditions

Figure 6.7 illustrates the initial geometry of the test; the Dirichlet and Neumann boundary conditions imposed on the flow are shown in Figure 6.8. In addition to the boundary conditions illustrated in Figure 6.8, friction boundary conditions are also imposed on the walls and the base of the L-box, as in the slump flow test above. In the numerical simulation of L-box casting approximately 2500 SPH particles were used to model the material shown shaded in Figure 6.7.

0.1m

0.6m

0.15m

0.18m

0.52m
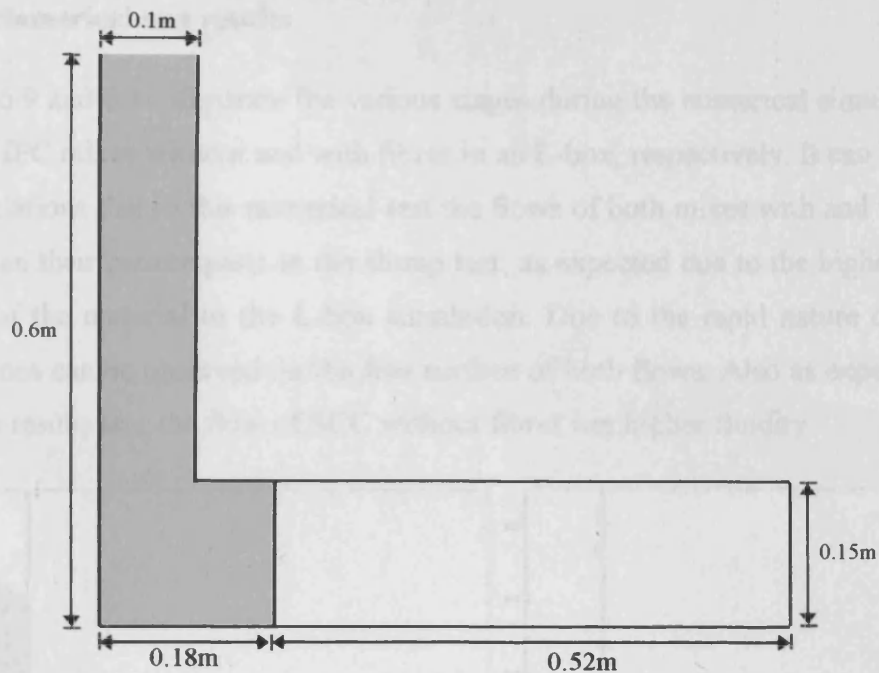
Figure 6.8: Initial configuration of the L-box concrete casting

$P = 0$

$$\frac{\partial P}{\partial n} = 0, v_n = 0, F_t = c_f v_t$$

$$\frac{\partial P}{\partial n} = 0,$$
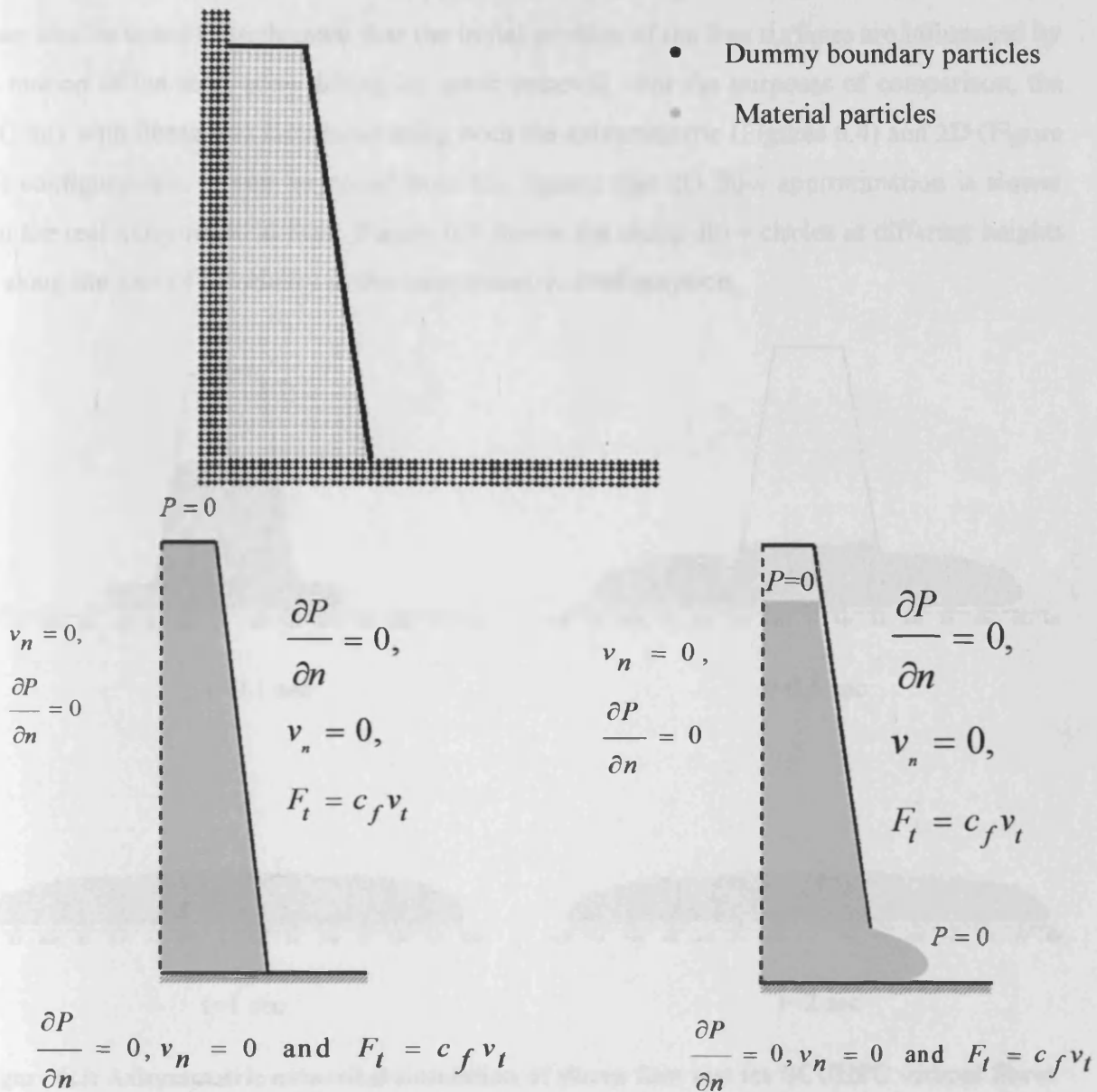$$v_n = 0$$

$$\frac{\partial P}{\partial n} = 0, v_n = 0, F_t = c_f v_t$$
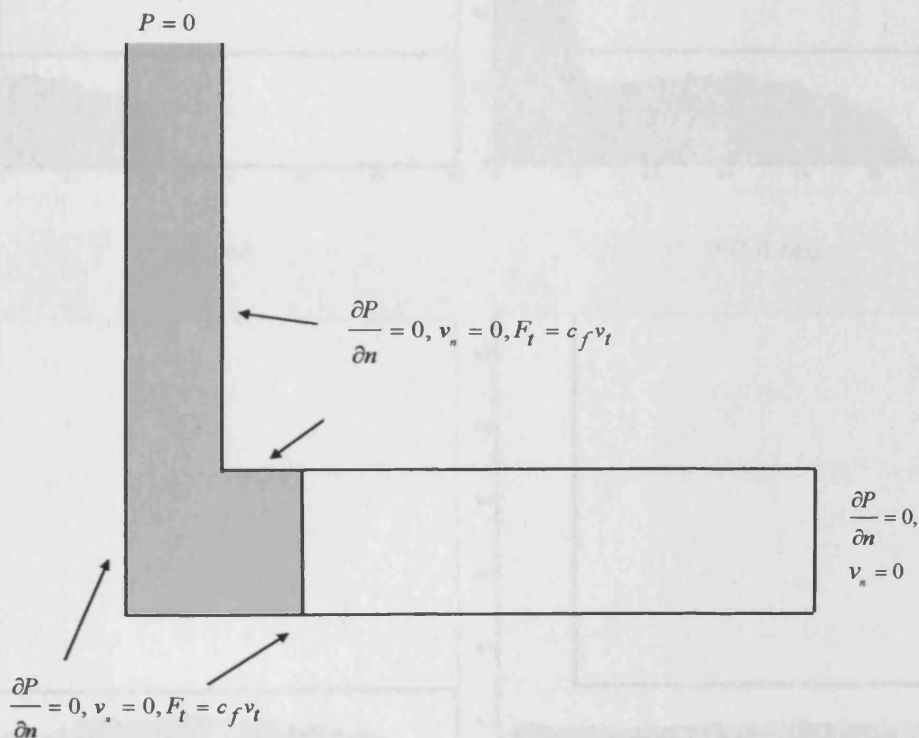
Figure 6.9: Boundary conditions (P- pressure, v_n- normal velocity, v_t -tangential velocity and c_f - dynamic coefficient of friction).

6.6.3.2 Numerical test results

Figures 6.9 and 6.10 illustrate the various stages during the numerical simulation of the flow of SCUHPC mixes without and with fibres in an L-box, respectively. It can be observed from the simulations that in this numerical test the flows of both mixes with and without fibres are faster than their counterparts in the slump test, as expected due to the higher initial potential energy of the material in the L-box simulation. Due to the rapid nature of the flow, more undulations can be observed on the free surface of both flows. Also as expected, it is evident from the results that the flow of SCC without fibres has higher fluidity.

t=0.2 sec   t=0.4 sec

t=0.8 sec   t=1.1 sec
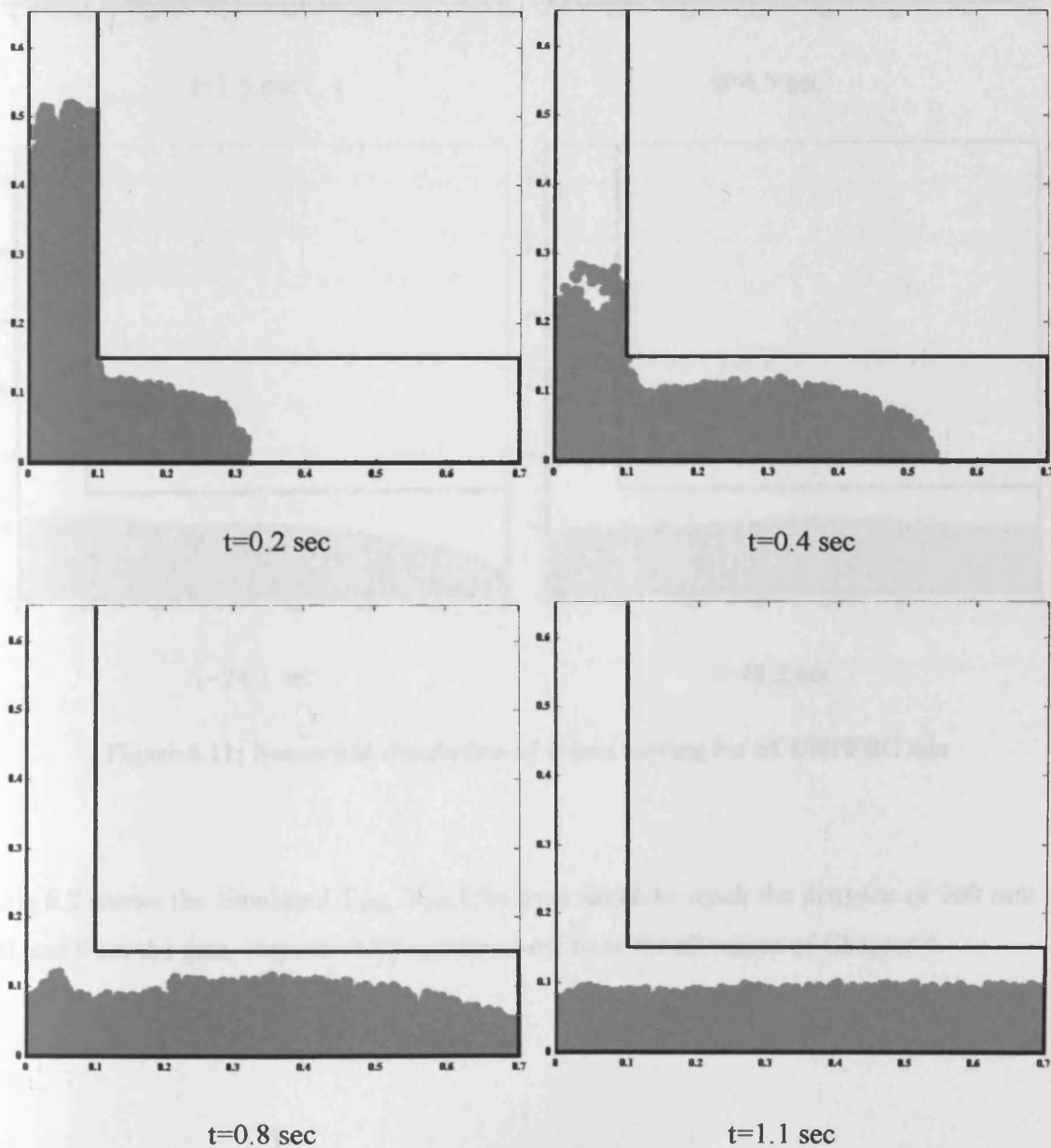
Figure 6.10: Numerical simulation of L-box casting for SCUHPC mix without fibres
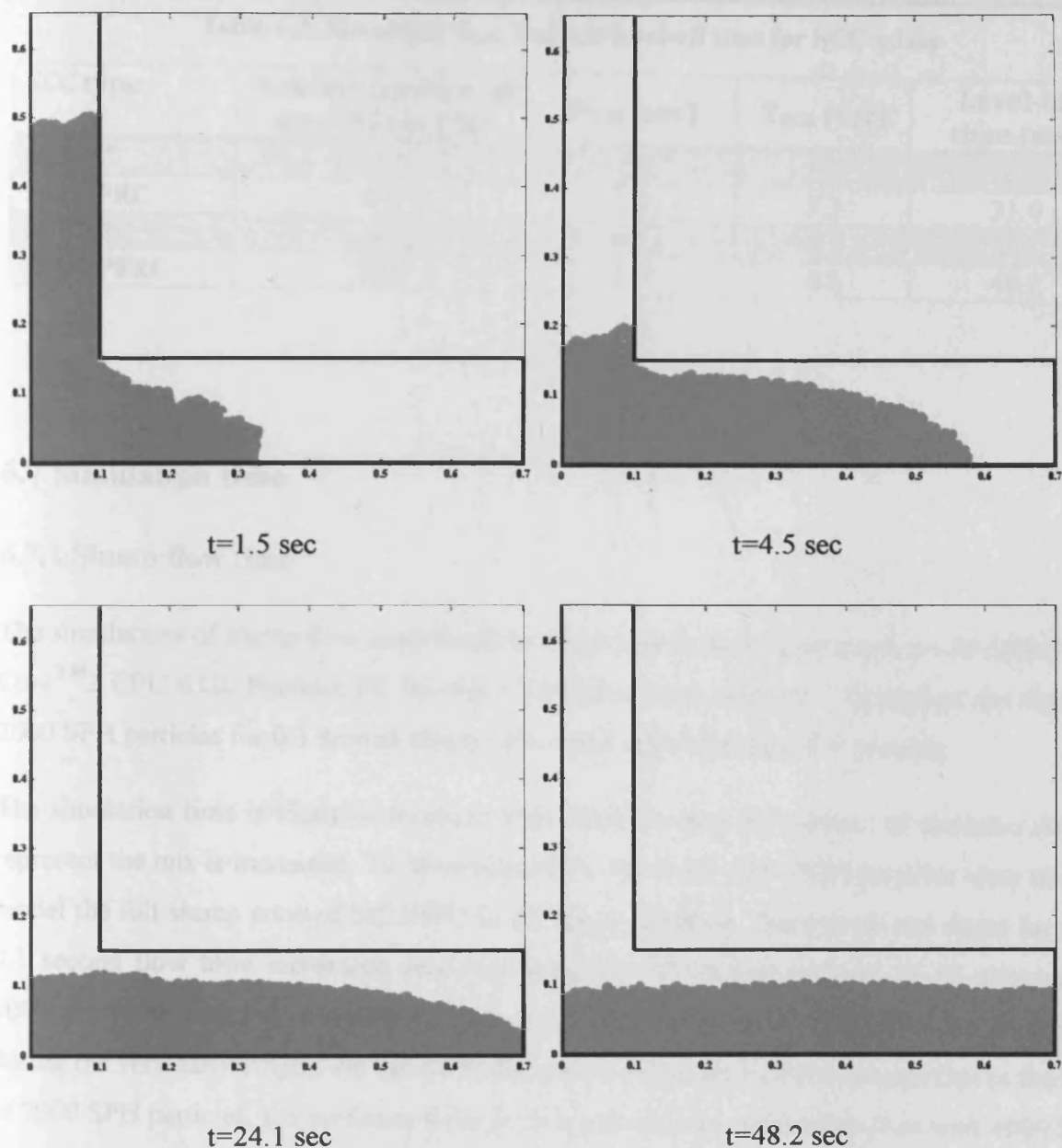
Figure 6.11: Numerical simulation of L-box casting for SCUHPFRC mix

Table 6.2 shows the simulated T_{200}, T_{400} (the time taken to reach the distance of 200 mm and 400 mm from the gate, respectively) and level-off time for all mixes of Chapter 4.

Table 6.2: Simulated T_{200}, T_{400} and level-off time for SCC mixes

SCC type	Volume fraction of steel fibres (%)	T_{200} (sec)	T_{400} (sec)	Level-off time (sec)
SCHPC	---	0.9	1.2	2.9
SCHPFRC	0.5	1.3	3.7	31.0
SCUHPC	---	0.3	0.7	0.9
SCUHPFRC	2.5	1.7	4.8	48.2

6.7 Simulation time

6.7.1 Slump flow time

The simulations of slump flow until the flow stops require several hours on a 1.86 GHz Intel® Core™2 CPU 6320 Pentium PC having 1.98 GB of core memory. The typical run time for 2000 SPH particles for 0.1 second slump flow takes approximately 6-7 minutes.

The simulation time is likely to increase significantly when the number of particles used to represent the mix is increased. To investigate this, 4000 and 7000 SPH particles were used to model the full slump cone of SCUHPC in 2D approximation. The typical run times for each 0.1 second flow time increment was approximately 50-54 minutes and 18-19 minutes for 7000 and 4000 particles, respectively. Figure 6.11 shows the flow of SCUHPC at three times during the very early stages. As can be observed the flows are identical except that in the case of 7000 SPH particles, the surfaces of the flow are show less undulations than with 4000 SPH particles.

t=0.1 sec

t=0.2 sec

t=0.3 sec
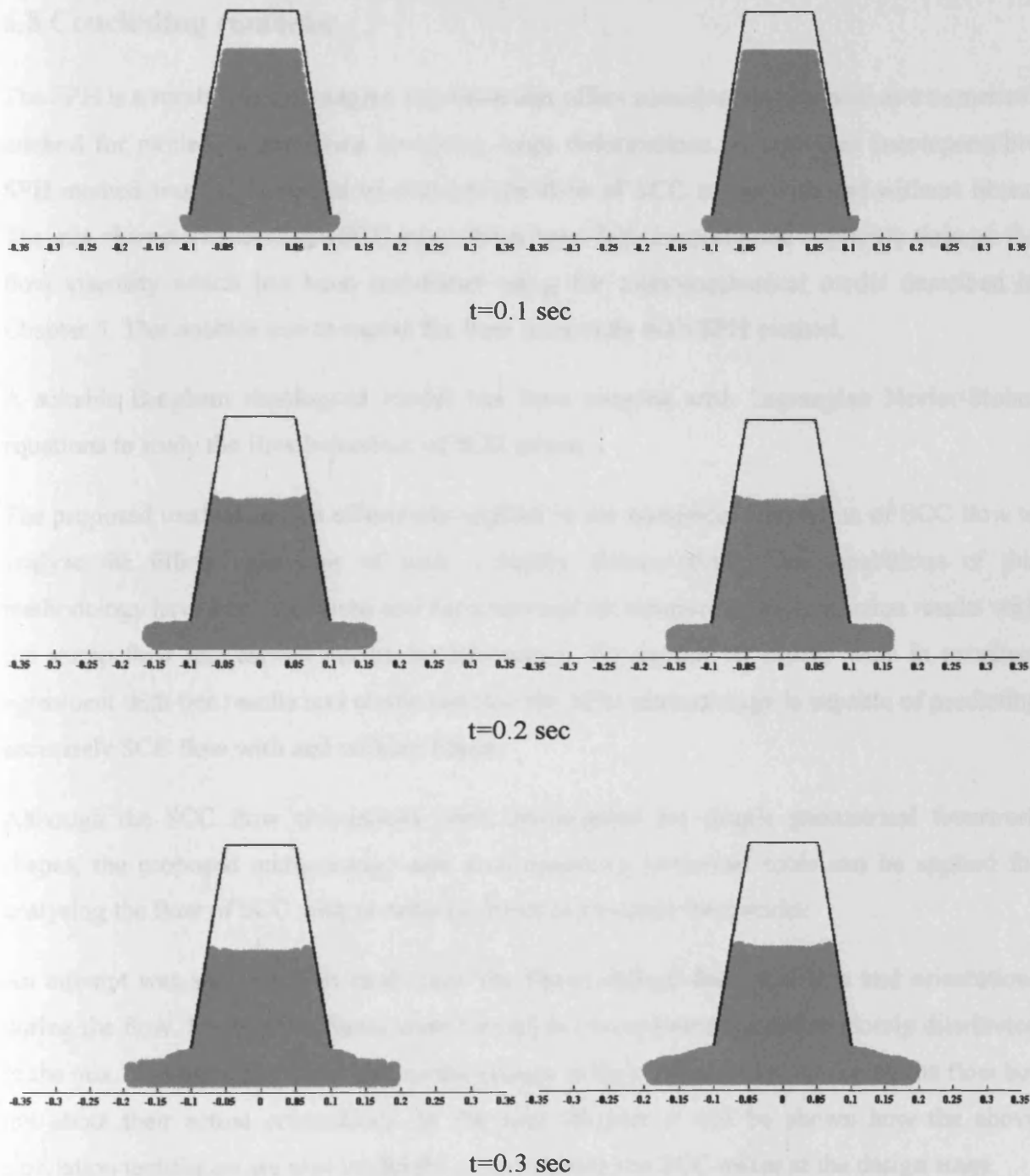
Figure 6.12: Numerical simulation of slump flow test for SCUHPC in 2D approximation using 4000 (left) and 7000 (right) particles

6.7.2 L-box time

The simulations of the L-box until the flow levels off require several hours on a 1.86 GHz Intel® Core™2 CPU 6320 Pentium PC having 1.98 GB of memory. The typical run time for 0.1 second flow takes approximately 7-8 minutes.

6.8 Concluding remarks

The SPH is a mesh-less Lagrangian approach that offers considerable potential as a numerical method for modelling problems involving large deformations. A corrected incompressible SPH method was implemented to simulate the flow of SCC mixes with and without fibres. The mix characteristics of the SCC mixes have been fully incorporated implicitly through the flow viscosity which has been calculated using the micromechanical model described in Chapter 5. This enables one to model the flow accurately with SPH method.

A suitable Bingham rheological model has been coupled with Lagrangian Navier-Stokes equations to study the flow behaviour of SCC mixes.

The proposed method can be effectively applied in the numerical simulation of SCC flow to analyse the filling behaviour of such a highly viscous fluid. The capabilities of this methodology have been validated and demonstrated by comparing the simulation results with the slump flow test carried out in the laboratory. The numerical results were in excellent agreement with test results and confirmed that the SPH methodology is capable of predicting accurately SCC flow with and without fibres.

Although the SCC flow simulations were investigated for simple geometrical formwork shapes, the proposed methodology and accompanying numerical tools can be applied for analysing the flow of SCC with or without fibres in complex formworks.

An attempt was also made to study how the fibres change their positions and orientations during the flow. For this the fibres were treated as concentrated masses randomly distributed in the mix. This gave a general idea of the change in their centres of mass during the flow but not about their actual orientations. In the next Chapter it will be shown how the above simulation techniques are also useful for proportioning the SCC mixes at the design stage.

The typical run time for 2000 SPH particles for 0.1 second slump flow takes approximately 6-7 minutes, whereas for 2500 SPH particles for 0.1 second L-box flow takes approximately 7-8 minutes.

A comparative study was carried out on simulation times. 7000 and 4000 SPH particles were used to simulate the full slump cone. It was observed that the run time was considerably increased (by at least 3 times) when the number of SPH particles was increased from 4000 to 7000.

Chapter 7

Guidelines for Mix Proportioning

of

Self-Compacting

High and Ultra High

Performance Concretes

With and Without

Steel Fibres

7.1 Introduction

In the previous Chapter the numerical techniques were used to simulate the flow of pre-designed SCC with or without fibres in moulds at the application stage. The same techniques are also useful for proportioning the SCC mixes at the design stage. They provide an alternative tool for the mix design of SCC, thus avoiding expensive and time-consuming tests in laboratories or on site.

The design tools are often more useful than the experimental methods in providing insightful and complete information through an extensive parametric study that cannot be easily performed by other means.

In this Chapter, the simulations of SCC mixes are used as an aid in the mix design stage of such concretes. Self-compacting high and ultra-high performance concrete (SCHPC/SCUHPC) mixes with and without steel fibres (SCHPFRC/SCUHPFRC) will be designed to cover a wide range of plastic viscosity. All these mixes will meet the flow and passing ability criteria, thus ensuring that they will flow properly into the moulds.

The various steps in the design of SCC mixes with or without steel fibres are as follows.

- Firstly, the slump flow test is carried out with the aid of the numerical simulation technique described in Chapter 6 on a series of SCC mixes having different plastic viscosities and volume fractions of steel fibre. The T_{500} (the time from lifting of the cone to the concrete spreading to a 500 mm diameter) for each mix is obtained with a view to investigating whether or not a correlation exists between T_{500} and the plastic viscosity.

- Secondly, in order to further analyse the flow of SCC in a mould, the flow of the same mixes is studied in an L-box configuration, and the T_{200}, T_{400} (the time taken by the mix to reach a distance of 200 mm (T_{200}) or 400 mm (T_{400}) from the gate) and level-off time are obtained, again with a view to ascertaining whether or not a correlation exists between these flow times and the mix plastic viscosity. It should be emphasized that at this stage in the mix design process the actual mix proportions are still unknown, apart from the volume fraction of fibres and the plastic viscosity of the mix.

- Finally, guidance is given for proportioning the mixes such that they will attain the given plastic viscosity and the T_{500}, T_{200}, T_{400}, and the level-off times.

7.2 Types of SCC mixes

As mentioned in Chapter 2, three different types of SCC can be distinguished depending on the method of ensuring the required plastic viscosity. These are the powder-type, the VMA type and the combined type. In this thesis two main mixes of the powder type were examined, i.e. SCHPFRC and SCUHPFRC (Chapter 4). These mixes are characterized by high powder content and a low water to powder ratio. Their self-compacting ability was achieved by adjusting the water to binder ratio and the superplasticiser dosage. However, in view of the high powder content, the powder-type SCC mixes are sensitive to changes in the constituent materials. This must be borne in mind during the proportioning of the mixes.

Okamura and Ozawa (1995) have proposed a heuristic mix proportioning method for this type of SCC (see, Chapter 2, Figure 2.6). According to their method, the coarse and fine aggregate contents are fixed and the self-compacting ability is obtained by adjusting the water to powder ratio and the amount of superplasticiser. However, as the SCC base mixes used here differ in terms of their fine constituents, type of superplasticiser and mixing procedures (see Chapter 4 and Tables (4.5) and (4.11)), the heuristic mix design method is not very appropriate. Instead, the three-step mix design method outlined above based on the actual simulation of the mixes were used.

7.3 Slump flow test

Slump flow simulations were carried out on a series of self-compacting high and ultra-high performance concretes with (SCHPFRC/SCUHPFRC) and without fibres (SCHPC/SCUHPC). The volume fractions of steel fibres were only varied out in the mixes: 0.5% and 1% in SCHPFRC mixes, and 1.5%, 2%, 2.5% and 3% in SCUHPFRC mixes. The target plastic viscosity of SCHPC mixes was chosen in the range from 4 Pas to 12 Pas, whilst that of SCUHPC mixes was from 2 Pas to 6 Pas. The lower plastic viscosity of the latter mixes is due to the absence of coarse aggregates in them. The target plastic viscosities of corresponding mixes with fibres were obtained using Equation (5.40). Table 7.1 gives the slump flow times (T_{500}) of this series of mixes obtained using the simulation technique described in Chapter 6.

According to the latest mix design rules for self-compacting concretes (BS EN 206-9, 2010) the maximum aggregate size is limited to 40 mm and two viscosity classes are introduced: viscosity class 1 (VS1) and viscosity class 2 (VS2) depending on whether $T_{500} < 2$ sec or $T_{500} \geq 2$ sec. The mixes considered below all belong to viscosity class 2.

Table 7.1: Slump flow time (T_{500}) for SCHPFRC and SCUHPFRC mixes with different volume fractions of steel fibre and target plastic viscosities

SCC type	Volume fraction of fibres (%)	Plastic viscosity of mix without fibres (Pas)	Plastic viscosity of mix with fibres (Pas)	T_{500} (s)
SCHPFRC	0.5	4	17.26	1.9
		6	25.89	2.1
		8	34.52	2.4
		10	43.15	3.0
		12	51.78	3.2
	1	4	30.52	2.2
		6	45.78	2.8
		8	61.04	3.3
		10	76.30	3.8
		12	91.56	4.2
SCUHPFRC	1.5	2	21.89	1.8
		3	32.84	2.0
		4	43.78	2.6
		5	54.73	3.2
		6	65.67	3.4
	2	2	28.52	2.0
		3	42.78	2.5
		4	57.04	2.9
		5	71.30	3.4
		6	85.56	3.7
	2.5	2	35.15	2.2
		3	52.73	2.8
		4	70.30	3.1
		5	87.88	3.6
		6	105.45	4.1
	3	2	41.78	2.4
		3	62.67	2.8
		4	83.56	3.4
		5	104.45	4.1
		6	125.34	4.8

Figure 7.1 shows that the T_{500} and the plastic viscosity of the above mixes are reasonably well correlated.
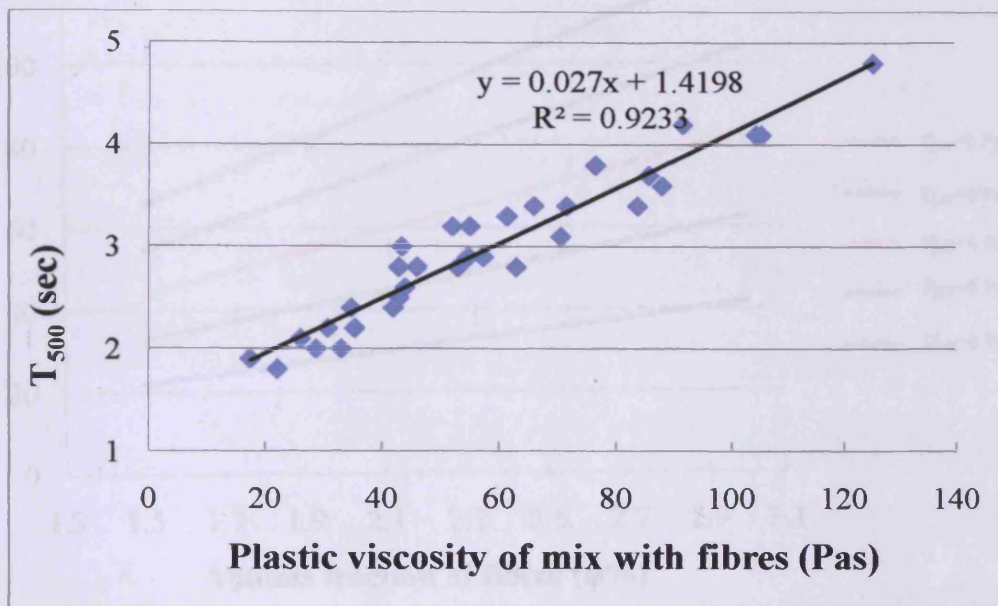
Figure 7.1: Simulated T_{500} vs. plastic viscosity of different mixes with steel fibres

Figures 7.2 and 7.3 show fan-shaped relationships between the plastic viscosity of SCHPFRC and SCUHPFRC mixes and the steel fibre volume fraction as the plastic viscosity of the base mixes without fibres increases.
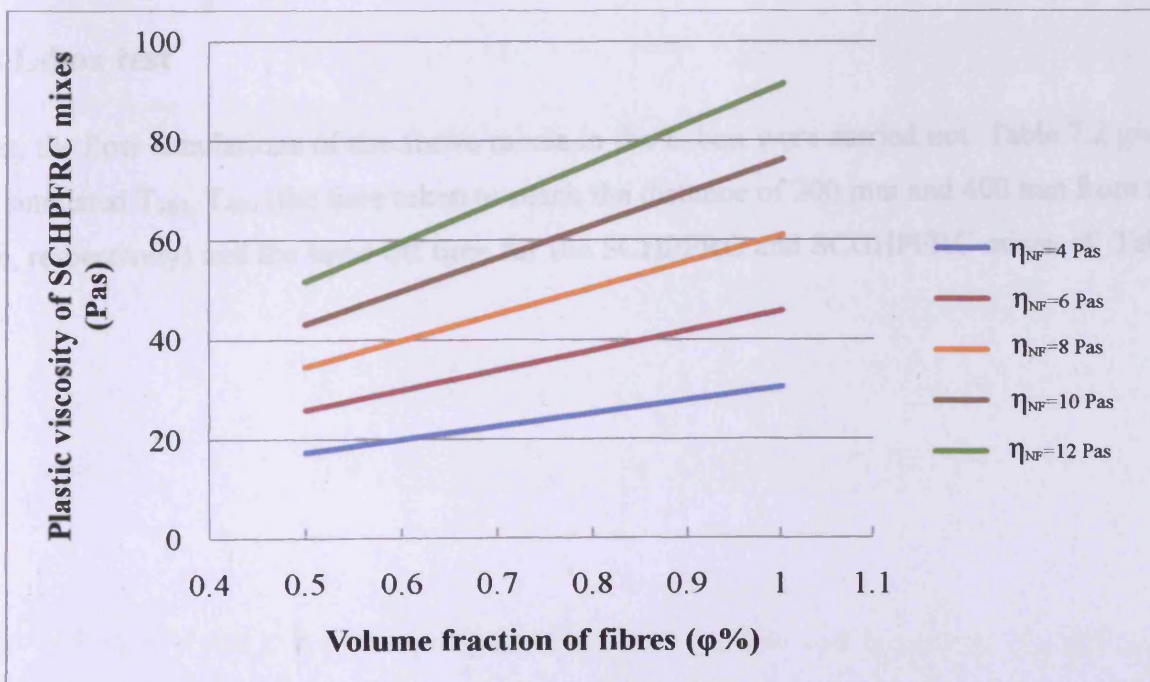
Figure 7.2: Fan-shaped correlation between plastic viscosities of SCHPFRC and steel fibre volume fractions (η_{NF} is the plastic viscosity of SCHPC mix without fibres)
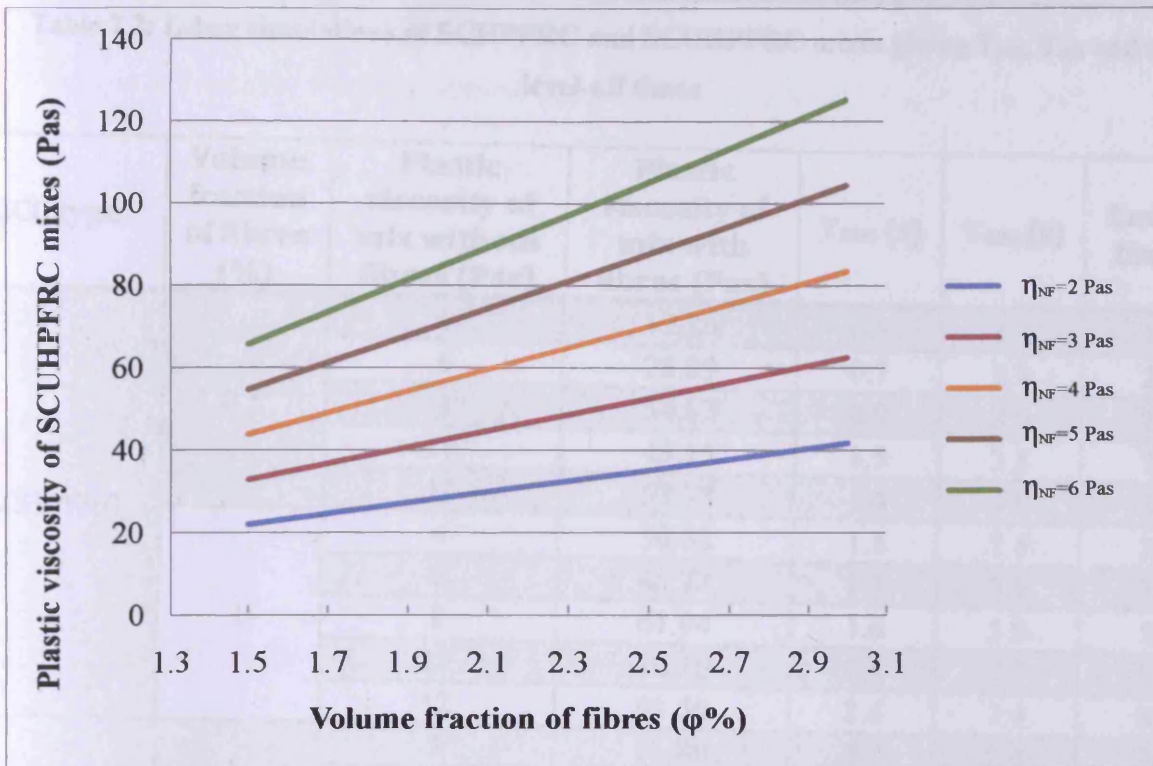
Figure 7.3: Fan-shaped correlation between plastic viscosities of SCUHPFRC and steel fibre volume fractions (η_{NF} is the plastic viscosity of SCUHPC mix without fibres)

7.4 L-box test

Next, the flow simulations of the above mixes in the L-box were carried out. Table 7.2 gives the simulated T_{200}, T_{400} (the time taken to reach the distance of 200 mm and 400 mm from the gate, respectively) and the level-off time for the SCHPFRC and SCUHPFRC mixes of Table 7.1.

Table 7.2: L-box simulations of SCHPFRC and SCUHPFRC mixes giving T_{200}, T_{400} and the level-off times

SCC type	Volume fraction of fibres (%)	Plastic viscosity of mix without fibres (Pas)	Plastic viscosity of mix with fibres (Pas)	T_{200} (s)	T_{400} (s)	Level-off time (s)
SCHPFRC	0.5	4	17.26	0.5	1.4	16.0
		6	25.89	0.7	2.8	23.2
		8	34.52	0.9	3.6	28.1
		10	43.15	1.5	3.8	31.7
		12	51.78	1.4	4.9	37.0
	1	4	30.52	1.1	2.8	27.9
		6	45.78	1.3	3.9	33.9
		8	61.04	1.6	5.0	58.5
		10	76.30	2.4	7.1	55.0
		12	91.56	2.4	7.4	87.7
SCUHPFRC	1.5	2	21.89	0.7	2.4	20.3
		3	32.84	0.9	3.4	25.5
		4	43.78	1.6	3.6	36.8
		5	54.73	1.7	5.0	44.6
		6	65.67	1.8	6.8	49.5
	2	2	28.52	0.9	2.5	20.7
		3	42.78	1.2	4.0	35.5
		4	57.04	2.0	4.9	40.7
		5	71.30	2.4	7.2	64.5
		6	85.56	2.3	7.9	65.7
	2.5	2	35.15	1.2	2.9	34.5
		3	52.73	1.8	4.8	45.2
		4	70.30	2.0	6.6	50.7
		5	87.88	2.7	8.0	75.3
		6	105.45	3.0	8.8	87.6
	3	2	41.78	1.1	3.9	31.5
		3	62.67	2.0	5.8	48.6
		4	83.56	2.4	8.7	70.1
		5	104.45	3.2	8.6	93.5
		6	125.34	4.6	12.1	96.3

Figure 7.4 depicts the trend between T_{200}, T_{400}, and the level-off times and the different plastic viscosity of the above mixes.

The data in Figure 7.4 shows that the various times correlate well with the plastic viscosity of
the mixes in the entire range of volume fractions of steel fibres (0.5-3.0%) studied.
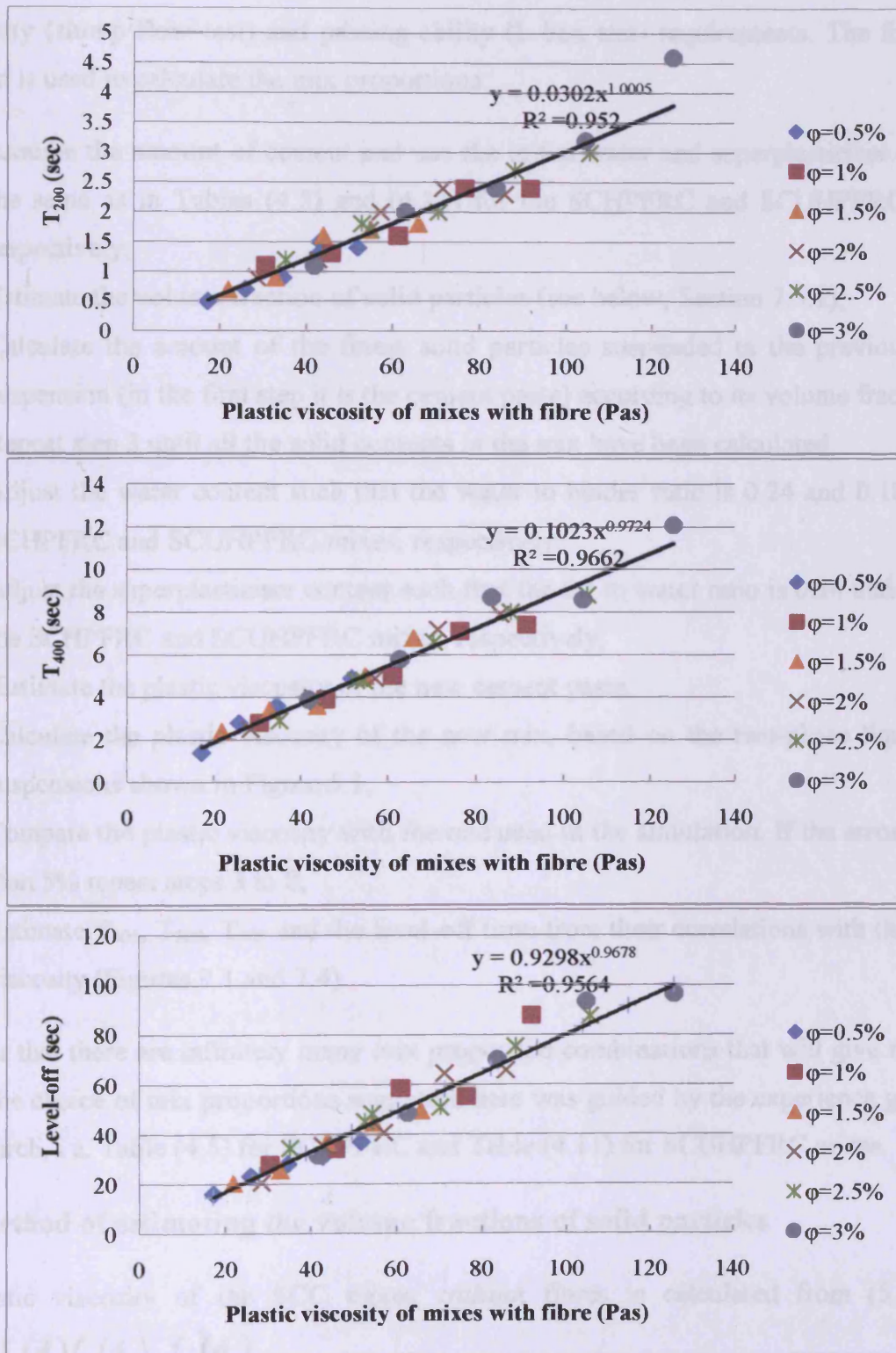
Figure 7.4: T_{200}, T_{400} and the level-off times vs the plastic viscosity of mixes for various fibre
volume fractions

7.5 Mix proportioning

The final step in the mix design process is to choose the mix proportions that will meet the flow-ability (slump flow test) and passing-ability (L-box test) requirements. The following algorithm is used to calculate the mix proportions:

1. Assume the amount of cement and use the initial water and superplasticiser contents the same as in Tables (4.5) and (4.11) for the SCHPFRC and SCUHPFRC mixes, respectively;

2. Estimate the volume fraction of solid particles (see below, Section 7.5.1);

3. Calculate the amount of the finest solid particles suspended in the previous liquid suspension (in the first step it is the cement paste) according to its volume fraction;

4. Repeat step 3 until all the solid contents in the mix have been calculated;

5. Adjust the water content such that the water to binder ratio is 0.24 and 0.18 for the SCHPFRC and SCUHPFRC mixes, respectively;

6. Adjust the superplasticiser content such that the SP to water ratio is 0.14 and 0.28 for the SCHPFRC and SCUHPFRC mixes, respectively;

7. Estimate the plastic viscosity of the new cement paste;

8. Calculate the plastic viscosity of the new mix, based on the two-phase liquid-solid suspensions shown in Figure 5.1;

9. Compare the plastic viscosity with the one used in the simulation. If the error is more than 5% repeat steps 3 to 8;

10. Estimate T_{500}, T_{200}, T_{400} and the level-off time from their correlations with the plastic viscosity (Figures 7.1 and 7.4).

It is clear that there are infinitely many mix proportion combinations that will give the same result. The choice of mix proportions suggested here was guided by the experience gained in this research, i.e. Table (4.5) for SCHPFRC and Table (4.11) for SCUHPFRC mixes.

7.5.1 Method of estimating the volume fractions of solid particles

The plastic viscosity of the SCC mixes without fibres is calculated from (5.41) i.e.

$$f_i(\phi_i) = f_1(\phi_1)f_2(\phi_2)\cdots f_n(\phi_n).$$

where $f_i(\phi_i)$ can be replaced by its equivalent, relative plastic viscosity, i.e. plastic viscosity

of SCC mix without fibre (η_{NF}) divided by the plastic viscosity of paste (η_{paste}). Therefore

(5.41) can be rewritten as

$$\eta_{NF} = \eta_{paste}\left\{ f_1(\phi_1)f_2(\phi_2)..f_n(\phi_n)\right\}$$ (7.1)

where

n: is total number of solid phases in the mix, such as coarse aggregate, sand, and cement
additives;

η_{paste} : is the plastic viscosity of the cement paste;

η_{NF} : is the plastic viscosity of SCC mix without fibres.

As stated in Chapter 5, the Krieger and Dougherty equation (5.11) is the most suitable for

cement pastes. Therefore (5.11) will be used here to obtain $f_i(\phi_i)$. The value of $[\eta] = 2.5$ and

$\phi_m = 0.63$ are used, as before.

For a given η_{NF} and η_{paste}, equation (7.1) can be rewritten as

$$(0.63-\phi_1)(0.63-\phi_2)(0.63-\phi_3)...(0.63-\phi_n)=u$$ (7.2)

where u is a constant number. The value of ϕ_i is given by

$$\phi_i = 0.63-t_i x$$ (7.3)

where $x = \sqrt[n]{u}$ and t_i is a factor such that

$$t_1 \times t_2 \times ... \times t_n = 1$$ (7.4)

An example of mix proportioning is given at the end of this Chapter.

7.5.2 Typical SCHPFRC mix proportions

Tables (7.3) and (7.4) give typical SCHPFRC mix proportions calculated in accordance with

the procedure described above. In these tables, ϕ_f, η_{NF} (error%) and η_{WF} represent the volume

fraction of fibre, the error in the plastic viscosity of the base SCHPC mix without fibres

(compared with the one used in simulations) and the plastic viscosity of SCHPFRC mix with

fibres, respectively.

Table 7.3: Typical mix proportions of SCHPFRC mixes with ϕ_f =0.5%

Constituents (kg/m³)	Cement	540	505	455	358	350
	Micro-silica	244	281	276	215	225
	Limestone	330	393	396	314	334
	Sand < 2 mm	451	556	573	463	500
	Coarse aggregates < 10 mm	590	753	796	654	716
	Water	188	189	175	138	138
	Superplasticiser	27	27	25	20	20
	Fibres	39	39	39	39	39
Ratios	Water/binder	0.24	0.24	0.24	0.24	0.24
	SP/water	0.14	0.14	0.14	0.14	0.14
Plastic viscosity	η_{Paste} (Pas)	0.30	0.29	0.31	0.36	0.36
	η_{NF} (Pas)	3.96	6.04	7.95	10.00	11.87
	η_{NF} (error%)	1.0	0.6	0.6	0.0	1.1
	η_{WF} (Pas)	17.09	26.04	34.31	43.14	51.22
Slump	T_{500} (Slump flow test) (sec)	1.9	2.1	2.3	2.6	2.8
L-box	T_{200} (L-box test) (sec)	0.5	0.8	1.0	1.3	1.5
	T_{400} (L-box test) (sec)	1.6	2.4	3.2	4.0	4.7
	Level-off time (L-box test) (sec)	14.5	21.8	28.5	35.5	42.0

Table 7.4: Typical mix proportions of SCHPFRC mixes with ϕ_f =1%

Constituents (kg/m³)	Cement	550	520	425	410	397
	Micro-silica	249	288	250	265	277
	Limestone	337	403	358	387	410
	Sand < 2 mm	461	570	519	571	614
	Coarse aggregates < 10 mm	603	772	720	806	880
	Water	192	194	162	162	162
	Superplasticiser	28	28	23	23	23
	Fibres	78	78	78	78	78
Ratios	Water/binder	0.24	0.24	0.24	0.24	0.24
	SP/water	0.14	0.14	0.14	0.14	0.14
Plastic viscosity	η_{Paste} (Pas)	0.30	0.29	0.32	0.32	0.32
	η_{NF} (Pas)	3.93	5.89	7.99	10.02	12.10
	η_{NF} (error%)	1.9	1.9	0.1	0.2	0.8
	η_{WF} (Pas)	29.96	44.93	60.97	76.44	92.34
Slump	T_{500} (Slump flow test) (sec)	2.2	2.6	3.1	3.5	3.9
L-box	T_{200} (L-box test) (sec)	0.9	1.4	1.8	2.3	2.8
	T_{400} (L-box test) (sec)	2.8	4.1	5.6	6.9	8.3
	Level-off time (L-box test) (sec)	25.0	37.0	49.7	61.8	74.2

7.5.3 Typical SCUHPFRC mix proportions

Tables (7.5), (7.6), (7.7) and (7.8) give typical SCUHPFRC mix proportions calculated in
accordance with the procedure described above.

Table 7.5: Typical mix proportions of SCUHPFRC mixes with ϕ_f =1.5%

Constituents (kg/m³)	Cement	660	550	480	435	402
	Micro-silica	263	283	294	303	310
	Ground granulated blast furnace slag (GGBS)	185	232	263	288	307
	Quartz Sand 9-300 μm	341	411	460	499	533
	250-600 μm	408	509	584	646	700
	Water	195	187	182	180	179
	Superplasticiser	55	52	51	50	50
	Fibres	117	117	117	117	117
Ratios	Water/binder	0.18	0.18	0.18	0.18	0.18
	SP/water	0.28	0.28	0.28	0.28	0.28
Plastic viscosity	η_{Paste} (Pas)	0.31	0.30	0.30	0.29	0.29
	η_{NF} (Pas)	2.01	3.04	4.09	5.12	6.11
	η_{NF} (error%)	0.6	1.2	2.3	2.3	1.9
	η_{WF} (Pas)	22.01	33.22	44.82	56.00	66.91
Slump	T_{500} (Slump flow test) (sec)	2.0	2.3	2.6	2.9	3.2
L-box	T_{200} (L-box test) (sec)	0.7	1.0	1.4	1.7	2.0
	T_{400} (L-box test) (sec)	2.1	3.1	4.1	5.1	6.1
	Level-off time (L-box test) (sec)	18.5	27.6	36.9	45.7	54.3

Table 7.6: Typical mix proportions of SCUHPFRC mixes with ϕ_f =2%

Constituents (kg/m³)	Cement	650	535	480	435	400
	Micro-silica	151	178	196	209	219
	Ground granulated blast furnace slag (GGBS)	306	342	371	392	408
	Quartz Sand 9-300 μm	339	406	460	500	533
	250-600 μm	406	503	584	647	699
	Water	195	185	184	182	180
	Superplasticiser	55	52	52	51	51
	Fibres	156	156	156	156	156
Ratios	Water/binder	0.18	0.18	0.18	0.18	0.18
	SP/water	0.28	0.28	0.28	0.28	0.28
Plastic viscosity	η_{Paste} (Pas)	0.31	0.30	0.29	0.29	0.29
	η_{NF} (Pas)	2.00	3.06	4.01	5.00	6.01
	η_{NF} (error%)	0.2	2.1	0.2	0.1	0.2
	η_{WF} (Pas)	28.59	43.71	57.17	71.36	85.70
Slump	T_{500} (Slump flow test) (sec)	2.2	2.6	3.0	3.3	3.7
L-box	T_{200} (L-box test) (sec)	0.9	1.3	1.7	2.2	2.6
	T_{400} (L-box test) (sec)	2.7	4.0	5.2	6.5	7.8
	Level-off time (L-box test) (sec)	23.9	36.0	46.7	57.8	69.0

Table 7.7: Typical mix proportions of SCUHPFRC mixes with ϕ_f =2.5%

Constituents (kg/m³)	Cement	630	550	480	435	400
	Micro-silica	188	216	231	243	251
	Ground granulated blast furnace slag (GGBS)	261	308	335	357	374
	Quartz Sand 9-300 μm	251	326	376	416	448
	250-600 μm	481	592	666	729	781
	Water	190	189	184	182	180
	Superplasticiser	53	53	52	51	50
	Fibres	195	195	195	195	195
Ratios	Water/binder	0.18	0.18	0.18	0.18	0.18
	SP/water	0.28	0.28	0.28	0.28	0.28
Plastic viscosity	η_{Paste} (Pas)	0.31	0.30	0.29	0.29	0.29
	η_{NF} (Pas)	2.07	2.98	4.02	5.02	6.03
	η_{NF} (error%)	3.6	0.6	0.5	0.3	0.4
	η_{WF} (Pas)	36.46	52.44	70.65	88.18	105.90
Slump	T_{500} (Slump flow test) (sec)	2.4	2.8	3.3	3.8	4.3
L-box	T_{200} (L-box test) (sec)	1.1	1.6	2.1	2.7	3.2
	T_{400} (L-box test) (sec)	3.4	4.8	6.4	8.0	9.5
	Level-off time (L-box test) (sec)	30.2	42.9	57.3	71.0	84.7

Table 7.8: Typical mix proportions of SCUHPFRC mixes with ϕ_f =3%

Constituents (kg/m³)	Cement	650	540	480	435	400
	Micro-silica	177	202	220	231	240
	Ground granulated blast furnace slag (GGBS)	279	318	348	369	385
	Quartz Sand 9-300 µm	132	201	253	292	325
	250-600 µm	594	691	770	832	884
	Water	194	187	184	182	180
	Superplasticiser	54	52	52	51	51
	Fibres	234	234	234	234	234
Ratios	Water/binder	0.18	0.18	0.18	0.18	0.18
	SP/water	0.28	0.28	0.28	0.28	0.28
Plastic viscosity	η_{Paste} (Pas)	0.31	0.30	0.29	0.29	0.29
	η_{NF} (Pas)	2.01	3.04	4.01	5.01	6.02
	η_{NF} (error%)	0.4	1.3	0.4	0.2	0.3
	η_{WF} (Pas)	41.93	63.48	83.86	104.68	125.72
Slump	T_{500} (Slump flow test) (sec)	2.6	3.1	3.7	4.2	4.8
L-box	T_{200} (L-box test) (sec)	1.3	1.9	2.5	3.2	3.8
	T_{400} (L-box test) (sec)	3.9	5.8	7.6	9.4	11.3
	Level-off time (L-box test) (sec)	34.6	51.6	67.6	83.8	100.0

As can be seen from Tables (7-3) to (7-8), in order to increase the plastic viscosity of SCC mixes, the amount of binder should be increased, whereas that of liquids (water and superplasticiser) should be decreased.

7.6 Concluding remarks

Various SCC mixes with different plastic viscosity and steel fibres content were studied. These mixes were characterised as a powder-type SCC.

Slump flow and L-box numerical simulations were performed on a series of mixes to test their flow ability and passing ability as measured by the T_{500} (for slump flow test), T_{200}, T_{400} and level-off time (for L-box test). At this stage in the mix design process the actual mix proportions were still unknown, apart from the volume fraction of fibres and the plastic viscosity of the mix.

Finally, guidance was given for proportioning the mixes such that they will attain the given plastic viscosity and the T_{500}, T_{200}, T_{400}, and the level-off times. This guidance followed a step by step algorithm. An example is given below to illustrate this algorithm.

7.7 An example of mix proportioning

As an example of the application of the mix proportioning method described in Section 7.5, let us calculate the mix proportions of a SCUHPFRC mix with ϕ_f=3% , assuming that the viscosity of the base SCUPHC mix without fibres is η_{NF}=4 Pas and that of the cement paste is η_{paste}=0.30 Pas

1. The amount of cement (c) is assumed to be 520 kg/m^3. The initial amount of water (w) and superplasticiser (sp) are the same as in Table (4.11) i.e. 188 kg/m^3 and 52.64 kg/m^3, respectively.

2. In order to estimate the volume fractions of micro-silica ϕ_{ms}, GGBS ϕ_g, fine quartz sand (9-300 µm) ϕ_{s1} and coarse quartz sand (250-600 µm) ϕ_{s2} we proceed as per the algorithm above. We first use Equation (7.1) as follows.

$$\eta_{NF} = \eta_{paste} \times \left(1-\frac{\phi_{ms}}{0.63}\right)^{-2.5\times0.63} \times \left(1-\frac{\phi_g}{0.63}\right)^{-2.5\times0.63} \times \left(1-\frac{\phi_{s1}}{0.63}\right)^{-2.5\times0.63} \times \left(1-\frac{\phi_{s2}}{0.63}\right)^{-2.5\times0.63} =$$

$$\frac{\eta_{paste}}{\left((0.63)^4\right)^{-2.5\times0.63}}\left[(0.63-\phi_{ms})(0.63-\phi_g)(0.63-\phi_{s1})(0.63-\phi_{s2})\right]^{-2.5\times0.63} \qquad (7.5)$$

Substituting η_{NF}=4 Pas and η_{paste}=0.30 Pas into (7.5) yields

$$u = (0.63-\phi_{ms})(0.63-\phi_g)(0.63-\phi_{s1})(0.63-\phi_{s2}) = 0.030417 \qquad (7.6)$$

Therefore

$$x=\sqrt[4]{u} = 0.417618 \qquad (7.7)$$

Using (7.3) i.e. $\phi_i = 0.63 - t_i x$ with $t_1 = 34/33$, $t_2 = 33/34$, $t_3 = 6/5$ and $t_4 = 5/6$ (note that $t_1 t_2 t_3 t_4 = 1$), (7.6) gives the following volume fractions of solid phases

$$\phi_{ms} = 0.199727$$
$$\phi_g = 0.224665$$
$$\phi_{s1} = 0.128859$$
$$\phi_{s2} = 0.281985$$

(7.8)

There is an infinite choice in the selection of t_is, as mentioned before.

3. The amount of finest solid particle i.e. micro-silica (ms) suspended in cement paste is calculated according to its volume fraction (ϕ_{ms}) to give

$$\phi_{ms} = \frac{\dfrac{ms}{\rho_{ms}}}{\left(\dfrac{c}{\rho_c} + \dfrac{w}{\rho_w} + \dfrac{sp}{\rho_{sp}} \right) + \dfrac{ms}{\rho_{ms}}}$$

(7.9)

Using $\rho_c = 2950$ kg/m^3, $\rho_w = 1000$ kg/m^3, $\rho_{sp} = 1070$ kg/m^3 and $\rho_{ms} = 2200$ kg/m^3 in (7.9) gives the amount of micro-silica as $ms = 227$ kg/m^3.

4. Step 3 is repeated until all the solid contents in the mix have been calculated i.e. GGBS (g), fine quartz sand (9-300 μm)(s1) and coarse quartz sand (250-600 μm) (s2). The amounts of GGBS ($\rho_g = 2400$ kg/m^3) and of the quartz sands ($\rho_{s1} = \rho_{s2}$ =2650 kg/m^3) work out to be $g = 359$ kg/m^3, $s1 = 261$ kg/m^3 and $s2 = 796$ kg/m^3.

5. The amount of water is adjusted such that water-binder ratio is 0.18. Therefore $w = 195$ kg/m^3.

6. The amount of superplasticiser is adjusted such that SP-water ratio is 0.28. Therefore $sp = 55$ kg/m^3.

7. The value of plastic viscosity of cement paste in relation to the original cement paste used in Table 4.11 is estimated to be 0.29 pas.

8. The plastic viscosities of SCC mix with and without fibres are calculated according to procedures described in Chapter 5. This gives $\eta_{NF} = 8.9$ Pas.

9. This value of plastic viscosity is compared with the one used in the simulation (i.e.
η_{NF} =4 Pas). This gives an error in η_{NF} > 5% which is not acceptable. Therefore steps
3 to 8 have to be repeated with a lower trial amount of cement in order to reduce the
plastic viscosity.

- 3 (repeat): try cement=450 kg/m^3, giving ms=214 kg/m^3.
- 4 (repeat): calculate corresponding g=339 kg/m^3, $s1$=246 kg/m^3 and $s2$=750 kg/m^3.
- 5 (repeat): the amount of water is w=176 kg/m^3.
- 6 (repeat): the amount of superplasticiser is sp=49 kg/m^3.
- 7 (repeat): viscosity of cement paste is calculated as 0.30 Pas.
- 8 (repeat): the plastic viscosity of new mix will be η_{NF}=4.32 Pas.
- 9 (repeat): the error in the plastic viscosity is 7.4% which is again not acceptable.
  Therefore steps 3 to 8 have to be repeated again with a new trial amount of cement.

- 3 (repeat): try cement=480 kg/m^3, gives ms=220 kg/m^3.
- 4 (repeat): repeat the previous step yields: g=348 kg/m^3, s1=253 kg/m^3 and s2=770 kg/m^3.
- 5 (repeat): the amount of water is w=184 kg/m^3.
- 6 (repeat): the amount of superplasticiser is sp=52 kg/m^3.
- 7 (repeat): viscosity of cement paste is calculated as 0.29 Pas.
- 8 (repeat): the plastic viscosity of new mix will be η_{NF}=4.01 Pas.
- 9 (repeat): the error in the plastic viscosity is 0.4% (<5%) which is acceptable.

---

10. T_{500}, T_{200}, T_{400} and level-off times are estimated based on their correlation with plastic
viscosity (see Figures (7.1) and (7.4)). Table 7.9 gives the SCUHPFRC constituents.

Table 7.9: SCUHPFRC constituents

Constituents (kg/m³)	Cement	480
	Micro-silica	220
	Ground granulated blast furnace slag (GGBS)	348
	Quartz Sand 9-300 μm	253
	250-600 μm	770
	Water	184
	Superplasticiser	52
	Fibres	234
Ratios	Water/binder	0.18
	SP/water	0.28
Plastic viscosity	η_{Paste} (Pas)	0.29
	η_{NF} (Pas)	4.01
	η_{NF} (error%)	0.4
	η_{WF} (Pas)	83.86
Slump	T_{500} (Slump flow test) (sec)	3.7
L-box	T_{200} (L-box test) (sec)	2.5
	T_{400} (L-box test) (sec)	7.6
	Level-off time (L-box test) (sec)	67.6

7.7.1 Remarks on the choice of t_i

As mentioned previously, for a given viscosity of the paste, there are many (theoretically infinitely many) mix combinations that will lead to the desired viscosity of the SCUHPC. This is reflected in the choice of t_i. The best starting point is to choose $t_1=t_2=t_3=t_4=1$ and to check the error in the resulting viscosity of the mix. If this error is more than the acceptable limit (5%) then the new trial values of t_i need to be chosen such that $t_1t_2t_3t_4=1$ and the process of mix proportioning repeated until the error in the viscosity η_{NF} is less than 5%.

Chapter 8

Conclusions
and
Recommendations
for
Future Research

8.1 Conclusions

The main conclusions on the basis of the research work embodied in Chapters 4 to 7, inclusive, are summarised below:

- The development of self-compacting high-performance and ultra high-performance concrete mixes is a complex process requiring the resolution of conflicting demands of flow-ability and non-segregation. Whilst these demands can be reconciled by increasing the paste content and decreasing the large aggregate volume, the resulting self-compacting mixes may not reach the target compressive strength (Chapter 4).

- The easiest way to meet the strength requirement is to include steel fibres in the mix. This can however compromise the ability of the mix to flow smoothly through gaps in the reinforcement and to cause segregation of the fibres (Chapter 4).

- Self-compacting high- and ultra high-performance concrete mixes without fibres may be designed to satisfy only the flow-ability and cohesiveness criteria using the slump flow test. However, when long steel fibres are present in the mixes, it is additionally necessary to check that the mixes meet the passing ability criterion using the J-Ring apparatus (Chapter 4).

- The micromechanical procedure developed in Chapter 5 estimates the plastic viscosity of SCC mixes with or without steel fibres from the knowledge of the plastic viscosity of cement paste alone or of the cement paste with SP and/or VMA. In this procedure, the SCC mix is regarded as a succession of two-phase suspensions- solid and liquid phases (Chapter 5).

- It was noted that the influence of the discrete solid phase on the plastic viscosity of the continuous liquid phase depends only on the volume fraction of the solid phase ϕ_i, if it is less than 10%. This influence was captured by the Einstein equation (or many of its later modifications) which contains the intrinsic viscosity $[\eta]$ (Chapter 5).

- However, when the volume fraction of the solid phase exceeds 10% but is less than the maximum possible volume fraction ϕ_m, then the relative viscosity depends not only on the volume fraction of the discrete solid phase but also on how it is dispersed in the fluid and on the shape of the solid particles. In this case the formula proposed by Krieger and Dougherty (1959) was used (Chapter 5).

- The fibres were regarded as rigid slender bodies in a viscous medium whose free translation and rotation are restrained by the viscous concrete mix (Chapter 5).

- The plastic viscosity, together with the yield stress of the SCC mixes with or without fibres, is needed to simulate the flow both at the mix design stage and at the industrial use stage to simulate the flow in the formwork. However the yield stress of SCC mix is practically unchanged over a large range of plastic viscosity (Chapter 5).

- The SPH is a mesh-less Lagrangian approach that offers considerable potential as a numerical method for modelling problems involving large deformations. A corrected incompressible SPH method was implemented to simulate the flow of SCC mixes with and without fibres (Chapter 6).

- A suitable Bingham rheological model was coupled with Lagrangian Navier-Stokes equations to study the flow behaviour of SCC mixes (Chapter 6).

- The capabilities of this methodology were validated by comparing the simulation results with the slump flow test carried out in the laboratory. The numerical results were in excellent agreement with test results and confirmed that the SPH methodology is capable of predicting accurately SCC flow with and without fibres (Chapter 6).

- An attempt was also made to get a qualitative idea of how the fibres change their positions and orientations during the flow. For this a limited number of fibres were treated as concentrated masses randomly distributed in the mix. This gave a general idea of the change in their centres of mass during the flow but not about their actual orientations (Chapter 6).

- Several powder-type high- and ultra high-performance SCC mixes with different plastic viscosity and steel fibre content were proportioned using the SPH simulations as a mix design tool (Chapter 7).

- Guidance was given for proportioning the mixes such that they will attain the given plastic viscosity and the T_{500}, T_{200}, T_{400}, and the level-off times. This guidance was presented as a step by step algorithm for ease of use (Chapter 7).

8.2 Recommendations for future research

- In most practical applications of SCHPFRC/SCUHPFRC using 30mm long Dramix steel fibres, the volume fraction of steel fibres is usually less than 3% for workability reasons. In this case the dilute concentration approximation of slender steel fibres made in Chapter 5 is adequate. The expressions derived in Chapter 5 are accurate for needle-shaped steel fibres with aspect ratio up to 85 in dilute concentrations. The fibres were regarded as rigid slender bodies in a viscous medium whose free translation and rotation are restrained by the viscous concrete mix. However, for steel fibres in larger concentrations and/or larger aspect ratios, the interaction of steel fibres needs to be considered. In this case the assumptions that the fibres are rigid and that they are statistically homogeneously distributed in the mix need to be re-examined.

- The flow of SCHPFRC/SCUHPFRC affects the orientation of the fibres. To exploit the full potential of SCHPFRC/SCUHPFRC, the orientations of the fibres need to be monitored during the flow. In this thesis, only a limited number of fibres was treated as lumped masses and randomly distributed in the diametrical section using a random number generator. However, in order to find the actual orientations of the fibres during the flow, it is necessary to treat all the fibres in the mix not as lumped masses but as slender bodies.

- In this thesis, the L-box was simulated in a 2D configuration. However, in order to understand fully the flow of SCHPC/SCUHPC with or without fibres, a full 3D simulation is required.

- The run time was considerably increased (by at least 3 times) when the number of SPH particles representing the SCC mix was increased from 4000 to 7000. The simulation algorithm should be modified in order to accelerate the run times, thus reducing the computational cost. This can be done by either rearranging the memory allocations for each argument or using parallel computations.

References

Aiad, I., Abd El-Aleem, S. and El-Didamony, H., 2002, Effect of delaying addition of some concrete admixtures on the rheological properties of cement pastes, *Cement and Concrete Research*, Vol. 32, pp. 1839-1843.

ASTM C1240 and EN 13263, Silica fumes for use in concrete, mortar and grout. Definitions, specifications and conformity criteria.

Aydin, A.C., 2007, Self compact ability of high volume hybrid fibre reinforced concrete, *Construction and Building Materials*. Vol. 21, No. 6, p.p 1149-1154.

Bakker, P., Ramohalli Gopala, V., Lycklama à Nijeholt, J.A., Koenders, E., Grünewald, S. and Walraven, J., 2010, Simulation and testing of the grout backfill process in a case-study related to a nuclear waste disposal gallery in self-compacting concrete (SCC). In: *Proceedings of the 2010 International RILEM Symposium on Self-Compacting Concrete*. Design, production and placement of self-consolidating concrete eds. Khayat KH. and Feys. D. Canada; 2010. pp. 197-208.

Banfill, P.B.G., Beaupré, D., Chapdelaine, F., de Larrard, F., Domone, P.L., Nachbaur, L., Sedran, T., Wallevik, J.E. and Wallevik, O., 2001, In Ferraris, C.F. and Brower, L.E. (eds), Comparison of concrete rheometers: *International tests at LCPC (Nantes, France)* in October 2000. NISTIR 6819, National institute of standards and technology, Washington, USA, October.

Barnes, H. A., Hutton, J. F. and Walters, K., 1993, *An introduction to rheology*, Elsevier, pp. 119-128.

Bartos, P.J.M., Marrs, D.L., 1999, Development and testing of self-compacting grout for the production of SIFCON, Proceedings *of international workshop on high performance fibre reinforced cement composites*, eds H.W. Reinhardt and, A.E. Maaman, Germany, pp. 171-180.

Batchelor, G.K., 1971, The stress generated in a non-dilute suspension of elongated particles by pure straining motion, *Journal of Fluid Mechanics Digital Archive*, Vol. 46, pp. 813-829.

Batchelor, G.K., 1977, The effect of Brownian motion on the bulk stress in a suspension of spherical particles, *Journal of Fluid Mechanics Digital Archive*, Vol. 83, pp. 97-117.

References

Bennenk, I. H. W., 2005, Self-compacting concrete - five years of experience with SCC in the netherlands, in *Proceedings of the 18th BIBM International Congress*, Amsterdam, pp. 211-218.

Benson, S.D.P. and Karihaloo B.L., 2005a, CARDIFRC®-Development and mechanical properties. Part I: Development and workability. *Magazine of Concrete Research*, Vol. 57, No. 6, pp. 347-352.

Benson, S.D.P. and Karihaloo, B.L., 2005b, CARDIFRC®-Development and mechanical properties. Part III: Uniaxial tensile response and other mechanical properties, *Magazine of Concrete Research*, Vol. 57, No. 8, pp. 433-443.

Benson, S.D.P., Nicolaides, D and Karihaloo, B.L., 2005, CARDIFRC®-Development and mechanical properties. Part II: Fibre distribution. *Magazine of Concrete Research* , Vol. 57, No. 7, pp. 421-432.

Billberg, P., 1999, Self-compacting concrete for civil engineering structures-the Swedish experience, Report no 2:99, *Swedish Cement and Concrete Research Institute*, Stockholm, pp. 121-129.

Billberg, P., Petersson, O., Westerholm, M., Wustholz, T. and Reinhardt, H., 2004, Summary report on work package 3.2: Test methods for passing ability, pp. 48-62.

Bonen, D. and Sarkar, S.L., 1995, The superplasticiser adsorption capacity of cement pastes, pore solution composition, and parameters affecting flow loss. *Cement and Concrete Research*, Vol. 25, No.7, pp. 1423-1434

Bonet, J and Lok, T.S., 1999, Varational and momentum aspects of smooth particle hydrodynamics formulations, *Computer Methods in Applied Mechanics and Engineering*, Vol. 180, pp. 97-115.

Bonet, J. and Kulasegaram, S., 2000, Correction and stabilization of smooth particle hydrodynamic methods with application in metal forming simulations, *International Journal of Numerical Methods in Engineering*, Vol. 47, pp. 1189-1214

References

Bouzoubaa, N. and Lachemib, M., 2001, Self compacting concrete incorporating high-volumes of class f fly ash: preliminary results, *Cement and Concrete Research*, Vol. 31, No. 3, pp. 413-420.

Brite, E.R., 2000, Self compacting concrete, proposal No. BE96-3801, No.10, pp. 1-48.

Bui, V.K., Akkaya, Y. and Shah, S.P., 2002, Rheological model for self-consolidating concrete, *ACI Materials Journal*, Vol. 99, No. 6, pp. 549-559.

Carlsward J, Emborg M, Utsi S, Oberg P., 2003, Effects of constituents on the workability and rheology of self-compacting concrete. In: The *3rd International RILEM Symposium on Self-Compacting Concrete*, Wallevik OH, Nielsson I, editors, RILEM Publications S.A.R.L, Bagneux, France, pp. 143-153.

Chhabra, R.P., Richardson, J.F., 2008, *Non-newtonian flow and applied rheology engineering applications*, Elsevier second edition, pp. 11-63.

Chindaprasirt, P., Hatanaka, S., Chareerat, T., Mishima, N. and Yuasa, Y., 2008, Cement paste characteristics and porous concrete properties, *Construction and Building Materials*, Vol. 22, pp. 894-901.

Chindaprasirt, P., Jaturapitakkul, C. and Sinsiri, T., 2005, Effect of fly ash fineness on compressive strength and pore size of blended cement paste, *Cement and Concrete Composites*, Vol. 27, No. 4, pp. 425–428.

Chong, J. S., Christiansen, E. B. and Baer, A. D., 1971, Rheology of concentrated suspensions, *Journal of Applied Polymer Science*, Vol. 15, pp. 2007-2021.

Chorin, A.J., 1968, Numeical solution of the Navier-Stokes equations, *Mathematics of Computation*, Vol. 22, pp. 745-762.

Chu, H, Machida, A. and Suzuki, N., 1996, Experimental investigation and DEM simulation of filling capacity of fresh concrete, *Transactions of the Japan Concrete Institute*, Vol. 16 pp. 9-14.

Crofton, M. W., 1885, probability, *Encyclopedia Brittanica*, 9th ed., Vol. 19, pp. 768-788.

References

Cummins, S.J. and Rudman, M., 1999, An SPH projection method, *Journal of Computational Physics*, Vol. 152, No. 2, pp. 584-607.

Cussigh, F., 1999, Self-compacting concrete stability, *Proceedings of First RILEM International Symposium on Self Compacting Concrete*, Stockholm, Å. Skarendahl 13-15 September.

Cyr, M., Legrand, C. and Mouret, M., 2000, Study of the shear thickening effect of superplasticizers on the rheological behaviour of cement pastes containing or not mineral additives, *Cement and Concrete Research*, Vol. 30, pp. 1477-1483.

David, B. and Shah, S. P., 2004, Concrete construction-fresh and hardened properties of self-consolidating concrete, *Progress in Structural Engineering and Materials*, Vol. 7, pp. 14-26.

de Castro, A.L. and Liborio, J.B.L., 2006, Initial rheological description of high performance concretes, *Materials Research*, Vol. 9, pp. 405-410.

de Kruif, C.G., van Iersel, E.M.F., Vrij, A. and Russel, W.B., 1985, Hard sphere colloidal dispersions: Viscosity as a function of shear rate and volume fraction, *The Journal of Chemical Physics*, AIP, pp. 4717-4725.

de Larrard, F., Hu, C., Sedran, T., Szitkar, J.C., Joly, M., Claux, F. and Derkx, F., 1997, A new rheometer for soft-to-fluid fresh concrete. *ACI Materials Journal*, Vol. 94 No. 234-243.

Dietz, J. and Ma, J., 2000, Preliminary examinations for the production of self-compacting concrete using lignite fly ash, *LACER* No. 5, pp.125-139.

Domone, P. L., 2003, Fresh concrete, in *Advanced concrete technology*, eds. J Newman, B S Choo, Elsevier, Vol. 2, Ch 1.

Domone, P.L. and Thurairatnam, H., 1988, The effect of water/cement ratio, plasticizers and temperature on the rheology of cement grouts, *Advances in Cement Research*, Vol. 1, No. 4, pp. 203-214.

Domone, P.L., Chai, H., 1998, The slump flow test for high workability concrete, *Cement and Concrete Research*, Vol. 28, pp. 117-182.

Domone, P.L., Xu, Y. and Banfill, P.F.G., 1999, Developments of the two-point workability test for high-performance concrete. *Magazine of Concrete Research*, Vol. 51, pp. 171–179.

Dransfield, J., 2003, Admixtures for concrete, mortar and grout, In: *Advanced concrete technology*. eds. Newman J and Choo BS. Elsevier, Vol. 2, Ch 4.

Druta, C., 2003, Tensile strength and bonding characteristics of self-compacting concrete. M.Sc. Thesis, Louisiana state university and agricultural and mechanical college.

Dufour, F. and Pijaudier-Cabot, G., 2005, Numerical modelling of concrete flow: homogeneous approach, *International Journal for Numerical and Analytical Methods in Geomechanics*, Vol. 29, pp. 395-416.

Duval, R. and Kadri, E.H., 1998, Influence of silica fume on the workability and the compressive strength of high-performance concretes, *Cement and Concrete Research*, Vol. 28, No. 4, pp.533-547.

Eilers, H., 1941, The viscosity of emulsions of highly viscous substances as function of the concentration, Coloid Zh, Vol. 97, pp. 313.

EN 15167-1 and EN 15167-2 (or BS 6699), 2006, Ground granulated blast furnace slag for use in concrete, mortar and grout, definitions, specifications and conformity criteria.

EN 206-9:2010, Concrete. Additional rules for self-compacting concrete (SCC), published April 2010.

Esping O., 2007, Slump flow values versus Bingham parameters for high flowable mortars and concretes, *Proceedings of the 5th International RILEM Symposium-SCC*, Ghent, Belgium, pp. 315-322.

European guidelines for self-compacting concrete, specification, production and use, 2005, pp. 1-68.

Fernàndez-Altable, V. and Casanova, I., 2006, Influence of mixing sequence and superplasticiser dosage on the rheological response of cement pastes at different temperatures, *Cement and Concrete Research*, Vol. 36, pp. 1222-1230.

References

Ferraris, C.F., 2000, Comparison of concrete rheometers, International tests at LCPC (Nantes, France) October, National Institute of Standards and Technology (USA), pp. 127-139.

Ferraris, C.F., de Larrard, F.and Martys, N.S., 2001a, Fresh concrete rheology: recent developments. *Materials science of concrete* VI, In: S. Mindess, J. Skalny (Eds.), Proceedings, American Ceramic Society. December 2001, American Ceramic Society, Westerville, OH, pp. 215-241.

Ferraris, C.F., Obla, K.H. and Hill, R., 2001b, The influence of mineral admixtures on the rheology of cement paste and concrete, *Cement and Concrete Research*, Vol. 31, pp. 245-255.

Feys, D., Heirman, G., De Schutter, G., Verhoeven, R., Vandewalle, L. and Van Germet, D., 2007, Comparison of two concrete rheometers for shear thickening behaviour of SCC, Magnel Laboratory for Concrete Research, Ghent University, Belgium, pp. 407-418.

Flatt, R.J., 2004a, Dispersion forces in cement suspensions, *Cement and Concrete Research*, Vol. 34, No. 3, pp. 399–408.

Flatt, R.J., 2004b, Towards a prediction of superplasticized concrete rheology, *Materials and Structures*, Vol. 37, pp. 289-300.

Frankel, N.A. and Acrivos, A., 1967, On the viscosity of a concentrated suspension of solid spheres, *Chemistry and Engineering Science*, Vol. 22, pp. 847-853.

Gaimster, R. and Dixon, N., 2003, Self-compacting concrete, in *Advanced concrete technology*, eds. J Newman, B S Choo Elsevier London, Vol. 3, Ch 9.

Gingold, R.A. and Monaghan, J. J., 1977, Smoothed Particle Hydrodynamics: theory and application to non-spherical stars, *Monthly Notices of the Royal Astronomical Society*, Vol. 181, pp.375-389.

Gjorv, O.E., 1997, Concrete workability: a more basic approach needed, in selected research studies from Scandinavia, report TVBM-3078, Lund institute of technology, pp. 45–56.

Goodier, C.I., 2003, Development of self-compacting concrete, *Structures Building*, Vol. 156, Issue SB4, pp. 405-414.

References

Groth, P., 2000, Fibre reinforced concrete-fracture mechanics methods applied on self-compacting concrete and energetically modified binders. Ph.D. thesis, Department of civil and mining engineering division of structural engineering Luleå University of technology Luleå, Sweden.

Grünewald, S. and Walraven, J. C., 2003, Rheological measurements on self-compacting fibre reinforced concrete, *Proceedings of the 3rd International RILEM Symposium on Self-Compacting Concrete*, eds. Ó. Wallevik, I. Nielsson, pp. 49-58, RILEM S.A.R.L, France.

Grünewald, S., 2004, Performance-based design of self-compacting fibre reinforced concrete, Ph.D. Thesis of Delft university (Netherlands), pp. 48-61.

Grzeszczyk, S. and Lipowski, G., 1997, Effect of content and particle size distribution of high-calcium fly ash on the rheological properties of cement pastes, *Cement and Concrete Research*, Vol. 27, pp. 907-916.

Gupta, R. K., 2000, *Polymer and composite rheology, Morgantown, USA*, CRC Press, pp. 177-179.

Guth, E. and Simha, A. R., 1936, Viscosity of suspensions and solutions, *Kolloid-Z*, Vol. 74, No. 266.

Hassan, A.A.A, Lachemi, M. and Hossain, K.M.A., 2010, Effect of metakaolin on the rheology of self-consolidating concrete. In: *Proceedings of the 2010 International RILEM Symposium on Self-Compacting Concrete*. Design, production and placement of self-consolidating concrete eds. Khayat KH. and Feys. D. Canada; 2010. pp. 103-113.

Heirman, G., Vandewalle, L., Van Gemert, D. and Wallevik, Ó., 2008, Integration approach of the Couette inverse problem of powder type self-compacting concrete in a wide-gap concentric cylinder rheometer, *Journal of Non-Newtonian Fluid Mechanics*, Vol. 150, pp. 93-103.

Jacobs, F. and Hunkeler, F., 1999, Design of self-compacting concrete for durable concrete structures. *Proceedings of Self-Compacting Concrete Stockholm*, Sweden, pp. 397 - 407

References

Johnston, C.D., 1996, *Proportioning, mixing and placement of fibre-reinforced cements and concretes, Production Methods and Workability of Concrete*, Edited by Bartos, Marrs and Cleland, E&FN Spon, London. pp. 155-179.

Khayat, K.H. and Z. Guizani., 1997, Use of viscosity-modifying admixture to enhance stability of fluid concrete, *ACI Materials Journal*, Vol. 94, No. 4, pp.332-340.

Khayat, K.H. Ghezal, A. and Hadriche, M.S., 1999, Factorial design models for proportioning self-consolidating concrete, *Materials and Structures*, Vol. 32, pp. 679–686.

Khayat, K.H., 1999, Workability, testing, and performance of self-consolidating concrete, *ACI Materials Journal*, Vol. 96, No. 3, pp. 339-346.

Khayat, K.H., M.Vachon, and M. C. Lanctot., 1997, Use of blended silica fume cement in commercial concrete mixtures, *ACI Materials Journal*, Vol. 94, No. 3, pp.183-192.

Khayat, K.H., Roussel, Y., 2000, Testing and performance of fibre-reinforced self-consolidating concrete, First Int. Symposium on SCC, Stockholm, edited by Skarendahl and Petersson, RILEM publications PRO 7, pp. 509-521.

Kim, J.K., Han, S.H., Park, Y.D., Noh, J.H., Park, C.L., Kwon, Y.H. and Lee, S.G., 1996, Experimental research on the material properties of super flowing concrete, In: P.J.M. Bartos, D.L.Marrs, D.J.Cleland (Eds), *Production Methods and Workability of Concrete*, E&FN Spon London, pp.271-284

Kong, H.J., Bike, G. S. and Li V.C., 2003, Development of self-consolidating engineered cementitious composite employing electrosteric dispersion/stabilization, *Cement and Concrete Composites*, Vol. 25, pp. 301-309.

Koshizuka, S., Nobe, A. and Oka, Y., 1998, Numerical analysis of breaking waves using moving particle semi-implicit method, *International Journal for Numerical Methods in Fluids*, Vol. 26, pp.751-769.

Krieger, I.M. and Dougherty, T.G., 1959, A mechanism for non-Newtonian flow in suspensions of rigid spheres, *Journal of Rheology*, Vol. 3, pp. 137–152.

References

Kuder, K.G., Ozyurt, N., Mu, E.B. and Shah, S.P., 2007, Rheology of fibre-reinforced cementitious materials, *Cement and Concrete Research*, Vol. 37, pp. 191-199.

Kulasegaram, S., Bonet, J., Lewis, R.W. and Profit, M., 2002, mould filling simulation in high pressure die casting by mesh-less method, WCCMV, *Fifth world congress on computational mechanics* July 7-12, 2002, Vienna, Austria Eds.: H.A. Mang, F.G. Rammerstorfer, J. Eberhardsteiner.

Kulasegaram, S., Bonet, J., Lewis, R.W. and Profit, M., 2004, A variational formulation based contact algorithm for rigid boundaries in two-dimensional SPH applications, *Computational Mechanics*, Vol. 33, pp. 316-325.

Kurita, M. and Nomura, T., 1998, High-flowable steel fibre-reinforced concrete containing fly ash, Proceedings, *Sixth CANMET/ACI international conference on fly ash, silica fume, slag, and natural pozzolans in concrete*, SP-178, V. M. Malhotra, ed., American Concrete Institute, Farmington Hills, Michigan, pp. 159-179.

Kurokawa, Y., Taniwawa, Y., Mori, H. and Komura, R., 1994, A study on the slump test and slump-flow test of fresh concrete, *Transactions of the Japan Concrete Institute*, Vol. 16, pp. 25-32.

Kurokawa, Y., Tanigawa, Y., Mori, H. and Nishinosono, Y., 1996, Analytical study on effect of volume fraction of coarse aggregate on Bingham's constants of fresh concrete, *Transactions of the Japan Concrete Institute*, Vol. 18, pp. 37-44.

Lachemi, M., Hossain, K.M.A., Lambros, V., Nkinamubanzi, P.C. and Bouzoubaâ, N., 2004, Performance of new viscosity modifying admixtures in enhancing the rheological properties of cement paste, *Cement and Concrete Research*, Vol. 34, pp. 185-193.

Laskar, A.I. and Talukdar, S., 2008, Rheological behaviour of high performance concrete with mineral admixtures and their blending, *Construction and Building Materials*, Vol. 22, pp. 2345-2354.

Li, S.F. and Liu, W.K, 1996, Moving least square Kernel Galerkin method (II) Fourier analysis, *Computer Methods in Applied Mechanics and Engineering*, Vol. 139, No. 4, pp. 159-193.

References

Liu, G.R. and Liu, M.B., 2003, *Smoothed particle hydrodynamics: A mesh-free particle method*, published by World Scientific Publishing Co. Pte. Ltd, Singapore.

Liu, M., 2009, Wider application of additions in self-compacting concrete. Ph.D. thesis. Department of civil, environmental and geomatic engineering, University College London. pp. 45-55.

Lucy L.B., 1977, Numerical approach to testing the fission hypothesis, *Astronomical Journal*, Vol. 82, pp.1013-1024.

Ma, J., Dietz, J. and Dehn, F., 2003, Ultra high performance self compacting concrete (2003) pp. 136-144, In: *Self-Compacting Concrete, Proceedings, 3rd Intern. RILEM Symp.* Eds. O. Wallevik and I Nielsson, RILEM Publications S.A.R.L. August 17-20, 2003.

Martys, N.S., 2005, Study of a dissipative particle dynamics based approach for modelling suspensions, *Journal of Rheology*, Vol. 49, No. 2, pp. 401-424.

Mikanovic, N. and Jolicoeur, C., 2008, Influence of superplasticisers on the rheology and stability of limestone and cement pastes, *Cement and Concrete Research*, Vol. 38, pp. 907-919.

Mindess, S., Young, J. F. and Darwin, D., 2003, *High-performance construction materials: science and applications*, Second Edition, Prentice Hall USA, pp. 12-18.

Mittal, K. L. and Kumar, P., 1999, *Handbook of microemulsion science and technology*, CRC Press, pp. 357-362.

Monaghan, J.J., 1992, Smoothed particle hydrodynamics, *Annual Review of Astronomy and Astrophysics*, Vol. 30, pp. 543-574.

Monaghan, J.J., 1994, Simulating free surface flows with SPH, *Journal of Computational Physics*, Vol. 110, pp. 399-406.

Mooney, M., 1957, The viscosity of a concentrated suspension of spherical particles, *Journal of Colloid Science*, Vol. 6, pp. 162-170.

Mori, H. and Tanigawa, Y, 1992, Simulation methods for fluidity of fresh concrete, memoirs of the school of engineering, Nagoya University, Vol. 44, pp. 71-133.

References

Morton, R. R. A., 1966, The expected number and angle of intersections between random curves in a plane, *Journal of Applied Probability*, Vol. 3, pp. 559-562.

Nehdi, M. and Rahman, M.A., 2004, Estimating rheological properties of cement pastes using various rheological models for different test geometry, gap and surface friction, *Cement and Concrete Research*, Vol. 34, pp. 1993-2007.

Neophytou, M.K.A, Pourgouri, S., Kanellopoulos, A.D., Petrou, M.F., Ioannou, I, Georgiou, G. and Alexandrou, A., 2010, Determination of the rheological parameters of self-compacting concrete matrix using slump flow test, *Journal of applied rheology*, Vol. 20 DOI: 10.3933/ApplRheol-20-62402.

Nguyen, T., Roussel, N. and Coussot, P., 2006, Correlation between l-box test and rheological parameters of a homogeneous yield stress fluid, *Cement and Concrete Research*, Vol. 36, No. 10, pp. 1789-1796.

Nicolaides, D., 2004, Fracture and fatigue of CARDIFRC®, Ph.D. Thesis, Department of Civil Engineering, Cardiff University, pp. 148-153.

Nmai, C. and Violetta, B., 1996, The use of flowing concrete in congested areas, *Concrete International*, Vol. 18, No. 9, pp. 53-57.

Noguchi, T., Oh, S. and Tomosawa, F., 1999, Rheological approach to passing ability between reinforcing bars of self-compacting concrete, In: *The 1st International RILEM Symposium on Self-Compacting Concrete*, Skarendahl A, Petersson O, editors, RILEM Publications S.A.R.L, France pp. 59-70.

Noor, M.A. and Uomoto T., 1999, Three-dimensional discrete element simulation of rheology tests of self-compacting concrete, In: *Proceedings of the 1st International RILEM Symposium on Self-Compacting Concrete*, Skarendahl Å, Petersson Ö (eds). RILEM: Cachan, pp. 35-46.

Oh, S. G., Noguchi, T and Tomosawa, F., 1997, Evaluation of pass ability of self-compacting concrete by visualization model, *Proceedings of Japan Concrete Institute*, Vol. 19, No.1. pp. 37-42.

References

Okamura, H. and Ouchi, M., 2003a, Applications of self-compacting concrete in Japan. In: *The 3rd International RILEM Symposium on Self-Compacting Concrete*, Wallevik OH, Nielsson I, editors, RILEM Publications S.A.R.L. Bagneux France, pp. 3-5.

Okamura, H. and Ouchi, M., 2003b, Self-compacting concrete, *Journal of Advanced Concrete Technology*, Vol. 1, No. 1, pp. 5-15.

Okamura, H. and Ozawa, K., 1995, Mix design for self-compacting concrete, *Concrete Library of JSCE*, Vol. 25, pp. 107-120.

Okamura, H. Ouchi, M. Hibino, M. and Ozawa, K., 1998, A rational mix-design method for mortar in self-compacting concrete, *The 6th East Asia-Pacific Conference on Structural Engineering & Construction*, Vol. 2, pp. 1307–1312.

Okamura, H., 1999, Self compacting concrete development, present use and future, *Proceedings of First RILEM International Symposium on Self Compacting Concrete*, Stockholm, 13–15 September, pp. 120-128.

Okamura, H., Ozawa, K., Ouchi, M., 2000, Self compacting concrete, *Structural Concrete*, Vol 1, pp. 3–17.

Ouchi M, Hibino M and Okamura H., 1996, Effect of superplasticiser on self-compact ability in fresh concrete, transportation research record, *Journal of the Transportation Research Board*, Vol. 1574, pp. 37-40.

Ouchi, M. and Hibino-Nagaoka, M., 2000, Development, applications and investigations of self-compacting concrete, Kochi University of Technology, Japan, pp. 1-14.

Ouchi, M., 1999, State-of-the-art report on self-compact ability evaluation, *Proceedings of the International Workshop on Self-Compacting Concrete (CD-ROM)*, Kochi, Japan, March 1999, Also available from concrete engineering series, No. 30, Japan society of civil engineers, pp. 15-21.

Ouchi, M., Nakamura, S., Osterson, T., Hallberg, S. and Lwin, M., 2003, Applications of self-compacting concrete in Japan, Europe and the United States, ISHPC, p 2-5.

References

Ozawa, K. Maekawa, K. Kunishama, M and Okamura, H., 1989, Development of high performance concrete based on the durability design of concrete structures, *Proceedings of the 2nd East-Asia and Pacific Conference on Structural Engineering and Construction (EASEC-2)*, Vol 1, pp. 445–450.

Ozawa, K., Maekawa, K., Okamura, H., 1990, High performance concrete with high filling capacity, *Proceedings of RILEM International Symposium on Admixtures for Concrete: Improvement of Properties*, ed. E Vasquez, Barcelona, pp. 51–62.

Papadakis, V.G., 1999, Experimental investigation and theoretical modelling of silica fume activity in concrete, *Cement and Concrete Research*, Vol. 29, pp.79-86

Papanastasiou, T.C., 1987, Flows of materials with yield, *Journal of Rheology*, Vol. 31, pp. 385-404.

Pashias, N., Boger, D., Summers, J. and Glenister, D., 1996, A fifty-cent rheometer for yield stress measurement, *Journal of Rheology*, Vol. 40, pp. 1179-1189.

PCI, 2003, Interim guidelines for the use of self-consolidating concrete in precast pre-stressed concrete institute member plants, pp. 14-18.

Petersson, Ö., 2003, Simulation of self-compacting concrete - laboratory experiments and numerical modelling of testing methods, j ring and l-box tests, In: Proceedings of the 3rd *International RILEM Symposium*, Pro 33, Wallevik O , Nielsson I (eds). RILEM: Cachan, pp. 202-207.

Petit, J.-Y., Wirquin, E., Vanhove, Y. and Khayat, K., 2007, Yield stress and viscosity equations for mortars and self-consolidating concrete, *Cement and Concrete Research*, Vol. 37, pp. 655-670.

Phan-Thien, N. and Huilgol, R.R., 1980, A micromechanic theory of chopped-fibre-reinforced materials, *Journal of Fibre Science and Technology*, Vol. 13, pp. 423-433.

Phan-Thien, N. and Karihaloo, B.L., 1994, Materials with negative poisson's ratio: A qualitative microstructural model, *Journal of Applied Mechanics*, Vol. 61, pp. 1001-1004.

References

Quemada, D., 1984. Models for rheological behaviour of concentrated disperse media under shear. In: *Advances in Rheology* (eds. B. Mena, A. Garcia-Rejon, C. Rangel –Nafaile), Universidad Nacional Autonama de Mexico, Mexico City, pp. 571–582.

Ramachandran, V. S., Feldman, R. F. and Beaudoin, J. J., 1981, *Concrete Science*, Heyden and Son Ltd London, ISBN 0855017031, pp. 141-155.

Reinhardt, H.W. and Wustholz, T., 2006, About the influence of the content and composition of the aggregates on the rheological behaviour of self-compacting concrete, *Materials and structures*, Vol. 39, pp. 683-693.

Richard, P. and Cheyrezy, M., 1995, Composition of reactive powder concrete, *Cement and Concrete Research*, Vol.25, No.7, pp.1501-1511.

RILEM (2002), Workability and rheology of fresh concrete: compendium of test. Report of technical committee TC145-WSM. Bartos, P.J.M., Sonebi M. and Tamimi, A.K. (eds), RILEM, Paris, pp. 23-35.

RILEM TC 174 SCC, 2000, Self- compacting concrete State-of-the-art report of RILEM technical committe 174-SCC. Skarendahl A, Petersson O, editors, RILEM Publications S.A.R.L., France.

Robinson, J.V., 1957. The viscosity of suspension of spheres: sediment volume as a determining parameter. *Transactions of the Society of Rheology*, Vol. 1, p. 15.

Roussel, N., 2006, A theoretical frame to study stability of fresh concrete, *Materials and Structures*, Vol. 39, No. 285, pp. 75–84.

Roussel, N., 2007a, A thixotropy model for fresh fluid concretes: Theory and applications, Proceedings of the 5th *International RILEM Symposium-SCC 2007*. 1, pp 267-272, Ghent, Belgium.

Roussel, N., 2007b, Rheology of fresh concrete: from measurements to predictions of casting processes, *Materials and Structures*, Vol. 40, pp. 1001-1012

Roussel, N., and Coussot, P., 2005, fifty-cent rheometer for yield stress measurements: From slump to spreading flow, *Journal of Rheology*, Vol.49, No. 3, pp. 705–718.

References

Roussel, N., Geiker, M.R., Dufour, F. ,Thrane, L.N. and Szabo, P., 2007, Computational modelling of concrete flow : general overview, *Cement and Concrete Research*, Vol.37, pp.1298-1307.

Roussel, N., Staquet, S., D'Aloia Schwarzentruber, L., Le Roy, R. and Toutlemonde, F, 2007, SCC casting prediction for the realization of prototype VHPC-precambered composite beams, *Materials and Structures*, Vol. 40, No. 9, pp. 134-144.

Roussel, N., Stefani, C. and Leroy, R., 2005, From mini-cone test to abrams cone test: measurement of cement-based materials yield stress using slump tests, *Cement and Concrete Research*, Vol. 35, No. 5, pp. 817–822.

Roziere, E., Granger, S., Turcry, Ph., and Loukili, A., 2007, Influence of paste volume on shrinkage cracking and fracture properties of self compacting concrete, *Cement and Concrete Composites*, Vol. 29, No. 8, pp. 626-636. doi:10.1016/j.cemconcomp.2007. 03.010.

Russel, W.B., 1973, On the effective moduli of composite materials: Effect of fiber length and geometry at dilute concentrations, Zeitschrift *für Angewandte Mathematik und Physik (ZAMP)*, Vol. 24, pp. 581-600.

Russell, H. G., 1997, High performance concrete-from buildings to bridges, *Concrete International*, Vol. 19, No. 8, pp.62-63.

Saak W.A., Jennings H.M. and Shah S.P., 2001, New methodology for designing SCC, *ACI Materials Journal*, Vol. 98, pp. 429-439.

Saito, N., 1950, Concentration dependence of the viscosity of high polymer solutions. I, *Journal of the Physical Society of Japan*, Vol. 5, pp. 4-8.

Sedran, T. and De Larrard, F., 1999, Optimization of self compacting concrete thanks to packing model, *Proceedings of First RILEM International Symposium on Self Compacting Concrete*, Stockholm, 13–15 September, pp. 168-180.

Shao, S. and Lo, E.Y.M., 2003, Incompressible SPH method for simulating Newtonian and non-Newtonian flows with a free surface, *Advances in Water Resources*, Vol. 26, pp. 787-800.

References

Shenoy, A.V., 1999, *Rheology of filled polymer systems*, Springer USA, pp. 136-149.

Simha, R., J., 1952, Mathematics of solid-liquid suspension, *Journal of Applied Physics*, Vol. 23, pp. 102-111.

Sobolev, K. G., 1999, High performance concretes, Dundee, Scotland. *4th International Conference - Creating with Concrete*, 6-10 September 1999, Edited by Ravindra K Dhir and Kevin A Paine, pp. 125-136.

Sonebi, M. and Bartos, P., 2005, Filling ability and plastic settlement of self compacting concrete, *Materials and structures*, Vol. 35, pp. 462-469.

Sonebi, M., 2004, Medium strength self-compacting concrete containing fly ash: Modelling using factorial experimental plans, *Cement and Concrete Research*, Vol. 34, No.7, pp. 1199-1208.

Sonebi, M., Zhu, W. and Gibbs, J., 2001, Bond of reinforcement in self-compacting concrete, *Cement and Concrete Research*, Vol. 35, No. 7, pp. 26-28.

Solomon, H., 1978, Geometric probability. Society for industrial and applied mathematics, USA.

Spangenberg, J., Roussel, N., Hattel, J.H., Thorborg, J., Geiker, M.R., Stang, H. and Skocek, J., 2010, Prediction of the impact of flow-induced inhomogeneities in self-compacting concrete (SCC). In: *Proceedings of the 2010 International RILEM Symposium on Self-Compacting Concrete*. Design, production and placement of self-consolidating concrete eds. Khayat KH. and Feys. D. Canada; 2010. p. 209-14.

Struble, L. and Sun, G.-K., 1995, Viscosity of portland cement paste as a function of concentration, *Advanced Cement Based Materials*, Vol. 2, pp. 62-69.

Su, N., Hsu, K.C. and Chai, H.W., 2004, A simple mix design method for self-compacting concrete, *Cement and Concrete Research*, Vol. 31, pp.1799-1807.

Sun, Z., Voigt, T. and Shah, S.P., 2006, Rheometric and ultrasonic investigations of viscoelastic properties of fresh Portland cement pastes, *Cement and Concrete Research*, Vol. 36, pp. 278-287.

References

Tattersall, G.H., 1991, *Workability and quality control of concrete*, E&FN Spon, London, pp. 27-36.

The European Guidelines for self-compacting concrete; specification, production and use. *www.efnarc.org*. 2005.

Thrane, L., Szabo, P., Geiker, M., Glavind, M. and Stang, H., 2004, Simulation of the test method "l-box" for self-compacting concrete, *Annual Transactions of the Nordic Rheology Society*, Vol. 12, pp. 47-54.

Thrane, L.N., 2007, Form filling with self-compacting concrete. Ph.D. Thesis concrete centre danish technological institute department of civil engineering department of chemical engineering technical university of Denmark. ISBN 97-8877-8772-473.

Tregger, N., Ferrara, L. and Shah, S.P., 2007, Empirical relationships between viscosity and flow time measurements from mini-slump tests for cement pastes formulated from SCC, Proceedings of the 5th *International RILEM Symposium-SCC 2007*, Ghent, Belgium, pp. 273-278.

Tregger, N., Ferrara, L. and Shah, S.P., 2008, Identifying viscosity of cement paste from mini-slump-flow test, *ACI Materials Journal*, Vol.105, pp. 558-566

Utracki, L.A., 2003, *Polymer Blends Handbook*, Springer London, pp. 459-461.

Utsi, S., 2008, Performance based concrete mix design-aggregate and micro mortar optimization applied on self-compacting concrete containing fly ash. Ph.D. Thesis, Luleå, Sweden: division of structural engineering, Luleå University of Technology, pp. 142-150.

Utsi, S., Emborg, M and Carlsward, J., 2003, Relation between workability and rheological parameters, In: *Proceedings of the 3rd International RILEM Symposium*, Pro 33, Wallevik O, Nielsson I (eds). RILEM: Cachan, pp. 154-160.

Vand, V., 1948, Viscosity of solutions and suspensions. II, experimental determination of the viscosity & concentration function of spherical suspensions, *The Journal of Physical and Colloid Chemistry*, Vol. 52, pp. 300-314.

References

Vasilic, K., Roussel, N., Meng, B. and Kühne, H.C., 2010, Computational modeling of SCC flow through reinforced sections in self-compacting concrete (SCC), In: *Proceedings of the 2010 International RILEM Symposium on Self-Compacting Concrete*. Design, production and placement of self-consolidating concrete eds. Khayat KH. and Feys. D. Canada; 2010. pp. 187-195.

Vikan, H. and Justnes, H., 2003, Influence of silica fume on rheology of cement paste, *Proceeding of international symposium. Self-Compacting Concrete*, Reykjavik, Iceland, 17-20 August, 2003, pp. 238-252.

Wallevik J.E., 2006, Relationship between the Bingham parameters and slump, *Cement and Concrete Research*, Vol. 36, pp. 1214-1221.

Wallevik, O.H. and Gjorv, O.E., 1990, Development of a coaxial cylinders viscometer for fresh concrete, eds. Wiereg, H.J., *Properties of Fresh Concrete*, Chapman and Hall. London, pp. 213-224.

Wendt, J. F. (1992), *Computational fluid dynamics, an introduction*, Springer London, pp. 15-35.

Westerholm, M., Lagerblad, B., Silfwerbrand, J. and Forssberg, E., 2008, Influence of fine aggregate characteristics on the rheological properties of mortars, *Cement and Concrete Composites*, Vol. 30, pp. 274-282.

Williams, D.A., Saak, A.W. and Jennings, H.M., 1999, The influence of mixing on the rheology of fresh cement paste, *Cement and Concrete Research*, Vol. 29, pp. 1491-1496.

Wildemuth, C.R. and Williams, M.C. 1984, Viscosity of suspensions modelled with a shear-dependent maximum packing fraction, *Rheologica Acta*, Vol. 23, pp. 627-635.

Willis, J. R. and Acton, J. R., 1976, The overall elastic moduli of a dilute suspension of spheres, *The Quarterly Journal of Mechanics and Applied Mathematics*, Vol. 29, pp. 163-177.

Wu, Z., Zhang, Y., Zheng, J. and Ding, Y., 2009, An experimental study on the workability of self-compacting lightweight concrete, *Construction Building material*, Vol. 23 pp. 2087-2092.

References

www.ermco.org., 2010, European ready-mixed concrete industry statistics

Yahia, A., Tanimura, M., Shimabukuro, A. and Shimoyama, H., 1999, Effect of limestone powder on rheological behaviour of highly flowable mortar, _Proceeding of Japan Conference_, Vol. 21, No. 2, pp. 559–564

Yamada, K., Takahashi, T., Hanehara, S. and Matsuhisa, M., 2000, Effects of the chemical structure on the properties of polycarboxylate-type superplasticiser, _Cement and Concrete Research_, Vol. 30, No. 2, pp. 197–207.

Zhang, X. and Han, J., 2000, The effect of ultra-fine admixture on the rheological property of cement paste, _Cement and Concrete Research_, Vol. 30, pp. 827-830.

Appendix A

A.1 Corrected SPH integration

The basic SPH approximations as given by equation (3.44) or (3.47) do not accurately reproduce or approximate the functions $\phi(\mathbf{x})$ and $\nabla\phi(\mathbf{x})$. Therefore, in the past, corrected SPH equations were developed to address these issues (Bonet and Lok, 1999; Bonet and Kulasegaram, 2000). The main aim of the correction techniques is to satisfy the conservation of angular momentum which, unlike the linear momentum, is not automatically satisfied. For two neighbouring particles, a and b, it can be shown (Bonet and Lok, 1999) that the angular momentum is preserved if

$$\sum_{b=1}^{N}\frac{m_b}{\rho_b}(\mathbf{x}_b-\mathbf{x}_a)\otimes\nabla W_b(\mathbf{x}_a)=\mathbf{I} \tag{A.1}$$

where $\mathbf{x}_a$ and $\mathbf{x}_b$ are the position vectors of particles a and b, respectively. In order to correct the SPH algorithms, either the gradient of the kernel is addressed directly (Bonet and Lok, 1999) or the kernel function itself is modified (Li and Liu, 1996). Another possible way is to mix the kernel and gradient corrections (Bonet and Kulasegaram, 2000; Bonet and Lok, 1999). In following these methods are discussed in more detail.

A.1.1 Gradient correction

The kernel gradient is modified by introducing a correction matrix $\mathbf{L}$ such that

$$\tilde{\nabla}W_b(\mathbf{x})=\mathbf{L}\nabla W_b(\mathbf{x}) \tag{A.2}$$

In (A.1), if general SPH equation (for any particle i.e. without subscript a) is used and the term $\nabla W_b(\mathbf{x})$ is replaced by its corrected one (A.2), we have

$$\sum_{b=1}^{N}\frac{m_b}{\rho_b}(\mathbf{x}_b-\mathbf{x})\otimes\mathbf{L}\nabla W_b(\mathbf{x})=\mathbf{I} \tag{A.3}$$

Therefore, $\mathbf{L}$ is given by

$$\mathbf{L}=\left(\sum_{b=1}^{N}\frac{m_b}{\rho_b}\nabla W_b(\mathbf{x})\otimes(\mathbf{x}_b-\mathbf{x})\right)^{-1} \tag{A.4}$$

A.1.2 Kernel correction

The kernel can be modified to ensure that polynomial functions up to a given degree are exactly interpolated. The linear kernel correction is given by

$$\tilde{W}_b(x) = W_b(x)\alpha(x)\{1 + \beta(x)(x - x_b)\} \tag{A.5}$$

For any linear field, such as velocity, the correction formulation is

$$v_0 + v_1 x = \sum_{b=1}^{N} \frac{m_b}{\rho_b}(v_0 + v_1 x_b)\, \tilde{W}_b(x) \tag{A.6}$$

The following completeness conditions must be satisfied

$$\sum_{b=1}^{N} \frac{m_b}{\rho_b}\, \tilde{W}_b(x) = 1 \tag{A.7}$$

$$\sum_{b=1}^{N} \frac{m_b}{\rho_b}(x - x_b)\, \tilde{W}_b(x) = 0 \tag{A.8}$$

The vector parameter, $\beta(x)$ is obtained by substituting (A.5) into (A.8)

$$\beta(x) = \frac{\displaystyle\sum_{b=1}^{N} \frac{m_b}{\rho_b}(x - x_b)W_b(x)}{\displaystyle\sum_{b=1}^{N} \frac{m_b}{\rho_b}(x - x_b)\otimes(x - x_b)W_b(x)} \tag{A.9}$$

Substituting (A.5) into (A.7) gives the scalar parameter, $\alpha(x)$ as

$$\alpha(x) = \frac{1}{\displaystyle\sum_{b=1}^{N} \frac{m_b}{\rho_b}\{1 + \beta(x)(x - x_b)\}W_b(x)} \tag{A.10}$$

As can be seen from (A.9) and (A.10) both $\alpha(x)$ and $\beta(x)$ are functions of x and therefore make this correction expensive in terms of the computational time. A possible way to make the correction less time consuming is by ignoring $\beta(x)$, i.e. the kernel is corrected by using a constant rather than a linear correction. Therefore the interpolation of the field function $v(x)$ becomes

$$v(\mathbf{x}) = \sum_{b=1}^{N} \frac{m_b}{\rho_b} v_b \tilde{W}_b(\mathbf{x}) \qquad (A.11)$$

where

$$\tilde{W}_b(\mathbf{x}) = \frac{W_b(\mathbf{x})}{\sum_{b=1}^{N} \frac{m_b}{\rho_b} W_b(\mathbf{x})} \qquad (A.12)$$

A.1.3 Combined kernel and gradient correction

Another possible correction technique is by mixing the kernel and gradient corrections described above. The corrected gradient of the corrected kernel is given by

$$\tilde{\nabla} \tilde{W}_b(\mathbf{x}) = \mathbf{L} \nabla \tilde{W}_b(\mathbf{x}) \qquad (A.13)$$

$\nabla \tilde{W}_b(\mathbf{x})$ can be obtained by differentiation of (A.12) to give

$$\nabla \tilde{W}_b(\mathbf{x}) = \frac{\nabla W_b(\mathbf{x}) - \varepsilon(\mathbf{x})}{\sum_{b=1}^{N} \frac{m_b}{\rho_b} W_b(\mathbf{x})} \qquad (A.14)$$

where

$$\varepsilon(\mathbf{x}) = \frac{\sum_{b=1}^{N} \frac{m_b}{\rho_b} \nabla W_b(\mathbf{x})}{\sum_{b=1}^{N} \frac{m_b}{\rho_b} W_b(\mathbf{x})} \qquad (A.15)$$

Similar to (A.14), the correction matrix $\mathbf{L}$ is given by

$$\mathbf{L} = \left(\sum_{b=1}^{N} \frac{m_b}{\rho_b} \nabla \tilde{W}_b(\mathbf{x}) \otimes \mathbf{x}_b \right)^{-1} \qquad (A.16)$$

Note that, in (A.16), the term $\mathbf{x}$ is no longer required since only the constant kernel is used instead of a linear one. Using the corrected gradient of the corrected kernel, the SPH equations (3.44) and (3.47) can be rewritten as

$$\phi(\mathbf{x}) = \sum_{b=1}^{N} \frac{m_b}{\rho_b} \phi_b \tilde{W}_b(\mathbf{x}) \qquad (A.17)$$

$$\nabla\phi(\mathbf{x}) = \sum_{b=1}^{N} \frac{m_b}{\rho_b} \phi_b \tilde{\nabla}\tilde{W}_b(\mathbf{x}) \qquad (A.18)$$

Appendix B

Mix compositions of the reference mixes of series OS used in Chapter 5
(after Grünewald, 2004)

		Mix 1	Mix 2	Mix 3	Mix 4	Mix 5	Mix 6	Mix 7
Constituent (kg/m³)	CEM III 42.5 N	155	149	149	143	335	352	367
	CEM I 52.5 R	249	263	249	269	0	0	0
	Water	172	181	171	181	155	164	173
	SP CUGLA (20% solid) LR	2.58	2.88	2.59	2.78	2.1	2.1	2.17
	SP CUGLA (35% solid) HR	1.58	1.44	2.12	1.85	1.26	1.18	1.09
	Fly ash 1	0	0	0	0	168	192	217
	Fly ash 2	142	173	146	173	0	0	0
	Sand (0.125-4mm) round	913	876	1089	1045	1134	1089	1045
	CA (4-16mm) round	682	655	508	487	528	508	487
Ratios	Water/Cement	0.42	0.44	0.43	0.44	0.46	0.47	0.47
	Water/Binder	0.38	0.39	0.39	0.39	0.43	0.44	0.44

Appendix C

Number of steel fibres cut by the diametrical vertical section of the slump cone (after Nicolaides, 2004)

The number of steel fibres that will theoretically be seen in one cut section of the particular volume is given by the theory of geometric probability or more precisely by the solution of the so-called Buffon problem in three dimensions (Solomon 1978). Although the proof of the particular problem is beyond the scope of the current work, some basic points are described below. The original problem called the "the Buffon needle problem" is about the probability of a needle (line segment) of length l that is dropped "at random" on a set of equidistant parallel lines in a plane that are d units apart, $l \leq d$ intersecting a line (see Figure C.1). The problem is solved by considering a finite number of possible positions for the needle as equally likely outcomes and then treating the limiting case as a representation of the problem. This includes a definition of randomness for the distance x of the needle's midpoint to the nearest line and the acute angle φ formed by the needle and a perpendicular form the midpoint to the line. The solution is obtained by computing the ratio of favourable outcomes to the total set of outcomes and passing to the limit.
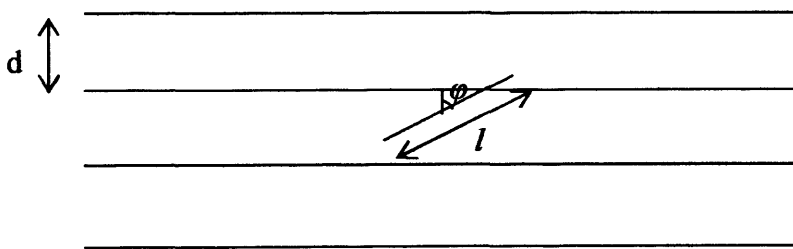
Figure C.1: Buffon needle problem in two-dimensions

Buffon's problem is also extended to those situations where the needle is larger than the shortest distance between grid lines, and therefore multiple intersections can be seen. However, a more general extension of the problem is the one provided by Morton (1966), who proved an important and remarkable result on the expected number of intersections and distribution of angles of intersections for a random set of rectifiable curves in the plane.

The three dimensional situation takes as its point of departure a result by Crofton (1885) which shows that if a line is repeatedly placed at random over a plane containing a closed figure, the average length of the chord $E(c)$ intersected by the figure will be

$$E(c) = \pi \frac{\text{area}}{\text{perimeter}} \qquad \text{(C.1)}$$

no matter what the shape of the figure, as long as its boundary is a convex curve.

However, before this result could be employed for estimating volume-surface area ratios it required the following modifications:

1. it had to be made applicable to line segments;

2. a simple procedure for measuring chord length had to be found;

3. it had to be extended to cover non-convex figures (e.g. figures with re-entrant corners);

4. it had to be extended to provide an estimate not only of the area-perimeter ratio in the focal plane under observation but the volume-surface ratio in the three dimensions of which the observed focal plane is a two-dimensional representation.

The first three of these modifications were accomplished by a single device. A line of finite length, say l, was considered and the number of times each of the two end points fell in the interior of a plane figure was counted. This number was denoted by $E(h)$ for hits and the number of times the line intersected the perimeter of the figure was denoted by $E(c)$ for cuts.

Then, in a very large number of throws it will be found that

$$l \frac{E(h)}{E(c)} = \pi \frac{\text{area}}{\text{perimeter}} \qquad \text{(C.2)}$$

for all closed figures including the non-convex ones.

The fourth and important modification was provided by a mathematical result. When a line of length l is placed at random in three-dimensional space containing a closed figure, for a very large number of throws it may be shown that

$$l\frac{E(h)}{E(c)}=4\frac{\text{volume}}{\text{surface area}} \qquad\qquad (C.3)$$

This result satisfied condition 4. Since placing a line at random in three dimensions could be shown to be formally equivalent to placing a plane at random in three dimensions and placing the line at random on the resulting two-dimensional plane section.

If the space contains a series of figures of different volumes and surfaces, then

$$l\frac{E(h)}{E(c)}=4\frac{\sum\text{volumes}}{\sum\text{surface areas}} \qquad\qquad (C.4)$$

Here $E(h)$ is the number of hits, i.e. the number of times each of the two end points of the line fall in the interior of the plane closed figure and $E(c)$ is the number of times the line intersects the perimeter of the figure. As in two dimensions, this result applies irrespective of whether the closed figure is convex or not.

The above theoretical result is used here to calculate how many 30 mm long steel fibres will be cut by the diametrical vertical section of the slump cone.

Volume of truncated cone =

$$V=\frac{\pi h}{3}\left(R^2+r^2+Rr\right)=\frac{\pi\times300}{3}\left(100^2+50^2+100\times50\right)=5497787.14 \text{ mm}^3$$

Volume of each fibre with 0.55 mm diameter and 30 mm length = 7.127 mm^3

Number of fibres (2.5 % by volume) in the truncated cone $=\dfrac{2.5}{100}\times\dfrac{5497787.14}{7.127}=19242$

Let us subdivide the cone volume into cubes of 40 mm side, thus (C.4) becomes

$$30\times\frac{E(h)}{E(c)}=4\times\frac{64000}{6\times1600}\Rightarrow E(h)=\frac{8}{9}E(c)$$

Number of fibres in a 40 mm cube = $E(h)+E(c)=\dfrac{64000\times2.5}{100\times7.127}=225$

Therefore, the number of fibres cut by 40×40 mm section is $E(c)=119$

Area of the diametrical vertical section of slump cone is 45000 mm^2.

Therefore the number of fibres that will be cut by the diametrical vertical section =

$$\frac{119}{1600} \times 45000 = 3347$$

Appendix D

Data Sheets and Health and Safety Sheets

Health and Safety Information – Blue Circle Portland Cements

This datasheet provides the information required by the Chemicals (Hazard Information and Packaging) Regulations.

IRRITANT

HEALTH & SAFETY INFORMATION
BLUE CIRCLE PORTLAND CEMENTS

Autumn 2006

BLUE CIRCLE PORTLAND CEMENTS

1. Identification of Substance/ Supplier Section

An odourless white to grey powder mainly insoluble in water. When water is added it becomes a binder for construction applications. This datasheet applies to the following Blue Circle cements:

- Portland (CEM I) cements
- Mastercrete Original
- Extra Rapid
- Cement
- Procem
- Portland Limestone Cement
- Ferrocrete
- Sulfacrete
- Snowcrete
- Phoenix
- Microcem
- CEMblend.

*Lafarge Cement United Kingdom
Manor Court
Chilton OX11 0RN
Technical helpline: 0870 609 0011*

2. Composition/Information on Ingredients

2.1. Chemical Description
The principal constituents of these cements are calcium silicates, aluminates, ferro-aluminates and sulfates. Small amounts of alkalis, lime and chlorides are also present together with trace amounts of chromium compounds. Additional constituents may also be present eg pulverized-fuel ash, limestone, and granulated blastfurnace slag. CAS: 65997-15-1.

2.2. Hazardous Ingredients
a) The lime, calcium silicates and alkalis within the cement are partially soluble and when mixed with water will give rise to a potentially hazardous alkaline solution.

b) Hexavalent chromium salts in these cements are soluble and when mixed with water, will give rise to a potentially hazardous solution.

3. Hazards Identification

When cement is mixed with water such as when making concrete or mortar, or when the cement becomes damp, a strong alkaline solution is produced. If this comes into contact with the eyes or skin it may cause serious burns and ulceration. The eyes are particularly vulnerable and damage will increase with contact time.

Strong alkaline solutions in contact with the skin tend to damage the nerve endings first before damaging the skin, therefore chemical burns can develop without pain being felt at the time.

Cement mortar and concrete mixes may until set cause both irritant and allergic contact dermatitis:

- Irritant contact dermatitis is due to a combination of the wetness, alkalinity and abrasiveness of the constituent materials.

- Allergic contact dermatitis is caused mainly by the sensitivity of an individuals skin to hexavalent chromium salts.

4. First Aid Measures

Eye Contact
Wash eyes immediately with clean water for at least 15 minutes and seek medical advice without delay.

Skin Contact
Wash the affected area thoroughly with soap and water before continuing. If irritation, pain or other skin trouble occurs, seek medical advice. Clothing contaminated by wet cement, concrete or mortar should be removed and washed thoroughly before use.

Ingestion
Do not induce vomiting. Wash out mouth with water and give patient plenty of water to drink.

Inhalation
If irritation occurs, move to fresh air. If nose or airways become inflamed seek medical advice.

5. Fire Fighting Measures
Cements are not flammable and will not facilitate combustion with other materials.

6. Accidental Release Measures

6.1. Personal Precautions
(See 8.3. overleaf)

6.2. Method of Cleaning
Recover the spillage in a dry state if possible. Minimise generation of airborne dust. The product can be slurried by the addition of water but will subsequently set as a hard material. Keep children away from clean up operation.

7. Storage and Handling

7.1. Storage
Bags should be stacked in a safe and stable manner.

7.2. Handling
When handling cement bags due regard should be paid to the risks outlined in the Manual Handling Operations Regulations. Some bags may have a small amount of cement on the outer surface. Appropriate personal protective clothing (see 8.3) should therefore be used whilst handling.

7.3. Control of Hexavalent Chromium
From 17 January 2005, those cements which naturally contain more that 2 ppm of soluble hexavalent chromium (chromium (VI)) by dry weight of cement, will be treated with a chemical reducing agent (such as ferrous sulfate) that maintains the level of hexavalent chromium in the cement to below 2 ppm by dry weight of cement. The effectiveness of the reducing agent reduces with time, therefore cement bags and/or delivery documents will contain information on the period of time ('shelf life') for which the manufacturer has established that the reducing agent will continue to limit the level of hexavalent chromium to less than 2 ppm by dry weight of cement. They will also indicate the appropriate storage conditions for maintaining the effectiveness of the reducing agent.

Blue Circle™ is a brand of **LAFARGE**

If cements are incorrectly stored, or used after the end of the declared 'shelf life', the level of hexavalent chromium may rise above 2 ppm by dry weight of cement, with a consequent increase in the potential risk of allergic contact dermatitis.

Note: White Portland cement is typically low in soluble hexavalent chromium and would be exempt from these requirements.

8. Exposure Controls

8.1. Workplace Exposure Limits (WEL's)
WELs 8hr Time Weighted Average (TWA)

Total inhalable dust 10mg/m³   8hr TWA
Respirable dust   4mg/m³   8hr TWA

8.2. Engineering Control Measures
Where reasonably practicable, dust exposures should be controlled by engineering methods.

8.3. Recommended Protective Equipment

Respiratory Protection
Suitable respiratory protection should be worn to ensure that personal exposure is less than the WEL.

Hand and Skin Protection
Protective clothing should be worn which ensures that cement, or any cement/water mixture eg concrete or mortar, does not come into contact with the skin. In some circumstances such as when laying concrete, waterproof trousers and wellingtons may be necessary.

Particular care should be taken to ensure that wet concrete does not enter the boots and persons do not kneel on the wet concrete so as to bring the wet concrete into contact with unprotected skin.

Should wet mortar or wet concrete get inside boots, gloves or other protective clothing then this protective clothing should be immediately removed and the skin thoroughly washed as well as the protective clothing/footwear.

Eye Protection
Dust-proof goggles should be worn wherever there is a risk of cement powder or any cement/water mixtures entering the eye.

9. Physical/Chemical Properties

9.1. Physical Data

Physical state	Particulate
Mean particle size	5–30 micron
Odour	Not applicable (N/A)
pH	pH of wet cement 12-14
Viscosity	N/A
Freezing point	N/A
Boiling point	N/A
Melting point	N/A
Flash point	Not flammable
Explosive properties	Not explosive

Density	2800-3200 kg/m³
Solubility	N/A

9.2. Chemical Compounds
Mainly a mixture of: $3CaO.SiO_2$, $2CaO.SiO_2$, $3CaO.Al_2O_3$, $4CaO.Al_2O_3$, $Fe_2O_3.CaSO_4$.

Contains less than 1% crystalline silica.

10. Stability and Reactivity
Conditions contributing to chemical instability: None.

Hazardous decomposition products: None.

Special precautions: None.

11 Toxicological Information

11.1. Short Term Effects

Eye Contact
Cement is a severe eye irritant. Mild exposures can cause soreness. Gross exposures or untreated mild exposures can lead to chemical burning and ulceration of the eye.

Skin
Cement powder or any cement/water mixture may cause irritant contact dermatitis, allergic (chromium) dermatitis, and/or burns.

Ingestion
The swallowing of small amounts of cement or any cement/water mixtures is unlikely to cause any significant reaction. Larger doses may result in irritation to the gastro intestinal tract.

Inhalation
Cement powder may cause inflammation of mucous membranes.

11.2. Chronic Effects
Repeated exposures in excess of the WEL have been linked with rhinitis and coughing. Skin exposure has been linked to allergic (chromium) dermatitis. Allergic dermatitis more commonly arises through contact with cement/water mixtures than dry cement.

12. Ecological Information

12.1. Aquatic Toxicity Rating
LC50 aquatic toxicity rating not determined. The addition of cements to water will, however, cause the pH to rise and may therefore be toxic to aquatic life in some circumstances.

12.2. Biological Oxygen Demand (BOD)
Not applicable.

13. Disposal Considerations
Dispose of empty bags or surplus cement to a place authorised to accept builder's waste (non-hazardous materials landfill).

Keep out of the reach of children.

14. Transport Information
Classification for conveyance: Not required.

15. Regulatory Information

15.1. Chemicals (Hazard Information & Packaging) Regulations
Classification: Irritant.

15.2. Risk Phrases
● Contains chromium (VI). May produce an allergic reaction.
● Risk of serious damage to eyes.
● Contact with wet cement, wet concrete or wet mortar may cause irritation, dermatitis or burns.
● Contact between cement powder and body fluids (eg sweat and eye fluid) may also cause skin and respiratory irritation, dermatitis or burns.
● R 37/38/41/43.

15.3. Safety Phrases
● Avoid eye and skin contact by wearing suitable eye protection, clothing and gloves.
● Avoid breathing dust.
● Keep out of reach of children.
● On contact with eyes or skin, rinse immediately with plenty of clean water. Seek medical advice after eye contact.
● S 2/22/24/25/26/37/39.

16. Legislation and Other Information
● CONIAC Health Hazard Information Sheet No 26, Cement.
● Health & Safety at Work Act 1974.
● Control of Substances Hazardous to Health (Regulations).
● HSE Guidance Note EH40 (Workplace Exposure Limits).
● Any authorised manual on First Aid by St. Johns/St. Andrews/Red Cross.
● Manual Handling Operations Regulations 1992.
● Environmental Protection Act.

LAFARGE
CEMENT

United Kingdom

A leading company...

and a leading brand

The information in this datasheet is accurate at the time of printing, but Lafarge Cement UK reserve the right to amend details as part of their product development programme.   HS:3:10/06

Elkem Microsilica®

CONCRETE

Guidance for the Specification of Silica Fume

General

Silica Fume (also often termed condensed silica fume and microsilica) is a powerful pozzolanic material and has been used as an addition to concrete for some 30 years.

However, until more recently only a few international standards have been available for the specification of the material. This datasheet reviews the main standards and provides advice on how silica fume should be specified.

History

The first patent for a 'Silica Modified Cement' was granted in the USA in 1946. This was long before the first full-scale filtering came 'on-line'.

In 1986, Canada drew up a 'Standard for Supplementary Cementing Materials' – which included silica fume. This was revised in 1998.

In 1995, ASTM produced a Standard for the American market place and this undergoes almost annual review.

A new European Standard is under approval and will probably be issued in 2005.

These are the three main standards in global use, but many countries have now issued national standards for silica fume of which some are shown in Table 1.

Each should be checked for the date and only the latest edition used when specifying the silica fume.

Elkem Microsilica®

Elkem Materials produce Elkem Microsilica® which conforms to the mandatory requirements of the relevant standards from :
- **American Society for Testing and Materials**
- **European Committee for Standardisation**

Kindly see our Product Datasheets.

Standardisation Criteria

In order that the silica fume is of a suitable quality to use in concrete, a certain number of parameters have been set. While some of the values set may vary in 'National' Standards, the limits discussed here are considered the 'norm'.

Silicon Dioxide (SiO$_2$) – minimum 85%

While lower content fumes may be used under some National Standards, this is considered the lowest level for effective reaction in concrete use.

Specific Surface Area - 15 000 to 35 000 m^2/kg

SSA defines the size of the particles. The higher the value, the smaller the sphere size. A 'normal' number is around 20 000. Out of range high values could have negative physical effects in the fresh concrete.

Loss on Ignition – maximum 4 to 6%

This is the amount of organic contaminant in the material. The lower this figure, the higher the quality. The 6% value is derived from the standard for fly ash.
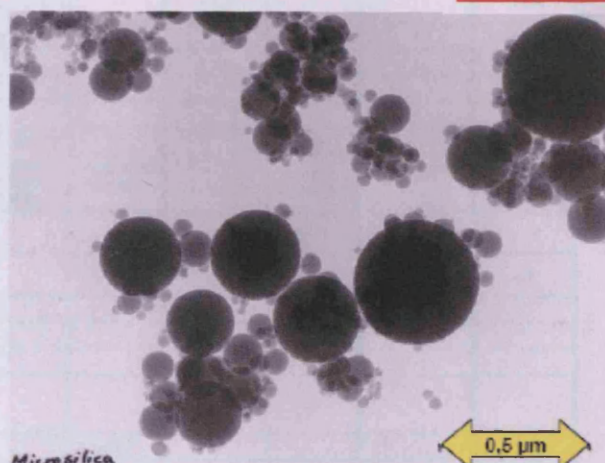
Microsilica

TEM (Transmission Electron Microscopy) picture of silica fume

Retained on 45 micron sieve – up to 10%

The 'oversize' particles in the fume. These may be agglomerates or crystalline material. The lower this figure, the higher the quality. This is probably the most variable figure, with tolerance being up to 10%, depending on the standard used.
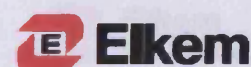
Pozzolanic Activity Index

The reactivity of the silica fume. This figure also varies from standard to standard depending on the design of the test mix and curing conditions. A good silica fume will always give a figure above 100% at 28 days.

Mix Proportioning

Due to the wide and varied nature of all the constituents of concrete – cements, aggregates, admixtures etc. – it is not feasible to give exact proportions for specific mixes – especially on a 'global' basis.

However, a review of past projects, and the mixes used, can give an insight into the level of silica fume dosage that may be advantageous for certain applications. These are quite simply, starting points for mix designs, until sufficient 'local' information has been determined. In almost all circumstances silica fume concrete is produced using a plasticiser or superplasticiser.

Table 2 sets out examples of the percentages that are suitable for the types of mixes given. Dosage levels will be relative to the environmental conditions and the performance requirements, hence the ranges given and the stress on trial mix work. The table shows areas of overlap.

Elkem

Mandatory chemical and physical requirements	American ASTM C1240–04	European EN 13263:2005	Canadian CAN/CSA A23.5-98	Japanese JIS A 6207 2000	Chinese GB/T18736 -2002	Brazilian NBR 13956:1997	Korean KS F 2567 2003	Vietnamese TCXDVN 311-2003	Indian IS 15388:2003
SiO₂ (%)	> 85.0	> 85	> 85	> 85	> 85	> 85	> 85	> 85	> 85.0
SO₃ (%)		< 2.0	< 1.0	< 3.0			< 3.0		
Cl (%)		< 0.3		< 0.1	< 0.2		< 0.3		
Free CaO (%)		< 1.0		< 1.0					
MgO (%)				< 5.0			< 5.0		
Free Si (%)		< 0.4							
Available alkalis (Na₂O equivalent, %)	Report					< 1.5			< 1.5
Moisture (%)	< 3.0			< 3.0	< 3.0	< 3.0		< 3.0	< 3.0
Loss on ignition (%)	< 6.0	< 4.0	< 6.0	< 5.0	< 6.0	< 6.0	< 5.0	< 6.0	< 4.0
Specific surface (m²/gram)	> 15	15 - 35		> 15	> 15		> 15		> 15
Bulk density, undensified	Report								
Pozzolanic Activity Index (%)	> 105 @ 7d, accel. curing	> 100 @ 28d, std curing		> 95 @ 7d / > 105 @ 28d, std curing	> 85 @ 28d, std curing		> 95 @ 7d, accel curing	> 85 @ 7d	> 85.0 @ 7d, 27 °C curing
Retained on 45 micron sieve (%)	< 10		< 10				< 5.0	< 10	< 10
Variation from average on 45 micron sieve (%-points)	< 5								< 5
Density (kg/m³)	Report								
Autoclave expansion (%)			< 0.2						
Foaming			No foam						
Dry mass (%-points deviation from declared in slurry)		< 2					< 2		
Water requirement ratio (%)					< 125				

Table 1. Comparison of main international silica fume standards. Please note that the table gives the mandatory chemical and physical requirements. Some of the standards also contain optional requirements. Where there are blanks, no mandatory requirements exist.

A low permeability concrete may also give high strength, and a high strength shotcrete will also give a very low permeability. This is where the 'fine tuning' of the mix design comes in, to achieve both fresh and hardened performance. This may include the use of blended cements, retarding and other admixtures, different aggregate types or the use of hot/cold weather concreting techniques (chilled or hot water, flaked ice, etc.)

Elkem Materials offers technical and practical assistance in determining mix parameters and designing silica fume concrete mixes. This knowledge has been established from many diverse projects world-wide.

Application	Dosage level [a], %
Pumping Aid	2 – 3
Normal Concrete	4 – 7
Self Compacting Concrete	4 – 10
High Strength	7 – 10[**]
Low Permeability	7 – 10[**]
Underwater	12 – 15
Shotcrete	8 – 12
[a] the silica fume percentage is always given as dry weight by weight of the cementitious materials	
[**] higher percentages may be used under specific conditions to achieve certain performance characteristics	

Table 2. General recommended dosage levels of silica fume

The information given on this datasheet is accurate to the best knowledge of Elkem Materials. The information is offered without guarantee, and Elkem Materials accepts no liability for any direct or indirect damage from its use. The information is subject to change without notice. For latest update or further information or assistance, please contact your local representative, the internet address or the e-mail address given on this datasheet.

CONCRETE	GENERAL INFORMATION	NOVEMBER 2005	C1-05

Contact/representative:

Elkem Materials

Internet: www.concrete.elkem.com
e-mail: microsilica.materials@elkem.no

◻ ■ BASF

The Chemical Company

SAFETY DATA SHEET
Glenium Ace 333

1 IDENTIFICATION OF THE SUBSTANCE/PREPARATION AND COMPANY/UNDERTAKING

PRODUCT NAME   Glenium Ace 333

APPLICATION   Admixture for precast concrete

SUPPLIER   BASF Construction Chemicals
Albany House
Swinton Hall Road
Swinton Manchester M27 4DT
(+44) 161 794 7411
NOTE : In cases of emergency outside
working hours, use Telephone Number
above. Follow instructions from recorded
message.
(+44) 161 727 8547

2 COMPOSITION/INFORMATION ON INGREDIENTS

COMPOSITION COMMENTS

Aqueous solution containing polycarboxylate ether

3 HAZARDS IDENTIFICATION

Not regarded as a health or environmental hazard under current legislation.

4 FIRST-AID MEASURES

INHALATION

Move the exposed person to fresh air at once. Provide fresh air, warmth and rest, preferably in a comfortable upright sitting position. Get medical attention if any discomfort continues.

INGESTION

DO NOT INDUCE VOMITING! NEVER MAKE AN UNCONSCIOUS PERSON VOMIT OR DRINK FLUIDS! Rinse mouth thoroughly. Promptly get affected person to drink large volumes of water to dilute the swallowed chemical. Obtain medical advice Provide rest, warmth and fresh air.

SKIN CONTACT

Remove affected person from source of contamination. Remove contaminated clothing. Wash the skin immediately with soap and water. Get medical attention if irritation persists after washing.

EYE CONTACT

Make sure to remove any contact lenses from the eyes before rinsing. Promptly wash eyes with plenty of water while lifting the eye lids. Continue to rinse for at least 15 minutes. Get medical attention if any discomfort continues.

5 FIRE-FIGHTING MEASURES

EXTINGUISHING MEDIA

This product is not flammable. Use fire-extinguishing media appropriate for surrounding materials.

SPECIAL FIRE FIGHTING PROCEDURES

No specific fire fighting procedure given.

6 ACCIDENTAL RELEASE MEASURES

PERSONAL PRECAUTIONS

Wear protective clothing as described in Section 8 of this safety data sheet.

ENVIRONMENTAL PRECAUTIONS

Avoid subsoil penetration. Prevent product from entering drains. Do not contaminate surface water.

SPILL CLEAN UP METHODS

Wear necessary protective equipment. Stop leak if possible without risk. Absorb in vermiculite, dry sand or earth and place into containers. Flush with plenty of water to clean spillage area. Do not contaminate water sources or sewer.

1 / 3

7 HANDLING AND STORAGE

USAGE PRECAUTIONS

Avoid spilling, skin and eye contact. Observe good industrial hygiene practices.

STORAGE PRECAUTIONS

Keep in original container. Protect against Freezing Store Between 5 and 30 Degrees C

8 EXPOSURE CONTROLS/PERSONAL PROTECTION

PROTECTIVE EQUIPMENT

ENGINEERING MEASURES

No particular ventilation requirements.

RESPIRATORY EQUIPMENT

If ventilation is insufficient, suitable respiratory protection must be provided.

HAND PROTECTION

Use protective gloves. Rubber gloves are recommended.

EYE PROTECTION

Use approved safety goggles or face shield.

OTHER PROTECTION

Wear appropriate clothing to prevent any possibility of skin contact.

HYGIENE MEASURES

DO NOT SMOKE IN WORK AREA! Wash at the end of each work shift and before eating, smoking and using the toilet. Wash promptly if skin becomes wet or contaminated. Promptly remove any clothing that becomes contaminated. When using do not eat, drink or smoke.

9 PHYSICAL AND CHEMICAL PROPERTIES

APPEARANCE	Liquid		
COLOUR	Brown		
ODOUR	Characteristic		
SOLUBILITY	Miscible with water.		
MELTING POINT (°C)	0	RELATIVE DENSITY	1.07 @ 20 °c
VAPOUR PRESSURE	n/a mbar	pH-VALUE. CONC. SOLUTION	7.5

10 STABILITY AND REACTIVITY

STABILITY

Stable under normal temperature conditions and recommended use.

CONDITIONS TO AVOID

Avoid excessive heat for prolonged periods of time.

HAZARDOUS DECOMPOSITION PRODUCTS

None other than those associated with the packaging

11 TOXICOLOGICAL INFORMATION

TOXIC DOSE 1 - LD 50   > 2000 mg/kg (oral rat)

TOXICOLOGICAL INFORMATION

No toxilogical data is available for the finished product. The LD50/LC50 values mentioned referes to individual raw materials:

polycarboxylates

GENERAL INFORMATION

Not irritating

HEALTH WARNINGS

No specific health warnings noted.

Other Health Effects

May cause sensitisation to susceptible persons

Glenium Ace 333

12 ECOLOGICAL INFORMATION

ECOTOXICITY

There is no data available for the product itself. The EC50/LC50/IC50 values mentioned refers to individual raw materials: polycarboxylates
The product should not be allowed to enter drains or water courses or be deposited where it can affect ground or surface waters.

13 DISPOSAL CONSIDERATIONS

DISPOSAL METHODS
Dispose of waste and residues in accordance with local authority requirements.
WASTE CLASS
16 03 06: Off-specification batches and unused products; organic wastes other than those mentioned in 16 03 05

14 TRANSPORT INFORMATION

ROAD TRANSPORT NOTES   Not classified for road transport.
RAIL TRANSPORT NOTES   Not classified for rail transport.
SEA TRANSPORT NOTES   Not classified for sea transport.

15 REGULATORY INFORMATION

RISK PHRASES
                NC   Not classified.
SAFETY PHRASES
                NC   Not classified.
ENVIRONMENTAL LISTING
Rivers (Prevention of Pollution) Act 1961. Control of Pollution (Special Waste Regulations) Act 1980.
EU DIRECTIVES
System of specific information relating to Dangerous Preparations. 2001/58/EEC. Dangerous Preparations Directive 1999/45/EEC.
STATUTORY INSTRUMENTS
Chemicals (Hazard Information and Packaging) Regulations. Control of Substances Hazardous to Health.
APPROVED CODE OF PRACTICE
Classification and Labelling of Substances and Preparations Dangerous for Supply.
GUIDANCE NOTES
Workplace Exposure Limits EH40. Introduction to Local Exhaust Ventilation HS(G)37. CHIP for everyone HSG(108).

16 OTHER INFORMATION

ISSUED BY
HS&E Manager.
REVISION DATE   03/04/06
REV. NO./REPL. SDS GENERATED Issue 1
SDS NO.   SDS11343

3 / 3

Page 226

□ ■ **BASF**

The Chemical Company

Safety data sheet

BASF Safety data sheet according to Regulation (EC) No.1907/2006

Date / Revised: 13.08.2008   Version: 1.1

Product: **GLENIUM STREAM 2006L**

(30438165/SDS_GEN_GB/EN)

Date of print 13.08.2008

1. Substance/preparation and company identification

GLENIUM STREAM 2006L

Use: additive for cement based and other inorganic suspensions of solids in water

Company:

BASF PLC - PO Box 4, Earl Road

Cheadle Hulme, Cheshire, SK8 6QG

GREAT BRITAIN

Telephone: +44 161 485-6222

Telefax number: +44 161 4274

E-mail address: product-safety-north@basf.com

Emergency information:

International emergency number:

Telephone: +49 180 2273-112

2. Hazard Identification

No specific dangers known, if the regulations/notes for storage and handling are considered.

3. Composition/information on ingredients

Chemical nature

BASF Safety data sheet according to Regulation (EC) No.1907/2006

Date / Revised: 13.08.2008   Version: 1.1

Product: **GLENIUM STREAM 2006L**

(30438165/SDS_GEN_GB/EN)

Date of print 13.08.2008

High molecular weight synthetic copolymer

4. First-aid measures

General advice:
First aid personnel should pay attention to their own safety. Remove contaminated clothing.

If inhaled:
Keep patient calm, remove to fresh air.

On skin contact:
Wash thoroughly with soap and water. If irritation develops, seek medical attention.

On contact with eyes:
Wash affected eyes for at least 15 minutes under running water with eyelids held open.

On ingestion:
Rinse mouth and then drink plenty of water.

Note to physician:
Treatment: Symptomatic treatment (decontamination, vital functions).

5. Fire-fighting measures

Suitable extinguishing media:
foam, water spray, dry extinguishing media

Unsuitable extinguishing media for safety reasons:
water jet

Specific hazards:
harmful vapours
Evolution of fumes/fog.

Special protective equipment:
Wear a self-contained breathing apparatus.

Further information:
The degree of risk is governed by the burning substance and the fire conditions. Contaminated extinguishing water must be disposed of in accordance with official regulations.

6. Accidental release measures

Personal precautions:
Do not breathe vapour/aerosol/spray mists. Use personal protective clothing. Handle in accordance with good industrial hygiene and safety practice.

BASF Safety data sheet according to Regulation (EC) No.1907/2006

Date / Revised: 13.08.2008   Version: 1.1

Product: **GLENIUM STREAM 2006L**

(30438165/SDS_GEN_GB/EN)

Date of print 13.08.2008

Environmental precautions:
Contain contaminated water/firefighting water. Do not discharge into drains/surface
waters/groundwater.

Methods for cleaning up or taking up:
For small amounts: Contain with absorbent material (e.g. sand, silica gel, acid binder, general purpose
binder, sawdust). Correctly dispose of recovered product immediately.
For large amounts: Pump off product.

Additional information: Forms slippery surfaces with water.

7. Handling and storage

Handling

Avoid aerosol formation. No special measures necessary provided product is used correctly.

Protection against fire and explosion:
The substance/product is non-combustible. The product does not contribute to the spreading of
flames, nor is it self combustible, not explosive. Take precautionary measures against static
discharges.

Storage

Further information on storage conditions: Containers should be stored tightly sealed in a dry place.
Keep away from heat. Store protected against freezing. Keep only in the original container.

8. Exposure controls and personal protection

Personal protective equipment

Respiratory protection:
Respiratory protection in case of vapour/aerosol release. Combination filter for gases/vapours of
organic, inorganic, acid inorganic and alkaline compounds (e.g. EN 14387 Type ABEK).

Hand protection:
impermeable gloves
rubber
Manufacturer's directions for use should be observed because of great diversity of types.

Eye protection:
Wear safety goggles at working overhead and danger of sputtering.

Body protection:
Body protection must be chosen depending on activity and possible exposure, e.g. apron, protecting
boots, chemical-protection suit (according to EN 14605 in case of splashes or EN ISO 13982 in case of
dust).

BASF Safety data sheet according to Regulation (EC) No.1907/2006

Date / Revised: 13.08.2008   Version: 1.1

Product: **GLENIUM STREAM 2006L**

(30438165/SDS_GEN_GB/EN)

Date of print 13.08.2008

General safety and hygiene measures:
In order to prevent contamination while handling, closed working clothes and working gloves should be used. Handle in accordance with good building materials hygiene and safety practice. When using, do not eat, drink or smoke. Hands and/or face should be washed before breaks and at the end of the shift. At the end of the shift the skin should be cleaned and skin-care agents applied. Gloves must be inspected regularly and prior to each use. Replace if necessary (e.g. pinhole leaks).

9. Physical and chemical properties

Form:	aqueous solution
Colour:	colourless to lightly coloured
Odour:	characteristic
pH value:	6.5 - 8.5
	(20 °C)

Information on: water
solidification temperature: *0 °C*

Information on: water
boiling temperature: *100 °C*
                         (1,000 hPa)

Flash point:

         Not applicable

Ignition temperature:

         Not applicable

Information on: water
Vapour pressure: *23 mbar*
                        (20 °C)

Density: 1.01 - 1.02 g/cm3
                     (20 °C)

Miscibility with water:

         miscible in all proportions